



NTNU – Trondheim
Norwegian University of
Science and Technology

The Effect of Liquid Exposure on PTMSP/TiO₂ Nanocomposite Membranes for Gas-Liquid Membrane Contactors for Removal of CO₂ from Natural Gas

Henriette Iselin Mortensen

Chemical Engineering and Biotechnology

Submission date: June 2014

Supervisor: May-Britt Hägg, IKP

Co-supervisor: Karen Nessler Seglem, IKP

Norwegian University of Science and Technology
Department of Chemical Engineering

Preface

This master's thesis has been carried out at Department of Chemical Engineering at the Norwegian University of Science and Technology (NTNU) during spring 2014. The work is a continuation of a specialization project conducted during fall 2013 and is part of an ongoing Ph.D. project. The latter is part of a project called *A GREEN Sea*, for which the overall objective is to identify, mature and evaluate new technologies and concepts for acid gas removal from natural gas. One of the technologies is membrane contactors. The Ph.D. project is conducted in collaboration with SINTEF Materials and Chemistry. Industrial partners are Statoil, Gassco and Petrobras.

First of all, I would like to express my sincere gratitude to my supervisor Karen Nessler Seglem who has provided me with valuable and highly appreciated guidance, help and advice on the laboratory work as well as on the report. I would also like to thank my supervisor May-Britt Hägg, professor and head of the Memfo group, for giving me the opportunity to take part in this project.

I am grateful to all the people who have answered my questions, given me guidance and helped me solve any practical challenges both inside and outside the laboratory. Thank you, Mats, for standing by my side through five years of hard studies. Without you, I am afraid I would have gone through with my plan to make the terrifying Calculus 1 exam not only my first, but also my last at NTNU. To my fellow students and friends: thank you for making my student days brighter! When I look back on the years in Trondheim, I will not only remember the "inhumane" third semester spent in the organic lab, the oh-so stressful weeks each December and May and the endless amount of curriculum, but also the good times I spent with you!

Finally, I would like to address a word of thanks to my family. You have always believed that I could make it, even when I was convinced that I would not. And as it turns out, you were often right.

Declaration of compliance

I declare that this is an independent work according to the exam regulations of the Norwegian University of Science and Technology (NTNU).

Trondheim, 13.06.2014

_____

Henriette Mortensen

Abstract

This project concerns the development of membrane materials for use in gas-liquid membrane contactors for the removal of CO₂ from natural gas. In this application, the membrane is primarily intended to prevent any phase dispersion and to secure a high gas flow across the gas-liquid interface. The CO₂ selectivity is provided by the liquid absorbent, which is usually an amine solution. In addition to the importance of high permeability, the membrane-liquid compatibility is crucial to secure high performance and long-term stability.

Flat sheet nanocomposite membranes based on poly(1-trimethylsilyl-1-propyne) (PTMSP) have been prepared. PTMSP is a glassy, high free volume polymer exhibiting the highest gas permeability of all known polymers. Titanium dioxide (TiO₂) nanoparticles are dispersed in the polymer matrix as a mean to disrupt the chain packing and thereby enhance the transport of gas. Three different types of particles are employed. One is the commercial Aeroxide® TiO₂ T 805. The particles are in form of covalently bonded aggregates in the range of 100-250 nm. The second and third type are custom made by SINTEF Materials and Chemistry. These are delivered in the form of clustered particles in toluene in the size ranges 15-400 nm and >1 μm, respectively. The nanocomposite membranes contained 5 and 20 wt% TiO₂.

The air-facing side (upside) of the nanocomposite membranes were exposed to deionized water, 2 M MDEA and 4.2 M MDEA (aqueous solutions). The membranes were exposed for 1 day and up to about 9 weeks. After exposure, pure gas permeability tests were conducted using CO₂ and CH₄ at 2, 4 and 6 bar. The permeability decreased as the time of exposure increased. The rate of change was highest during the first weeks of exposure. For the membranes exposed to 4.2 M MDEA, a significant decrease was observed already after 1 day of exposure. Long-term exposure to 2 M MDEA resulted in permeabilities comparable to those exposed to 4.2 M MDEA. At this point, the permeability of the membranes exposed to MDEA solution was less than 10% of the initial value. Thus, the nanocomposite membranes investigated in this work have shown poor performance at long-term exposure to MDEA solution. The membranes exposed to water showed a better performance. After 67 days of exposure, the measured CO₂ permeability was higher than 10 000 Barrer for all membranes.

Contact angle measurements confirmed the hydrophobicity of PTMSP and the nanocomposites. The water contact angle was highest on the upside of the membranes. For the liquid-exposed membranes, the measured contact angles decreased as the time of exposure increased. The membranes exposed to water experienced a more significant decrease in contact angle than the ones exposed to MDEA solutions.

Scanning electron microscopy (SEM) was used to characterize the surface morphology of the flat sheet nanocomposite membranes. The images confirmed the suspected difference between the upside and downside of the membranes. Alterations of the surface was observed after exposure to liquid. At the maximum time of exposure, both sides of the membranes were clearly affected both by water and the MDEA solutions. The morphological changes coincided with the reduction in permeability.

Sammendrag

I denne masteroppgaven er det fokusert på testing og utvikling av et membranmateriale til bruk i en gass-væske-membrankontaktor for fjerning av CO₂ fra naturgass. I denne prosessen muliggjør membranen direkte kontakt mellom gass og væske uten at de to fasene blandes. Membranens primære oppgave er å sikre en høy gjennomstrømning av gass. Absorpsjonsvæsken, som ofte er en aminløsning, sørger for CO₂-selektiviteten. For å sikre en langsiktig ytelse av membrankontaktoren er det svært viktig at membranmaterialet er kompatibelt med absorpsjonsvæsken.

Det har blitt laget flate nanokomposittmembraner basert på den glassaktige polymeren poly(1-trimetylsilyl-1-propyn) (PTMSP). Denne polymeren har et ekstremt høyt fritt volum og dermed den høyeste permeabiliteten av alle kjente polymerer. Tre forskjellige partikkeltyper av titandioksid (TiO₂) har blitt inkorporert i polymermatriksen for å forbedre permeabiliteten av gass. Den ene typen er den kommersielle Aeroxide® T 805 TiO₂ som er i form av kovalent bundede aggregater med en størrelse på 100-250 nm. De to andre partikkeltypene er laget av SINTEF Materialer og Kjemi og er i form av partikkelklynger i toluen. Den ene løsningen inneholder partikler i størrelsesorden 15-400 nm, mens den andre inneholder partikler >1 µm. De tillagede nanokomposittmembranene inneholdt henholdsvis 5 og 20 vektprosent TiO₂.

Oversiden av membranene har blitt eksponert for deionisert vann, samt 2 M og 4.2 M vandig MDEA-løsning. Varigheten av eksponeringen varierte fra 1 dag til omtrent 9 uker. Etter eksponering ble permeabilitetsmålinger gjennomført med bruk av CO₂ og CH₄ ved 2, 4 og 6 bar. Målingene viste at permeabiliteten minket med økende varighet av eksponering. En kraftig reduksjon i permeabilitet ble observert allerede etter 1 dag for membranene eksponert for 4.2 M MDEA. For membranene eksponert for 2 M MDEA varierte permeabiliteten noe i løpet av de første ukene. Etter omtrent 9 ukers eksponering var CO₂-permeabiliteten for membranene eksponert for 2 M og 4.2 M MDEA-løsning omtrent lik. I begge tilfeller var permeabiliteten lavere enn 10% av den opprinnelige verdien for de ikke-eksponerte membranene. Nanokomposittmembranene eksponert for vann viste en bedre ytelse. Etter nærmere 10 ukers eksponering var CO₂-permeabiliteten fortsatt høyere enn 10 000 Barrer for alle typer membraner.

Kontaktvinkelmålinger bekreftet at polymeren og nanokomposittmembranene var hydrofobe. På oversiden av membranene var kontaktvinkelen større enn 100°, mens den på undersiden var tydelig lavere. For de væskeeksponerte membranene minket kontaktvinkelen med økende varighet av eksponering. Membranene som var eksponert for vann, viste en større reduksjon i kontaktvinkel enn de som var eksponert for MDEA-løsning.

Morfologien av membranene ble undersøkt ved hjelp av scanningelektronmikroskopi (SEM). Bildene bekreftet at det var en forskjell på de to sidene av membranen og at dette kunne forklare den observerte forskjellen i kontaktvinkel. Tydelige endringer på overflaten av væskeeksponerte membraner ble observert. For de langtidseksponerte membranene ble det observert en tydelig endring også på undersiden, dette til tross for at denne siden ikke hadde vært i direkte kontakt med væsken. Endringene i morfologi samsvarer med reduksjonen i permeabilitet.

Table of contents

Preface	i
Abstract	iii
Sammendrag	v
List of symbols.....	xi
List of figures.....	xv
List of tables	xix
1. Background.....	1
2. Introduction.....	3
3. Membranes and polymers	5
3.1 <i>Polymers and their properties</i>	5
3.1.1 State of the polymer and the glass transition temperature.....	5
3.1.2 Free volume.....	6
3.2 <i>Polymeric membranes</i>	6
3.3 <i>Transport in membranes</i>	8
3.3.1 Transport of gases through porous membranes	8
3.3.2 Transport of gases through nonporous membranes	9
3.3.3 The dual sorption model	11
3.3.4 Membrane selectivity.....	12
3.4 <i>Poly(1-trimethylsilyl-1-propyne) (PTMSP)</i>	13
4. Mixed matrix membranes.....	17
5. Gas-liquid membrane contactors	19
5.1 <i>Positive and negative aspects of membrane contactors</i>	19
5.2 <i>Types of membrane contactors</i>	21
5.3 <i>The membrane-solvent system</i>	21
5.3.1 The solvent in a gas-liquid membrane contactor	21
5.3.2 The membrane in a gas-liquid membrane contactor	22
5.4 <i>Basic principles of mass transfer in a gas-liquid membrane contactor</i>	25
6. Literature review	27
6.1 <i>Nanocomposite membranes</i>	27
6.2 <i>Gas-liquid membrane contactors</i>	31
7. Experimental	35
7.1 <i>Materials and preparation</i>	35

7.1.1	Polymer	35
7.1.2	Nanoparticles	35
7.1.3	Other chemicals and gases	36
7.1.4	Polymer solutions.....	36
7.1.5	Membrane preparation.....	37
7.1.6	Exposure of nanocomposite membranes to liquid	38
7.2	<i>Membrane characterization</i>	39
7.2.1	Gas permeability measurements	39
7.2.2	Membrane thickness.....	41
7.2.3	Scanning electron microscopy (SEM)	41
7.2.4	Contact angle measurements	42
8.	Previous work	45
9.	Results and discussion	49
9.1	<i>Gas permeability results</i>	49
9.1.1	Effect of gas and feed pressure on gas permeabilities.....	49
9.1.2	Uncertainty in permeability measurements	49
9.1.3	Aging of membranes	50
9.1.4	Permeability of unexposed membranes	51
9.1.5	Liquid-exposed nanocomposite membranes	53
9.1.6	Summary of permeability results	64
9.2	<i>Contact angle measurements</i>	67
9.2.1	Uncertainty in contact angle measurements	67
9.2.2	Contact angles of PTMSP and nanocomposite membranes	67
9.2.3	Contact angles of membranes prepared on casting plates of Teflon.....	69
9.2.4	Contact angles of liquid-exposed nanocomposite membranes	69
9.2.5	Summary of contact angle measurements	73
9.3	<i>Scanning electron microscopy (SEM) images</i>	75
9.3.1	Uncertainty in SEM analysis	75
9.3.2	Unexposed membranes	75
9.3.3	Membranes prepared on casting plates of Teflon	80
9.3.4	Liquid-exposed nanocomposite membranes	81
9.3.5	Summary of SEM images.....	89
9.4	<i>Summary of results</i>	90
10.	Conclusion	93
10.1	<i>Nanocomposite membranes of PTMSP and TiO₂</i>	93
10.2	<i>Effects of liquid exposure</i>	94
10.3	<i>Effect of different types of TiO₂ particles</i>	94
10.4	<i>Comparison of results</i>	95
11.	Further work	97
12.	References	99
APPENDIX	I	
A.	<i>Permeation rig flowsheets</i>	I

<i>B. Gas permeability results</i>	<i>III</i>
<i>C. Contact angle measurements</i>	<i>XIII</i>
<i>D. SEM images</i>	<i>XV</i>
<i>E. Risk assessments</i>	<i>XXIX</i>

List of symbols

Symbol	Explanation	Unit
<u>Latin characters</u>		
A	area	m ²
b	hole affinity constant	atm ⁻¹
C or c	concentration	kg/m ³ , mol/m ³
C	total concentration of gas in polymer	m ³ (STP)/m ³
C _D	Henry's law sorption	m ³ (STP)/m ³
C _H	Langmuir sorption	m ³ (STP)/m ³
C' _H	hole saturation constant	m ³ (STP)/m ³
D	diffusivity, diffusion coefficient	m ² /s
D _A	diffusivity coefficient of gas A	m ² /s
D _B	diffusivity coefficient of gas B	m ² /s
d	diameter	m
E	tensile modulus	N/m ²
E	enhancement factor	
H	Henry's law constant	m ³ (STP)/m ³ ·atm
J	flow rate	m ³ (STP)/s
J _i	diffusion flux of component i	mol/m ² ·s
k	Boltzmann constant	
k _D	Henry's law solubility constant	m ³ (STP)/m ³ ·atm
k _G	mass transfer coefficient of the gas phase	m/s
k _L	mass transfer coefficient of the liquid phase	m/s
k _m	mass transfer coefficient of the membrane	m/s
K	overall mass transfer coefficient	m/s
K _i	overall mass transfer coeff. of comp. i	m/s
L	length	m
l	thickness	m
M _w	molecular weight	g/mol
p	pressure	Pa
P	permeability	Barrer
P _i	permeability coefficient of comp. i	Barrer
P _A	permeability coefficient of gas A	Barrer
P _B	permeability coefficient of gas B	Barrer
P _p	permeability coefficient of pure polymer	Barrer
R	gas constant	J/mol·K
r or r _p	pore radius	m

S	sorption, solubility coefficient	$\text{m}^3(\text{STP})/\text{m}^3\text{bar}$
S_A	solubility coefficient of gas A	$\text{m}^3(\text{STP})/\text{m}^3\text{bar}$
S_B	solubility coefficient of gas A	$\text{m}^3(\text{STP})/\text{m}^3\text{bar}$
S_f	solubility coefficient of fillers	$\text{m}^3(\text{STP})/\text{m}^3\text{bar}$
S_p	solubility coefficient of polymer	$\text{m}^3(\text{STP})/\text{m}^3\text{bar}$
T	temperature	K
T_g	glass transition temperature	K
T_m	melting temperature	K
V	volume	m^3
v	velocity	m/s
x	distance in x direction	m

Greek characters

α	selectivity	
γ	surface tension	N/m
γ_L	surface tension of liquid	N/m
γ_{SL}	solid-liquid interfacial energy	N/m
γ_{SV}	solid-vapor interfacial energy	N/m
γ_{LV}	liquid-vapor interfacial energy	N/m
Δ	delta, finite difference	
δ	thickness	m
ε	porosity	
η	viscosity	Pa·s
θ	contact angle	°
v	specific volume of membrane	m^3/kg
v_0	volume occupied by molecules	m^3/kg
v_f	fractional free volume	
ϕ_F^N	nominal volume fraction	
ϕ_f	volume fraction of filler	
ϕ_p	volume fraction of polymer	

Abbreviations

AFM	atomic force microscopy
BAA	4,4-diazidobenzophenone
DEA	diethanolamine
FFV	fractional free volume
FT-IR	Fourier transform infrared spectroscopy
FS	fumed silica
G-L	gas-liquid
HFM	hollow fiber membrane
MEA	monoethanolamine
MDEA	methyldiethanolamine
MgO	magnesium oxide
MMM	mixed matrix membrane
NaOH	sodium hydroxide
PALS	positron annihilation lifetime spectroscopy
PE	polyethylene
PES	polyether sulfone
PDMS	polydimethylsiloxane (silicon rubber)
PP	polypropylene
PTFE	polytetrafluoroethylene
PTMSP	poly(1-trimethylsilyl-1-propyne)
SEM	scanning electron microscopy
TEA	triethanolamine
TEM	transmission electron microscopy
TiO ₂	titanium dioxide
TMSG	trimethylsilylglucose
WAXD	wide angle X-ray diffraction
wt%	weight percentage
XPS	X-ray photoelectron spectroscopy

Conversions

Barrer	$10^{-10} \text{ cm}^3(\text{STP})\text{cm}/\text{cm}^2\cdot\text{s}\cdot\text{cmHg}$ $27.4\cdot 10^{-10} \text{ m}^3(\text{STP})\text{m}/\text{m}^2\cdot\text{h}\cdot\text{bar}$ $3.34\cdot 10^{-16} \text{ kmol}\cdot\text{m}/\text{m}^2\cdot\text{s}\cdot\text{kPa}$
Å	10^{-10} m

List of figures

- FIGURE 3-1: THE BASIC MEMBRANE GAS SEPARATION PROCESS [11].
- FIGURE 3-2: THE THREE BASIC TYPES OF MEMBRANES: POROUS (A), NONPOROUS (B) AND CARRIER MEMBRANE (C) [7].
- FIGURE 3-3: COMPONENTS ARE SEPARATED BY MOLECULAR FILTRATION IN POROUS MEMBRANES (TO THE LEFT). IN NON-POROUS MEMBRANE, SEPARATION IS OBTAINED DUE TO DIFFERENCES IN SOLUBILITY AND DIFFUSIVITY (TO THE RIGHT) [11].
- FIGURE 3-4: PERMEATION OF NONCONDENSABLE AND CONDENSABLE GAS MIXTURES THROUGH A MICROPOROUS MEMBRANE. (A) KNUDSEN DIFFUSION, (B) MOLECULAR SIEVING, (C) KNUDSEN DIFFUSION AND SURFACE DIFFUSION, (D) SURFACE DIFFUSION AND CAPILLARY CONDENSATION [11].
- FIGURE 3-5: SORPTION ISOTHERMS FOR (A) IDEAL AND (B AND C) NON-IDEAL SYSTEMS [7].
- FIGURE 3-6: GAS SORPTION IN GLASSY POLYMERS BY THE DUAL SORPTION MODEL. LANGMUIR SORPTION AND HENRY'S LAW SORPTION CONTRIBUTES TO THE TOTAL SORPTION [11].
- FIGURE 3-7: THE STRUCTURE OF PTMSP [11].
- FIGURE 3-8: PERMEABILITY AS A FUNCTION OF LENNARD-JONES DIAMETER FOR DIFFERENT POLYMERS [7].
- FIGURE 4-1: ILLUSTRATION OF A MIXED MATRIX MEMBRANE.
- FIGURE 5-1: PRINCIPLE OF MEMBRANE GAS ABSORPTION [40].
- FIGURE 5-2: PARALLEL FLOW HOLLOW FIBER GAS-LIQUID MEMBRANE CONTACTOR (REDRAWN FROM [9] AND [46])
- FIGURE 5-3: GAS-LIQUID CONTACTORS WITH A POROUS MEMBRANE IN (A) NON-WETTED MODE AND (B) WETTED MODE. THE CORRESPONDING CONCENTRATION PROFILE IS SHOWN IN FIGURE (C) AND (D). [7].
- FIGURE 5-4: CONTACT ANGLES OF LIQUID DROPLETS ON A SOLID (NONPOROUS) MATERIAL [7]. (A) $\Theta > 90^\circ$, (B) $\Theta = 90^\circ$ AND (C) $\Theta < 90^\circ$.
- FIGURE 5-5: GAS LIQUID CONTACTOR WITH (A) A COMPOSITE MEMBRANE (POROUS MEMBRANE WITH DENSE TOP LAYER) AND (B) A DENSE MEMBRANE. CORRESPONDING CONCENTRATION PROFILES ARE SHOWN IN FIGURE (C) AND (D) [7].
- FIGURE 5-6: MASS TRANSFER PROCESS IN A HOLLOW FIBER GAS-LIQUID MEMBRANE CONTACTOR [41].
- FIGURE 6-1: EFFECT OF TiO_2 CONCENTRATION ON (A) CO_2 AND CH_4 PERMEABILITY AND (B) PURE GAS CO_2/CH_4 SELECTIVITY AT $\Delta P = 3.4$ ATM AND 35°C [37].
- FIGURE 7-1: PTMSP COMMERCIALY AVAILABLE FROM GELEST [96].
- FIGURE 7-2: TiO_2 NANOPARTICLES PROVIDED BY SINTEF MATERIAL AND CHEMISTRY [96].
- FIGURE 7-3: SOLUTIONS OF PURE PTMSP (LEFT), PTMSP+5 WT% T 805 (MIDDLE) AND PTMSP+20 WT% T 805 (RIGHT).
- FIGURE 7-4: MEMBRANES WITH 20 WT% $>1 \mu\text{M}$ (LEFT) AND PURE PTMSP (RIGHT).
- FIGURE 7-5: DRY MEMBRANES WITH 5 WT% $>1\mu\text{M}$ (LEFT), 15-400 NM (MIDDLE) AND T 805 (RIGHT).
- FIGURE 7-6: ILLUSTRATIONS SHOWING THE PREPARATION (A), THE FINAL EXPOSURE UNIT WITH THE UPSIDE OF THE MEMBRANE POINTING UPWARDS (B) AND THE EXPOSURE OF THE UPSIDE OF THE MEMBRANE (C).
- FIGURE 7-7: ILLUSTRATIONS SHOWING (A AND B) THE TESTING UNIT AND (C AND D) THE MEMBRANE CELL.
- FIGURE 7-8: PICTURES SHOWING (A) THE SPUTTER COATER, (B) SEM SAMPLES AND (C) THE SAMPLE HOLDER AT NTNU NANOLAB.
- FIGURE 7-9: IMAGE FROM ONEATTENSION SOFTWARE SHOWING WATER DROP ON MEMBRANE SURFACE. THE BASE LINE IS GIVEN IN GREEN.
- FIGURE 7-10: (A) ATTENSION'S THETA LITE OPTICAL TENSIOMETER, (B) WATER DROP ON MEMBRANE SURFACE AND (C) MEMBRANE PIECES GLUED ONTO A MICROSCOPE SLIDE.
- FIGURE 8-1: RESULTS FROM PREVIOUS MASTER PROJECT SHOWING THE CO_2 PERMEABILITY AT 2 BAR FOR PURE PTMSP, CROSSLINKED PTMSP WITHOUT NANOPARTICLES AND CROSSLINKED PTMSP WITH NANOPARTICLES [99]. THE MEMBRANES ARE EXPOSED TO DEIONIZED WATER, 2 M MDEA AND 4.2 M MDEA.
- FIGURE 8-2: CO_2 PERMEABILITY AS A FUNCTION OF TIME OF EXPOSURE FOR MEMBRANES CONTAINING 20 WT% T 805. RESULTS FROM SPECIALIZATION PROJECT CONDUCTED DURING FALL 2013.

FIGURE 8-3: CO₂ PERMEABILITY AS A FUNCTION OF TIME OF EXPOSURE FOR MEMBRANES CONTAINING 20 WT% 15-400 NM. RESULTS FROM SPECIALIZATION PROJECT CONDUCTED DURING FALL 2013.

FIGURE 8-4: CO₂ PERMEABILITY AS A FUNCTION OF TIME OF EXPOSURE FOR MEMBRANES CONTAINING 20 WT% >1 μM. RESULTS FROM SPECIALIZATION PROJECT CONDUCTED DURING FALL 2013.

FIGURE 9-1: CO₂ (RED LINE) AND CH₄ (BLACK LINE) PERMEABILITY AS A FUNCTION OF FEED PRESSURE FOR (A) 5 WT% T 805 TESTED IN PR-1 AND (B) 5 WT% 15-400 NM TESTED IN PR-2.

FIGURE 9-2: CO₂ PERMEABILITY AT 2 BAR FOR UNEXPOSED MEMBRANES AS A FUNCTION OF AGE.

FIGURE 9-3: CO₂ PERMEABILITY AT 2 BAR FOR LIQUID EXPOSED MEMBRANES CONTAINING 5 WT% T 805 TiO₂. THE BROKEN LINE SHOWS THE PERMEABILITY OF THE UNEXPOSED NANOCOMPOSITE.

FIGURE 9-4: CO₂/CH₄ SELECTIVITY AT 2 BAR FOR LIQUID EXPOSED MEMBRANES CONTAINING 5 WT% T 805 TiO₂. THE BLACK BROKEN LINE CORRESPONDS TO THE SELECTIVITY OF THE UNEXPOSED NANOCOMPOSITE.

FIGURE 9-5: CO₂ PERMEABILITY AT 2 BAR FOR LIQUID EXPOSED MEMBRANES CONTAINING 20 WT% T 805 TiO₂. THE BROKEN LINE SHOWS THE PERMEABILITY OF THE UNEXPOSED NANOCOMPOSITE.

FIGURE 9-6: CO₂/CH₄ SELECTIVITY AT 2 BAR FOR LIQUID EXPOSED MEMBRANES CONTAINING 20 WT% T 805 TiO₂. THE BLACK BROKEN LINE CORRESPONDS TO THE SELECTIVITY OF THE UNEXPOSED NANOCOMPOSITE.

FIGURE 9-7: CO₂ PERMEABILITY AT 2 BAR FOR LIQUID EXPOSED MEMBRANES CONTAINING 5 WT% 15-400 NM TiO₂. THE BROKEN LINE IN BLACK SHOWS THE PERMEABILITY OF THE UNEXPOSED NANOCOMPOSITE.

FIGURE 9-8: CO₂/CH₄ SELECTIVITY AT 2 BAR FOR LIQUID EXPOSED MEMBRANES CONTAINING 5 WT% 15-400 NM TiO₂. THE BLACK BROKEN LINE CORRESPONDS TO THE SELECTIVITY OF THE UNEXPOSED NANOCOMPOSITE.

FIGURE 9-9: CO₂ PERMEABILITY AT 2 BAR FOR LIQUID EXPOSED MEMBRANES CONTAINING 5 WT% >1 μM NM TiO₂. THE BROKEN LINE IN BLACK SHOWS THE PERMEABILITY OF THE UNEXPOSED NANOCOMPOSITE.

FIGURE 9-10: CO₂/CH₄ SELECTIVITY AT 2 BAR FOR LIQUID EXPOSED MEMBRANES CONTAINING 5 WT% >1 μM TiO₂. THE BLACK BROKEN LINE CORRESPONDS TO THE SELECTIVITY OF THE UNEXPOSED NANOCOMPOSITE.

FIGURE 9-11: CO₂ PERMEABILITY AT 2 BAR FOR ALL FOUR TYPES OF NANOCOMPOSITES, BOTH UNEXPOSED MEMBRANES AND MEMBRANES EXPOSED TO LIQUID FOR THE MAXIMUM AMOUNT OF TIME.

FIGURE 9-12: CO₂/CH₄ SELECTIVITY AT 2 BAR FOR ALL FOUR TYPES OF NANOCOMPOSITES, BOTH UNEXPOSED MEMBRANES AND MEMBRANES EXPOSED TO LIQUID FOR THE MAXIMUM AMOUNT OF TIME.

FIGURE 9-13: WATER CONTACT ANGLES ON (A) UPSIDE AND (B) DOWNSIDE OF MEMBRANE PREPARED ON GLASS, AND (C) UPSIDE AND (D) DOWNSIDE OF MEMBRANE PREPARED ON TEFLON. BOTH MEMBRANES CONTAIN 5 WT% T 805 TiO₂.

FIGURE 9-14: CONTACT ANGLE OF WATER ON UPSIDE OF MEMBRANE CONTAINING 5 WT% T 805 TiO₂ AS A FUNCTION OF TIME OF LIQUID EXPOSURE.

FIGURE 9-15: CONTACT ANGLE OF WATER ON UPSIDE OF MEMBRANE CONTAINING 20 WT% T 805 TiO₂ AS A FUNCTION OF TIME OF LIQUID EXPOSURE.

FIGURE 9-16: CONTACT ANGLE OF WATER ON UPSIDE OF MEMBRANE CONTAINING 5 WT% 15-400 NM TiO₂ AS A FUNCTION OF TIME OF LIQUID EXPOSURE.

FIGURE 9-17: CONTACT ANGLE OF WATER ON UPSIDE OF MEMBRANE CONTAINING 5 WT% >1 μM TiO₂ AS A FUNCTION OF TIME OF LIQUID EXPOSURE.

FIGURE 9-18: WATER CONTACT ANGLES ON UPSIDE OF NANOCOMPOSITE MEMBRANES. THE EXPOSED MEMBRANES WITH 5/20 WT% TiO₂ HAVE BEEN IMMERSSED IN WATER FOR 66/67 DAYS AND IN 2 M AND 4.2 M MDEA FOR 63/64 DAYS.

FIGURE 9-19: SEM IMAGES SHOWING (A, C) UPSIDE AND (B, D) DOWNSIDE OF PTMSP MEMBRANE.

FIGURE 9-20: SEM IMAGES OF (A AND C) UPSIDE AND (B) DOWNSIDE OF MEMBRANE CONTAINING 5 WT% T 805 TiO₂.

FIGURE 9-21: SEM IMAGES OF (A, C, D) UPSIDE AND (B) DOWNSIDE OF MEMBRANE CONTAINING 20 WT% T 805 TiO₂.

FIGURE 9-22: SEM IMAGES OF (A AND C) UPSIDE AND (B AND D) DOWNSIDE OF MEMBRANE WITH 5 WT% 15-400 NM TiO₂.

FIGURE 9-23: SEM IMAGES OF (A, C, D) UPSIDE AND (B) DOWNSIDE OF MEMBRANE CONTAINING 5 WT% $>1 \mu\text{M}$ TiO_2 .

FIGURE 9-24: SEM IMAGE OF THE CROSS-SECTION OF A MEMBRANE CONTAINING 20 WT% 15-400 NM TiO_2 . BLUE AND RED LINE SHOWS THE UPSIDE AND DOWNSIDE OF THE MEMBRANE, RESPECTIVELY.

FIGURE 9-25: SEM IMAGES OF THE DOWNSIDE OF MEMBRANES PREPARED ON TEFLON CONTAINING (A, B) 5 WT% AND (C, D) 20 WT% T 805 TiO_2 NANOPARTICLES.

FIGURE 9-26: SEM IMAGES OF THE UPSIDE OF LIQUID-EXPOSED NANOCOMPOSITES CONTAINING 5 WT% T 805 TiO_2 .

FIGURE 9-27: SEM IMAGES OF DOWNSIDE NANOCOMPOSITES CONTAINING 5 WT% T 805 TiO_2 EXPOSED TO (A) WATER FOR 67 DAYS, (B) 2 M MDEA FOR 64 DAYS AND (C) 4.2 M MDEA FOR 64 DAYS..

FIGURE 9-28: SEM IMAGES OF LIQUID-EXPOSED NANOCOMPOSITES CONTAINING 20 WT% T 805 TiO_2 .

FIGURE 9-29: SEM IMAGES OF DOWNSIDE NANOCOMPOSITES CONTAINING 20 WT% T 805 TiO_2 . UPSIDE EXPOSED TO (A) WATER FOR 66 DAYS, (B) 2 M MDEA FOR 63 DAYS AND (C) 4.2 M MDEA FOR 63 DAYS.

FIGURE 9-30: SEM IMAGES OF LIQUID-EXPOSED NANOCOMPOSITES CONTAINING 5 WT% 15-400 NM TiO_2 .

FIGURE 9-31: SEM IMAGES OF DOWNSIDE NANOCOMPOSITES CONTAINING 5 WT% 15-400 NM TiO_2 . UPSIDE EXPOSED TO (A) WATER FOR 67 DAYS, (B) 2 M MDEA 64 DAYS AND (C) 4.2 M MDEA 64 DAYS.

FIGURE 9-32: SEM IMAGES OF LIQUID-EXPOSED NANOCOMPOSITES CONTAINING 5 WT% $>1 \mu\text{M}$ TiO_2 .

FIGURE 9-33: SEM IMAGES OF DOWNSIDE NANOCOMPOSITES CONTAINING 5 WT% $>1 \mu\text{M}$ TiO_2 . UPSIDE EXPOSED TO (A) WATER FOR 67 DAYS, (B) 2 M MDEA FOR 64 DAYS AND (C) 4.2 M MDEA FOR 64 DAYS.

FIGURE 9-34: CO_2 PERMEABILITY AT 2 BAR FOR PTMSP, CROSSLINKED PTMSP, CROSSLINKED NANOCOMPOSITES AND UNCROSSLINKED NANOCOMPOSITES OF PTMSP AND TiO_2 . THE MEMBRANES ARE EXPOSED TO WATER, 2 M MDEA AND 4.2 M MDEA FOR 9-10 WEEKS. THE CROSSLINKED NANOCOMPOSITES ARE EXPOSED TO LIQUID FOR 2 WEEKS.

FIGURE A-1: FLOWSHEET OF PERMEATION RIG 2 (PR-2).

FIGURE A-2: FLOWSHEET OF PERMEATION RIG 1 (PR-1)

FIGURE B-3: CH_4 PERMEABILITY OF NANOCOMPOSITES CONTAINING (A) 5WT% T 805, (B) 20 WT% T 805, (C) 5 WT% 15-400 NM AND (D) 5 WT% $>1 \mu\text{M}$.

FIGURE D-4: SEM IMAGES OF MEMBRANES CONTAINING 5 WT% T 805 TiO_2 .

FIGURE D-5: SEM IMAGES OF MEMBRANES CONTAINING 20 WT% T 805 TiO_2 .

FIGURE D-6: SEM IMAGES OF MEMBRANES CONTAINING 5 WT% 15-400 NM TiO_2 .

FIGURE D-7: SEM IMAGES OF MEMBRANES CONTAINING 5 WT% $>1 \mu\text{M}$ TiO_2 .

FIGURE D-8: SEM IMAGES (A AND B) AND (C AND D) DOWNSIDE OF MEMBRANES CONTAINING 5 WT% T 805 TiO_2 PREPARED ON CASTING PLATES OF TEFLON.

FIGURE D-9: CROSS-SECTION IMAGES OF (A, B) UNEXPOSED AND (C-F) MEMBRANE EXPOSED TO 2 M MDEA FOR 2 WEEKS CONTAINING 20 WT% 15-400 NM TiO_2 . UPSIDE IS POINTING UPWARDS IN IMAGE A-F, DOWNSIDE IS POINTING UPWARDS IN IMAGE F.

List of tables

- TABLE 6-1: PERMEABILITIES AND SELECTIVITIES OF PURE PTMSP, PTMSP/FS AND PTMSP/TIO₂ NANOCOMPOSITE MEMBRANES AT 35°C AND FEED PRESSURE OF 2 BAR [2].
- TABLE 6-2: CO₂ AND CH₄ PERMEABILITY, SOLUBILITY AND DIFFUSION COEFFICIENTS, AND CO₂/CH₄ SOLUBILITY AND DIFFUSIVITY SELECTIVITY IN TIO₂ FILLED PTMSP AT 35 °C [37].
- TABLE 6-3: SUMMARY OF THE STUDIES PERFORMED ON DENSE POLYMERIC MEMBRANES FOR CO₂ ABSORPTION IN MEMBRANE CONTACTORS [44].
- TABLE 9-1: CH₄ AND CO₂ PERMEABILITY OF PTMSP AND TIO₂-PTMSP NANOCOMPOSITES, BASED ON TWO AND THREE MEASUREMENTS, RESPECTIVELY.
- TABLE 9-2: CO₂/CH₄ SELECTIVITY OF PTMSP AND TIO₂-PTMSP NANOCOMPOSITES, BASED ON TWO AND THREE MEASUREMENTS, RESPECTIVELY.
- TABLE 9-3: CONTACT ANGLES OF WATER, 2 M MDEA AND 4.2 M MDEA ON THE UPSIDE AND DOWNSIDE OF PURE PTMSP.
- TABLE 9-4: CONTACT ANGLES ON UPSIDE AND DOWNSIDE OF NANOCOMPOSITE MEMBRANES.
- TABLE B-1: DESCRIPTION AND VALUES OF VARIABLES IN THE PERMEABILITY EQUATION.
- TABLE B-2: MEASURED PERMEABILITIES OF PURE PTMSP. ONE TEST CONDUCTED IN EACH OF THE PERMEATION RIGS.
- TABLE B-3: MEASURED PERMEABILITIES OF NANOCOMPOSITES CONTAINING 5 WT% T 805 TIO₂. THREE SAMPLES FROM SAME MEMBRANE TESTED IN PR-1.
- TABLE B-4: MEASURED PERMEABILITIES OF NANOCOMPOSITES CONTAINING 20 WT% T 805 TIO₂. THREE SAMPLES FROM SAME MEMBRANE TESTED IN PR-2.
- TABLE B-5: MEASURED PERMEABILITIES OF NANOCOMPOSITES CONTAINING 5 WT% 15-400 NM TIO₂. THREE SAMPLES FROM SAME MEMBRANE TESTED IN PR-2.
- TABLE B-6: MEASURED PERMEABILITIES OF NANOCOMPOSITES CONTAINING 5 WT% >1 μM TIO₂. THREE SAMPLES FROM SAME MEMBRANE TESTED IN PR-1.
- TABLE B-7: PURE GAS PERMEABILITY OF CH₄ AND CO₂ FOR MEMBRANES CONTAINING 5 WT% AEROXIDE[®] T 805 TIO₂ NANOPARTICLES EXPOSED TO SOLUTION (DEIONIZED WATER, 2 M MDEA AND 4.2 M MDEA), THE TIME OF EXPOSURE VARYING FROM 1 DAY TO 10 WEEKS. THE NUMBERS IN GREY GIVES THE PERCENTAGE CHANGE IN PERMEABILITY FROM THE INITIAL PERMEABILITY OF THE UNEXPOSED NANOCOMPOSITE MEMBRANE CONTAINING THE SAME TYPE AND AMOUNT OF NANOPARTICLES.
- TABLE B-8: PURE GAS PERMEABILITY OF CH₄ AND CO₂ FOR LIQUID-EXPOSED MEMBRANES CONTAINING 20 WT% AEROXIDE[®] T 805 TIO₂ NANOPARTICLES. THE NUMBERS IN GREY GIVES THE PERCENTAGE CHANGE IN PERMEABILITY FROM THE INITIAL PERMEABILITY OF THE UNEXPOSED NANOCOMPOSITE.
- TABLE B-9: PURE GAS PERMEABILITY OF CH₄ AND CO₂ FOR LIQUID-EXPOSED MEMBRANES CONTAINING 5 WT% 15-400 NM TIO₂ NANOPARTICLES. THE NUMBERS IN GREY GIVES THE PERCENTAGE CHANGE IN PERMEABILITY FROM THE INITIAL PERMEABILITY OF THE UNEXPOSED NANOCOMPOSITE.
- TABLE B-10: PURE GAS PERMEABILITY OF CH₄ AND CO₂ FOR LIQUID-EXPOSED MEMBRANES CONTAINING 5 WT% >1 μM TIO₂ NANOPARTICLES. THE NUMBERS IN GREY GIVES THE PERCENTAGE CHANGE IN PERMEABILITY FROM THE INITIAL PERMEABILITY OF THE UNEXPOSED NANOCOMPOSITE. THE MEMBRANE EXPOSED TO 4.2 M MDEA FOR 14 DAYS (MARKED WITH *) WAS TESTED IN PR-2 RATHER THAN PR-1.
- TABLE C-11: WATER CONTACT ANGLES ON UPSIDE AND DOWNSIDE OF MEMBRANES CONTAINING 5 AND 20 WT% T 805 TIO₂ PREPARED ON CASTING PLATES OF TEFLON.
- TABLE C-12: WATER CONTACT ANGLES ON UPSIDE OF MEMBRANES CONTAINING 5 AND 20 WT% COMMERCIAL T 805 TIO₂ EXPOSED TO WATER, 2 M MDEA AND 4.2 M MDEA. VALUES IN BOLD ARE MEASURED BEFORE GAS PERMEATION TEST.
- TABLE C-13: WATER CONTACT ANGLES ON UPSIDE OF MEMBRANES CONTAINING 5 WT% 15-400 NM AND >1 μM TIO₂ EXPOSED TO WATER, 2 M MDEA AND 4.2 M MDEA. VALUES IN BOLD ARE MEASURED BEFORE GAS PERMEATION TEST.

1. Background

This work is part of an ongoing Ph.D. project by Karen Nessler Seglem and is a continuation of a master's thesis conducted in 2013 by Tina Tomaša. In early phases of the project, the focus was on the optimization of the membrane preparation. Membranes were prepared from polymer solutions containing different concentrations of polymer (PTMSP), crosslinking agent (BAA) and nanoparticles (TiO_2). Crosslinking of the polymer was performed to increase the chemical and physical stability, as the performance of PTMSP is known to be unstable with time due to physical aging. The bis(aryl azide) 4,4'-diazidobenzophenone (BAA) was used as the crosslinking agent. As expected, crosslinking of the polymer reduced the permeability.

The starting point for the investigation was the expectation that smaller nanoparticles would give rise to a higher increase in permeability. Thus, the first batch of TiO_2 nanoparticles provided by SINTEF Materials and Chemistry were specially designed to be evenly distributed in toluene as 15 nm-particles. Unexpectedly, the dispersion of nanoparticles in crosslinked PTMSP further reduced the permeability, an observation opposite of what is reported in the literature [1-3]. It was suspected that the nanoparticles were too small, causing the particles to block the free volume elements rather than expanding them. In the following phase of the project, the experiments were repeated using commercial TiO_2 in the form of clusters in the range of 100-250 nm. The addition of these nanoparticles had already been reported to give the expected increase in permeability [2]. The same was observed in the studies at NTNU.

Liquid exposure tests have been conducted using water and aqueous MDEA solutions. For the crosslinked PTMSP without nanoparticles, permeation tests indicated that the permeability stability provided by crosslinking was eliminated as a result of liquid exposure. For the crosslinked nanocomposite membranes, a dramatic decrease in permeability was observed already after 2 weeks of exposure. This is a disadvantageous result, as it is crucial for the membrane material to be compatible with the absorption liquid.

The poor performance of the crosslinked nanocomposite membranes was further investigated in a specialization project conducted during fall 2013. From then on, the nanocomposites were no longer crosslinked. The aim was to reveal whether or not it was the addition of nanoparticles that caused the dramatic decrease in permeability of the liquid-exposed membranes. In addition to the commercial particles, TiO_2 nanoparticles in the size range 15-400 nm and $>1 \mu\text{m}$ were provided by SINTEF Materials and Chemistry. Nanocomposites containing 20 wt% TiO_2 were immersed in liquid for 1 day, 1 week and 2 weeks. The results showed that liquid-exposed nanocomposites had not experienced the same decrease in permeability as the crosslinked nanocomposites. This was especially true for the ones exposed to water and 2 M MDEA. The results indicated that it was not the nanoparticles alone that caused the poor performance of the crosslinked nanocomposites. It was not possible to draw any conclusion regarding the effect of different types of nanoparticles.

2. Introduction

Carbon dioxide is found as an impurity in natural gas in which methane is the major component. Removal of CO₂ and other acidic gases from raw natural gas is an important operation in the process industry in order to meet commercial specifications [4]. High amounts of CO₂ in natural gas reduce the heating value of the gas and may lead to corrosion in equipment and pipelines due to its acidic nature. The removal of carbon dioxide from natural gas, and other gas streams, is a potentially economic source of CO₂ for enhanced oil recovery. Finally, CO₂ capture is an important measure to prevent the greenhouse gas from entering the atmosphere.

The needs for efficient and economical CO₂ capture techniques have been given high priority in present research. A number of technologies are available today. In the industry, chemical and/or physical absorption processes are the most established methods for the separation of CO₂. The method is based on a chemical reaction between CO₂ and a liquid absorbent, most commonly an aqueous solution of alkanolamines. In the next step, CO₂ is released by heating in a separate unit and the absorption liquid is re-generated [5]. One of the main disadvantages of chemical absorption is the high energy consumption [6]. Additionally, the process requires extensive equipment and suffers from a number of operating issues limiting the process, such as flooding, entrainment and that the liquid and gas streams cannot be operated independently.

Gas separation membranes for removal of CO₂ from natural gas are becoming a promising alternative to the conventional absorption processes and have received a lot of attention during the past three decades of research. The membrane acts as a selective barrier with the ability to transport one component from the feed mixture, e.g. CO₂, with greater ease than the other component(s) [7]. Membrane processes are considered less energy intensive and more environmental friendly than absorption processes [8]. The challenge is to produce a membrane with high gas flux *and* high selectivity that is able to withstand the high pressures and temperatures as well as the presence of a variety of impurities. Additionally, the long-term stability of the membrane performance is very important.

Another natural gas sweetening technology is gas-liquid membrane contactors, a promising and potentially simple low-cost construction. The membrane in the contactor simply acts as a barrier between the gas and liquid phase, thereby avoiding any phase dispersion. As with ordinary membranes for gas separation, one component, e.g. CO₂, is selectively removed from the feed gas. Unlike conventional membranes, the selectivity is usually provided by the liquid absorbent and not the membrane itself. Gas-liquid membrane contactors benefit from the advantages of both membrane separation and absorption. The main drawbacks of the conventional amine absorption processes are eliminated or minimized, e.g. flooding, channeling and foaming [9]. Additionally, membrane contactors are usually more compact than conventional gas separation membranes [6]. This is an advantageous characteristic of gas-liquid membrane contactors in the case of gas separation on oil platforms [10].

3. Membranes and polymers

A membrane can be defined as a semi-permeable barrier between two homogeneous phases. The ability to control the permeation rate of different species is considered one of the most important properties of a membrane [7]. The components in the feed may be separated due to differences in shape, size or chemical structure, or as a result of differences in the interaction with the membrane itself.

The large variety of membranes existing today, both biological and synthetic, may be categorized by means of their structure, transport properties and separation mechanism. Organic membranes (polymeric membranes) are considered the most important class of membranes [7]. The majority of the membranes applied in gas separation is dense polymeric membranes [11]. Theory on polymers and polymeric membranes is given in the following sections.

3.1 Polymers and their properties

Polymers are high molecular weight components built up of repeating subunits (monomers), exhibiting a large range of properties [7]. The physical properties of a given polymer are closely related to the polymer structure. As the number of segments increases, i.e. the molecular weight increases, the physical, chemical and mechanical properties of the polymer change. These properties may also be affected by crosslinking, through which the chains are connected by covalent bonding. Chain flexibility is one of the main structural characteristics of a polymer. The flexibility of a polymer is determined by the character of the main chain as well as the presence and nature of the side groups of the polymer backbone [7]. The forces acting between the polymer chains also have an impact on the polymer properties.

In the case of dense, polymeric membranes – which are further described in the following parts of the report – the membrane performance is closely related to the choice of polymeric material. Two structural parameters which strongly affect membrane performance are the glass transition temperature (T_g) and the crystallinity [7]. Both T_g and the crystallinity are determined by structural factors, i.e. chain flexibility and chain interactions. The glass transition temperature is further described in the following.

3.1.1 State of the polymer and the glass transition temperature

The mechanical, chemical and thermal properties of a polymer are affected by the state of the polymer. The same applies to the permeation properties of a polymeric membrane. The state of the polymer is defined as the phase in which the polymer appears. A distinction is made between the glassy state and the rubbery state [7]. In the glassy state, the mobility of the polymer chains is very restricted. As the temperature increases, the thermal energy increases. At a certain point, the thermal energy

exceeds the steric hindrance along the polymer backbone and the polymer changes from a glassy polymer to a rubbery polymer, in which the segments can freely rotate along the main chain bonds. The temperature at which this transition takes place is called the glass transition temperature, T_g .

3.1.2 Free volume

The free volume of a polymer may be described as the sum of all the small spaces between the polymer chains [11]. Free volume in polymers arises as a result of inefficient packing of the polymer, which creates static voids. Thermally induced chain segment rearrangements may also create temporary gaps [1]. Free volume is important for the transport of molecules through a membrane. As the size and number of free volume elements in a polymer increase, the ability of a molecule to migrate increases. The free volume of a polymer mainly affects the diffusivity. However, rigid polymers having very high free volume sieve molecules poorly based on difference in size [12].

The free volume is an intrinsic property of the polymer material. Free volume can be expressed in terms of fractional free volume, v_f , (free volume/cm³ of polymer), which is given by the equation [11]

$$v_f = \frac{v - v_0}{v} \quad (3.1)$$

Here, v is the specific volume of the membrane and v_0 is the volume occupied by the molecules. The fractional free volume of rubbery glassy polymers is usually lower than that of rubbery polymers, as the polymer chains are no longer able to rotate freely. Most glassy polymers have a fractional free volume (FFV) of a few percent [7].

Recently, substituted polyacetylene polymers exhibiting unusual properties have been prepared. This group of polymers – the high-free-volume polymers – have extraordinarily rigid backbones, unusually high free volume and very high glass transition temperatures. Two examples of glassy high free volume polymers are poly(1-trimethylsilyl-1-propyne) (PTMSP) and poly(4-methyl-2-pentyne) (PMP). The properties of PTMSP is described in detail in Chapter 3.4.

3.2 Polymeric membranes

Figure 3-1 shows a schematic diagram of the basic membrane gas separation process. A gas mixture (feed) at an elevated pressure is passed across the membrane surface. The membrane is selectively permeable to one component of this gas mixture, and this component is transported through the membrane, producing a permeate stream enriched in this component. The residue leaving the membrane module has a lower concentration of the permeable species compared to the feed gas.

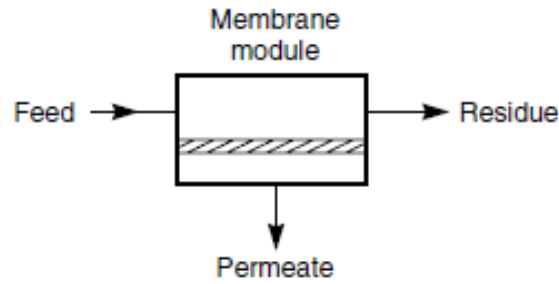


Figure 3-1: The basic membrane gas separation process [11].

Two types of solid, synthetic membranes may be distinguished: symmetric and asymmetric membranes. Asymmetric membranes consist of a dense top layer supported on a porous and much thicker sublayer. The porous support secures a high mechanical strength, while the membrane performance is governed by the dense top layer. The mass transfer resistance of an asymmetric membrane is determined by the thin top layer. For symmetric membranes, the resistance is determined by the total thickness of the membrane [7].

Polymeric membranes may be further classified according to their structure and separation principles as porous membranes, nonporous membranes or carrier membranes. A schematic drawing of the three basic types of membranes is shown in Figure 3-2. The structure of a membrane determines the separation mechanism and the application of the membrane [7]. In porous membranes, the selectivity is determined by the dimensions of the membrane pores. That is, one component is transported more readily through the membrane than another due its more compatible size, shape or structure. Porous membranes may be used for microfiltration or ultrafiltration, where the separation characteristics are mainly determined by the dimension of the pores. For the second category, nonporous membranes, the permeability and selectivity is determined by the intrinsic properties of the membrane material [7]. The choice of material used is therefore crucial for the membrane performance, in contrast to porous membranes, where the type of membrane material is important mainly for the stability of the membrane. Nonporous membranes are suitable for gas and vapor separation as they have the ability to separate components of approximately the same size. Finally, the transport in carrier membranes is determined by the presence of a carrier molecule, which facilitates the transport of a given molecule or particle. As a result of this facilitated transport, membranes based on carrier mediated transport can reach extremely high selectivities.

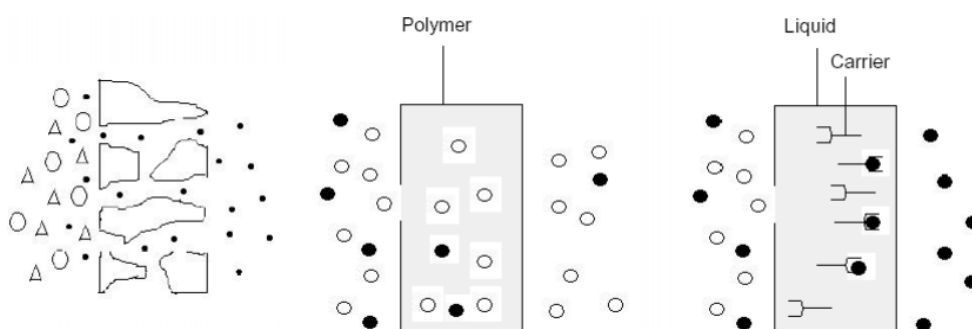


Figure 3-2: The three basic types of membranes: porous (a), nonporous (b) and carrier membrane (c) [7].

3.3 Transport in membranes

Driving forces acting on the components in the feed are responsible for the transport of a molecule or particle through a membrane. The driving force arises as a result of differences in chemical or electrical potential on the two sides of the membrane. The majority of the membrane processes takes place due to difference in chemical potential ($\Delta\mu$) arising from a gradient in pressure, concentration or temperature [7].

Gas separation makes use of the difference in concentration across the membrane as the driving force for separation. The transport of a gas component, J_i , proceeds via diffusion in the direction of the concentration gradient and may be described according to Fick's law of diffusion, which for a component i in the feed is given by [11]

$$J_i = -D_i \frac{dc_i}{dx} \quad (3.2)$$

Here, dc_i/dx is the concentration gradient representing the driving force and D_i is the diffusion coefficient, which is a measure of the mobility of the component.

In general, a distinction is made between two models describing the mechanism of permeation through a membrane [11]. One is the pore-flow model, in which the transport of a component is described as a pressure-driven convective flow. Separation between the components in the feed is obtained as one (or a few) of the components are allowed to pass through the narrow pores, while others are not. The pore flow model is suitable for describing the transport through porous membranes. The second model is the solution-diffusion model, which describes the transport of penetrants through a non-porous membrane. According to this model, a penetrant is dissolved in the membrane and then transported through the membrane by diffusion. The separation is obtained as a result of differences in solubility and/or diffusivity. Figure 3-3 shows a schematic drawing of the pore-flow model and the solution-diffusion model. The transport in porous and nonporous membranes is further described in the following sections.

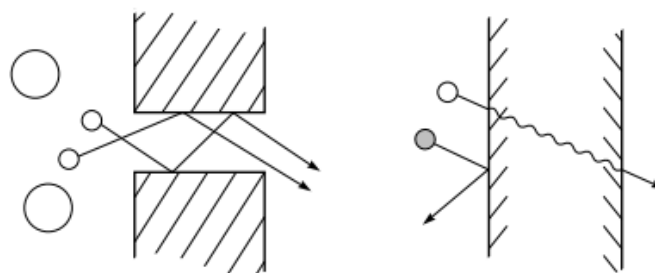


Figure 3-3: Components are separated by molecular filtration in porous membranes (to the left). In non-porous membrane, separation is obtained due to differences in solubility and diffusivity (to the right) [11].

3.3.1 Transport of gases through porous membranes

The transport of a penetrant through a porous membrane depends on the pore size of the membrane as well as the properties of the penetrant itself and the membrane material. As mentioned in the previous paragraph, the molecular transport through a porous membrane can be described according

to the pore-flow model. The exact transport mechanism depends on the pore size of the membrane. Commonly occurring mechanisms are molecular diffusion, Knudsen diffusion, surface diffusion, capillary condensation and micropore diffusion [13]. Molecular diffusion occurs when the mean free path of the molecules is smaller than the pore size, while Knudsen diffusion becomes important when the opposite is the case. When the pore radius becomes very small, gases are separated by a molecular sieving effect. When the pore diameter drops below 100 Å, adsorption onto the pore walls become noticeable. In small-pore-diameter membranes, surface adsorption and diffusion can make a significant contribution to the total gas permeation, especially if the gas is condensable. Figure 3-4 illustrates the different transport mechanisms in a microporous membrane.

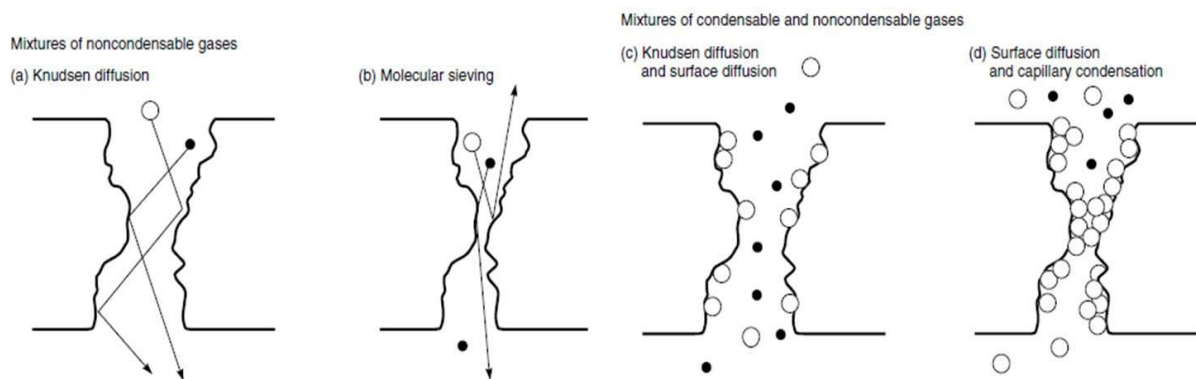


Figure 3-4: Permeation of noncondensable and condensable gas mixtures through a microporous membrane. (a) Knudsen diffusion, (b) Molecular sieving, (c) Knudsen diffusion and surface diffusion, (d) Surface diffusion and capillary condensation [11].

3.3.2 Transport of gases through nonporous membranes

The transport of a gas or vapor through a dense, nonporous polymeric membrane can be described by the solution-diffusion mechanism. The mechanism consists of three steps: first, the gas molecule is adsorbed on the high-pressure side of the membrane; then, the molecules diffuse through the membrane, and finally, the gas molecules desorb from the low-pressure side of the membrane [13]. According to the solution-diffusion model, the permeation of gas molecules is controlled by two major parameters: the diffusivity coefficient (D) and the solubility coefficient (S). According to this model, the permeability, P , is the product of the diffusivity and solubility, i.e. [7]

$$P = S \cdot D \quad (3.3)$$

The permeability coefficient is often given in Barrer units ($1 \text{ Barrer} = 10^{-10} \text{ cm}^3(\text{STP}) \cdot \text{cm} / \text{cm}^2 \cdot \text{s} \cdot \text{cmHg}$). The diffusivity (m^2/h) is a kinetic parameter describing the mobility of a penetrant, that is, how fast a penetrant is transported through the membrane. The thermodynamic solubility coefficient, S , is a measure of the amount of penetrant being sorbed by the membrane at equilibrium conditions. Both parameters are affected by the state of the polymer, the type of gas and the process conditions. The solubility coefficient of gases in polymers are relatively constant for a wide range of chemically different polymers [11]. The difference in the diffusion coefficient from one polymer to the other, on the other hand, may be significant.

The solubility is a measure of the energy required for the gas to be sorbed by the polymer, and depends on the condensability of a gas [7]. This is reflected in the critical temperature of the gas, which increases as the condensability of the gas increases. Since larger gas molecules condensate with greater ease than smaller molecules, the solubility coefficient tends to increase with increasing molecular size. This is the reverse of what is observed for the diffusivity coefficient. Also, as the affinity between a given gas molecule and polymer increases, the solubility of the gas increases [11].

In ideal systems, both the diffusivity and solubility of a gas penetrant is constant and independent of concentration of gas in the polymer. In such systems, Fick's law (equation 3.2) is obeyed and the solubility is given by Henry's law, i.e.

$$c = S \cdot p \quad (3.4)$$

According to this equation, there is a linear relationship between the concentration of a gas in the membrane (c) and the partial pressure of gas outside the membrane (p_i). Such a relationship may be the case for elastomers. A schematic drawing of the sorption isotherm in ideal systems is shown in Figure 3-5a. In non-ideal systems, the diffusivity and solubility are concentration-dependent parameters and the sorption isotherm becomes curved rather than linear (Figure 3-5b and c). Such non-ideal sorption behavior is observed for glassy polymers (Figure 3-5b) and is further described in Section 3.3.3.

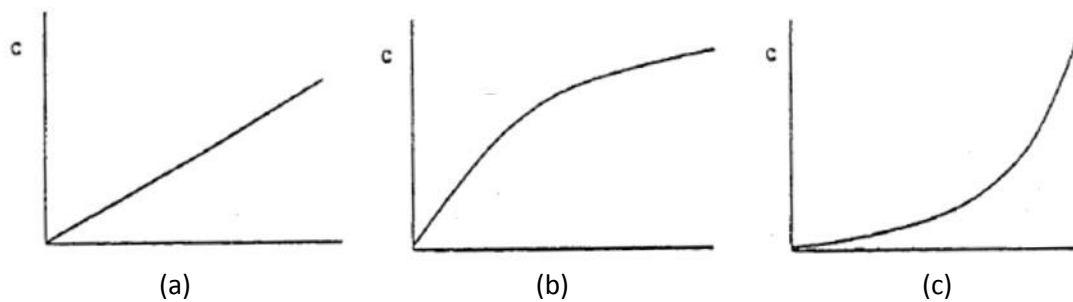


Figure 3-5: Sorption isotherms for (a) ideal and (b and c) non-ideal systems [7].

The magnitude of the diffusivity parameter is determined by the nature of the polymer and the size of the penetrant. The latter can be seen from the Stokes-Einstein equation, i.e.

$$D = \frac{kT}{6\pi\eta r} \quad (3.5)$$

The equation shows that the diffusivity coefficient, D , decreases as the particle size (expressed by the Stokes-Einstein radius, r) increases. The parameters k , T and η are the Boltzmann's constant, the absolute temperature and the viscosity, respectively. The decrease in diffusivity with molecular size is caused by the stronger interactions between larger molecules and the polymer chains [11]. In non-interacting systems, where the state of the polymer is hardly affected by the presence of the penetrant, the diffusivity coefficient is solely determined by the penetrant size. The mobility of a given

gas component may, however, also be affected the nature of the membrane material, and the interactions taking place between the polymer and the penetrant. This is the case for interacting systems, in which the state of the polymer may be affected by the presence of a penetrant.

The diffusivity coefficient is also dependent on the state of the polymer. In rubbery polymers, the thermal motion of the back-bone segments leads to higher diffusion coefficients. In glassy polymers, on the other hand, the segments are not as flexible and the thermal motion is therefore limited. As a result, the diffusivity coefficients of glassy polymers are commonly low [11]. No significant change in the solubility is observed at the transition from glassy to rubbery state.

Under steady-state conditions the flow rate across a membrane can be written as [7]

$$J_i = \frac{P_i}{l} \Delta p_i \quad (3.6)$$

The equation shows that the flux of a component i is proportional to the difference in partial pressure across the membrane (Δp_i) and inversely proportional to the membrane thickness, l . P_i is the permeability coefficient of component i .

The temperature dependency of permeability, diffusivity and solubility may be described as van't Hoff-Arrhenius relationships. These can be found in literature [1].

3.3.3 The dual sorption model

The deviation from ideal behavior observed for glassy polymers (Figure 3-5b) may be described by the dual sorption theory. According to this theory, two sorption mechanisms taking place in two different types of sites contribute to the total sorption of a gas in the polymer. The first one is the ideal sorption following Henry's law, depicted in Figure 3-5a. The second sorption mechanism contributing to the dual sorption is the Langmuir type sorption. Ideal sorption following Henry's law occurs in the equilibrium free volume parts of the polymer (C_D), while Langmuir sorption occurs in the excess free volume between the chains that exists in glassy polymers (C_H). The total sorption of gas in a glassy polymer, i.e. the total concentration of gas in the polymer, C , is the sum of the concentration in the two types of sites and may be expressed as [11, 14]:

$$C = C_D + C_H = k_D p + \frac{C'_H b p}{1 + b p} \quad (3.7)$$

where p is the pressure, k_D is Henry's law solubility coefficient, C'_H is the hole saturation constant and b is the hole affinity constant. The latter represents the ratio of the rate constants of gas adsorption and desorption in microcavities or defects. Figure 3-6 shows an illustration of the two contributions to the total sorption in glassy polymers, as predicted from the dual sorption model.

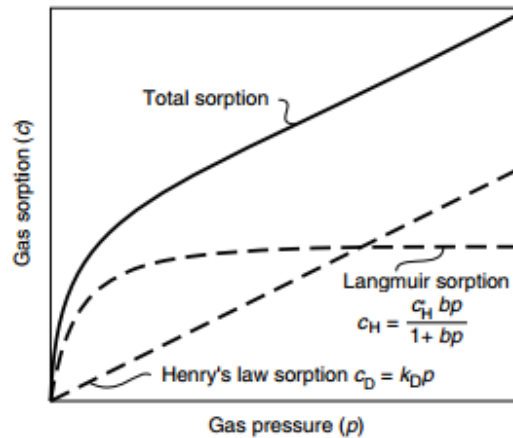


Figure 3-6: Gas sorption in glassy polymers by the dual sorption model. Langmuir sorption and Henry's law sorption contributes to the total sorption [11].

At low feed pressures, most glassy polymers show a decreasing permeability with increasing pressure [14]. This is consistent with the dual sorption model. However, as the driving pressure increases, an increase in permeability is often observed. This phenomenon is referred to as penetrant-induced plasticization. In the case of CO₂/CH₄ separation, plasticization occurs when the concentration CO₂ inside the polymer is high enough to increase the free volume and segmental mobility [15]. Due to swelling, the permeability of both gases increases and, in turn, the selectivity decreases. For conventional membrane separation, this is an unwanted phenomenon.

3.3.4 Membrane selectivity

The membrane selectivity is a measure of the membranes ability to separate two gases. The ideal selectivity is simply the ratio of the permeabilities of two different gases A and B, i.e.

$$\alpha_{A/B} = \frac{P_A}{P_B} \quad (3.8)$$

The permeability of a component is given as the product of solubility and diffusivity (cf. equation 3.3). Thus, equation 3.8 may also be written as

$$\alpha_{A/B} = \left(\frac{S_A}{S_B} \right) \left(\frac{D_A}{D_B} \right) \quad (3.9)$$

The ratio of the solubility coefficients S_A/S_B and the diffusivity coefficients D_A/D_B may be referred to as the solubility selectivity and the diffusivity selectivity, respectively. For polymers in their glassy state, the selectivity is normally governed by the diffusivity selectivity as the smaller molecules are favored over larger ones. In rubbery polymers, the selectivity is usually determined by the differences in solubility. As a result, larger molecules permeate with greater ease than smaller ones, contrary to what is the case for glassy polymers [11].

The permeability of a gas may also be affected by the presence of another gas component in the mixture. This is the case for the separation of methane and carbon dioxide, where the permeability of

methane is increased above the pure gas permeability value due to the simultaneous sorption of CO₂ [11]. As a result, the selectivity measured in a gas mixture of the two gases is lower than what is observed for pure gas systems, i.e. the ideal selectivity.

There is a reverse relationship between permeability and selectivity, making highly permeable polymers less selective, and vice versa [11]. The upper bound in a plot of selectivity as a function of permeability is known as Robeson's upper bound. The line defines the limit of performance for polymeric membranes investigated up to 1991 [11]. A lot of research has concerned the development of new types of membrane materials with a performance above Robeson's upper bound. One example is the mixed matrix membranes (MMMs). MMMs are addressed in Section 4.

3.4 Poly(1-trimethylsilyl-1-propyne) (PTMSP)

The glassy, high-free-volume polymer poly(1-trimethylsilyl-1-propyne) PTMSP was synthesized by Masuda and his coworkers in 1983 [16]. The polymer exhibited glass transition temperatures higher than 200 °C and densities as low as 0.75 g/cm³. The most striking feature was, however, the unusually high permeability. The permanent-gas permeabilities of PTMSP are orders of magnitude higher than those of conventional glassy polymers [17]. The values are even higher than those of the rubbery polydimethylsiloxane (PDMS), which had been considered one of the most permeable polymers until the discovery of PTMSP [16].

PTMSP is a silicon-substituted acetylene with bulky side groups. As can be seen from the chemical structure in Figure 3-7, the polymer contains a rigid main chain of alternating double bonds in addition to side groups of trimethylsilyl. These large, bulky side groups causes a severe hindrance to the rotation of the polymer chain giving PTMSP the lowest density of any known polymer [17]. Together with a low density, the polymer structure also secures the exceptionally high free volume which is characteristic of PTMSP. In fact, PTMSP may be considered as an interconnected porous network with pore sizes within the range of 5 Å [7]. The polymer is hydrophobic and soluble in a wide range of common solvents, e.g. toluene.

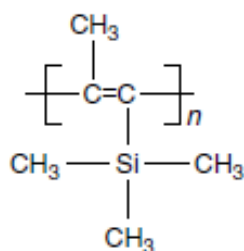


Figure 3-7: The structure of PTMSP [11].

The remarkably high permeability of PTMSP is the result of its extremely high free volume, which make up 20-25% of the total volume [17]. The high free volume provides a high sorption capacity and extremely high diffusivities [18]. The combination gives rise to the high permeabilities of PTMSP, which are significantly higher than for other conventional glassy polymers. For permanent gases, the

extremely high permeability is combined with very low selectivities. For this reason, PTMSP has not been considered a suitable membrane material for gas separation processes in the industry [17].

For glassy polymers in general, the diffusivity decreases as the penetrant size increases, causing a decrease in permeability. This is because the gas transport is controlled by the diffusivity term in equation 3.3 [17]. PTMSP deviates from this characterization, as it is more permeable to large, condensable organic vapors than to permanent gases [17]. This is because the gas transport is controlled by the solubility term in equation 3.3, which increases with increasing condensability of the gas [17]. For this reason, PTMSP is referred to as a reverse-selective polymeric membrane [12, 17]. The organic-vapor/permanent-gas selectivity based on pure gas permeabilities is low. In gas mixtures, however, the selectivity is much higher as the presence of the organic vapor lowers the permeability of the permanent gas [17]. The unique mixed-gas behavior makes PTMSP membranes attractive for several industrial gas separations. One example is the n-butane/methane mixture, for which PTMSP shows the highest selectivity ever observed for this mixture [17].

Figure 3-8 shows how the permeability changes as a function of the Lennard-Jones diameter for different polymeric materials, among others PTMSP [7]. As seen from the figure, the CO₂ permeability is higher than the CH₄ permeability for all polymers, including PTMSP. This is due to the fact that both the solubility coefficient and the diffusivity coefficient of CO₂ are higher than those of CH₄ [7, 17]. The difference in solubility is reflected in the critical temperature, which is higher for the non-ideal CO₂ than for CH₄ (304.2°C and 190.7°C, respectively) [7]. The difference in the diffusivity coefficient is caused by different size of CO₂ and CH₄, which is approximately 3.3 Å and 3.8 Å, respectively [7].

The permeability coefficients of PTMSP decreases with increasing pressure, most notably for CO₂ [19]. As mentioned, the permanent-gas selectivities of PTMSP are low and this is true also for the gas pairs CH₄ and CO₂. The low CO₂/CH₄ selectivity is, however, not a concern when the polymer is to be used in gas-liquid membrane contactors, a process described in Section 5.

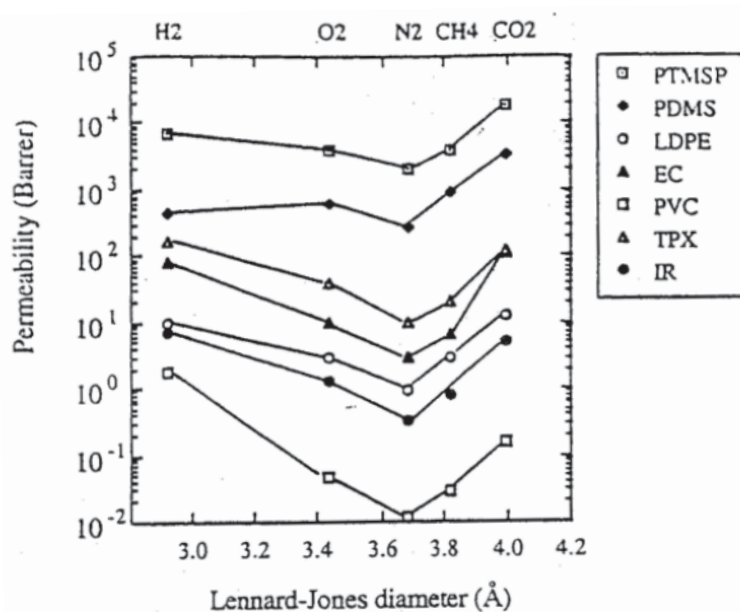


Figure 3-8: Permeability as a function of Lennard-Jones diameter for different polymers [7].

The transport taking place in glassy, high-free-volume polymers is more complex than for conventional dense membranes and do not conform completely to the solution-diffusion model [20]. The large amount of free volume elements appear to be connected in a finely microporous network [17]. PTMSP may therefore be considered an ultra-microporous membrane in which pore flow contributes to the total permeation [11]. Pinnau and Toy presented a hypothesis that gas transport in PTMSP occurs primarily through these interconnected free volume elements and that permeation through the dense matrix of the polymer is essentially negligible [17]. The hypothesis was supported by a study by Nakagawa and his coworkers [21].

For gas mixtures of condensable and non-condensable gases, the proposed transport mechanism in PTMSP occurs by competitive sorption and surface diffusion [17]. The condensation of gas causes capillary condensation, which increases the permeation of gas. At the same time, the adsorption of the condensable gas causes a blockage – either partially or completely – of the pores, which prevents the flow of noncondensable gas. The transport of gas through PTMSP may therefore be placed in a transition region between pore-flow and solution-diffusion transport [11]. The proposed transport mechanism helps explain the unique mixed-gas behavior of PTMSP.

Literature show a broad range of gas permeability values of PTMSP [22]. For example, CO₂ permeabilities ranges from 18 000 Barrer in a study by Takada et al. [23] to 37 000 Barrer in one by Robeson [24]. The permeability of PTMSP is closely related to the amount of free volume in the polymer. As summarized by Gomes et al. [25], the amount of free volume in PTMSP depends on the casting solvent, the main-chain conformation, the molecular weight of PTMSP, the drying conditions during film preparation, etc. [22, 23, 26-28]. The measured gas permeabilities are also affected by the experimental conditions. Additionally, PTMSP is subjected to physical aging, which also has a direct influence on the transport properties. Thus, the permeability of PTMSP is unstable and decreases with time. In a study by Jia and Baker [29], the permeability of PTMSP membranes stored under vacuum for one month declined to 70% of their initial value. Morlière et al. concluded that the mechanism behind this decrease in permeability is dependent of the nature of the penetrant [30]. According to the writers, a small decrease in hole size would have a stronger effect on narrow holes and at a certain point these holes would no longer serve as a diffusion pathway for the penetrants. As a result, the smaller gas molecules should be more affected by the aging of PTMSP. Crosslinking of PTMSP has proved to increase the stability of the polymer [29, 31]. However, this decreases the permeability of the polymer as the polymer structure becomes more compact. The incorporation of inorganic particles may restore the permeability of the crosslinked polymer. Such mixed matrix membranes are addressed in the following section of report.

4. Mixed matrix membranes

Inorganic particles, such as zeolites, carbon molecular sieves, silica and carbon nanotubes, are frequently employed to improve the performance of polymeric membranes, e.g. permeability, selectivity, mechanical strength and thermal and chemical stability. These systems are referred to as mixed matrix membranes (MMMs) and have been the subject of growing interest as they have the potential to overcome Robeson's upper limit. Ideally, the incorporation of these inorganic fillers into the polymer matrix can lead to a significant increase in the separation efficiency [32]. Figure 4-1 shows an illustration of a mixed matrix membrane.

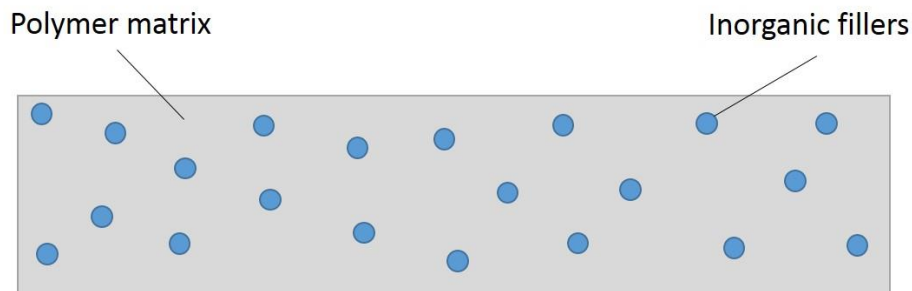


Figure 4-1: Illustration of a mixed matrix membrane.

In general, porous fillers separate the gas molecules by their size and shape, thereby acting as molecular sieving agents [33]. The porous fillers are often highly permeable and selective. Ideally, when these porous fillers are distributed in the polymer matrix, both the permeability and the selectivity increases [33]. This requires that the porous particles are completely wetted by the polymer chains and that the polymer-particle interface is defect free [33]. The addition of porous fillers may also induce selective surface flow, allowing more condensable/adsorbable component to adsorb and diffuse selectively through the particles [33, 34]. For example, this could be advantageous in natural gas sweetening, in which the more adsorbable CO_2 is separated from the less adsorbable CH_4 .

Nonporous fillers can improve the separation properties by manipulating the packing of the polymer chains, thereby increasing the separation properties by decreasing the diffusion of larger molecules [32, 33]. In the case of glassy polymers, the dispersion of nano-scale inorganic fillers can disrupt the chain packing and, in turn, increase the free volume of the polymer [33]. As a result, the gas permeability increases. The penetrant solubility of mixed matrix membranes may also increase if there is an interaction between functional groups on the surface of the nanoparticles and polar gases, e.g. CO_2 and SO_2 [35]. Even nanoparticle distribution is important to avoid the creation of defects in the membrane, leading to low selectivity [36]. A mixed matrix membrane with nanoparticle fillers is henceforth referred to as a nanocomposite membrane.

One model commonly used to describe gas permeability in heterogeneous materials is Maxwell's model [19, 37]. According to this model, the permeability of a composite, P , may be related to the pure polymer permeability (P_p) and the volume fraction of impermeable, spherical filler (ϕ_f):

$$P = P_p \left(\frac{1 - \phi_f}{1 + \frac{\phi_f}{2}} \right) \quad (4.1)$$

Maxwell's model predicts a decrease in permeability as the concentration of the impermeable filler increases, as observed in conventional filled polymer systems [1, 12].

The solubility coefficient, S , of a binary system consisting of filler and polymer can be described by the equation [38, 39]

$$S = \phi_p S_p + (1 - \phi_p) S_f \quad (4.2)$$

where S_p and ϕ_p is the solubility and the volume fraction of the polymer, respectively, and S_f and ϕ_f the corresponding parameters for the filler. In addition to the concentration of fillers, the gas solubility of a binary system also depends on the interaction between the filler particles and the polymer chains [38]. Sorption of light gases may occur both in the polymer matrix and the filler particles [37]. For glassy polymers, such as PTMSP, the sorption behavior follows the dual sorption model described by equation 3.7 [19].

For conventional filled polymer systems, the addition of nonporous fillers has caused a decrease in permeability and had little effect on the selectivity [1]. The reason is that the filler particles mixed with the polymer without increasing the free volume, but rather blocked the free volume elements. As a result, the diffusion pathway tortuosity across the polymer film increases [12]. Additionally, as penetrant-sorbing polymer is replaced with impermeable, non-sorbing particles, loss of penetrant gas solubility in the film contributes to the decrease in gas permeability [12]. Unexpectedly, studies conducted in the past two decades have shown that the addition of nonporous fillers have enhanced the permeability of glassy, high-free-volume polymers. This is the opposite of what is predicted by equation 4.1. The increase in permeability derives from an increase in penetrant diffusivity, penetrant solubility, or both. As previously mentioned, the dispersion of nonporous fillers can cause an increase in permeability due to a disruption of chain packing causing an increase in free volume [12]. The fillers may also create voids at the polymer-particle interface or within particle aggregates increasing the transport of gas through the mixed matrix membrane [37].

5. Gas-liquid membrane contactors

A membrane contactor is a device that allows two phases to come into direct contact with each other, while at the same time avoiding any dispersion of one phase into the other. The purpose of the membrane contactor is the mass transfer from one phase to the other. A distinction is made between gas-liquid and liquid-liquid membrane contactors [7]. Henceforth, only gas-liquid membrane contactors (G-L membrane contactors) are discussed.

The principle of gas-liquid membrane contactors is shown in Figure 5-1. In this case, flue gas and absorption liquid are separated by a microporous membrane, allowing the transport of carbon dioxide from the gas phase to the liquid phase. The CO₂-bearing gas, in this case flue gas, is fed along one side of the membrane. Gas diffuses through the gas filled pores of the membrane and carbon dioxide is selectively absorbed and removed by the liquid absorbent. The process is also referred to as a membrane gas absorption process.

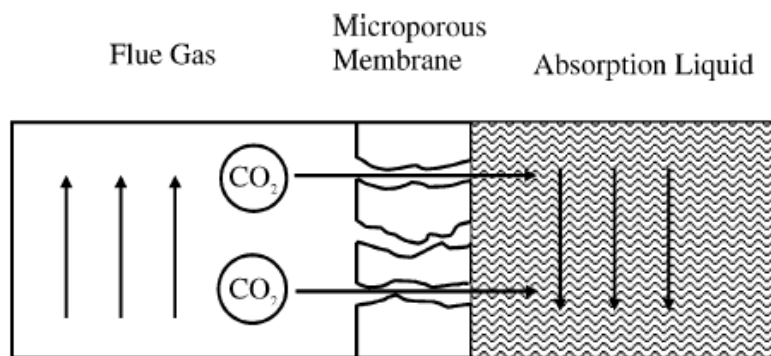


Figure 5-1: Principle of membrane gas absorption [40].

Hollow fiber membrane contactors have been studied extensively in the last decade. Usually, raw natural gas is obtained from the gas well with a typical pressure of 50 bar [41]. The removal of sour gas components such as CO₂ and H₂S should be carried out without pressure loss. For this application, the membrane (usually hollow fibers) must be chemically compatible with the solvent and compatible with high-pressure operations. Additionally, the gas-liquid membrane contactor must be economically attractive compared to conventional contactors. Theory on membrane contactors is given in the following chapters. Relevant literature is addressed in Section 6.2.

5.1 Positive and negative aspects of membrane contactors

Membrane contactors offer numerous advantages over conventional gas-liquid contactors. Unlike absorbers, there is no dispersion of the gas and liquid phase. As the two phases are kept apart, operational challenges such as flooding, foaming and entrainment are avoided [42]. Since the direct contact between the two phases is prevented, it is possible to monitor the gas and liquid flow rates

independently. Also, any contamination due to mixing of the phases is eliminated [43]. Membrane contactors are flexible, easy to control and easy to scale up due to its modular nature. Its modular design also allows a plant to operate over a wide range of capacities, simply by varying the number of modules being used [9]. The challenging task of developing membranes with high permeability *and* selectivity is also avoided, as a high permeability is the main focus for the membranes being used in contactors.

The high interfacial area between the two phases makes the membrane contactors smaller and lighter than other conventional gas absorption processes. Very high specific surface areas may be achieved by using modules of densely packed hollow fiber membranes (500-2000 m²/m³ [40], 1500-3000 m²/m³ [43]), which is significantly higher than for conventional contactors (100-300 m²/m³ [40], 20-1000 m²/m³ [43]). The reduction in size compared to conventional absorption equipment, e.g. packed columns, is one of the main advantages of gas-liquid membrane contactors [44]. As a result of the smaller size, the capital cost is reduced, making the membrane contactor more economical than conventional devices [45].

The interfacial area for mass transfer is known and equal to the geometrical membrane surface area, and thus, constant [43]. As a result, the interfacial area is unaffected by orientation and change in flow rates, allowing simple operation over a wide range of process conditions. This differs from conventional gas-liquid contactors, in which the process conditions have a strong influence on the interfacial area. Additionally, as the interfacial area is known and constant, the performance of a membrane contactor is easier to predict than that of conventional dispersed phase contactors [9]. The compact design and constant interfacial area makes the membrane contactor suitable for natural gas purification on offshore platforms. Other advantages that membrane contactors offer over dispersive contactors are higher efficiencies, low solvent holdup and lack of moving parts [9].

Membrane contactors also suffer from some limitations. One important limitation is the additional resistance to mass transfer caused by the presence of a membrane between the two phases [42]. In the case of microporous membranes, the phase inside the pores have a strong influence on the mass transfer resistance and therefore has a crucial role in the design of membrane contactors [43]. The range of operating pressure is limited and must be carefully controlled to avoid wetting (intrusion of liquid into pores) or any other unwanted dispersion between the two phases.

The membrane used in membrane contactor usually have a limited life-time, which could cause the cost of periodic replacement to be substantial [43]. It may also be subjected to fouling and have limited compatibility with the solvents used in the membrane contactor, which would lead to an unwanted loss in efficiency. Loss in efficiency could also be caused by shell-side bypassing in the case of hollow fiber modules [9]. The stability of the absorbent liquid is another issue that complicates the use of membrane contactors.

According to Gabelman and Hwang, “these relatively few disadvantages are often outweighed by the numerous advantages cited above” [9]. The limitations of the membrane contactor may be minimized by choosing the right kind of membrane, solvent and operational conditions. This way, the mass transfer resistance of the membrane is minimized, the stability of the system is increased and the membrane-liquid compatibility is secured.

5.2 Types of membrane contactors

The module configurations available for the membrane gas-liquid contactors are similar to those available for conventional membrane applications, with some modifications [43]. The membrane contactors can be classified into two groups: the flat sheet membrane contactors and the hollow fiber membrane contactors [43]. Due to its higher interfacial area, hollow fiber membrane contactors are the most common type. Two different modes of operation are available for this type of device: the parallel flow mode (both phases flow parallel to the axis of the fibers, either co-current or counter-current) and cross-flow mode (one fluid flow perpendicular to the axis of the fibers, the other fluid flows parallel to the axis of the fibers) [43]. The choice of operation mode depends on the system. A parallel flow hollow fiber module is illustrated in Figure 5-2.



Figure 5-2: Parallel flow hollow fiber gas-liquid membrane contactor (redrawn from [9] and [46])

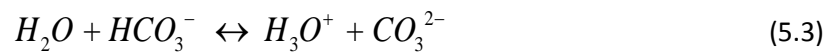
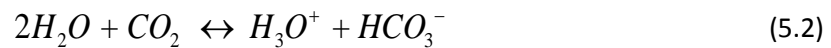
5.3 The membrane-solvent system

5.3.1 The solvent in a gas-liquid membrane contactor

As previously mentioned, the selectivity of the gas-liquid membrane contactor is determined by the solvent. The solvent in a membrane contactor could be of the same type as the one used in conventional gas absorption processes. According to Li and Chen [45], five criteria are important for the selection of liquid absorbent in a membrane contactor:

1. High reactivity with CO_2 : This secures higher absorption rate and mass fluxes.
2. Surface tension: The surface tension is related to the wetting ability of the liquid. Wetting should be avoided to secure that the pores remain gas-filled. Since the membrane used in a membrane contactor usually is hydrophobic, the liquid absorbent should have a high surface tension.
3. Chemical compatibility with the membrane material: The liquid-membrane compatibility is important to secure the long-term stability of the membrane.
4. Low vapor pressure and good thermal stability: The solvent should have a low vapor pressure to avoid any increase in mass transfer resistance due to vapor in the membrane pores. Additionally, the solvent should possess good thermal and chemical stability to avoid any thermal degradation.
5. Easiness of regeneration: The solvent should be easy to regenerate in the case of frequent recycling. Additionally, the absorption efficiency and the economy of the operation is determined by this criteria.

Commonly, aqueous solutions of amines are applied as absorbents for CO₂ capture [47]. These are weak bases reacting with carbon dioxide to form complexes with weak chemical bonds which are easily broken upon mild heating in the solvent regeneration step of the process [47]. The amines used in the case of CO₂ absorption are preferably the alkanolamines MEA (monoethanolamine), DEA (diethanolamine) and MDEA (methyldiethanolamine) [47]. Aqueous solutions of the given amines provide high CO₂ loading capacity, rapid absorption rate and low cost for regeneration [47]. In aqueous solutions, CO₂ react in an acid-base buffer mechanism with alkanolamines [48]:



Here, RR'R''N represents the alkanolamine. R is an alkyl group, alkanol group or hydrogen. In aqueous solutions, primary and secondary alkanolamines usually react with CO₂ to form stable carbamates. The reaction is not included here. Tertiary amines, on the other hand, react with CO₂ mainly by reaction 5.2, forming bicarbonate [48].

5.3.2 The membrane in a gas-liquid membrane contactor

The membrane in a contactor simply act as a support between the gas and liquid, enabling direct contact between the two phases. Mass transfer takes place from one phase to the other, through the membrane, without any dispersion of one phase into the other. Unlike in pure membrane processes, where both permeability and selectivity are important properties, the membranes used in contactors are seldom selective. The selectivity of the system is provided by the liquid absorbent, allowing the application of highly permeable membranes. The important factors regarding the membrane used in the membrane contactor are a high permeability and a high solvent compatibility. This is due to the fast chemical reaction taking place at the liquid side of the membrane and the fact that the membrane has to withstand long term contact with the liquid without being wetted or degraded [44]. As will be further discussed in the following parts of this chapter, a proper choice of membrane-solvent combination is crucial for the performance of the gas-liquid membrane contactor.

The membranes used in contactor devices are commonly microporous hollow fiber membranes [9]. Depending on the characteristics of the membrane material, the nature of the liquid phase and the operating pressure, the membrane pores may be filled with either gas or liquid. The two cases are referred to as the non-wetted mode and the wetted mode, respectively, and are illustrated in Figure 5-3. The corresponding concentration profiles are also shown in the figure. These concentration profiles indicate that the mass transfer resistance is normally located in the liquid phase. In the case of gas absorption, the non-wetted mode is preferred as the membrane resistance will be lower than if

the pores were filled with liquid [7]. Thus, to maintain a high performance, the prevention of membrane wetting is very critical [49]. As a result, a hydrophobic membrane is often used together with an aqueous solution [7].

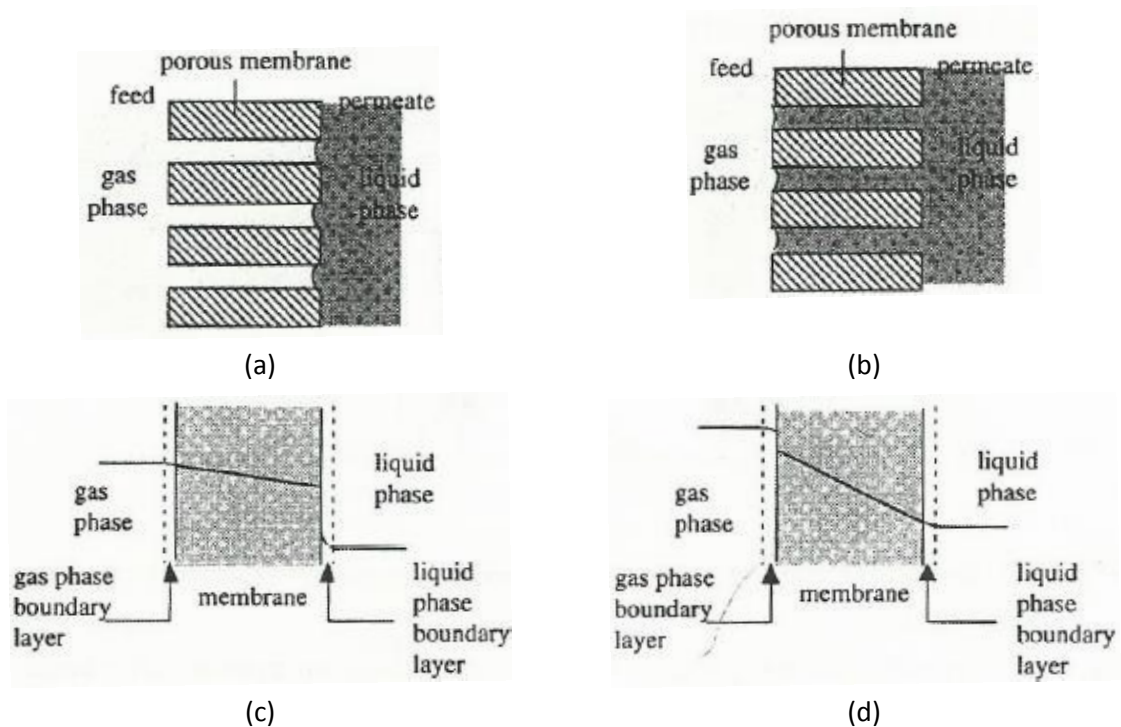


Figure 5-3: Gas-liquid contactors with a porous membrane in (a) non-wetted mode and (b) wetted mode. The corresponding concentration profile is shown in figure (c) and (d). [7].

In general, the higher the hydrophobicity of the membrane, the more resistant the membrane will be towards wetting [47]. An evaluation of hydrophobicity is made by measuring the contact angle [47]. Contact angles, θ , for liquid droplets on a solid material are illustrated in Figure 5-4. The contact angle between the liquid and the polymer depends on the affinity between the two phases. The smaller the interaction between liquid and polymer, the greater the contact angle will be. When the contact angle is larger than 90° (Figure 5-4a) the membrane material is not wetted by the liquid. For porous membranes, the liquid will fill the pores when wetting occurs, i.e. when θ is smaller than 90° (Figure 5-4c).

For an ideal, homogeneous solid surface, the contact angle can be described according to the Young equation [50]:

$$\cos \theta = \frac{\gamma_{SV} - \gamma_{SL}}{\gamma_{LV}} \quad (5.5)$$

According to this equation, the contact angle of a liquid drop on a solid surface is determined by three interfacial surface tensions: γ_{SV} (the solid-vapor interfacial energy), γ_{SL} (the solid-liquid interfacial energy) and γ_{LV} (the liquid-vapor interfacial energy).

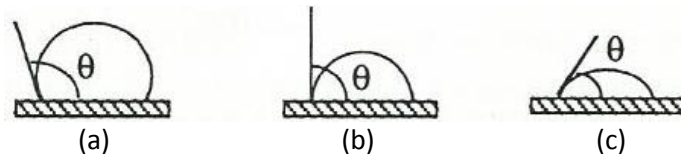


Figure 5-4: Contact angles of liquid droplets on a solid (nonporous) material [7]. (a) $\theta > 90^\circ$, (b) $\theta = 90^\circ$ and (c) $\theta < 90^\circ$.

Despite the hydrophobicity of the membrane material, an aqueous solution will penetrate the pores if the pressure exceeds a critical value known as the *breakthrough pressure* [7]. The pore characteristics of the membrane material are therefore another important factor in addition to the hydrophobicity. The pores of a hydrophobic membrane remain gas-filled as long as the applied pressure does not exceed the minimum breakthrough pressure for ideal cylindrical pores given by the Laplace equation [7],

$$\Delta p = \frac{2\gamma_l \cos \theta}{r} \quad (5.6)$$

where Δp is the pressure difference between liquid and gas, γ_l is the surface tension of the absorption liquid, θ is the contact angle of liquid on solid material and r is the pore radius.

To secure a long term non-wetting application of a gas-liquid membrane contactor, the breakthrough pressure should be as high as possible. As seen from the equation, this can be achieved by reducing the pore size of the membrane, using solvents with high surface tension and by increasing the contact angle. The latter could be achieved by using membranes with low surface tensions. Meeting these demands can be challenging, since most of the solvents used for CO_2 absorption have low surface tensions [43]. Additionally, by reducing the pore size, the gas transport through the membrane is reduced [43].

One possible solution to enhance the wetting resistance of the membrane is to use either a dense, self-standing membrane or a composite membrane where a dense thin layer is coated on the surface of the microporous membrane. These types of membranes were introduced in Section 3.2. An illustration is shown in Figure 5-5. In the case of the composite membrane, the dense layer prevents the liquid from penetrating the pores of the membrane and allows a higher operating pressure. To ensure minimal impact on the membrane mass transfer, the permeability of the dense layer should be as high as possible [42]. The composite membrane should be defect free and provide barrier properties against wetting [44]. Additionally, the dense layer should be very thin and the support very porous to minimize mass transfer resistance.

For membrane contactor applications, composite membranes are so far largely unexplored [44]. Some studies performed on dense polymeric membranes for CO_2 absorption in membrane contactors are summarized in Section 6.2.

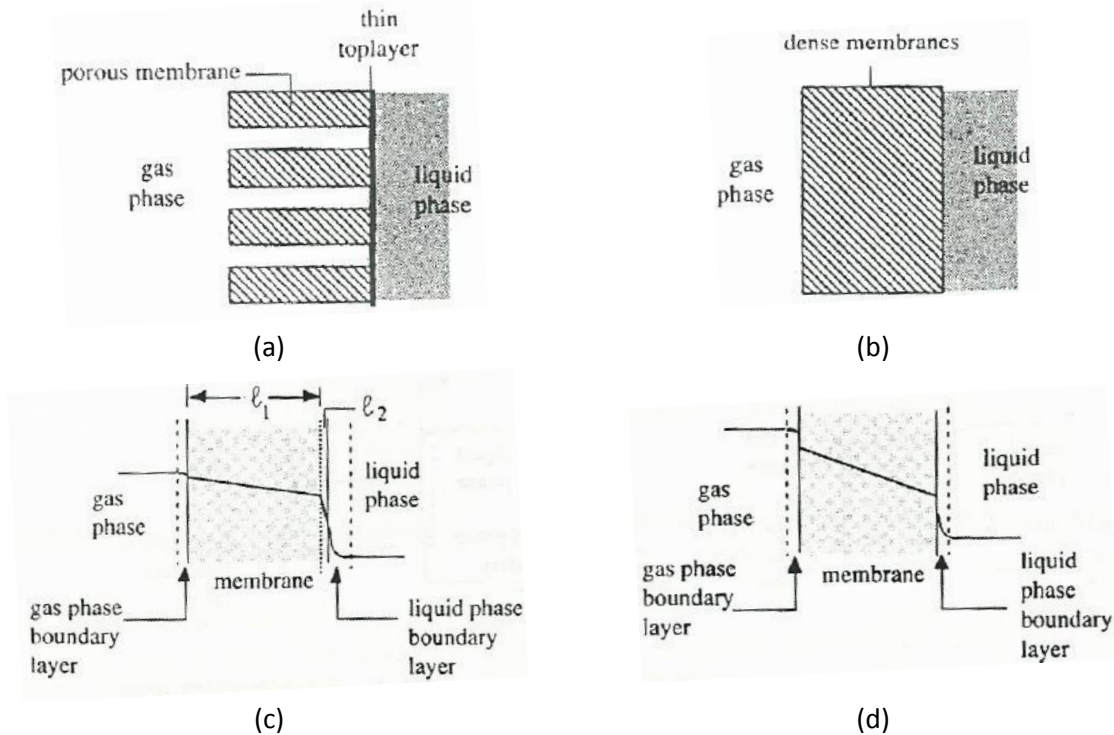


Figure 5-5: Gas liquid contactor with (a) a composite membrane (porous membrane with dense top layer) and (b) a dense membrane. Corresponding concentration profiles are shown in figure (c) and (d) [7].

5.4 Basic principles of mass transfer in a gas-liquid membrane contactor

The flux of a component i through the membrane can be written as [7]

$$J_i = K_i \Delta c_i \quad (5.7)$$

Here, Δc_i is the difference in concentration between the gas phase and the liquid phase and K_i is the overall mass transfer coefficient of component i . As seen from the equation, the driving force in a membrane contactor is provided by a difference in concentration across the membrane.

The mass transfer mechanism in a gas-liquid membrane contactor is commonly described according to the resistance-in-series model [47]. The mass transfer process consists of three steps: the transfer from gas phase to the membrane surface, transfer through the membrane, and finally, transfer from the liquid interface to the liquid bulk. Three resistances are encountered: resistance in the gas-membrane interface, in the membrane material and in the membrane-liquid interface.

For gas-liquid membrane contactors with chemical absorption, the resistance-in-series model can be expressed as [7, 44]

$$\frac{1}{K} = \frac{1}{k_G} + \frac{1}{k_M} + \frac{H}{Ek_L} \quad (5.8)$$

In the equation, K is the overall mass transfer coefficient based on the gas phase. k_G , k_M and k_L are the mass transfer coefficients in the gas phase, membrane and liquid phase, respectively. H is Henry's constant and E is an enhancement factor due to chemical reaction taking place in the liquid. The mass transfer coefficient in the liquid, k_L , is affected by the chemical reaction taking place between CO_2 (or any other solute) and the solvent. The mass transfer coefficient in the membrane phase, $k_{M,i}$, is dependent on the type of phase filling the pores of the membrane. As described in Section 5.3, the mass transfer resistance is smaller in the non-wetted mode than in the wetted mode. The aim should therefore be to prevent membrane wetting.

The mass transfer coefficients in membrane contactors are of the same size or smaller than those in conventional systems [42]. The enhanced efficiency of the membrane contactors is therefore the result of higher interfacial area rather than enhanced mass transfer. Studies have shown that the drawback of mass transfer resistance can be overcome by applying a highly permeable, non-wetting membrane combined with a high interfacial area between gas and liquid [44].

In the case of a composite membrane, where a thin dense layer is coated on top of a porous support (Figure 5-5), the dense top layer will represent an additional contribution to the overall mass transfer resistance [7]. The mass transfer resistance of the composite membrane should be minimized by using a support of high porosity and by using a dense top layer with a very high permeability [44]. One candidate for the dense layer of a composite membrane contactor for CO_2 capture is PTMSP, which was introduced in Section 3.4.

As mentioned, the membranes used in contactor devices are commonly microporous hollow fiber membranes (HFMs). The mass transfer process in HFMs may also be described according to the resistance-in-series model. An illustration is included in Figure 5-6 for a hydrophobic HFM with the liquid flowing inside the fibers.

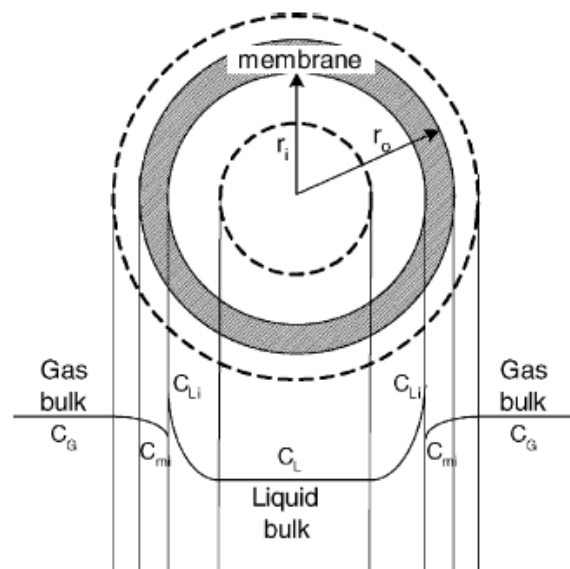


Figure 5-6: Mass transfer process in a hollow fiber gas-liquid membrane contactor [41].

6. Literature review

This section addresses the literature available on nanocomposite membranes and gas-liquid membrane contactors. In the first subsection, the focus is on nanocomposites of PTMSP and nonporous nanoparticle fillers. In the second one, research on gas-liquid membrane contactors for the use in natural gas sweetening is addressed, with emphasis on the interaction between membrane and absorption liquid. No literature on the performance of PTMSP/TiO₂ nanocomposites in gas-liquid contactors is available at this point.

6.1 Nanocomposite membranes

Numerous articles concerning nanocomposite membranes based on PTMSP are available, often with silica as the filler [1, 2, 25, 36, 51-55]. Other studies have involved fillers of trimethylsilylglucose (TMSG) [56], titanium dioxide (TiO₂) [2, 37] and magnesium oxide (MgO) [57]. Both crosslinked and uncrosslinked PTMSP have been investigated. Some of the studies are further described in the following.

Several studies on the addition of nanoparticles to high-free volume, stiff chain, glassy polymers have been conducted by Merkel et al. [1, 12, 36, 38]. The studies showed that the dispersion of nonporous, nanoscale fumed silica (FS) in PTMSP and PMP increased the permeability coefficients, in contrast to what had previously been observed for non-porous fillers. For PMP, the presence of the fillers also increased the vapor selectivity. This unusual property-enhancements differed from what was observed in unfilled polymers, in which the selectivity tends to decrease as the permeability increases, and vice versa. For PTMSP, the opposite results on selectivity were reported, as the vapor selectivity decreased upon filling. Experimental studies suggested that the dispersed particles enhanced the free volume of the polymer by altering the chain packing thereby increasing the diffusion coefficient [1]. The increase in free volume also explained the decrease in polymer size selectivity.

According to Gomes et al. [25], who also worked on PTMSP/silica nanocomposites, two different types of transport can occur in these nanocomposites. The incorporation of fumed silica can either increase the free volume without creating non-selective defects or it can create free volume elements large enough to permit non-selective Knudsen transport. The former would cause an increase in the gas permeation properties, while the latter would result in a decrease of selectivity. They also concluded that the addition of small particles (≈ 2 nm) into PTMSP could either fill the free volume or disrupt the chain packing, and that the final result could be a balance of both effects.

De Sitter and his coworkers also studied the performance of PTMSP/silica nanocomposites [51, 52, 58]. The researchers observed an increase in permeability and a decrease in vapor selectivity as the filler content increased. This was explained by an increase in the free volume size. Additionally, interstitial mesopores located between the particles of a silica agglomerate were observed in the nanocomposites. The size of these cavities increased with increasing filler concentration.

Shao studied crosslinking and stabilization of nanocomposite membranes of PTMSP [2]. Fumed silica (FS) and TiO₂ with primary particle sizes of 7 nm and 21 nm, respectively, were used as fillers. The results for the uncrosslinked nanocomposites are listed in Table 6-1 for CH₄ and CO₂. For the addition of fillers to uncrosslinked PTMSP, the permeability increased for all gases. The permeability increased with increasing filler content. The chemical stability of PTMSP increased upon crosslinking, while the permeability decreased compared to pure PTMSP. By adding nanoparticles (fumed silica/TiO₂), the permeabilities of crosslinked PTMSP again increased. The permeability and selectivity of the crosslinked nanofilled proved to be stable over time. The permeability of uncrosslinked PTMSP and PTMSP/filler membranes decreased significantly over time.

Table 6-1: Permeabilities and selectivities of pure PTMSP, PTMSP/FS and PTMSP/TiO₂ nanocomposite membranes at 35°C and feed pressure of 2 bar [2].

Filler content (wt%)	FS			TiO ₂		
	Permeability (Barrer)		Selectivity	Permeability (Barrer)		Selectivity
	CH ₄	CO ₂	CO ₂ /CH ₄	CH ₄	CO ₂	CO ₂ /CH ₄
0	12 670	28 590	2.3	12 670	28 590	2.3
15	12 970	28 960	2.2	12 780	28 870	2.3
25	16 750	36 750	2.2	16 210	36 210	2.2
35	18 320	39 280	2.1	18 220	38 980	2.1

Matteucci et al. [37] studied the influence of impermeable titanium dioxide (TiO₂), i.e. brookite, nanoparticles on pure gas permeability coefficients in PTMSP-based nanocomposites. Nanocomposites with a nanoparticle content ranging from 0 to 33 nominal vol% TiO₂ were prepared and, in turn, characterized. The nonporous, titanium dioxide nanoparticles – with a primary particle size of approximately 3 nm – have the potential to be dispersed individually or in nanoscale aggregates, unlike fumed silica which are chemically fused together. The particles do not permeate or sieve gas molecules, as zeolites do. Their role is to open up the structure of the polymer chains, thereby enhancing the permeability. At the same time, they do not introduce cavities large enough to promote free-phase flow mechanisms, such as Knudsen flow [12].

Matteucci et al. [37] used AFM, TEM, WAXD and FT-IR to characterize the nanocomposites, together with sorption, density and permeability measurements. WAXD and FTIR experiments demonstrated that the nanoparticles were non-interactive, as they were chemically stable in PTMSP and did not react with the polymer matrix or the gases considered. The particle distributions obtained from AFM images indicated that the particles were dispersed individually and in nanoscale aggregates (at low particle loading) and some micron-sized aggregates (at high particle loadings). TEM images showed that the aggregate concentration and size were higher in the sample containing the highest concentration of TiO₂. A potential explanation is the polymer's inability to disperse particles at high loadings, causing a less effective mixing and thereby an increase in aggregate size and concentration. It was also observed an increase in inter-aggregate spacing as the particle loading increased. With the inter-aggregate spacing taken into account, the writers concluded that the dispersion of TiO₂ nanoparticles in PTMSP should significantly influence the chain packing and further the transport properties of the polymer.

Density and permeability measurements showed that the nanocomposites exhibited two different regimes [37]. At low particle loadings (less than 6 nominal vol%) permeability was lower than that of the unfilled PTMSP and the density was slightly greater than expected based on pure component properties. These observations are consistent with the nanoparticles acting to reduce the free volume of the polymer. At higher loadings (greater than 7 nominal vol%), the permeability was higher than

that of the unfilled PTMSP and the densities were much lower than those predicted by a simple additive model. The density decrease was explained by a significant increase in void space within the nanocomposite.

Figure 6-1 shows the effect of TiO_2 concentration on CO_2 and CH_4 permeability and on the pure gas CO_2/CH_4 selectivity. At low loadings, the permeability decreases with TiO_2 concentration. At higher loadings, the permeability increases as the TiO_2 concentration increases. The CO_2/CH_4 selectivity is nearly constant as the filler content increases.

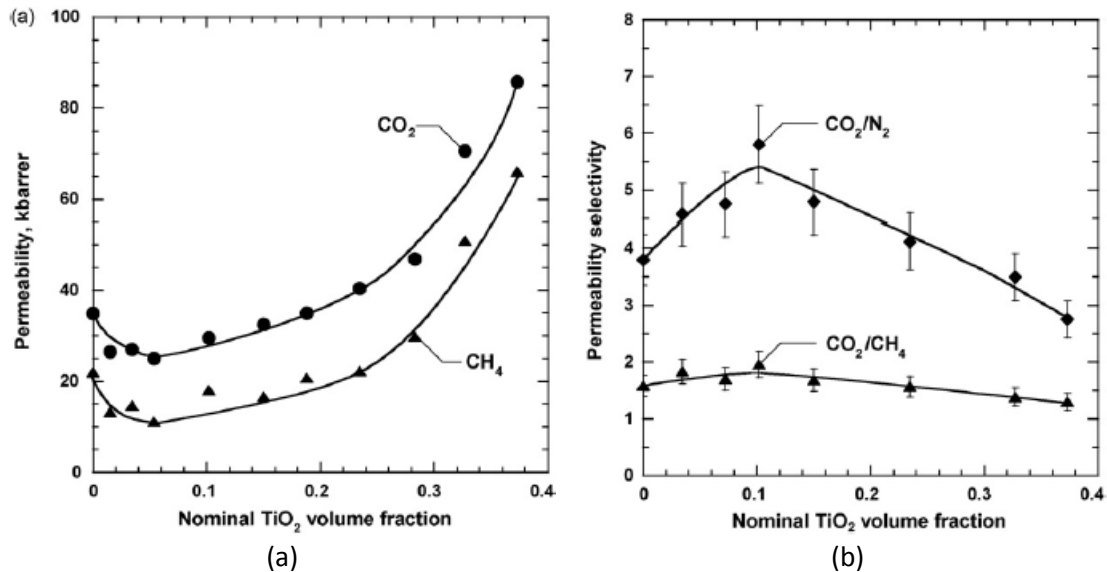


Figure 6-1: Effect of TiO_2 concentration on (a) CO_2 and CH_4 permeability and (b) pure gas CO_2/CH_4 selectivity at $\Delta p = 3.4 \text{ atm}$ and $35 \text{ }^\circ\text{C}$ [37].

Positron annihilation lifetime spectroscopy (PALS) have been used to study the size of the free volume elements in PTMSP [59]. The analysis indicated free volume elements with radii in two different size ranges: 2.5–4.0 Å and 5–7.5 Å. This is much lower than the primary particle size of titanium dioxide (3 nm). It is therefore unlikely that the nanoparticles can occupy the free volume elements. However, as the nanoparticles are present in the initial casting solution, they may influence the processing history of the nanocomposites and, in turn, cause an increase in density and a decrease in permeability. This is consistent with the observations made by Matteucci et al. at low particle loadings [37].

Sorption measurements showed that the TiO_2 nanoparticles adsorbed 9.3 and 12 times more CO_2 and CH_4 , respectively, than an equivalent volume of unfilled PTMSP. The experimental concentration of CO_2 and CH_4 was higher in the nanocomposite samples than in an unfilled PTMSP film. The light gas concentration increased with increasing particle loadings, a result that is consistent with substantial gas adsorption on the nanoparticles. In PTMSP containing 33 nominal vol% TiO_2 , the CO_2 and CH_4 concentration was 50% and 90% higher, respectively, than in unfilled PTMSP. The experimental sorption data were linearly interpolated to calculate solubility coefficients as a function of pressure. The results showed that the CO_2 solubility decreased with increasing pressure in both the unfilled polymer and in the nanocomposites. The CH_4 solubility in the nanocomposites were relatively pressure independent. These results were consistent with the observations made by Merkel et al. in a study of nanocomposites of PTMSP and fumed silica [1].

The CO₂ diffusion coefficients increased with pressure, while those of CH₄ decreased slightly. These observations were consistent with previously reported values for glassy polymers [19, 60]. As seen from Table 6-2 the diffusion coefficients of the nanocomposites containing 10 nominal vol% TiO₂ were lower than those of the unfilled PTMSP, which were consistent with the decrease in permeability. At the two highest particle loadings, the diffusion coefficients were higher than in unfilled PTMSP, which were explained by a possible onset of high concentration of voids through which CO₂ and CH₄ could diffuse rapidly.

As seen from Table 6-2, the addition of TiO₂ nanoparticles affected both gas solubility and diffusivity. The table also presents the solubility selectivity and the diffusivity selectivity for CO₂/CH₄. For the nanocomposite samples, the solubility selectivities were essentially equal to that of unfilled PTMSP. The diffusivity selectivity appeared to increase with increasing particle loading at low loadings, while at higher loadings the values decreased.

Table 6-2: CO₂ and CH₄ permeability, solubility and diffusion coefficients, and CO₂/CH₄ solubility and diffusivity selectivity in TiO₂ filled PTMSP at 35 °C [37].

φ_{F,TiO_2}^N	Permeability (kbarrer)		Solubility (cm ³ (STP)/cm ³ atm)		Diffusivity ($\times 10^6$ cm ² /s)		Solubility selectivity	Diffusivity selectivity
	CO ₂	CH ₄	CO ₂	CH ₄	CO ₂	CH ₄	CO ₂ /CH ₄	CO ₂ /CH ₄
0.00	35 ± 4	22 ± 2	5.5 ± 0.5	2.8 ± 0.3	48 ± 7	60 ± 9	2.0 ± 0.3	0.8 ± 0.2
0.03	27 ± 3	15 ± 2	6.8 ± 0.7	4.8 ± 0.5	30 ± 4	23 ± 3	1.4 ± 0.2	1.3 ± 0.4
0.07	30 ± 3	18 ± 2	5.3 ± 0.5	4.4 ± 0.4	43 ± 6	31 ± 4	1.2 ± 0.2	1.4 ± 0.5
0.10	33 ± 3	17 ± 2	7.5 ± 0.8	5.7 ± 0.6	33 ± 5	22 ± 3	1.3 ± 0.2	1.5 ± 0.5
0.15	35 ± 4	21 ± 2	7.5 ± 0.8	8.5 ± 2.0	36 ± 5	19 ± 7	0.9 ± 0.2	1.9 ± 0.6
0.23	56 ± 5	36 ± 3	7.5 ± 0.8	4.5 ± 0.5	57 ± 8	61 ± 9	1.7 ± 0.3	0.9 ± 0.3
0.33	71 ± 7	51 ± 5	7.5 ± 0.8	4.1 ± 0.1	72 ± 10	93 ± 13	1.8 ± 0.3	0.8 ± 0.2

Matteucci et al. also studied the physical aging of TiO₂-filled PTMSP [37]. As mention in previous parts of the report, PTMSP undergoes physical aging which causes the permeability to decrease over time. In their work, Matteucci et al. observed that the presence of nanoparticles seemed to retard the loss of permeability due to physical aging. Also, the severity of permeability loss were moderated at higher particle loadings. A possible, but not proven hypothetical explanation was based on the void spaces in the nanocomposites of high TiO₂ loadings, which might not decrease in size or volume with time since they are not necessarily associated with non-equilibrium polymer structure. The permeability loss with time could therefore be attributed to the aging of the polymer itself, and not the voids in the nanocomposites.

6.2 Gas-liquid membrane contactors

Initially, hydrophobic microporous membranes were used as gas-liquid contactors in studies on oxygenation of blood conducted in the 1970s and 1980s [61, 62]. Since then, several studies have been conducted on gas-liquid membrane contactors for a large range of applications, including removal of CO₂, SO₂, NO_x, H₂S, CO, VOC, NH₃ etc. from a variety of gas mixtures [7]. Applications of membrane contactors in the recovery/removal of acid gases from various gas mixtures, including their advantages and limitations, are reviewed by Ho and Sirkar [63], Gabelman and Whang [9] and Mansourizadeh and Ismail [64]. This section of the report provides a short overview of previous work on CO₂ removal using gas-liquid membrane contactors.

Gas-liquid membrane contactors can be used to remove CO₂ from flue gas, natural gas and biogas [7]. Qi and Cussler [65, 66] were the first to propose the idea of CO₂ absorption by aqueous solutions of sodium hydroxide and alkanolamines in a membrane contactor. The investigators studied the gas-liquid mass transfer in a hollow fiber module with microporous non-wetted polypropylene (PP) membranes. During the last three decades, absorption of CO₂ in hollow fiber membrane (HFM) contactors have been further investigated by numerous researches. In many cases, hollow fibers of microporous hydrophobic PP are used [67-72], but several other membrane materials have been investigated as well. Examples are polydimethylsiloxane (PDMS) [68, 73, 74], polyethersulfone (PES) [73], polyvinylidene fluoride (PVDF) [75, 76] and polyethylene (PE) [77]. Several studies have also involved polytetrafluoroethylene (PTFE), also known as Teflon [43, 77-81].

Effects of liquid contact on membranes have been studied by several researchers, and in many cases, a deterioration of the membrane performance is observed as a result of exposure [71, 72, 74]. Often, the reduced performance is associated with wetting of the membrane. Thus, membrane wettability is one of the main obstacles facing this technology and has been the center of attention in many studies. Some of these studies are addressed in the following.

Kreulen et al. [67, 68] continued the work initiated by Qi and Cussler and investigated the use of microporous HFM modules as gas-liquid contactors. These investigators reported the microporous membranes of PP may be wetted by the absorption liquid. A proposed solution was to coat the membrane with a very thin permeable layer on the liquid side. In the same period, Karoor and Sirkar [70] conducted a comprehensive experimental study of gas-liquid absorption of CO₂ in a microporous PP hollow fiber device. They used water as the absorbent and membranes in both non-wetted and wetted mode. Based on the results, the researchers concluded that it would not be advantageous to operate under wetted-mode conditions, as this caused the membrane-phase resistance to increase.

Another contribution to gas-liquid membrane contactors was provided by Rangwala [71], who studied the absorption of CO₂ into aqueous solutions using PP HFM modules. The study showed that the membrane mass transfer coefficients were much lower than those theoretically calculated for completely non-wetted pores. These observations indicated that the pores were partially wetted. Rangwala reported that even a marginal (< 2%) wetting of the pores could result in a membrane resistance that could be as high as 60% of the total mass transfer resistance.

In a study by Barbe et al. [82], the morphological changes of PP membranes exposed to water were linked to non-wetting pore intrusion by the liquid meniscus. This caused a significant increase in several morphology parameters. Solvent-induced morphological changes have also been studied by Kamo, Hirai and Kamuda [83]. In this study, microporous polyethylene (PE) HFMs were subjected to various

organic solvents. The results showed that the morphology of the pores were remarkably changed as a result of solvent treatment; the pore size expanded and the membrane shrunk in the longitudinal direction. The solvent-induced morphological changes were reported as a function of the surface tension of the liquids: the higher the surface tension of the solvent, the larger the change in morphology and permeation properties of the membrane.

Wang et al. [72] attempted to explore the impact of amine absorbents on the surface properties of membranes intended for use in G-L membrane contactors for CO₂ capture. The study concerned the impact of DEA solutions on porous PP HFMs. The experimental results showed that the pore structure and surface roughness changed as a consequence of the exposure to DEA solutions. Additionally, a decrease in the contact angles with water was observed. The longer the immersion time, the smaller the contact angle. A decrease in contact angle corresponds to an increase of the membrane surface tension. It was therefore concluded that the membrane hydrophobicity was reduced as a result of liquid immersion. A potential explanation of the reduction of contact angles was the chemical reaction between the membrane and the aqueous DEA solution. As speculated by Rangwala [71], partial wetting of polypropylene membrane by an amine solution would be possible in a membrane contactor intended used for CO₂ capture [72].

In another study by Wang et al. [49], a simulation of CO₂ absorption in water was developed for two extreme operating conditions: a non-wetted mode and a wetted mode. The results showed that the CO₂ absorption rates in the non-wetted mode were six times higher than in the wetted mode. The deterioration of the performance was mainly caused by the mass transfer resistance imposed by the liquid in the pores. The overall mass transfer coefficient in the liquid phase dropped with approximately 80% from non-wetted to completely wetted mode. As observed in several studies, the results presented in the article by Wang et al. [49] suggests that prevention of wetting is crucial to secure the high performance of a membrane contactor. In the experimental studies, a PP HFM was used together with an aqueous 2 M DEA solution as the absorbent. A performance drop of about 20% was observed after 4 days of operation. After this, no change in performance was observed. The reduction in the CO₂ flux was attributed to the wetting of the membrane. Membrane wetting was indirectly confirmed by the corresponding change in the morphologies of the immersed polypropylene hollow fibers. SEM images showed an increase in the membrane pore size after 4 days of exposure. For the hollow fibers immersed for more than 4 days, no noteworthy morphological changes were observed. The morphological changes therefore coincided with the change in the CO₂ flux. Additionally, the hydrophobicity of the membranes was altered by the liquid as a result of changes in surface energy. Regarding the overall mass transfer coefficient, decreasing values after 4 days of exposure were in good correspondence to the reduction of the CO₂ absorption and the morphological changes.

For hollow fiber membranes, the long-term compatibility with liquid is a very important criteria. Additionally, the separation system must be economically attractive compared to conventional contactors. For the application of gas-liquid membrane contactors for natural gas sweetening, another very important criteria is imposed: the HFM must be compatible with high-pressure operations. This requirement is difficult to meet when using microporous membranes, as these are subjected to wetting and, thus, mostly appropriate for low-pressure operation [84]. For both high- and low-pressure applications, the wetting problem may be overcome by using a dense, self-standing polymeric membrane. One obvious challenge related to the use of dense membranes is the increased mass

transfer resistance which may reduce the mass transfer rates [44]. Thus, the dense membrane must have a very high CO₂ permeability. Another approach to eliminate the wetting problem of hollow fiber membranes is to coat the porous membranes with a thin dense layer. Again, the dense layer of such composite membranes would contribute to the membrane resistance and possibly cause a reduction in the mass transfer rate.

Li and Teo [73] studied the absorption of CO₂ into aqueous NaOH solution through dense homogeneous PDMS. The study revealed two advantages of dense hollow fibers: (1) they eliminated the wetting problem encountered in microporous membranes, and (2) operations of the feed pressure were flexible. These advantages could overcome the disadvantage of the increase in the mass transfer resistance compared to microporous membranes. Al-Saffar and his coworkers [85] compared the performance of both porous (PP) and non-porous (PDMS) hollow fiber membranes in contact with water and DEA solutions. As expected, the gas removal rate was lower for PDMS than for PP. However, the improved CO₂ selectivity of the non-porous PDMS membrane compensated for the low permeation rate. Al-Marzouqi and Marzouk [84, 86] studied CO₂ removal from CO₂-CH₄ gas mixtures using different types of hollow fiber membrane contactors. As expected, the experimental study showed a higher CO₂ flux for the porous PP fibers than for the nonporous PDMS fibers [86].

As Nguyen et al. [44] concludes based on the studies addressed in the previous paragraph, self-standing dense polymeric films “logically cannot provide a high enough mass transfer coefficient compared to microporous membranes”. Thus, to obtain sufficiently high mass transfer coefficients and at the same time prevent wetting, composite membranes or asymmetric skinned membranes must be applied. For membrane contactor applications, composite membranes remain largely unexplored. Nguyen et al. [44] summarizes the few studies performed on composite/asymmetric membranes based on dense membranes for CO₂ absorption in membrane contactors. The summary is reproduced in Table 6-3. As the table shows, most attention has been given to the post-combustion removal of CO₂.

Table 6-3: Summary of the studies performed on dense polymeric membranes for CO₂ absorption in membrane contactors [44].

Polymer	CO ₂ permeability (Barrer)	Membrane type	System	Reference
PDMS	4550 [87]	Composite	CO ₂ /N ₂	[68, 73, 74]
PVTMS	190 [88]	Asymmetric	CO ₂ /N ₂	[89]
PMP	93 [90]	Composite	CO ₂ /N ₂	[91]
PPO	50 [92]	Asymmetric	CO ₂ /CH ₄	[93]
PTMSP	28 000 [94]	Composite	CO ₂ /N ₂	[44]
Teflon-AF 2400	3900 [95]	Composite	CO ₂ /N ₂	[44]

The studies performed by Kreulen et al. [68] and Falk-Pedersen and Dannström [74] on composite hollow fibers with PDMS as the dense layer shows that the polymer to be used as coating must be carefully selected to prevent liquid penetration.

Nguyen et al. [44] explored the possibility of using a dense layer of glassy polymers instead of elastomers. The potential advantage is the higher CO₂ permeability of some of the glassy high-free-volume polymers. Part of the work of Nguyen et al. was to develop a theoretical framework for the quantitative evaluation of the mass transfer performance of a membrane contactor. The researchers

concluded that to be able to compete with classical microporous membrane contactor materials, a dense layer thickness in the micrometer range of a highly permeable polymer with CO₂ permeability above 3000 Barrer is absolutely necessary. Two interesting candidates are the glassy high-free-volume polymers PTMSP (Section 3.4) and Teflon AF2400. As seen in Table 6-3, PTMSP has an extremely high CO₂ permeability compared to the other polymers. Teflon AF2400 has a CO₂ permeability comparable to that of PDMS, but its chemical and mechanical stability in solvents is much higher than that of PDMS.

To check the chemical and thermal resistance of PTMSP and Teflon AF2400 towards amines, Nguyen et al. [44] performed swelling experiments, in which the membranes were immersed in MEA, DEA and TEA. The results showed that the swelling of PTMSP was limited, confirming the stability of the polymer after exposure to polar liquids. Additionally, no macroscopic changes were observed. The same was observed for Teflon AF2400. Permeability measurements conducted after the immersion tests showed that the CO₂ permeability of Teflon AF2400 remained stable after exposure to MEA and DEA. For PTMSP, the permeability decreased nearly by a factor of 2. Even with this reduction in permeability, PTMSP remains the most permeable polymer for CO₂. These observations suggested that it is possible to achieve a high and stable CO₂ permeability based on these polymers.

Thin skin, defect free composite fibers were prepared with PTMSP and Teflon AF2400 coating. The hydrophobicity and the mechanical resistance of these composite materials were confirmed. However, the performance of the PTMSP coated fibers were surprisingly low, the thin layer representing a value of only 2 000 Barrer. The researchers suspected that the low performance was caused by the accelerated aging during the drying phase of the coating process which, in turn, affected the permeability and/or the penetration of the polymer solution inside the pores. The Teflon AF2400 coated fibers showed promising results with a performance similar to the porous PP membranes. Nguyen et al. [44] proved that wetting protection can be obtained without any reduction in the mass transfer performances for CO₂ absorption in MEA by a dense membrane contactor. For PTMSP coated fibers, improvements in the preparation have to be conducted to optimize the performance.

7. Experimental

7.1 Materials and preparation

7.1.1 Polymer

The polymer used in this project is the glassy, amorphous high-free-volume polymer poly(1-trimethylsilyl-1-propyne) (PTMSP). The polymer is available from Gelest Inc. (lot:2D-18172, 4A-22048) and distributed in Europe by Fluorochem Ltd. According to Gelest, the polymer is polymerized using a tantalum catalyst and has a molecular weight in the range 200 000-250 000 Da.



Figure 7-1: PTMSP commercially available from Gelest [96].

7.1.2 Nanoparticles

Three types of TiO₂ nanoparticles are used in this work:

1. Commercial TiO₂ nanoparticles
2. TiO₂ nanoparticles in the size range 15-400 nm prepared by SINTEF Materials and Chemistry
3. TiO₂ nanoparticles >1 μm prepared by SINTEF Materials and Chemistry

Hereinafter, the three types of nanoparticles are referred to as T 805, 15-400 nm and >1 μm , respectively.

The commercial nanoparticles are highly dispersed fumed titanium dioxide of the type Aeroxide[®] TiO₂ T 805 provided by Evonik Degussa. The particles are treated with octylsilane to achieve a hydrophobic surface. According to the producer, the particles have a specific surface area of $45 \pm 10 \text{ m}^2/\text{g}$ and an average primary size of 21 nm. The particles are delivered as covalently bounded aggregates in the range of 100-250 nm. These aggregates can not be broken apart by stirring or milling. SINTEF Material and Chemistry has measured the particle size to 1-3 μm . These particles have been reported to give the expected increase in permeability, as described in section 6.1 [2].

The custom-made particles provided by SINTEF Materials and Chemistry have a different surface modification than the commercial particles and are delivered in the form of clustered particles in toluene. In one of TiO₂-toluene solutions, the size of the aggregates ranges from 15 to 400 nm. In the other solution, the aggregates are larger than 1 μm .



Figure 7-2: TiO_2 nanoparticles provided by SINTEF Material and Chemistry [96].

7.1.3 Other chemicals and gases

Toluene was used as a solvent during the preparation of membranes. The toluene had a purity of 99.8% and was purchased from Sigma-Aldrich.

The membranes were exposed to solutions containing the tertiary amine N-methyldiethanolamine (MDEA). A $\geq 99\%$ grade MDEA purchased from Sigma-Aldrich was dissolved in deionized water to prepare aqueous 2 M and 4.2 M solutions.

Pure-gas permeability tests were conducted using methane (CH_4) and carbon dioxide (CO_2) at 2, 4 and 6 bar. Both gases were provided by Yara.

7.1.4 Polymer solutions

When preparing the solutions, dry polymer (PTMSP) was first dissolved in toluene. For all solutions, the amount of polymer corresponds to 2 wt% with respect to the total amount of toluene. Then, nanoparticles were added to the solution of polymer and toluene. The prepared solutions were mixed on an automatic rotator for several hours. To secure that the composition of polymer and nanoparticles is uniform throughout the membrane, it is important that the dispersions are very well mixed before being casted. Ahead of the membrane preparation, the solutions were magnetically stirred for several hours and then ultrasonically treated at about 6 A for a couple of minutes.

Two nanoparticle concentrations are used in this work: 5 wt% and 20 wt% with respect to the amount of polymer. Figure 7-3 shows three polymer solutions containing 2 wt% PTMSP without TiO_2 (to the left), with 5 wt% T 805 (in the middle) and with 20 wt% T 805 (to the right). As seen in the picture, the pure PTMSP solution is clear with a light yellow tint, while the two solutions containing nanoparticles are more opaque.

Due to limited amounts of nanoparticles from SINTEF Materials and Chemistry, only one solution of each type was prepared. These contained 5 wt% particles. In other words: no solutions containing 20 wt% 15-400 nm or $>1 \mu\text{m}$ were prepared in this work. However, solutions prepared in a previous phase of the project were available in the lab.

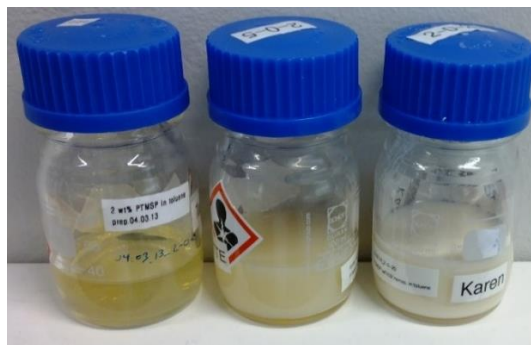


Figure 7-3: Solutions of pure PTMSP (left), PTMSP+5 wt% T 805 (middle) and PTMSP+20 wt% T 805 (right).

7.1.5 Membrane preparation

Dense films of PTMSP and nanoparticles were prepared by solution casting. The homogeneous polymer-nanoparticle solutions were poured in a glass Petri dish with a diameter of approximately 17 cm. The cast films were covered with perforated aluminum foil and left for slow evaporation at ambient conditions for a week. The residual solvent was completely removed in a vacuum oven for 24 hours. This procedure provided homogeneous membranes with a thickness of 20-60 μm . The dry membranes were carefully removed from the casting plates by using a small amount of water.

Figure 7-4 shows two membranes containing 20 wt% nanoparticles ($>1 \mu\text{m}$) and pure polymer, respectively. As seen, the pure polymer membrane is transparent with a light tint of yellow, while the one containing nanoparticles is semi-transparent.

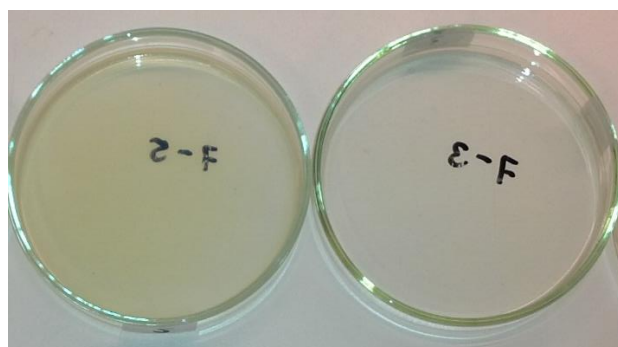


Figure 7-4: Membranes with 20 wt% $>1 \mu\text{m}$ (left) and pure PTMSP (right).

Figure 7-5 shows dry membranes prepared on 17 cm-glass dishes containing 5 wt% commercial nanoparticles (T 805). As the picture shows, the color of the dry films varies with the type of nanoparticles. The two membranes containing the largest nanoparticles ($> 1 \mu\text{m}$ and T 805) have similar colors and are the least transparent of the three. The one in the middle containing the smallest nanoparticles (15-400 nm) have a lighter tint of yellow and are more transparent than the two others.

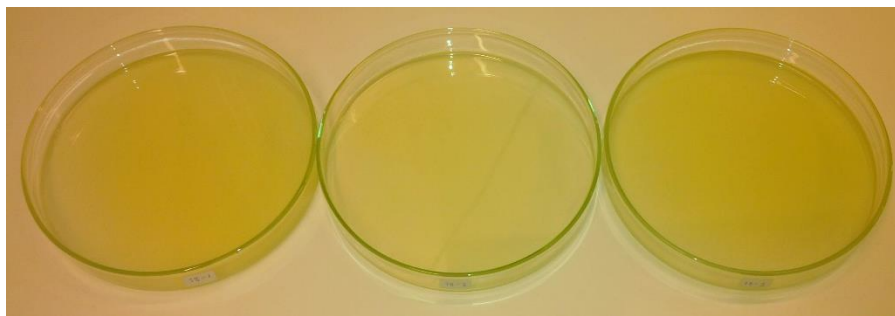


Figure 7-5: Dry membranes with 5 wt% $>1\mu\text{m}$ (left), 15-400 nm (middle) and T 805 (right).

For the commercial particles, large membranes containing both 5 and 20 wt% are prepared. As previously mentioned, only solutions containing 5 wt% particles from SINTEF Materials and Chemistry were prepared. Thus, no membranes containing 20 wt% 15-400 nm or $>1\mu\text{m}$ were prepared on large casting plates of glass. However, membranes were prepared in smaller petri dishes by using the remaining polymer solutions prepared in 2013. The area of these membranes were not big enough to provide the required amount of membrane samples for the exposure tests. Additionally, shortly after preparation, the two membranes became very brittle. The reason is not know, but the use of “old” solutions could have had an effect. Additionally, these membranes were stored in petri dishes of plastic rather than glass. The two membranes were too brittle to characterize, and, therefore, the focus of this work is on the membranes containing 5 wt% T 805, 20 wt% T 805, 5 wt% 15-400 nm and 5 wt% $>1\mu\text{m}$ TiO_2 . Additionally, two membranes containing 5 and 20 wt% T 805 TiO_2 were prepared on casting plates on Teflon.

Henceforth, the terms upside and downside of a membrane film refer to the air-side and casting plate-side, respectively.

7.1.6 Exposure of nanocomposite membranes to liquid

A method was invented to secure that only the upside of the membrane was exposed to liquid, while the downside was kept dry. The method is illustrated in Figure 7-6. The upside of the membrane was pasted over the hole of an aluminum tape. Then a filter paper was added to cover the downside of the membrane. Finally, a second aluminum tape (without hole) was laid on top of it all, giving an exposure unit as shown in Figure 7-6b. The upside of the membrane is available for liquid contact, while the downside of the membrane is kept dry. The filter paper secures that the downside of the membrane is not glued to the aluminum tape, allowing the exposed membrane to be cut out from the exposure unit and further tested. As Figure 7-6c illustrates, the exposure takes place in a beaker, with the exposure unit on top of the liquid surface, the upside of the unit/membrane facing downwards.

Membranes were exposed to deionized water, 2 M MDEA and 4.2 M MDEA, respectively. The time of immersion ranges from 1 day up to about 10 weeks. At the end of the immersion period, the membranes were taken out and washed with deionized water. Excess of liquid were carefully removed from the surface with a tissue. The membrane samples were kept at ambient conditions for several hours before being mounted in the cell and put into the permeation rig.

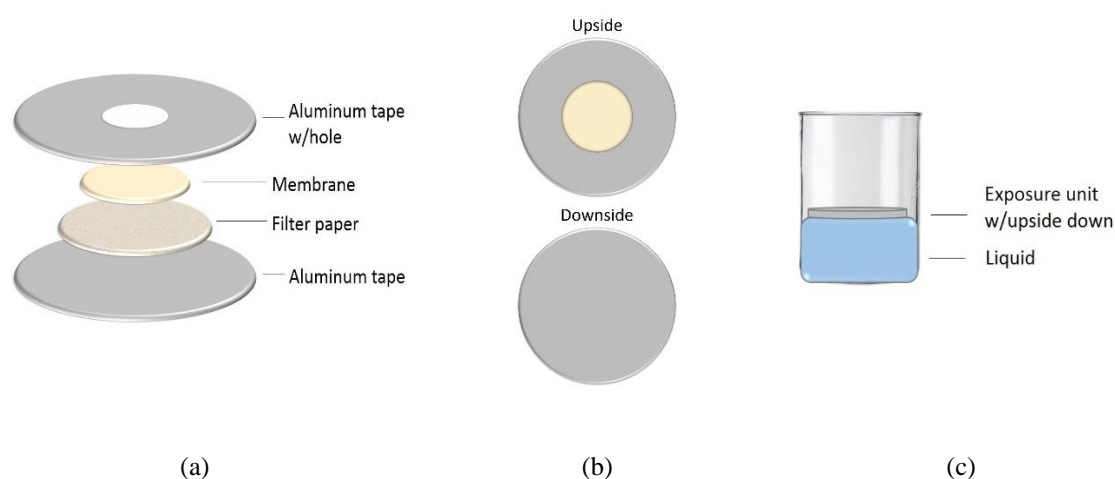


Figure 7-6: Illustrations showing the preparation (a), the final exposure unit with the upside of the membrane pointing upwards (b) and the exposure of the upside of the membrane (c).

7.2 Membrane characterization

The membranes were characterized by means of gas permeability tests, contact angle measurements and scanning electron microscopy (SEM). A general description of the methods are given in the following parts of the report, while the results are given in Section 9.

7.2.1 Gas permeability measurements

Pure gas permeabilities were measured using a constant-volume variable-pressure apparatus. As illustrated Figure 7-7, the membrane films to be tested are partially masked with impermeable aluminum tape on the top and bottom side to give a circular testing area with a diameter of 14 mm (approximate area of 1.5 cm²). Then, the testing unit is placed in a permeation cell with the downside (unexposed side) facing upwards. Finally, the cell is assembled, tightened and connected to the tubes in the permeation rig.

A constant-volume variable-pressure system measures the permeate flux by monitoring the pressure increase of collected permeate gas in a closed volume using a pressure transducer [97]. The change in the steady state pressure on the permeate side was detected by a MKS Baratron[®] manometer (0-100 mbar). The data was logged in the software LabView developed by National Instruments.

Before testing, the upstream and downstream volumes are evacuated (using a vacuum pump) for at least 8 hours to degas the film and the system. When testing, the feed gas at the desired pressure (2, 4 or 6 bar) is introduced to the upstream side of the membrane and the pressure rise in the downstream volume is recorded as a function of time. All experiments were conducted at room temperature of approximately 22°C. As mentioned in previous parts of the report, CO₂ may show some interaction with the membrane, while CH₄ is considered a non-interacting gas. The pure gas permeability of CH₄ was therefore measured first. Between the two tests, the system was evacuated for a minimum of 4 hours.

7. Experimental

The results were exported to Excel and the steady state pressure change (dp/dt) was calculated by applying linear regression to the pressure of the collected gas versus time. Finally, the permeability was calculated from the following equation:

$$P = \frac{lVT_0}{ATp_0(p_1 - p_2)} \frac{dp}{dt} \quad (7.1)$$

Here, l is the thickness of the membrane, V is the permeate volume, T_0 is the absolute zero, A is the tested area of the membrane sample, T is the temperature at which the test is conducted, and p_0 is the standard pressure. The two pressure terms, p_1 and p_2 , are the downstream pressure and the upstream pressure, respectively. The fraction dp/dt represents the steady-state pressure change. An example showing how the permeability is calculated is included in the appendix.

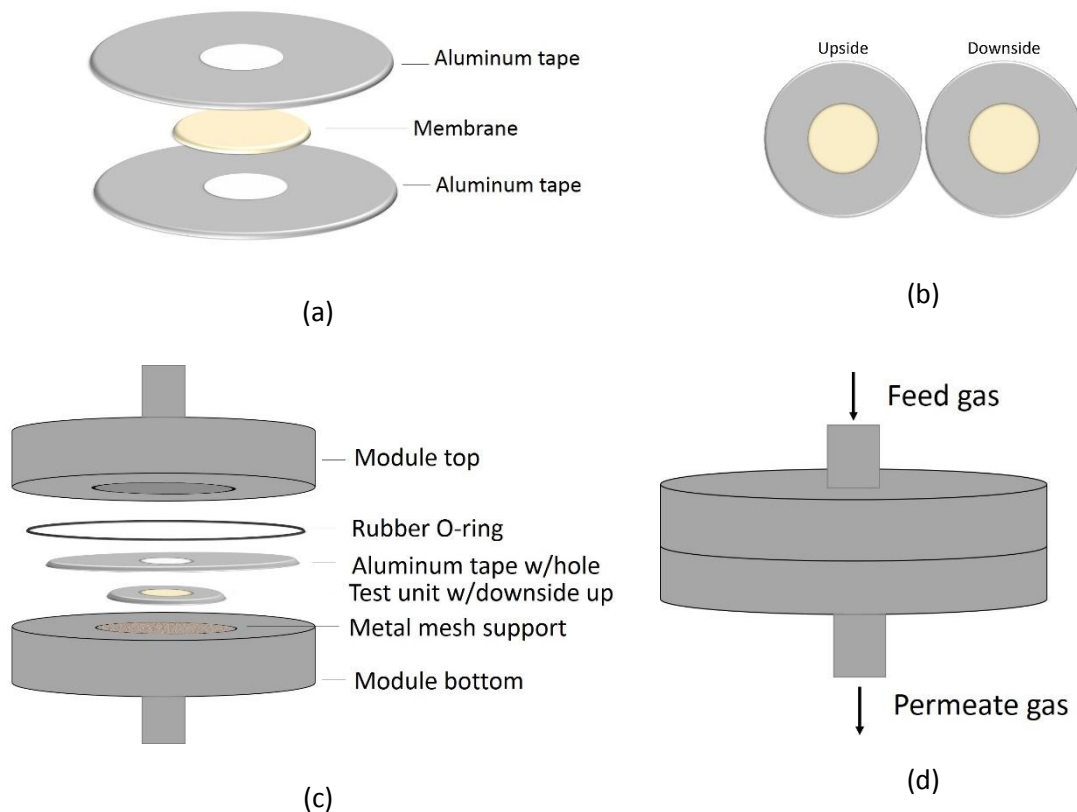


Figure 7-7: Illustrations showing (a and b) the testing unit and (c and d) the membrane cell.

The permeability tests were run in two different permeation rigs. Both rigs are constant-volume variable-pressure apparatus with some differences with respect to design. The flowsheets of the two permeation rigs are included in the appendix. Henceforth, the two permeation rigs are referred to as PR-1 and PR-2, respectively. The permeate volume, V , of the two rigs is 134 and 171 cm^3 , respectively. The installation of the permeation cell is somewhat more complicated in PR-2, as the gas tubes are fixed and not possible to adjust as the ones in PR-1 (see pictures in Appendix A). As a result, some leakage in PR-2 is sometimes observed, causing an increase in the measured permeability. Additionally,

it is observed that the gas permeation rigs give different results for almost identical samples. This inconvenience is taken into account by consistently running all tests for the individual membrane types in only one of the rigs.

7.2.2 Membrane thickness

The thickness of a membrane directly influences the gas permeability, as seen from equation 7.1. A digital precision micrometer (Digitrix II Disc Micrometer) was used to measure the thickness of the tested membranes. An average thickness was calculated by measuring the thickness of the tested membrane areas at 9 different locations on the surface. The membranes prepared during this project have a thickness ranging from 20 to 60 μm .

7.2.3 Scanning electron microscopy (SEM)

The surface morphology of the samples was investigated by a Hitachi S-5500 S(T)EM at NTNU NanoLab. This specific model is an in-lens cold field emission electron microscope with an attainable resolution of 0.4 nm. The acceleration voltage is 0.5-30 kV and the maximum beam current is 20 μA . An acceleration voltage in the range 3-10 kV and a beam current of 7 μA was used when investigating the membrane samples. The scanning electron microscope scans a focused electron beam over the sample surface, creating a number of signals from the surface. These signals are collected by detectors and used to form an image. The samples were glued to rectangular mounts by using carbon conductive tabs, as shown in Figure 7-8b. A Cressington 208 HR B sputter coater was used to produce a thin conducting layer on the non-conducting polymer samples. The membrane samples were coated with a 5 nm-layer of gold.

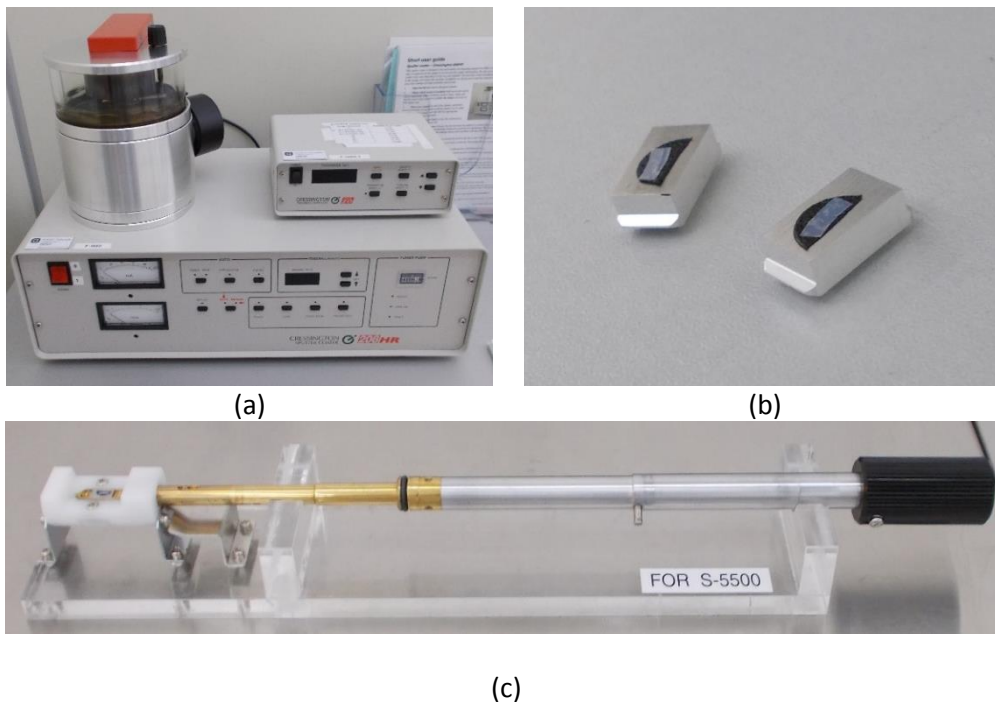


Figure 7-8: Pictures showing (a) the sputter coater, (b) SEM samples and (c) the sample holder at NTNU NanoLab.

In addition to SEM characterization, the plan was to investigate the nanocomposite membranes using AFM. However, the tool was out of order until late May and AFM studies are therefore not included in this work. Sorption measurements were also meant to be included in this work. However, due to problems with the sorption apparatus and lack of time, sorption measurements were not given priority. Both of these characterization methods are included in Section 11 as further work.

7.2.4 Contact angle measurements

Contact angles were measured with the sessile drop method using Attension's Theta Lite Optical Tensiometer, operated with the OneAttension Software. A piece of membrane was placed on a platform and a drop of liquid was placed on the surface using a micro syringe. All measurements were performed at room temperature. The contact angle was measured by manually placing a base line (green line in Figure 7-9). For each membrane sample, the contact angle of three to five drops was measured immediately after deposition, as well as 30 seconds and 1 minute after deposition. The measurements are used to calculate an average value as well as a standard deviation. The values listed in the following tables are the average values after 30 seconds.

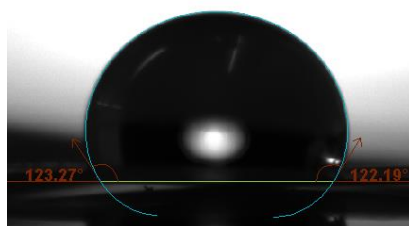


Figure 7-9: Image from OneAttension Software showing water drop on membrane surface. The base line is given in green.

To be able to measure the contact angle, the surface should be as smooth as possible. For a large number of membrane samples, the surface was too uneven to measure the contact angle. A method was found to make the contact angle measurements possible on samples that are not horizontal/smooth enough. By using double-sided tape, a membrane sample can be glued onto a microscope slide as shown in Figure 7-10. This way, the samples become completely horizontal.

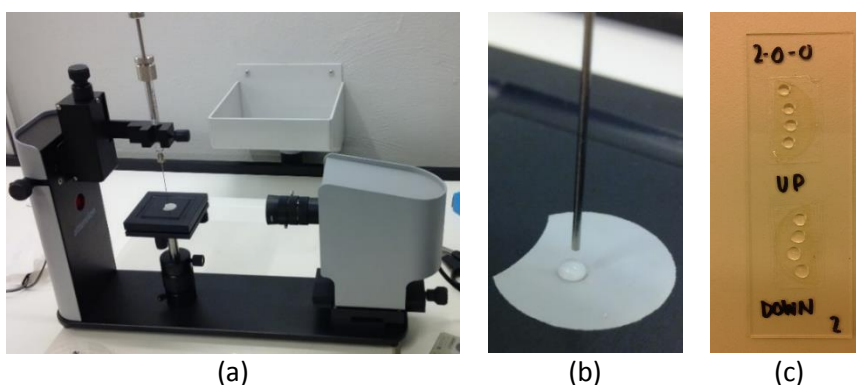


Figure 7-10: (a) Attension's Theta Lite Optical Tensiometer, (b) water drop on membrane surface and (c) membrane pieces glued onto a microscope slide.

Compared to the experimental work conducted during the specialization project in 2013, the following changes have been made:

- The prepared flat sheet membranes are larger (increased from 4 cm to 17 cm in diameter)
- The membranes are prepared on casting plates of glass rather than Teflon
- Only the upside of the membranes is exposed to liquid
- The membranes are exposed to liquid for a longer period of time

8. Previous work

Previous master student, now graduate, Tina Tomaša worked on a specialization and master project during fall 2012-spring 2013 with the same topic as the project addressed in this report, but on an earlier phase [98, 99]. The experimental work conducted during spring involved crosslinked, nanofilled PTMSP membranes. The bis(aryl azide) 4,4-diazidobenzophenone (BAA) was used as the crosslinking agent, while the nanoparticles used were of the type Aeroxide® T 805 TiO₂. The membranes were exposed to water, 2 M MDEA and 4.2 M MDEA, the time of exposure varying from 1 day to 10 weeks. The aim of the work was to study the effect of crosslinking and dispersion of nanoparticles on the pure gas permeability, stability and endurance in solution. Results relevant for this year's work is given in the following.

Figure 8-1 shows the CO₂ permeability at 2 bar with respect to time in solution. Three types of membranes are included in the figure: pure PTMSP, PTMSP crosslinked with 3 wt% BAA, and PTMSP crosslinked with 2 wt% BAA containing 20 wt% commercial Aeroxide® T 805 TiO₂. As the figure illustrates, the permeabilities decreases with time in solution. For the liquid-exposed PTMSP membranes, the results follow the same trend as the aging curve of PTMSP. These results indicate that PTMSP is not affected by liquid exposure and that the reduction in permeability is solely caused by physical aging of the membrane. The polymer's resistance towards water and MDEA solutions is linked to the hydrophobicity of the polymer.

A reduction in permeability was observed also for the crosslinked PTMSP membranes. Unlike the pure PTMSP membranes, it was concluded that the reduction in permeability with time was not related to aging, as the decrease in permeability did not follow the aging curve of PTMSP. Based on the selectivities, it was suspected that the reduction in permeability was linked to a reduction in solubility coefficients. For the crosslinked, nanofilled PTMSP membranes, a dramatic decrease in permeability was observed already after 2 weeks of exposure. For all concentrations, the measured CO₂ permeability was lower than 400 Barrer. As the nanoparticles are hydrophobic, it was expected that their presence would improve the membrane's resistance towards liquid. As further work, it was suggested that these observations should be further explored to reveal whether it was the addition of nanoparticles or the combination of nanoparticles and crosslinking that caused the dramatic decrease in permeability.

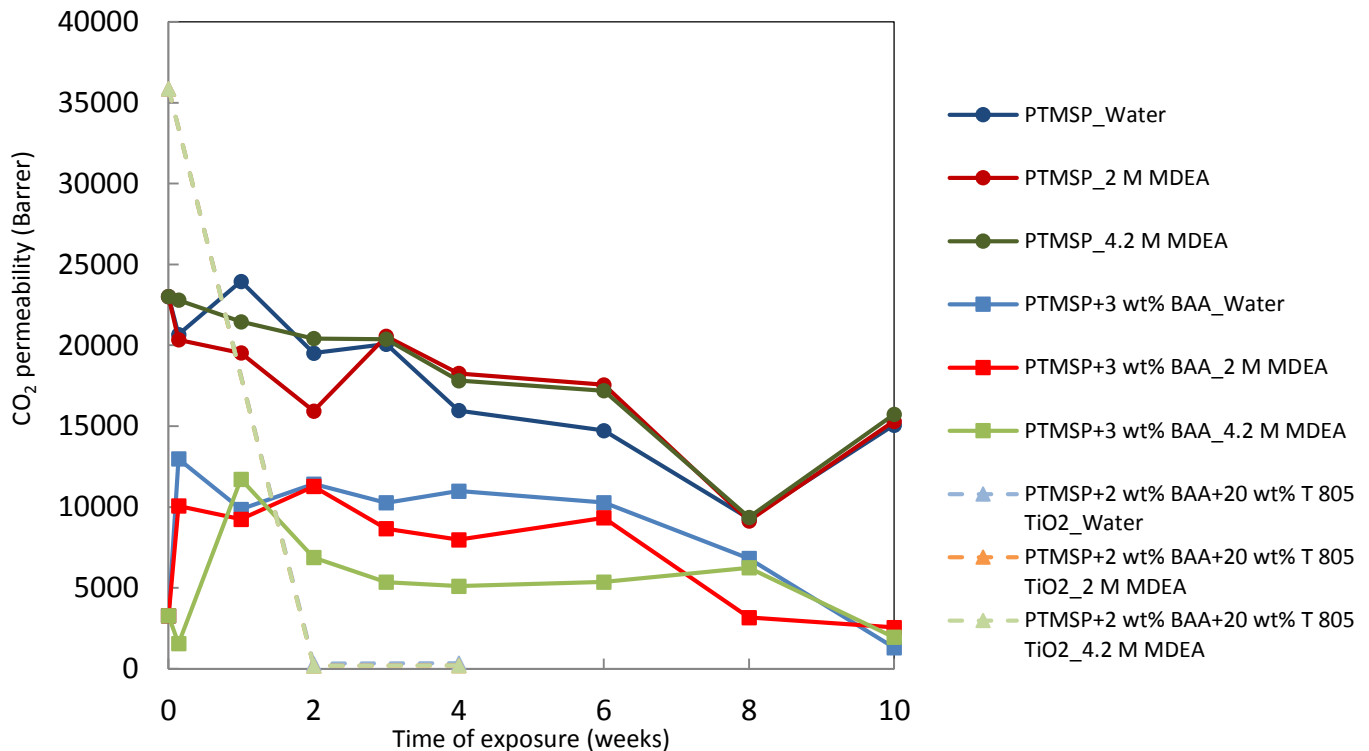


Figure 8-1: Results from previous master project showing the CO₂ permeability at 2 bar for pure PTMSP, crosslinked PTMSP without nanoparticles and crosslinked PTMSP with nanoparticles [99]. The membranes are exposed to deionized water, 2 M MDEA and 4.2 M MDEA.

For all membranes, the measured contact angle was higher than 90°, indicating that the membranes were hydrophobic. Compared to pure PTMSP, the addition of 20 wt% nanoparticles increased the contact angle. The increase was explained by an enhancement of hydrophobicity due to increased roughness and/or due to the fact that the TiO₂ nanoparticles are hydrophobic. For other compositions of BAA and nanoparticles, no specific trend was observed. The highest contact angles were measured for the ones exposed to 4.2 M MDEA, followed by 2 M MDEA and water. For the crosslinked nanofilled membranes, the highest angles were measured for the ones exposed to water.

The specialization project carried out during fall 2013 involved uncrosslinked PTMSP containing 20 wt% TiO₂ nanoparticles. These particles were of the same type as the ones applied in this master's thesis. The membranes were exposed to liquid for 1 day, 1 week and 2 weeks. Figure 8-2, Figure 8-3 summarize the permeability results from the specialization project. The permeability of unexposed membranes – shown as broken lines in the following figures – are based on results from preceding parts of the project. For the exposed membranes, each point on the graph is based on only one test. The uncertainty might therefore be significant.

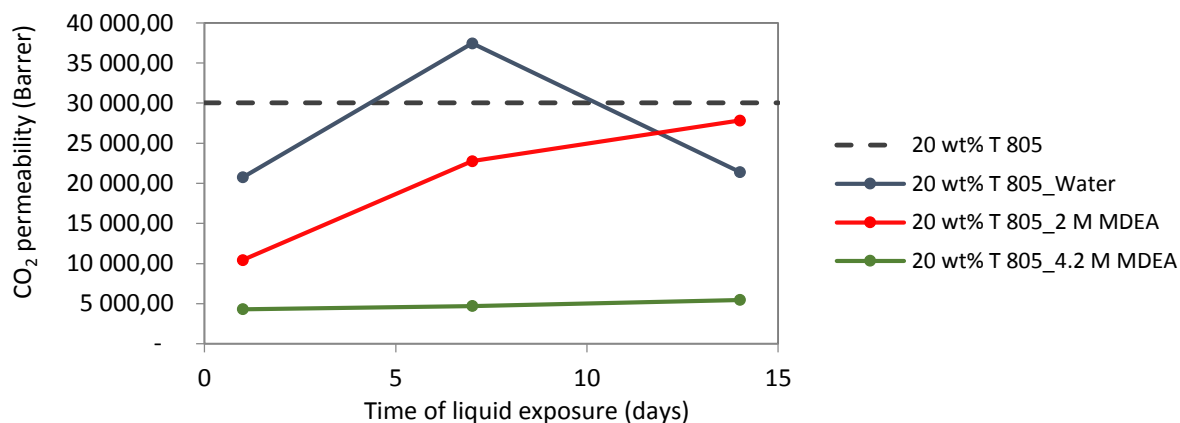


Figure 8-2: CO₂ permeability as a function of time of exposure for membranes containing 20 wt% T 805. Results from specialization project conducted during fall 2013.

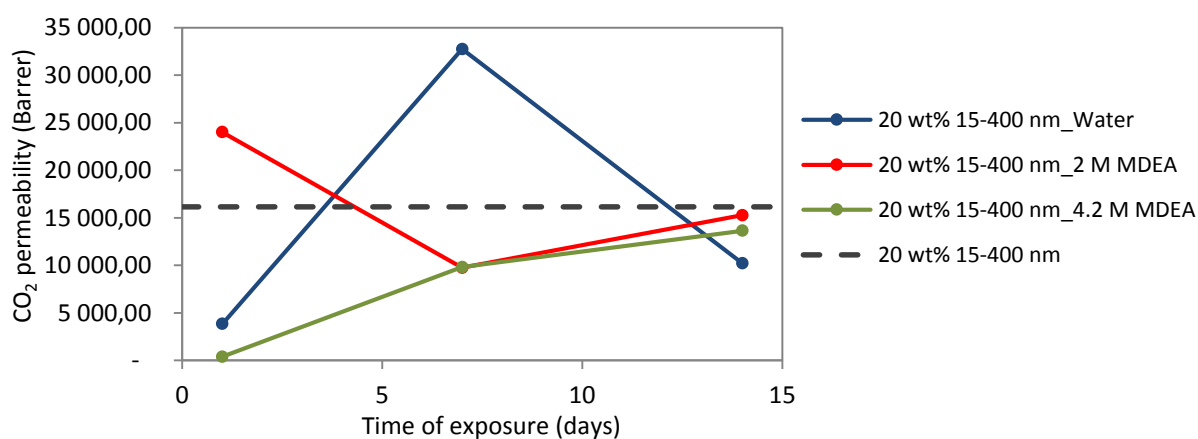


Figure 8-3: CO₂ permeability as a function of time of exposure for membranes containing 20 wt% 15-400 nm. Results from specialization project conducted during fall 2013.

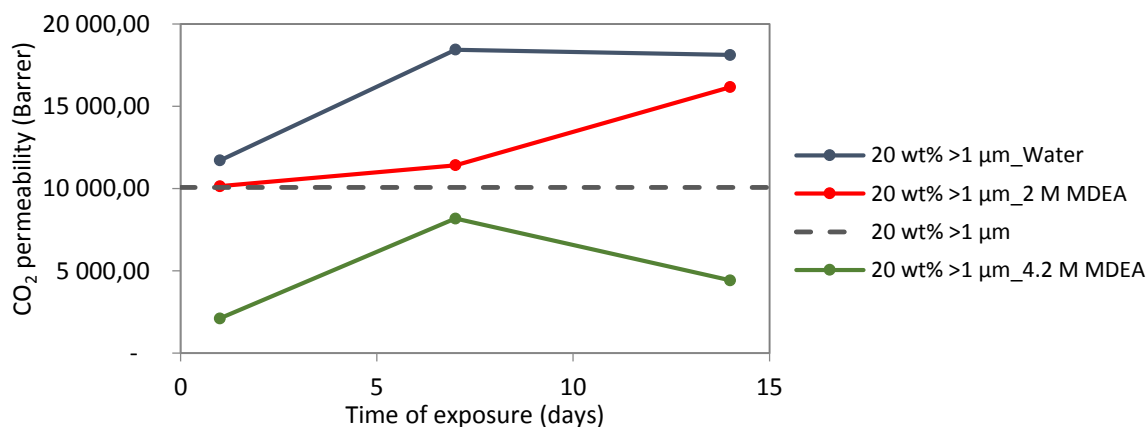


Figure 8-4: CO₂ permeability as a function of time of exposure for membranes containing 20 wt% >1 μm. Results from specialization project conducted during fall 2013.

As seen in the figures, the permeability of the membranes exposed to water and 2 M MDEA lies at a relatively high level after two weeks of exposure. For the highest concentration (4.2 M MDEA), the

permeability is lower at all times of exposure, except for the ones containing 20 wt% 15-400 nm. This could be a random deviation. As shown in Figure 8-1, previous results have indicated that pure PTMSP is unaffected by liquid exposure. This is not the case for the nanocomposites studied in the specialization project, indicating that the resistance towards liquid has changed due to the presence of nanoparticles.

The membranes exposed to liquid for 2 weeks did not suffer the same fate as the crosslinked, nanocomposite membranes (Figure 8-1). This observation suggests that the uncrosslinked nanocomposite membranes are more resistant towards liquid than the crosslinked nanocomposite membranes. As further work, it was suggested that nanocomposite membranes of several compositions of particles should be exposed to liquid for a longer period of time.

9. Results and discussion

9.1 Gas permeability results

9.1.1 Effect of gas and feed pressure on gas permeabilities

For all membranes investigated in this work, the permeability of CO₂ is higher than that of CH₄. Figure 9-1 illustrates a typical case. A slight increase in permeability is observed as the pressure increases. As mentioned in theoretical part of the report, the gas permeabilities of pure PTMSP are essentially independent of gas pressure [1, 2]. It was also mentioned that the CO₂ and CH₄ permeabilities should decrease with increasing feed pressure, most notably for CO₂ [19]. This is consistent with the dual sorption model introduced in Section 3.3.3. As mentioned in the same section of the report, the permeability of CO₂ may increase as the pressure increases due to plasticization [14]. However, this phenomenon usually appears at higher feed pressures [15]. Therefore, the slight increase in permeability observed in this work is not related to plasticization, but are rather expected to be caused by some leakage in the system.

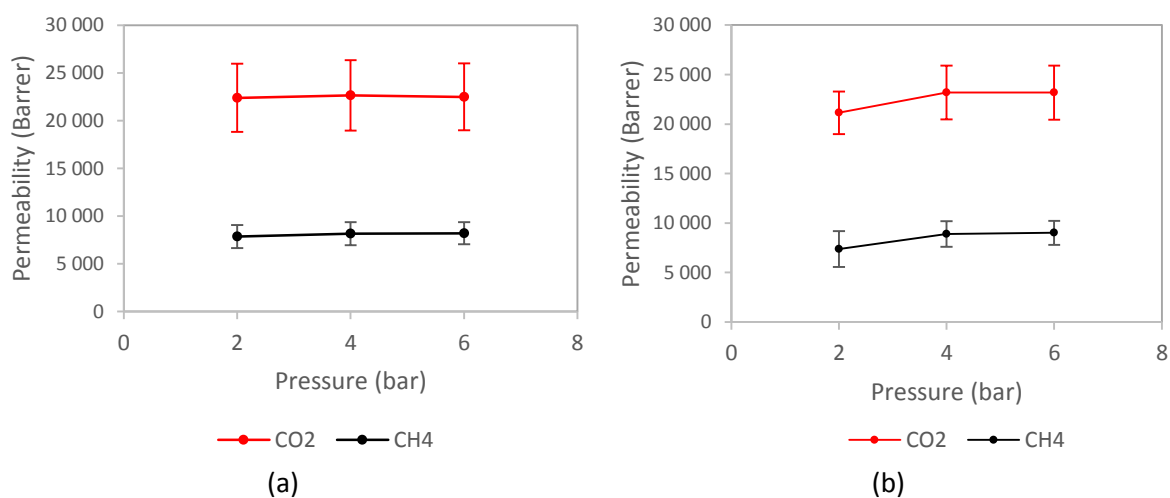


Figure 9-1: CO₂ (red line) and CH₄ (black line) permeability as a function of feed pressure for (a) 5 wt% T 805 tested in PR-1 and (b) 5 wt% 15-400 nm tested in PR-2.

9.1.2 Uncertainty in permeability measurements

Uncertainties exist in all measurements as a result of both instrumental and human errors. A tight schedule and very time-consuming permeability tests leave little or no time to run several tests for each parallel. As a consequence of this, the majority of the data points in the following graphs lack error bars. To get an indication of the uncertainty in the permeability measurements, the permeability of the non-exposed membranes was measured for three membrane areas from different parts of the initial membrane. The uncertainty in the results is quantified by using standard deviations. The standard deviations are included in Table 9-1. As seen, the values ranges from less than 50 Barrer to more than 4000 Barrer.

The gas permeation tests have involved the use of two different permeation rigs. Both systems are based on the same principle (constant-volume variable-pressure) and share the same operational procedure. As mentioned in Section 7.2.1, the two permeation rigs often give different results, and the permeabilities measured by PR-2 is suspected to be higher than those measured by PR-1. Additionally, the permeation results originating from PR-2 often show an obvious increase with increasing pressure. A typical example was shown in Figure 9-1b. During the specialization project, the difference between the two permeation rigs was not taken into account and testing was not done consistently. This year, however, one type of membrane is consistently tested in only one of the permeation rigs. This way, even though the two rigs may give different results, the individual types of membranes are at least sharing the same basis.

Another measure to minimize the uncertainty of the results is to let all tested samples share the same origin. Previously, the tested samples came from different membranes prepared on casting plates of Teflon. This year, as described in the experimental part of the report, large membranes (approximate diameter of 17 cm) were prepared on casting plates of glass. All tested samples therefore originate from the same membrane. Additionally, any impurities from the Teflon plate are eliminated.

9.1.3 Aging of membranes

As known, PTMSP undergoes a fast physical aging due to relaxation of non-equilibrium excess free volume. This leads to a decrease in permeability with time. The age of the membranes are given as the number of days from the polymer solutions were casted to form membranes. Results from the previous master project showed a decrease in permeability of PTMSP of 50% as the age increased from 15 to nearly 100 days. In this year's work, the age of the membranes ranges from about 15 to 100 days. Such a large span may be of great importance for the results, as aging may affect not only the permeability, but also the resistance toward liquid.

Prior to the startup of the experimental work, it was decided that all tested membrane areas should come from the same membrane and all were to be exposed to liquid for a maximum of 10 weeks. To meet these requirements, all membranes were prepared early in the semester (in middle of February). Therefore, the age of the membranes increases the further into the semester they were tested.

Ideally, unexposed membranes of all types should have been tested shortly after preparation to minimize the impact of aging. However, the permeability results for the unexposed membranes are generated throughout the semester, with an age ranging from 18 to 55 days. As a consequence of this, the membranes and, in turn, the gas permeabilities given in the following tables may be affected by aging. Figure 9-2 shows the permeabilities of the membranes as a function of age. As seen, the membranes tested several weeks after preparation still lie on level comparable to the PTMSP membranes tested only 8 days after preparation. This could indicate that the dispersion of TiO₂ nanoparticles has a stabilizing effect on the aging of PTMSP. The same is observed by Matteucci [37], for which the permeabilities of the PTMSP-TiO₂ were relatively stable after 60 days.

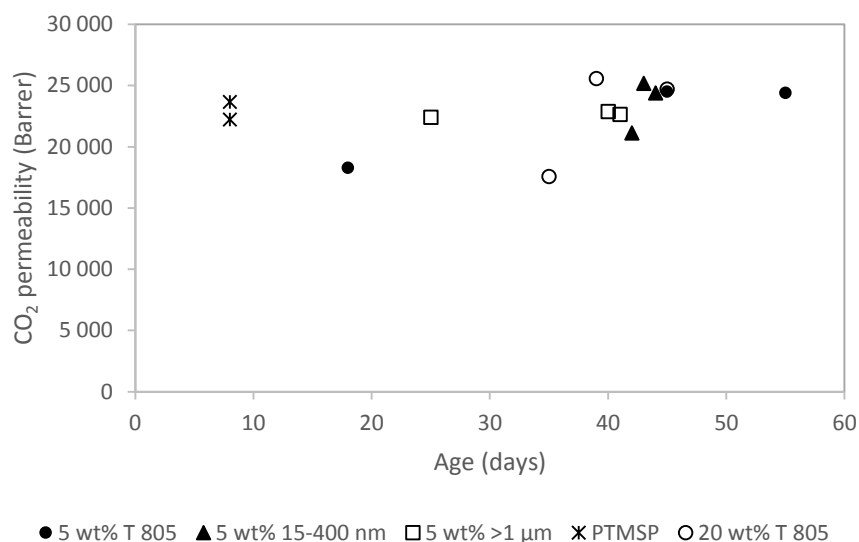


Figure 9-2: CO₂ permeability at 2 bar for unexposed membranes as a function of age.

9.1.4 Permeability of unexposed membranes

The average CH₄ and CO₂ permeability of pure PTMSP is given in Table 9-1. The values and standard deviations given in the table are based on two measurements conducted in each of the permeation rigs. As seen, the average CO₂ permeability at 2 bar is slightly below 23 000 Barrer.

At 2 bar, only one of the nanocomposite membranes exhibits a higher (average) permeability than that of PTMSP (5 wt% 15-400 nm). As the table shows, the standard deviations in the measurements are significant for all the membranes apart from the one containing 5 wt% >1 μm TiO₂. This is due to the fact that one of the three tests have given a CO₂ permeability considerably lower than the two others. This can be seen from the tables included in the appendix. The deviating results may be random errors. Another potential explanation is that the tested samples are taken from different parts of the main membranes. As mentioned, the morphology of the fillers is very important for the performance of the mixed matrix membrane. If the particles are not evenly distributed, it could reduce the effect of fillers on chain packing disruption and, in turn, the gas permeability.

The average CO₂ permeability is in the order 5 wt% 15-400 nm > PTMSP > 5 wt% >1 μm > 20 wt% T 805 > 5 wt% T 805. However, by considering the standard deviation in the results, the measured permeabilities all lie within the uncertainty of each other. By disregarding the deviating result, the standard deviation would become significantly lower (below 700 Barrer for all membranes) and the average permeability becomes somewhat higher. In this case, all membranes apart from the one containing 5 wt% >1 μm would have an average permeability higher than that of PTMSP. By disregarding the one deviating result, the highest permeability is observed for the membrane containing 20 wt% TiO₂ (25 154 Barrer). If this is really the case, it would be in agreement with what is observed in literature, where the permeability increases as the concentration of nanoparticles increases [2] (see Section 6.1). However, too few tests have been conducted in this work to draw any conclusions regarding the relative permeability of the individual membranes. Several tests would perhaps have minimized the uncertainty and given a more accurate average value.

9. Results and discussion

Table 9-1: CH₄ and CO₂ permeability of PTMSP and TiO₂-PTMSP nanocomposites, based on two and three measurements, respectively.

Membrane type	TiO ₂ content (wt%)	Permeation rig	Gas	Permeability (Barrer)		
				2 bar	4 bar	6 bar
PTMSP	0	PR-1, PR-2	CH ₄	9 093 ± 1 138	9 347 ± 1 250	9 349 ± 1 259
			CO ₂	22 952 ± 1 014	23 538 ± 231	23 442 ± 47
T 805	5	PR-1	CH ₄	7 862 ± 1 211	8 157 ± 1 208	8 199 ± 1 149
			CO ₂	22 397 ± 3 567	22 655 ± 3 689	22 488 ± 3 509
T 805	20	PR-2	CH ₄	11 805 ± 2 704	12 418 ± 2 495	12 612 ± 2 258
			CO ₂	22 631 ± 4 391	25 258 ± 3 576	26 756 ± 2 434
15-400 nm	5	PR-2	CH ₄	9 440 ± 1 816	10 333 ± 1 287	10 376 ± 1 210
			CO ₂	23 587 ± 2 153	26 317 ± 2 730	26 327 ± 2 732
>1 μm	5	PR-1	CH ₄	8 047 ± 335	8 228 ± 431	8 221 ± 396
			CO ₂	22 653 ± 240	23 032 ± 601	22 534 ± 518

The CO₂/CH₄ selectivities of the unexposed membranes are given in Table 9-2. As seen, the average selectivity of pure PTMSP is about 2.5. At 2 bar, the average selectivity is in the order 5 wt% T 805 > 5 wt% >1 μm > PTMSP > 5 wt% 15-400 nm > 20 wt% T 805. The fact that lowest selectivity is observed for the membrane containing the highest concentration of TiO₂ is consistent with results reported in literature [2]. This could indicate that the dispersion of particles has opened up the polymer structure and, in turn, increased the diffusivity of CH₄.

Table 9-2: CO₂/CH₄ selectivity of PTMSP and TiO₂-PTMSP nanocomposites, based on two and three measurements, respectively.

Membrane type	TiO ₂ content (wt%)	CO ₂ /CH ₄ selectivity		
		2 bar	4 bar	6 bar
PTMSP	0	2.55 ± 0.43	2.54 ± 0.36	2.53 ± 0.34
T 805	5	2.85 ± 0.27	2.78 ± 0.30	2.75 ± 0.28
T 805	20	1.93 ± 0.09	2.05 ± 0.17	2.15 ± 0.24
15-400 nm	5	2.54 ± 0.31	2.55 ± 0.12	2.54 ± 0.05
>1 μm	5	2.82 ± 0.10	2.80 ± 0.08	2.74 ± 0.07

The permeabilities of the unexposed PTMSP and TiO₂-PTMSP nanocomposites given in Table 9-1 are all lower than those measured by Matteucci [37] (Table 6-2) and Shao [2] (Table 6-1).

Table 6-1). Neither of the two researching groups investigated nanocomposites containing exactly 5 and 20 wt% TiO₂, but similar filler contents did indeed give higher permeabilities. However, the nanocomposites investigated by these researchers contained other types of particles and were tested

at other conditions. As mentioned in Section 3.4, the polymer is sensitive to the processing history of the sample. As a result, the measured permeability of PTMSP varies from one article to another.

The nanocomposite membranes containing 5 wt% 15-400 nm and 20 wt% T 805 TiO₂ were tested in PR-2. The rest were tested in PR-1. As seen from the table, the permeability of both gases increases with pressure to a greater extent than for the membranes tested in PR-1. This is particularly evident for the CO₂ permeability in the membrane containing the commercial particles, where the average value increases from about 22 600 to about 26 800 Barrer as the pressure increases from 2 to 6 bar. This is probably due to a leakage in the system. The leakage is assumed to have the least impact on the results at low pressure. As a result, the values at 2 bar are used in the figures in the following sections.

9.1.5 Liquid-exposed nanocomposite membranes

In the following figures, the solid lines in blue, red and green represent the membranes exposed to water, 2 M MDEA and 4.2 M MDEA, respectively. The dashed lines in black represent the average permeability of the unexposed membranes. These values are given with error bars, which are the standard deviations of three measurements. For the exposed membranes, the points on the graphs are based on one single test. Two tests have been performed in some of the cases where the results of the first test seemed very strange. The results from the second test are shown with a dashed line. The measured permeabilities at 2, 4 and 6 bar for all membranes are given in the appendix. The corresponding graphs for the CH₄ permeability at 2 bar are also included in the appendix.

9.1.5.1 Membranes containing 5 wt% T 805 TiO₂

Figure 9-3 shows the CO₂ permeability at 2 bar for the nanocomposites containing the commercial Aeroxide® T 805 TiO₂ nanoparticles. The broken line represents the average CO₂ permeability at 2 bar for the unexposed membrane, which is approximately 22 397 Barrer. The error bars show the standard deviation of ±3 567 Barrer. For the first 14 days of exposure, the results are somewhat unstable. The permeabilities of the membranes exposed to 4.2 M MDEA lie at a significantly lower level during the first weeks of exposure than the ones exposed to water and 2 M MDEA. As the figure shows, the long-term exposure to MDEA solutions of different concentrations have resulted in approximately equal CO₂ permeabilities. The same trend is observed for CH₄ (see appendix).

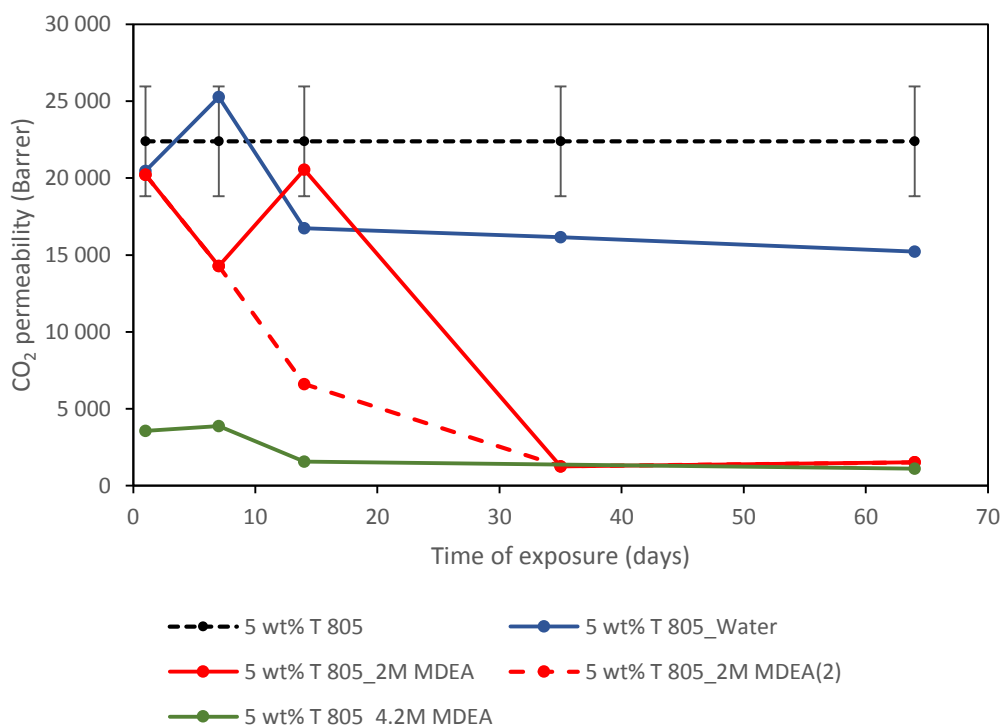


Figure 9-3: CO₂ permeability at 2 bar for liquid exposed membranes containing 5 wt% T 805 TiO₂. The broken line shows the permeability of the unexposed nanocomposite.

For the membranes exposed to water, only a slight decrease in permeability is observed as the time of exposure increases from 14 to 67 days (approximately 16 700 to 15 200 Barrer). The CO₂ permeability measured after 67 days of exposure is 68% of the initial permeability of the unexposed membrane.

At 14 days of exposure to 2 M MDEA, two membranes were tested. The first membrane (solid line) exhibited a CO₂ permeability more than twice as high as for second membrane (dashed line). The two tested areas originate from the same membrane and have been exposed to the same solvent for the same amount of time. Ideally, the two samples would therefore give the same results. The two membranes were tested 34 and 71 days after preparation, respectively. This could explain why the permeability of the second membrane is so much lower. However, as was illustrated in Figure 9-2, the permeability loss due to aging seems to be reduced due to the presence of nanoparticles. If this is the case, the decrease in permeability of the membrane measured 71 days after preparation is probably not caused by aging alone. It could be, however, that aging has an effect on the membrane's resistance towards liquid. The fact that the samples originates from different areas of the main membrane may also have affected the results. Both the properties and the effect of liquid contact may vary from one sample to the other.

After 35 days of exposure to 2 M MDEA, the measured CO₂ permeability has dropped to 1 400 Barrer. As the time of exposure further increases, the permeability remains about constant. The observations suggest that a decisive change in one or more of the membrane properties takes place at a time of exposure between 14 and 35 days. After 64 days, the permeability equals approximately 1 500 Barrer. This value is only 7% of the initial permeability of the unexposed membrane.

At the highest concentration (4.2 M MDEA), the membrane experiences a significant reduction in permeability already after 1 day of exposure. Compared to the unexposed membrane, the CO₂

permeability after 1 day exposure is only 16% of the initial value. At 14 days of exposure, the measured CO_2 permeability equals about 1 600 Barrer. As the time of exposure increases from 14 to 64 day, the CO_2 permeability is further decreased to approximately 1 100 Barrer. This value is only 5 % of the initial value. For the long-term exposed membrane sample, a sudden increase in the gas flux was observed while running the permeation test at 6 bar. It is suspected that a fracture in the sample occurred during testing, eliminating the resistance toward gas flow. This could be a coincidence, or it could indicate that the long-term exposure has had an effect on the mechanical stability of the membrane. The same was observed for the membrane containing 5 wt% $>1 \mu\text{m}$ TiO_2 (Section 9.1.5.4).

Figure 9-4 shows the pure gas CO_2/CH_4 selectivity for the nanocomposites containing 5 wt% Aeroxide® T 805 TiO_2 nanoparticles. The broken line in black represents the average selectivity at 2 bar for the unexposed membrane, which is 2.9. The standard deviation of ± 0.27 is also included. As for the CO_2 permeability (Figure 9-3) the values vary quite a lot in the first two weeks of exposure. In the beginning, the selectivity of the membranes exposed to 4.2 M MDEA is higher than that of the membranes exposed to water and 2 M MDEA. This is the opposite of what is observed for the permeabilities during the first weeks of exposure.

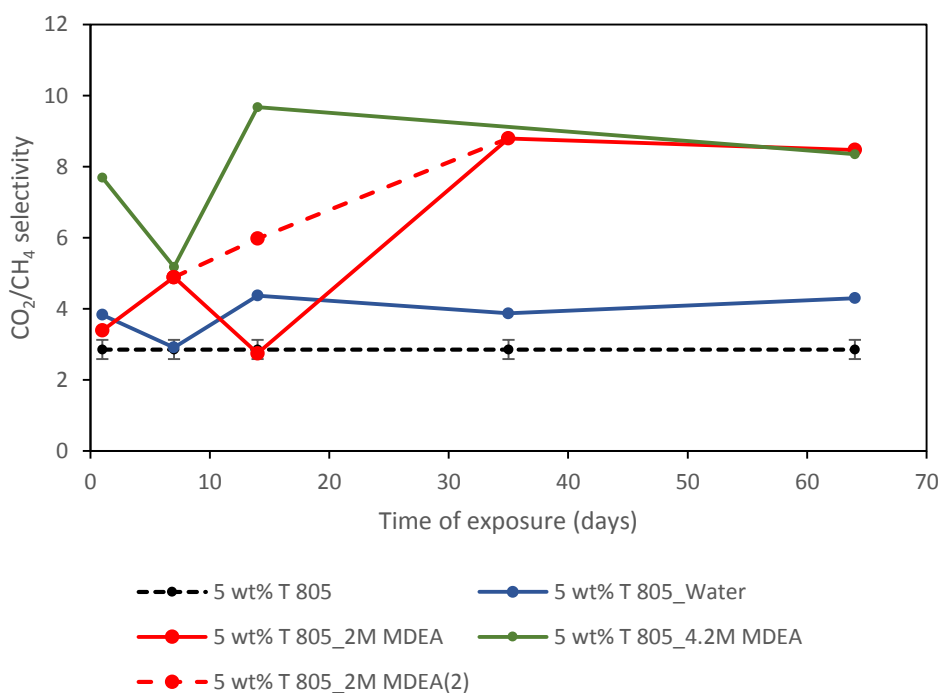


Figure 9-4: CO_2/CH_4 selectivity at 2 bar for liquid exposed membranes containing 5 wt% T 805 TiO_2 . The black broken line corresponds to the selectivity of the unexposed nanocomposite.

As observed for the permeability, the CO_2/CH_4 selectivity of the water-exposed membranes levels off beyond 14 days of exposure. Only a slight change is observed. After 67 days of exposure, the selectivity equals 4.30. This represents a 51% increase in selectivity compared to the unexposed membrane.

For the membrane exposed to 2 M MDEA, the selectivity has increased to about 8.8 after 35 days of exposure. As observed for the permeability, the selectivity remains about constant as the time of exposure further increases. After 64 days, the selectivity is 8.5, a value that is three times as high as for the unexposed membrane.

As Figure 9-4 shows, the highest CO₂/CH₄ selectivity is observed for the membrane exposed to 4.2 M MDEA for 14 days. At this point, the selectivity equals 9.7. As the time of exposure to 4.2 M MDEA increases to 64 days, the selectivity decreases to 8.4. Thus, long-term exposure to MDEA solutions of different concentrations have resulted in approximately the same CO₂/CH₄ selectivity. This was also observed for the permeability.

9.1.5.2 Membranes containing 20 wt% T 805 TiO₂

Figure 9-5 shows the CO₂ permeability at 2 bar for the liquid-exposed membranes containing 20 wt% commercial Aeroxide® T 805 TiO₂. The broken line represents the average CO₂ permeability at 2 bar for the unexposed membrane, which is approximately 22 631 Barrer. The error bars show the standard deviation of ±4 391 Barrer.

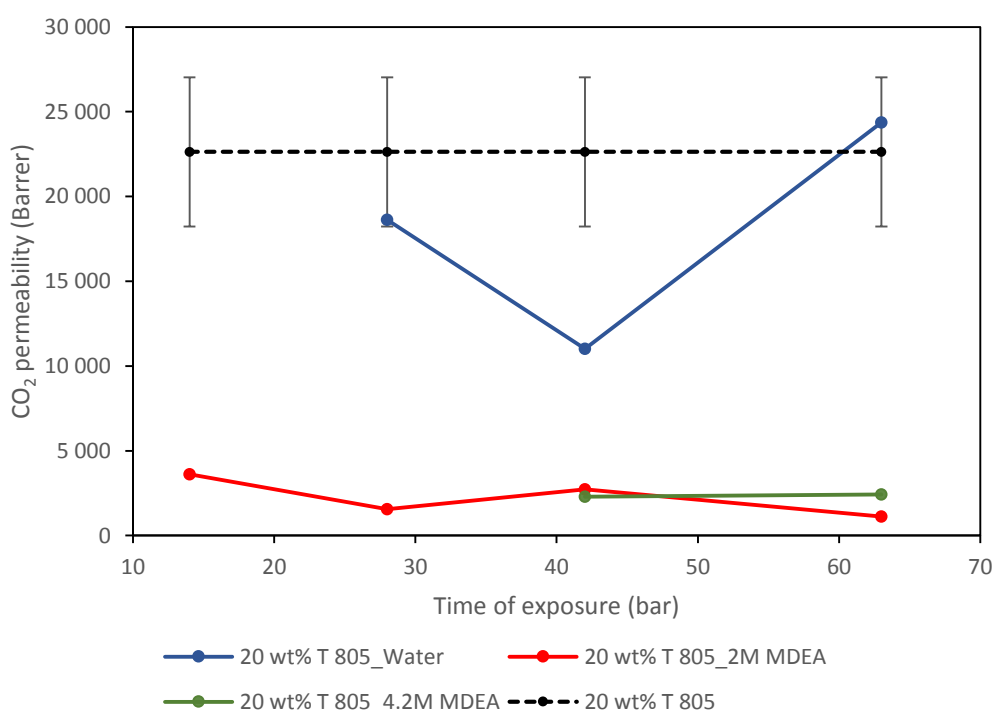


Figure 9-5: CO₂ permeability at 2 bar for liquid exposed membranes containing 20 wt% T 805 TiO₂. The broken line shows the permeability of the unexposed nanocomposite.

The lack of data at 14 days of exposure to water is caused by a fracture in the membrane sample. Due to lack of time, a second test was not given priority. For exposure to water for 28, 42 and 66 days, the results vary quite a lot. This differs from what was observed for the membrane containing 5 wt% of the same type of nanoparticles, for which the permeability stabilized after 14 days of exposure (Figure 9-3). After 28, 42 and 66 days in contact with water, the CO₂ permeability is approximately 18 600, 11 000 and 24 000 Barrer, respectively. The first and last value both lies within the uncertainty range of the unexposed membrane. An increase in permeability was also observed for CH₄ in the last interval (48-66 days). The increase may have been caused by irregularities in the system. The membrane was tested in PR-2, which is suspected to have a significant risk of leakage. A second test should have been conducted to reveal whether or not this was a random result.

For a liquid concentration of 2 M MDEA, the membrane has suffered a significant decrease in permeability already after 14 days of exposure. At this point, the CO₂ permeability equals about 3 600 Barrer. As the time of exposure increases, only slight changes in the permeability are observed. After 63 days of exposure, the permeability has decreased to approximately 1 100 Barrer. This represents a 95% decrease in permeability compared to the average permeability of the unexposed membrane. This is slightly lower than the CO₂ permeability of the membrane containing 5 wt% of the same type of nanoparticles exposed to 2 M MDEA for the same amount of time.

For the highest concentration of liquid, only two tests are conducted; one at 42 days, the other at 63 days. The measured CO₂ permeability of the membrane exposed to 4.2 M MDEA for 42 days equals about 2 300 Barrer. As the time of exposure increases to 63 days, the permeability is about 2 400 Barrer, which is 11% of the initial value. This value is more than twice as high as for the membrane exposed to 2 M MDEA for the same amount of time. However, by taking the expected uncertainty in the measurements into account (see Table 9-1), it may be concluded that exposure to MDEA solutions of different concentrations have resulted in approximately the same permeabilities.

Figure 9-6 gives the CO₂/CH₄ selectivity of the membranes containing 20 wt% T 805 TiO₂. As the broken line illustrates, the average selectivity of the unexposed nanocomposite membrane is 1.9. The standard deviation of ±0.1 is also included, though barely visible. For all liquid-exposed membranes, the selectivity is higher than that of the unexposed membrane. The difference is most prominent for the ones exposed to MDEA solutions. Long-term exposure to water has resulted in a selectivity equal to 3.1, which is 63% higher than the initial selectivity. As seen in Figure 9-5, the increased selectivity is accompanied by a permeability somewhat higher than the average value of the unexposed membrane. At this point, the permeability of CH₄ and CO₂ at 2 bar has decreased with 34% and increased with 8%, respectively, compared to the initial value. However, compared to the results obtained after 42 days, the permeability of both gases increases. As mentioned, this could be a random result affected by leakage.

For 2 MDEA, the relatively stable CO₂ permeability (84-90% lower than the initial value) is accompanied by a relatively stable selectivity. After 14 days of exposure, the selectivity is 8.6. As the time of exposure increases, a slight change in the selectivity is observed. Long-term exposure to 2 M MDEA (63 days) have resulted in a selectivity of 10.7. This value is 5.5 times higher than that of the unexposed membrane. When comparing the permeability and selectivity of the membranes exposed to 2 M MDEA, the highest and lowest permeability at 14 days and 63 days is accompanied by the lowest and highest selectivity, respectively.

The highest CO₂/CH₄ selectivity is observed for the membrane exposed to 4.2 M MDEA for 42 days. At this point, the selectivity equals 12.6. This value is 6.5 times higher than that of the unexposed membrane. As the time of exposure increases to 64 days, the selectivity decreases to 8.8. As seen in Figure 9-5, the decrease in selectivity is accompanied by a slight increase in permeability. For the long-term exposure to MDEA solutions, the membrane exposed to the highest concentration exhibits the highest permeability and lowest selectivity of the two.

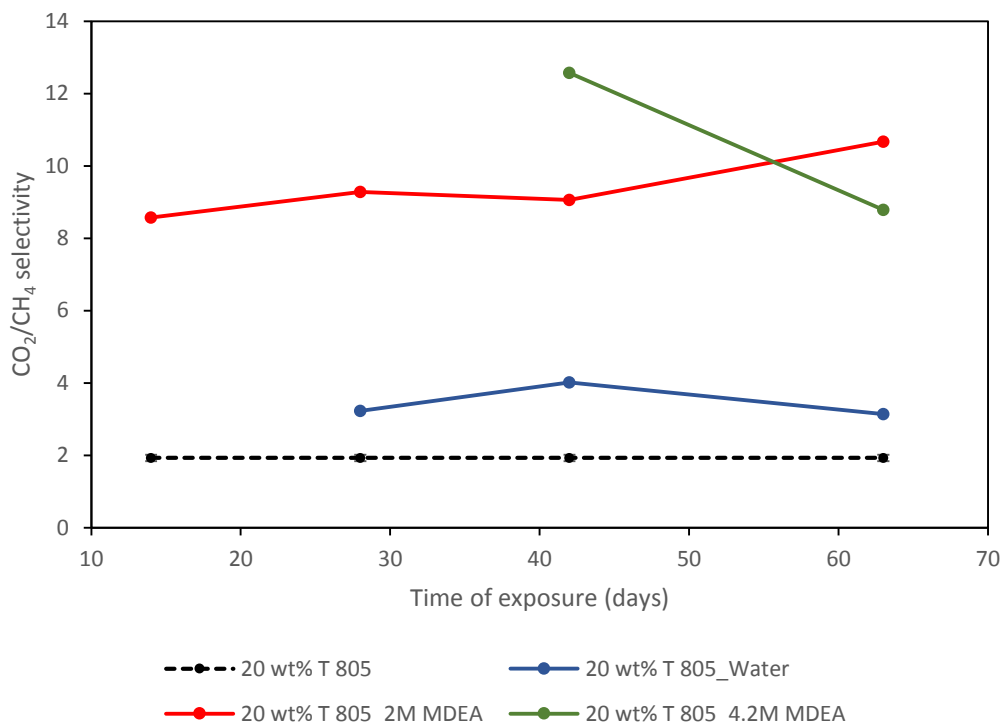


Figure 9-6: CO₂/CH₄ selectivity at 2 bar for liquid exposed membranes containing 20 wt% T 805 TiO₂. The black broken line corresponds to the selectivity of the unexposed nanocomposite.

9.1.5.3 Membranes containing 5 wt% 15-400 nm TiO₂

Figure 9-7 shows the CO₂ permeability at 2 bar for the membranes containing the smallest TiO₂ nanoparticles provided by SINTEF Materials and Chemistry (15-400 nm). The broken line represents the average CO₂ permeability at 2 bar for the unexposed membrane, which is 23 587 Barrer. The error bars show the standard deviation of ± 2 153 Barrer. During the first 14 days of exposure, the permeability decreases for all concentrations as the time of exposure increases. Apart from the membrane exposed to water for 1 day, the measured permeabilities are lower than that of the unexposed membrane for all concentrations and durations of exposure.

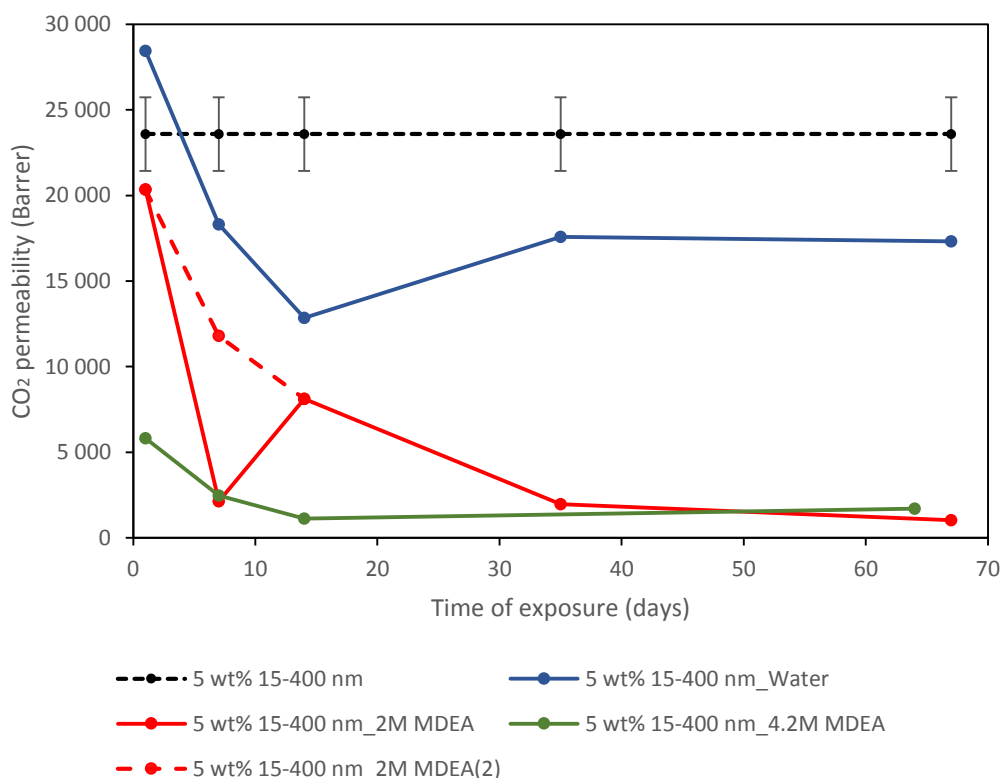


Figure 9-7: CO₂ permeability at 2 bar for liquid exposed membranes containing 5 wt% 15-400 nm TiO₂. The broken line in black shows the permeability of the unexposed nanocomposite.

After 1 day of exposure to water, the CO₂ permeability is higher than that of the unexposed membrane and lies above the uncertainty range. The corresponding permeability of CH₄ is lower than the average initial value, but is still within the uncertainty range (see appendix). The liquid can have affected the membrane in such a manner that the CO₂ permeability has increased. However, this is unlikely for water after only 1 day of exposure. Another explanation could be that the specific sample is taken from an area on the main membrane where the properties, e.g. free volume and nanoparticle dispersion, secures a better transport of gas. The value obtain is about 28 500 Barrer, which is within the range of the values reported for nanocomposites of PTMSP and TiO₂ in literature [2, 37]. Leakage in the permeation rig (PR-2) may also have contributed to the high permeability.

After 14 days of exposure to water, the permeability is reduced to approximately 12 900 Barrer. As the time of exposure increases to 35 days, an increase in the CO₂ permeability is observed. At this point, the value is about 17 600 Barrer. Beyond 35 days of exposure, the permeability levels off. Long-term exposure (67 days) to water results in a CO₂ permeability of about 17 300 Barrer. This represents a 27% decrease in CO₂ permeability compared to the unexposed membrane.

For the membrane exposed to 2 M MDEA, an overall decrease in permeability is observed as the time of exposure increases. At 7 days of exposure, two tests are conducted, as the dashed line in red illustrates. For both membranes, a reduction in permeability is observed. However, the first membrane suffered a more drastic reduction in permeability compared to the other. A clear difference between two tests was also observed for 5 wt% T 805 exposed to 2 M MDEA for 14 days (Figure 9-5). Again, the age of the two membrane samples differs, the second membrane being twice as old as the first. However, unlike what is observed in Figure 9-5, the second membrane showed the highest permeability. Based on the age of the membranes, the oldest membrane is expected to have the

lowest permeability. As previously mentioned, the properties of the membrane samples may differ as they are taken from different areas of the main membrane. As a result, the effect of liquid exposure may also differ, causing the first membrane to be more severely affected by 2 M MDEA than the second one.

As for the water-exposed membranes, the rate of change is highest during the first weeks of exposure to 2 M MDEA. As the time of exposure increases, the values seem to level off. When going from 1 day to 35 days, the CO₂ permeability decreases from about 20 400 to 2 000 Barrer (-540 Barrer/day). From 35 to 64 days, the permeability decreases to approximately 1 000 Barrer (-32 Barrer/day). This value is only 4% of the initial permeability of the unexposed membrane.

As observed for the majority of the nanocomposites investigated both in the specialization project and this master project, the membranes exposed to 4.2 M MDEA have suffered a dramatic decrease in permeability already after 1 day of exposure. For this membrane, the CO₂ permeability is only 25% of the initial value after 1 day. The permeability continues to decrease as the time of exposure increases. After 64 days, the permeability is approximately 1 700 Barrer, which is only 7% of the initial value. Long-term exposure to 4.2 M MDEA have resulted in a CO₂ permeability 700 Barrer higher than that of the membrane exposed to 2 M MDEA for the same amount of time. However, by taking the uncertainty in the measurements into account, it may be assumed that the long-term exposure to MDEA solutions have resulted in approximately the same permeabilities.

Figure 9-8 shows the CO₂/CH₄ selectivity at 2 bar for the membranes containing 5 wt% 15-400 nm TiO₂. As for the other types of membranes, the results vary somewhat during the first weeks of exposure. As the broken line in black illustrates, the selectivity of the unexposed nanocomposite membrane is 2.5. The standard deviation of ±0.3 is also included. For all liquid-exposed membranes, the selectivity is higher than this, the value increasing with liquid concentration and time of exposure. After 1 day of exposure, the selectivity increases in the order: water > 2 M MDEA > 4.2 M MDEA. The permeability decreased in the same order.

Beyond 14 days of exposure, the trends are somewhat different than what is observed for the other types of membranes. As the figure shows, the selectivity of the membranes exposed to water and 2 M MDEA continue to increase as the time of exposure increases. This is because the permeability of CH₄ decreases at a higher rate than the permeability of CO₂.

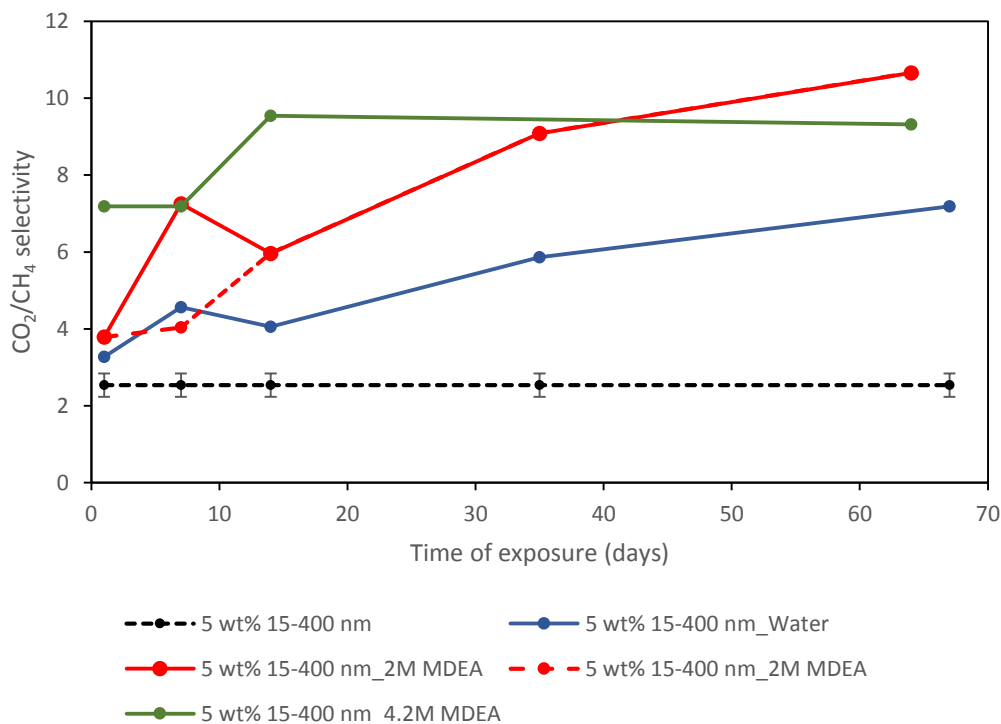


Figure 9-8: CO_2/CH_4 selectivity at 2 bar for liquid exposed membranes containing 5 wt% 15-400 nm TiO_2 . The black broken line corresponds to the selectivity of the unexposed nanocomposite.

For the water-exposed membranes, the CO_2/CH_4 selectivity increases from 4.1 to 5.9 as the time of exposure increases from 14 to 35 days. As seen in Figure 9-7, the CO_2 permeability levels off beyond 35 days of exposure, the value decreasing with only 1% when going from 35 to 67 days. The CH_4 permeability, on the other hand, decreases with 20% in the same interval (see appendix). As a result, the CO_2/CH_4 selectivity continues to increase. After 67 days of exposure to water, the selectivity has increased to 7.2. Compared to the unexposed membrane, this value is nearly three times higher.

As for the water-exposed membranes, fluctuations in the selectivity during the first 14 days of exposure are followed by a steady increase for the membranes exposed to 2 M MDEA. After 14 days of exposure, the selectivity is 6.0. The 76% decrease in permeability observed when going from 14 days to 35 days is accompanied by a 52% increase in selectivity (from 6.0 to 9.1). After 63 days of exposure, the selectivity has further increased to 10.7. Though the permeability of both gases decreases, the selectivity increases because the permeability of CH_4 decreases more than that of CO_2 . This could be a combined effect of diffusivity and solubility.

The membrane exposed to 4.2 M MDEA for 1 day has a CO_2/CH_4 selectivity of 7.2. This value is nearly three times higher than the initial selectivity of the unexposed membrane. Compared to the membranes exposed to water and 2 M MDEA for 1 day, the selectivity is about twice as high. As mentioned in the previous paragraph, the selectivity increases due to the fact that the permeability of CH_4 decreases more than that of CO_2 . This can be seen from Table B-9 in the appendix.

9.1.5.4 Membranes containing 5 wt% $>1 \mu\text{m}$ TiO_2

Figure 9-9 shows the CO_2 permeability at 2 bar for the membrane containing 5 wt% $>1 \mu\text{m}$ TiO_2 . The broken line represents the average CO_2 permeability at 2 bar for the unexposed membrane, which is approximately 22 653 Barrer. The error bars show the standard deviation of ± 240 Barrer. As observed

for the other types of membranes, the values are fluctuation somewhat during the first 14 days of exposure. The measured permeability of all membranes lies below that of the unexposed membrane. Beyond 14 days of exposure, a steadier decrease in permeability is observed.

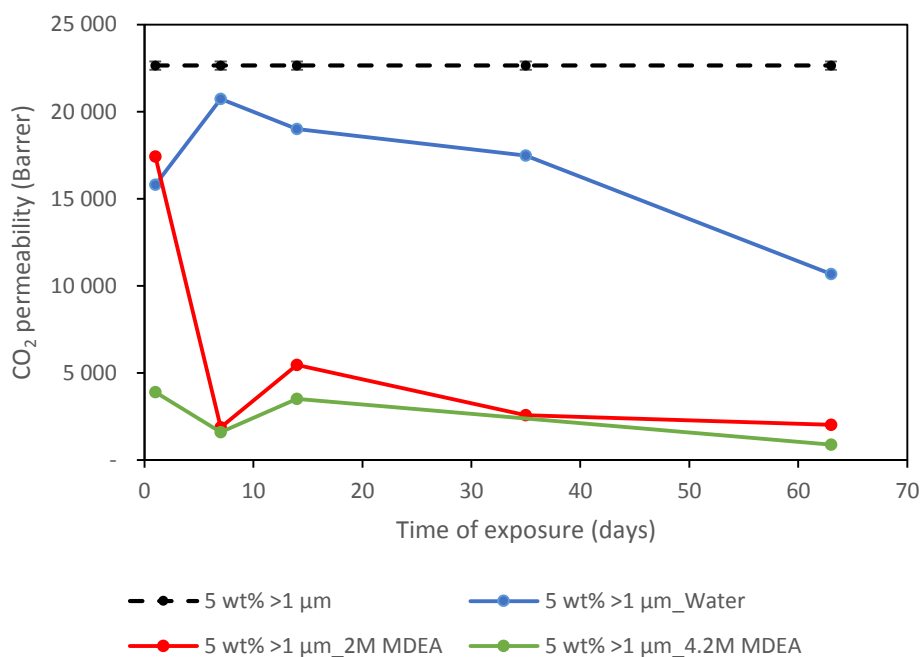


Figure 9-9: CO₂ permeability at 2 bar for liquid exposed membranes containing 5 wt% >1 μm nm TiO₂. The broken line in black shows the permeability of the unexposed nanocomposite.

After 1 day of exposure to water, the CO₂ permeability has decreased to approximately 15 800 Barrer. In the second interval (1-7 days), the permeability of the water-exposed membrane increases to about 20 700 Barrer. From then on, the permeability decreases as the time of exposure increases. Unlike the membranes containing 5 wt% T 805 and 15-400 nm, the permeability does not level off as the time of exposure increases. Instead, a steady decrease in permeability is observed both for CO₂ and CH₄. After 67 days of exposure, the permeability has reached a value of approximately 10 700 Barrer, representing a 53% decrease in permeability compared to that of the unexposed membrane. This is the lowest permeability measured among the membranes exposed to water for this amount of time.

For the membranes exposed to 2 M MDEA, the permeability after 1 day is slightly higher than that of the water-exposed membrane (17 400 Barrer). In the second interval (1-7 days), the permeability has dropped to a fairly low level. For this particular sample, it was observed that liquid had penetrated the exposure unit and, thus, the downside may have been in contact with the liquid for some period of time. The fact that both sides are exposed to liquid may have reinforced the effect on the membrane performance, causing the marked reduction in permeability. After 14 days of exposure to 2 M MDEA, the permeability is almost 3 600 Barrer higher than after 1 week. This could indicate that the penetration of liquid has had a deteriorating effect on the membrane performance. Beyond 14 days of exposure, a steady decrease in permeability is observed for both CO₂ and CH₄. In the last interval (35-64 days), the measured CO₂ permeability decreases from about 2 600 to 2 000 Barrer. Thus, long-term exposure to 2 M MDEA has resulted in a CO₂ permeability that is only 9% of the initial value of the unexposed membrane.

Finally, for the membranes exposed to 4.2 M MDEA, the CO₂ permeability has dropped with 83% already after 1 day of exposure. In the second interval (1-7 days), a further decrease in permeability is observed. At 14 days, a slight increase in permeability is observed. This is probably due to the fact that this membrane was tested in PR-2- rather than PR-1. In the last interval, the CO₂ permeability is reduced to approximately 900 Barrer. This is only 4% of the initial value of the unexposed membrane. Another noteworthy observation is the sudden increase in gas flux that was observed while running the permeation test at 4 bar. It is suspected that a fracture in the sample occurred during testing, eliminating the resistance toward gas flow. The same was observed for the membrane containing 5 wt% T 805 TiO₂ exposed to 4.2 M MDEA for the same amount of time. These observations could indicate that the exposure to 4.2 M MDEA has decreased the mechanical stability of the membrane. As a result, the membranes may no longer be able to withstand the flow of gas at higher pressures.

Figure 9-10 shows the CO₂/CH₄ selectivity of the membranes containing 5 wt% >1 μm TiO₂. The broken line represents the average selectivity at 2 bar for the unexposed membrane, which is equal to 2.8. The standard deviation of ±0.1 is also included, though barely visible. Except for the membrane exposed to water for 1 day, all membranes exhibit selectivities higher than that of the unexposed membrane.

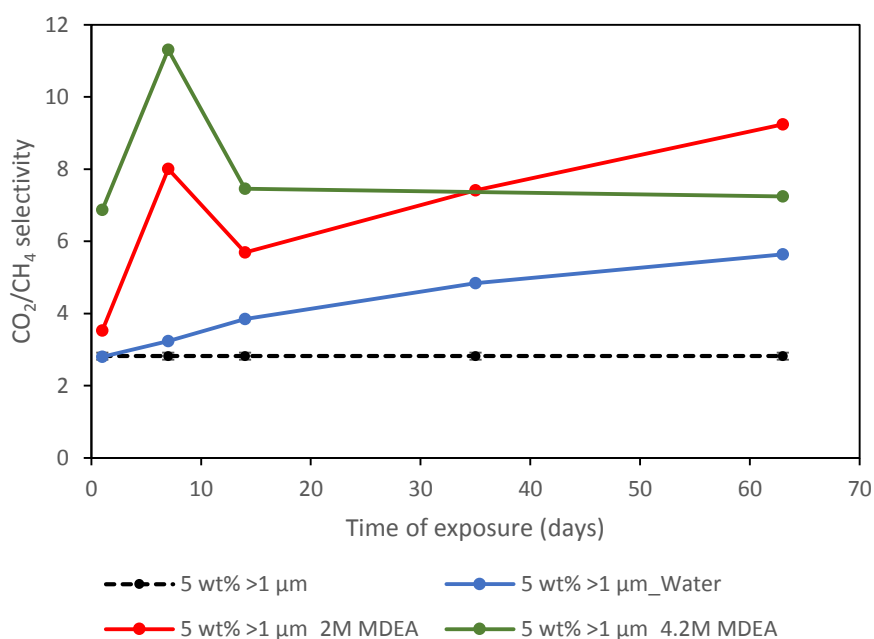


Figure 9-10: CO₂/CH₄ selectivity at 2 bar for liquid exposed membranes containing 5 wt% >1 μm TiO₂. The black broken line corresponds to the selectivity of the unexposed nanocomposite.

After 1 day of water-exposure, the selectivity is equal to that of the unexposed membrane. This is due to the fact that the relative decrease in the permeability is approximately the same for both CO₂ and CH₄. Beyond 1 day of exposure, a steady increase in selectivity is observed as the time of exposure increases. For the second interval (1-7 days), the increase in selectivity is accompanied by an increase in CO₂ permeability (Figure 9-9). This is because the relative change in CO₂ permeability within this interval is more than twice as high as that in CH₄. For the rest of the intervals, the decrease in CO₂ permeability is accompanied by an increase in selectivity. Again, this is because the decrease in the permeability of CH₄ is larger than that of CO₂. After 67 days of exposure to water, the selectivity has

increased to 5.6, which represents a doubling of the selectivity compared to the unexposed membrane.

For the membranes exposed to 2 M MDEA, a similar trend as for the water-exposed membranes is observed, only the values fluctuate somewhat during the first 14 days of exposure. 1 day of exposure has resulted in a selectivity of 3.5. At 7 days, the significant decrease in permeability observed for both gases is accompanied by a peak in the selectivity. This is due to the fact that the CH₄ permeability has decreased to a greater extent than that of CO₂. Beyond 14 days of exposure, a steady increase in selectivity is observed as the time of exposure increases. This matches the increase in permeability seen in Figure 9-9. Long-term exposure to 2 M MDEA has resulted in a selectivity of 9.2, which is three times as high as that of the unexposed membrane.

After 1 day, the membrane exposed to 4.2 M MDEA exhibits the lowest permeabilities and the highest selectivity. At this point, the permeability of CO₂ is nearly 7 times higher than that of CH₄. A peak in the selectivity is observed at 7 days of exposure. The selectivity is equal to 11.3, which is the highest value obtained for the membranes containing this type of nanoparticles. The peak in selectivity is accompanied by a drop in the CO₂ permeability, as seen in Figure 9-9. After 14 days of exposure, the selectivity is 7.5. In the last interval (14-64 days), the selectivity decreases to 7.3. This value is almost 160% higher than that of the unexposed membrane. Compared to the membranes exposed to 2 M MDEA for the same amount of time, the value is somewhat lower.

9.1.6 Summary of permeability results

Figure 9-11 shows the CO₂ permeability at 2 bar for all types of membranes exposed to liquid for the maximum amount of time (63-67 days). The corresponding CO₂/CH₄ selectivities are given in Figure 9-12. The initial values for the individual nanocomposites are also included for comparison. As seen in the first figure, the unexposed membranes exhibit approximately the same permeability. Except for the water-exposed membrane containing 20 wt% T 805, the permeabilities of the liquid-exposed membranes are lower than those of the unexposed membranes. This is especially true for the membranes exposed to MDEA solutions, for which the permeability of all membranes are less than 10% of the initial value. The water-exposed membranes exhibit a larger range of permeabilities compared to the unexposed membranes and the ones exposed to MDEA solutions.

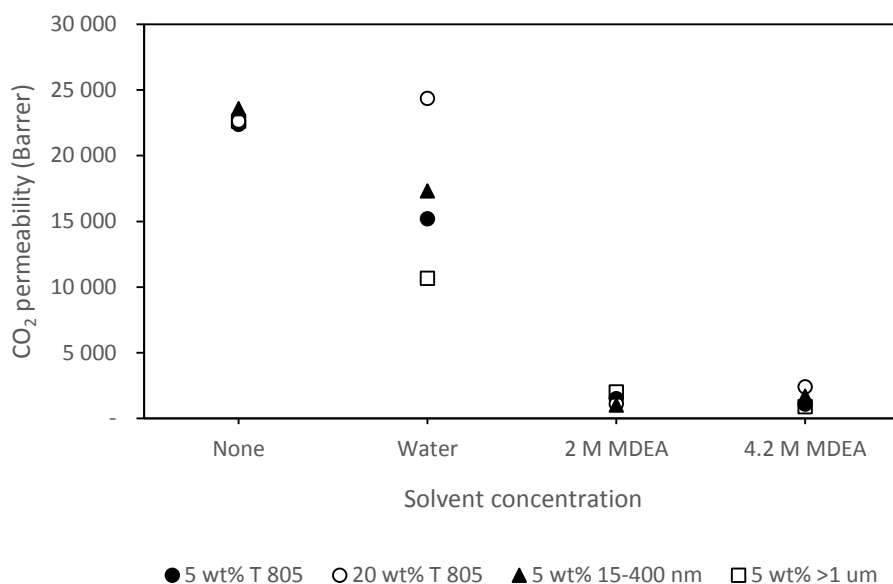


Figure 9-11: CO₂ permeability at 2 bar for all four types of nanocomposites, both unexposed membranes and membranes exposed to liquid for the maximum amount of time.

As seen in Figure 9-12, the CO₂/CH₄ selectivities are higher for the long-term liquid-exposed membranes than for the unexposed membranes. The values are higher for the membranes exposed to MDEA solution than for the ones exposed to water. Compared to unexposed membranes, the relative difference between the individual membranes is somewhat larger for the liquid-exposed membranes, especially for the ones exposed to water.

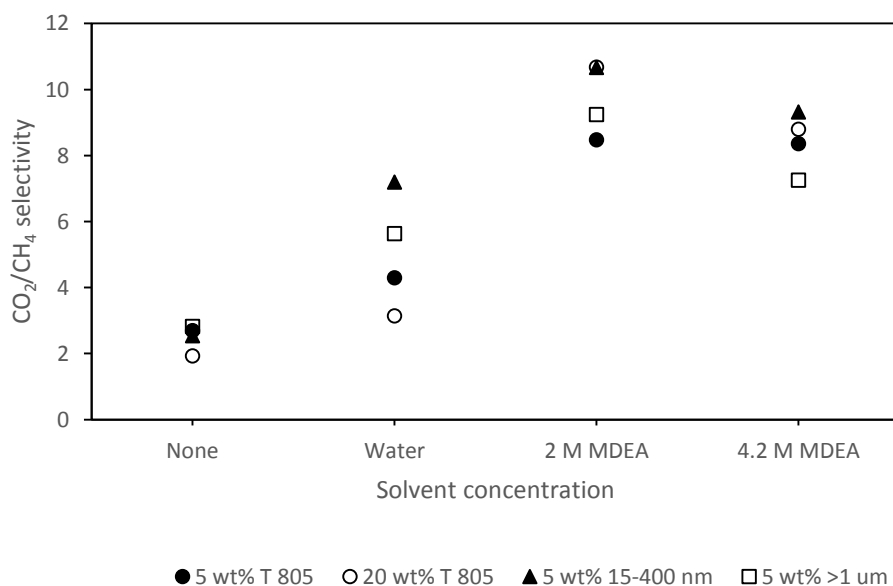


Figure 9-12: CO₂/CH₄ selectivity at 2 bar for all four types of nanocomposites, both unexposed membranes and membranes exposed to liquid for the maximum amount of time.

For a majority of the membranes presented in the previous figures, a decrease in the permeability is accompanied by an increase in CO₂/CH₄ selectivity. The observations have been explained by the larger decrease in the permeability of CH₄ than that of CO₂. According to equation 3.8, this gives rise to a

higher selectivity. As stated in the theoretical part of the report, permeability changes derive from changes in the diffusion coefficient, the solubility coefficient, or both (see equation 3.3). For mixed matrix membranes based on PTMSP, the addition of TiO₂ particles is meant to disrupt the chain packing, increase the free volume and, in turn, increase the diffusivity. The fillers may also affect the solubility coefficients. When a decrease in permeability is observed after liquid exposure, the opposite may have occurred. That is, the liquid exposure may have affected the membrane in such a manner that the free volume has decreased. This would cause a decrease in diffusivity and, as a result, a decrease in permeability. Such a densification of the polymer structure would affect the permeability of both CO₂ and CH₄. However, as CH₄ is a somewhat bigger molecule than CO₂ (3.8 Å and 3.3 Å), the decrease in free volume is expected to have a stronger effect on the transport of CH₄ than that of CO₂. This could explain the increase in the CO₂/CH₄ selectivity. The hole geometry may also have been affected by liquid exposure. The CO₂ and CH₄ molecules have a linear and tetrahedral geometry, respectively, and thus, the two penetrants are affected by changes in the hole geometry to different extents.

Changes in the gas permeability may also be linked to changes in the solubility coefficient. However, this effect is somewhat more difficult to visualize. The liquid contact may have affected the membranes in such a manner that the sorption of gas decreases. According to equation 3.3, this would cause a decrease in the permeability. An increase in the CO₂/CH₄ selectivity could indicate that the solubility coefficient of CO₂ is less affected than that of CH₄. This could be due to the fact that CO₂ is more condensable and interacts more strongly with the polymer and the TiO₂ particles. Thus, the diffusivity coefficient and/or the solubility coefficient of both gases may have been reduced as a result of the exposure to liquid. This would explain the reduction in permeability. Since CO₂ is smaller and more condensable than CH₄, it may be expected that the reduction in the coefficients would be less than for CH₄. This would explain the increase in selectivity. However, this is only assumptions and the effect of liquid exposure could be much more complex.

When an increase in permeability is observed for both CO₂ and CH₄, this could be caused by trans-film defects. This is especially true when the permeability increases with increasing feed pressure. Additionally, leakage in the permeation system would also contribute to higher values of the permeability. The liquid may have affected the polymer in such a manner that the membranes have become more susceptible to swelling by CO₂. However, this is probably not likely to occur due to the large amount of free volume in the polymer matrix [19]. Additionally, no swelling of PTMS with water is reported in literature [53]. For PTMSP immersed in primary MEA, secondary DEA and tertiary TEA, the swelling is reported to be limited [44]. Based on these observations, swelling of PTMSP in water and aqueous solutions of the tertiary MDEA is expected to be limited for the membranes investigated in this work.

The liquid-exposed membrane areas are taken from different parts of the main membrane. The prepared membranes have quite a large area and can therefore have local varieties with respect to thickness, morphology and particle dispersion. This could, in turn, affect the performance of the samples taken from different parts of the membrane. As seen in the previous figures, two tests performed on the same type of membrane with the same exposure have in some cases given two very different results (see Figure 9-3 and Figure 9-7). The fact that the tested membrane areas originate from different parts of the main membrane might have an influence on the impact of liquid exposure on the individual testing areas. As mentioned, only the upside of the membranes are exposed to liquid. Ideally, the downside is kept completely dry. However, for some membranes the liquid has penetrated the exposure unit. Therefore, the downside of the membranes may in some cases have been in contact with the liquid for some period of time. This may have affected the results.

If liquid is present inside the polymer matrix, this would increase the resistance toward gas transport, causing a decrease in permeability (see Section 5.4). The liquid-exposed membrane samples investigated in this work have been stored at ambient conditions for at least one day before ahead of testing. Additionally, the membrane cell and permeation system is evacuated for at least 8 hours. Therefore, it is assumed that no liquid is present inside the membrane samples. This assumption has not been further investigated. However, neither changes in chemical structure or traces of solvent were detected by FT-IR spectroscopy in previous studies at NTNU [99].

9.2 Contact angle measurements

9.2.1 Uncertainty in contact angle measurements

As the contact angle apparatus is manually operated (droplet deposition, stage level, stage tilt, baseline), the experimental error in the measurements is expected to be significant. The calibration is also done manually and contributes to the overall uncertainty in the measurements. One of the greatest sources of uncertainty in the measurement is perhaps the determination of the baseline, as it is very difficult to obtain an accurate position.

To quantify the uncertainty in the results, the contact angle is measured on several places on the membrane surface. For the unexposed membrane, the procedure is repeated on several samples from different areas on the main membrane. The uncertainty is given in form of standard deviations and these are included in Table 9-3 and Table 9-4. As seen, the uncertainty ranges approximately 1.1 to 7.4°.

In a previous phase of the project, it was observed that the contact angle of a drop on a membrane surface was unstable with time. The same was observed in this year's work. It was decided to use the value of the contact angle measured 30 seconds after deposition. At this point, it was expected that the liquid droplet would be in equilibrium.

As previously mentioned, the contact angle is a quantitative measure of the wetting of a solid by a liquid. The contact angle is affected by the surface chemistry as well as by the surface roughness. To obtain an accurate value of the contact angle, the surface should be as smooth and even as possible. Several of the membranes investigated in this work has proven to be very uneven and, therefore, contact angle measurements have been difficult to carry out. The high degree of surface roughness will have a considerable effect on the measured contact angle. The values given in the following may therefore not be representative for the membrane material, but rather reflect the surface topography.

9.2.2 Contact angles of PTMSP and nanocomposite membranes

As described in Section 5.3, liquids offering higher values of surface tension, γ_L , have lower wetting potential than those offering lower values [100]. The surface tension of aqueous solutions of alkanolamines are less than that of water [101]. As a result, the breakthrough pressure is lower for MDEA solutions than for water. According to literature, the surface tension of aqueous MDEA solution decreases with increasing MDEA concentration [100]. The wetting ability of the three liquids used in

this work is therefore expected to increase in the following order: water > 2 M MDEA > 4.2 M MDEA. The same order is expected to be observed for the contact angles.

The contact angles of water, 2 M MDEA and 4.2 M MDEA on the upside and downside of pure PTMSP are given in Table 9-3. The values given in the table are the average of eight measurements made on two membrane samples from two different parts of the same membrane. The measurements were made shortly after preparation. The results show that the apparent contact angle is higher on the upside of the polymer film than on the downside. Based on these observations, it was concluded that the upside of the membrane should be exposed to liquid, while the downside should be kept dry. Another observation is that the contact angle on both sides of the polymer film decreases as the concentration of the liquid increases. In the case of water, the results indicate that the upside of the membrane is hydrophobic, as the contact angles larger than 90°. For 2 M and 4.2 M MDEA, the contact angles on both sides of the polymer film are lower than 90°. As for water, the contact angle on the downside is lower than that on the upside.

Table 9-3: Contact angles of water, 2 M MDEA and 4.2 M MDEA on the upside and downside of pure PTMSP.

Liquid	Contact angle (°)	
	Upside	Downside
Water	103.41 ± 2.41	85.83 ± 6.98
2 M MDEA	83.13 ± 2.43	75.85 ± 3.81
4.2 M MDEA	80.21 ± 2.60	65.72 ± 1.99

As stated in the theoretical part of the report, the contact angle is affected by the surface chemistry as well as by the surface roughness. Increasing roughness enhances the existing wetting behavior. In the case of very rough surfaces, the measured contact angles reflect surface topography rather than surface energetics. The higher contact angle on the upside of the membrane could be explained by the surface topography on this side of the membrane. A difference between the two sides of the membranes is visible even to the naked eye. The upside seems rougher than the downside, with particles protruding from the surface. The downside of the membranes appear smoother. This is further investigated by SEM analysis (Section 9.3).

Table 9-4: Contact angles on upside and downside of nanocomposite membranes.

Membrane type	Contact angle (°)			
	Water		2 M MDEA	
	Upside	Downside	Upside	Downside
5 wt% T 805	104.15 ± 1.14	82.22 ± 1.51	78.50 ± 1.60	77.27 ± 2.17
20 wt% T 805	100.88 ± 1.51	73.10 ± 2.30	82.57 ± 3.84	78.02 ± 7.42
5 wt% 15-400 nm	107.90 ± 6.39	86.16 ± 6.45	84.94 ± 4.91	80.10 ± 2.98
5 wt% >1 μm	105.23 ± 1.73	84.62 ± 4.71	84.72 ± 1.40	73.35 ± 5.63

9.2.3 Contact angles of membranes prepared on casting plates of Teflon

Membranes containing 5 and 20 wt% commercial Aeroxide® T 805 TiO₂ were prepared on casting plates of Teflon. Figure 9-13 shows images of a drop of water on the upside and downside of membranes containing 5 wt% T 805 prepared on glass and Teflon, respectively. For the membrane prepared on glass, the water contact angle is higher on the upside of the membrane than on the downside. The opposite is observed for the membrane prepared on a casting plate of Teflon. The contact angle of the water drop displayed in Figure 9-13d is approximately 126°. The corresponding value of the membrane containing 20 wt% T 805 is approximately the same. These values are almost 20° higher than on the upside of the membranes prepared on glass. The results clearly indicate that there is a difference between the membranes prepared on Teflon and glass. This is further explored in Section 9.3 concerning SEM analysis.

According to the figure, the water contact angle is higher on the upside of the membrane prepared on glass than on the membrane prepared on Teflon. This is not expected to be caused by the use of different casting plates.

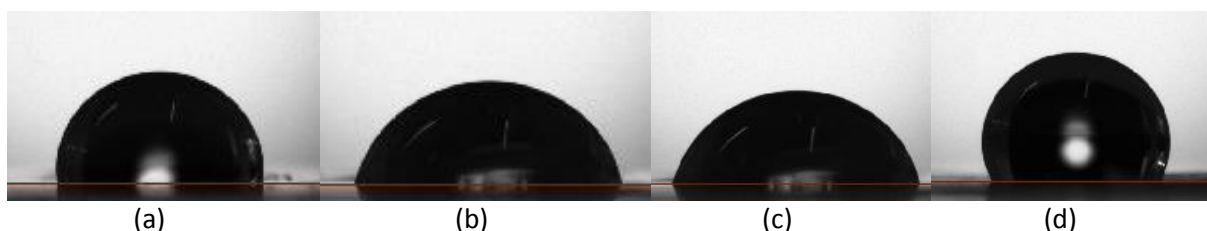


Figure 9-13: Water contact angles on (a) upside and (b) downside of membrane prepared on glass, and (c) upside and (d) downside of membrane prepared on Teflon. Both membranes contain 5 wt% T 805 TiO₂.

9.2.4 Contact angles of liquid-exposed nanocomposite membranes

The water contact angles of the different types of nanocomposites are presented in the following. Both values of unexposed and liquid-exposed nanocomposites are included, showing how the contact angle changes as the time of exposure increases. All results are listed in tables in the appendix. The results presented in the following are based on measurements conducted towards the end of the semester after the membranes had been tested in the gas permeation rigs. Therefore, the obtained results may be affected both by aging of the membrane and by interaction with gas. As the tables in the appendix show, a few measurements were made ahead of the permeations tests. In some of the cases, the two tests have given very different results. This could indicate that the interaction between membrane and gas has resulted in some changes on the membrane surface. Another explanation is that the membrane samples are taken from different parts of the main membrane. As the membrane is not perfectly homogeneous, the properties of the membrane may vary, causing a variation in contact angles.

Only the contact angles on the upside of the membrane samples were measured. This was the side of the membrane exposed to liquid and therefore the one expected to be most affected by the liquid contact.

9.2.4.1 Membranes containing 5 wt% T 805 TiO₂

Figure 9-14 shows how the water contact angle changes as the time of exposure increases for membranes containing 5 wt% T 805 TiO₂. The broken line represents the average value of the unexposed membrane, which is 104°. As the figure shows, the contact angle decreases rapidly during

the first 14 days of exposure. Apart from the membrane exposed to 4.2 M MDEA for 1 day, all membranes exhibit contact angles lower than 90°.

For the water-exposed membranes, the contact angle has decreased to a value slightly below 60° after 14 days of exposure. After 64 days of exposure, the measured contact angle is somewhat higher, but still significantly lower than for the membranes exposed to MDEA solutions. Compared to the unexposed membrane, long-term exposure to water has resulted in a decrease in contact angle of almost 40%. For the membranes exposed to MDEA solutions, the results follow the same trend. At 1 day and 14 days of exposure, the contact angles on the membrane surfaces exposed to 4.2 M MDEA are somewhat higher. After 64 days of exposure, the opposite is observed. At this point, the contact angles of the membranes exposed to aqueous MDEA solutions are both lower than 90°.

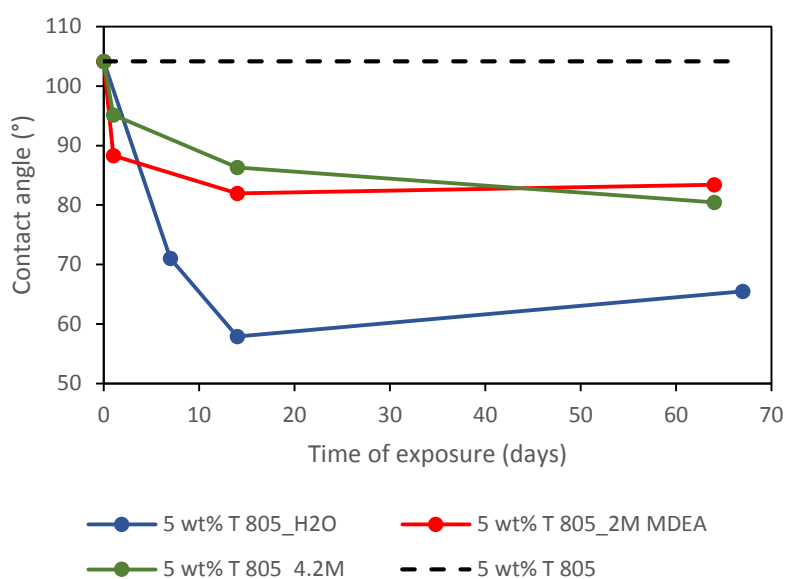


Figure 9-14: Contact angle of water on upside of membrane containing 5 wt% T 805 TiO₂ as a function of time of liquid exposure.

9.2.4.2 Membranes containing 20 wt% T 805 TiO₂

The results for the membrane containing 20 wt% T 805 TiO₂ are shown in Figure 9-15. Again, the broken line represents the unexposed membrane having an average water contact angle of 101°. These membranes were exposed to water and MDEA solutions for a minimum of 14 days. Contact angles are measured on surfaces exposed to liquid for 28 and 42 days. As seen for the membranes containing 5 wt% T 805 TiO₂, the results for the membranes exposed to MDEA solutions are approximately similar. For both membranes containing 5 and 20 wt% commercial particles, the measured contact angles are in the range 80-90° for the membranes exposed to 2 M and 4.2 M MDEA. After 63 days of exposure, both membranes show contact angles approximately equal to 90°.

As for the membranes containing 5 wt% T 805 TiO₂, a more significant decrease in contact angle is observed for the membranes exposed to water. After 28 days of exposure, the measured contact angle is approximately 60°, which represents a 40% decrease compared to the unexposed membrane. After 42 days of exposure, the measured contact angle is nearly unchanged.

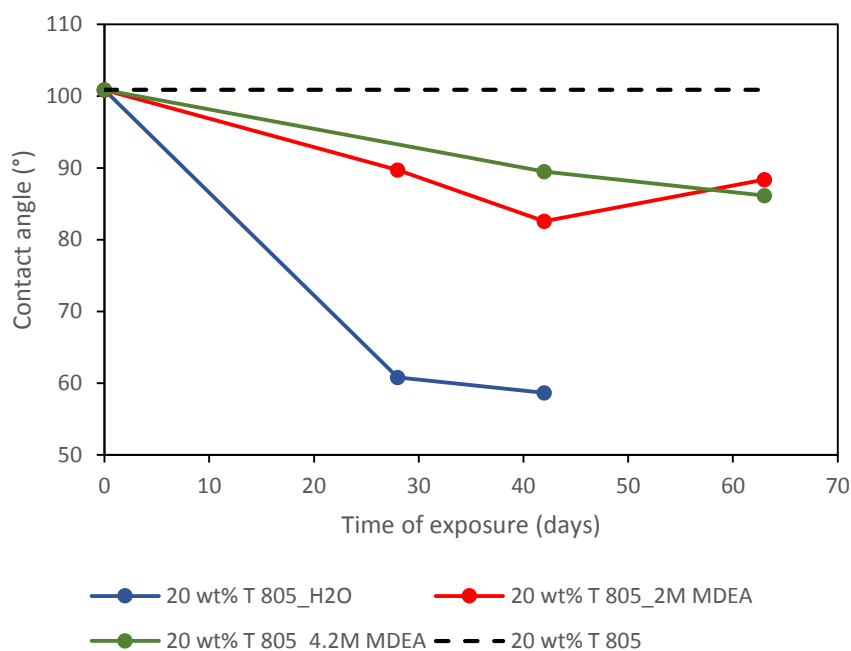


Figure 9-15: Contact angle of water on upside of membrane containing 20 wt% T 805 TiO_2 as a function of time of liquid exposure.

9.2.4.3 Membranes containing 5 wt% 15-400 nm TiO_2

Figure 9-16 shows the water contact angles on the upside of the membranes containing 5 wt% 15-400 nm TiO_2 provided by SINTEF Materials and Chemistry. The unexposed membrane – represented by the broken line in the figure – has an average contact angle of 108° . The trends observed for this membrane are comparable to those observed for the membrane containing 5 wt% commercial T 805 TiO_2 . The results for the membranes exposed to MDEA solutions follow the same trend, while the ones exposed to water lie at a lower level. After 1 day of exposure, the measured contact angle decreases in the order 4.2 M MDEA, 2 M MDEA, water. The same order is observed after long-term exposure, only the relative differences have increased.

Except for the membranes exposed to MDEA solutions for 1 day, all contact angles are below 90° . For the membranes exposed to MDEA solutions, the lowest contact angle is slightly below 80° . For the water-exposed membranes, the measured contact angle is below 70° after 14 days of exposure. After 67 days, the contact angle is approximately 60° , a value equal to about 55% of the initial value for the unexposed membrane.

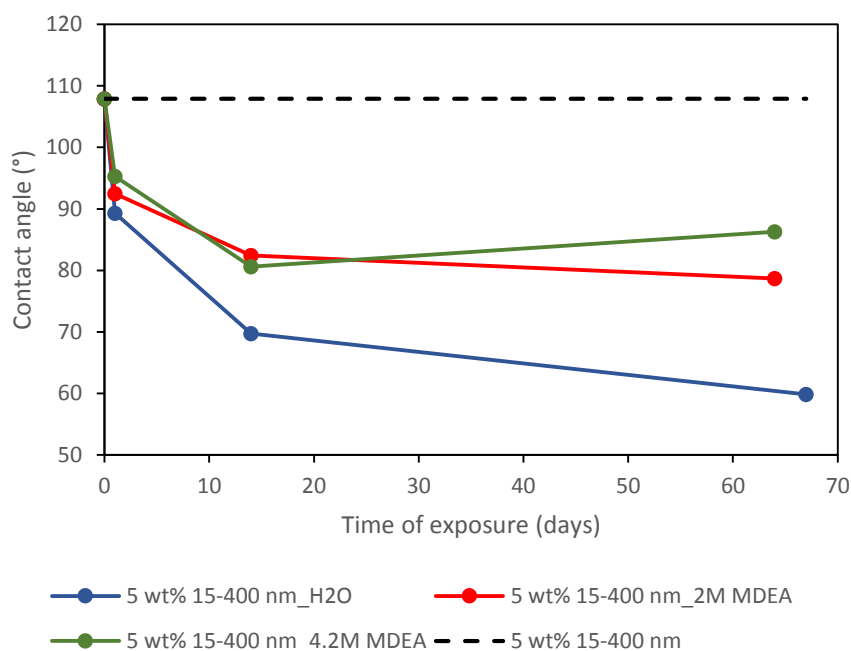


Figure 9-16: Contact angle of water on upside of membrane containing 5 wt% 15-400 nm TiO_2 as a function of time of liquid exposure.

9.2.4.4 Membranes containing 5 wt% $>1 \mu\text{m}$ TiO_2

Figure 9-17 shows the results for the membranes containing 5 wt% $>1 \mu\text{m}$ TiO_2 provided by SINTEF Materials and Chemistry. For the unexposed membrane, the average water contact angle is about 105° . As for the other types of membranes, a decrease in contact angle is observed already after 1 day of exposure, the value decreasing in the order 4.2 M MDEA $>$ 2 M MDEA $>$ water. As the time of exposure increases, the apparent contact angles continue to decrease. After 67 days of water-exposure, the contact angle is slightly above 60° . Long-term exposure to 2 M and 4.2 M MDEA have resulted in contact angles of between 80 - 90° . Thus, as previously observed, long-term exposure to water appears to have given the lowest contact angle.

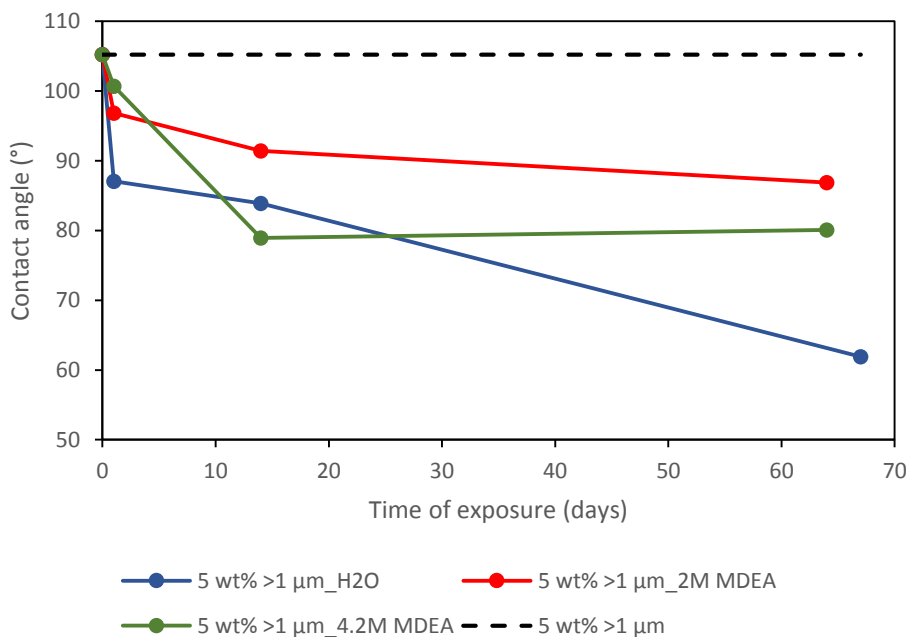


Figure 9-17: Contact angle of water on upside of membrane containing 5 wt% >1 μm TiO₂ as a function of time of liquid exposure.

9.2.5 Summary of contact angle measurements

For pure PTMSP, the average water contact angle on the upside and downside is measured to 103° and 86°, respectively. The former confirms the expected hydrophobicity of the polymer. The contact angles of MDEA solutions are lower than those of water and below 90°.

For the nanocomposite membranes, the water contact angle on the upside of the membranes are all higher than 100°. The average contact angle decreases in the following order: 5 wt% 15-400 nm, 5 wt% >1 μm, 5 wt% T 805, 20 wt% T 805. However, the uncertainties in the measurements are expected to be significant, and it is not possible to draw any conclusion regarding the degree of wettability for the different types of membranes. With 2 M MDEA as the liquid, the measured contact angle is lower than that of water and below 90° degrees for all types of membranes. As for pure PTMSP, the contact angles are higher on the upside than on the downside of the membrane

For the membranes prepared on Teflon, the water contact angle on the downside is higher than that on the upside. This is opposite of what is observed for the membranes prepared on casting plates of glass. The results clearly indicate that there is a difference between the membranes prepared on Teflon and glass. This is further explored in the following section concerning SEM analysis.

For all types of nanocomposites prepared on glass, the measured water contact angles are lower for the liquid-exposed membranes than for the unexposed membranes. In a majority of the cases, the water contact angle decreases as the duration of exposure increases. At the maximum time of exposure, all contact angles are lower than 90°. At this point, the contact angle decreases in the order 2 M MDEA, 4.2 M MDEA, water for all membranes apart from the ones containing 15-400 nm TiO₂, for which the membrane exposed to 4.2 M MDEA shows the highest contact angle.

Figure 9-18 shows the water contact angles for all types of membranes exposed to liquid for the maximum amount of time. As the figure illustrates, the contact angles on the water-exposed membranes lie on a lower level than for the ones exposed to MDEA solutions. The same was observed in a previous phase of the project for membranes containing 20 wt% T 805 TiO₂ (see Section 8) [99]. As mentioned in Section 6.2, previous research on gas-liquid membrane contactors have shown that membranes with high hydrophobicity is more resistant to wetting [49, 75, 100]. However, the hydrophobicity of a membrane may be altered as a result of liquid exposure. One potential explanation is a chemical reaction taking place between the membrane material and the aqueous MDEA solution. This may have increased the membrane surface tension and thereby increased the contact angle. In addition to a change in the chemistry of the membrane surface, the surface morphology may also be affected both by water and aqueous MDEA solutions. The individual effect of water and MDEA solutions on the surface chemistry and morphology may explain the results observed in Figure 9-18. The morphology of the liquid-exposed membranes is further addressed in the following section.

No obvious trend is observed for the different types of nanocomposite membranes. Therefore, it is difficult to draw any conclusions regarding the effect of liquid exposure on the membranes containing the different types of TiO₂ nanoparticles.

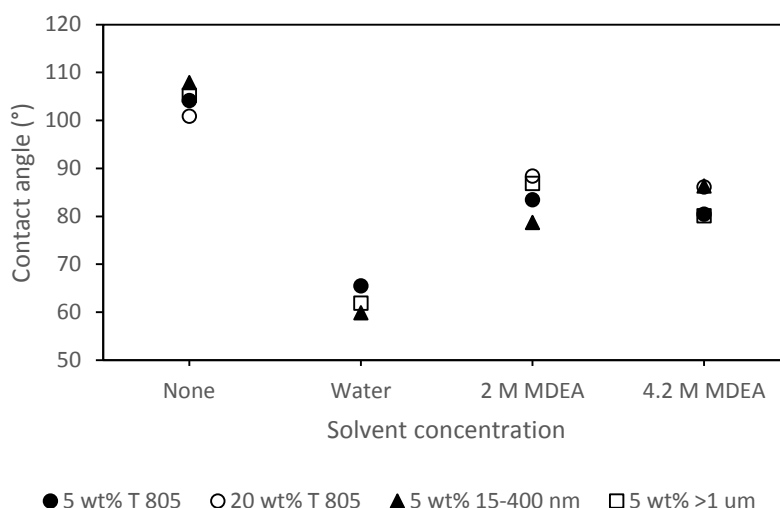


Figure 9-18: Water contact angles on upside of nanocomposite membranes. The exposed membranes with 5/20 wt% TiO₂ have been immersed in water for 66/67 days and in 2 M and 4.2 M MDEA for 63/64 days.

As mentioned, some of the membranes were tested ahead of the permeation tests. The values are included in the appendix. The results from these tests indicate that the contact angles on the membranes exposed to 4.2 M MDEA are lower than those on the water-exposed membranes. However, these measurements were made shortly after the membranes were removed from the beakers with liquid. Therefore, the membranes were probably not completely dry. This could explain why the values are lower for these membranes. The observations are not further investigated or discussed.

9.3 Scanning electron microscopy (SEM) images

9.3.1 Uncertainty in SEM analysis

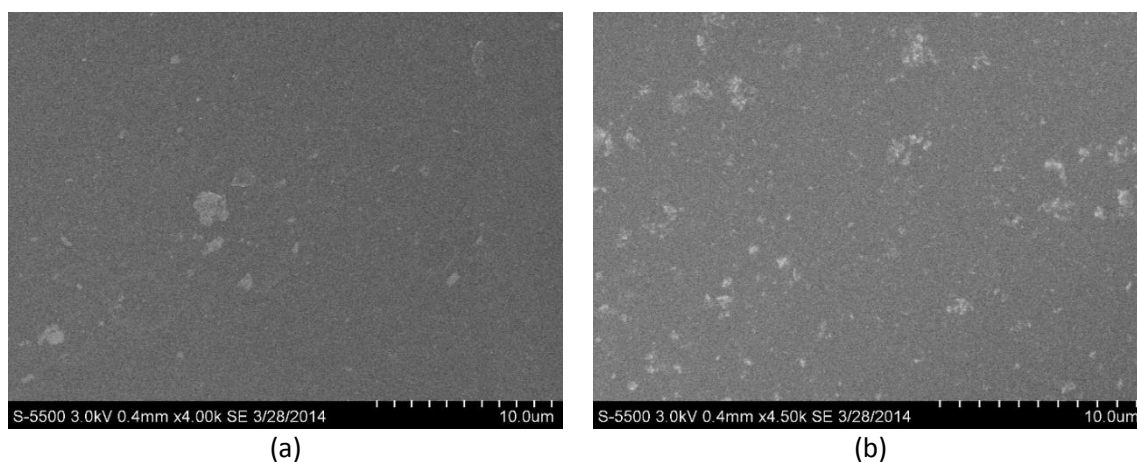
As the polymer samples are non-conducting, a conducting layer must be coated on top of the samples ahead of the characterization. This is crucial to obtain images of high quality. Usually, a 5 nm-layer of gold is sufficient. However, some images appear somewhat indistinct and some details may therefore be omitted from the image.

Only a tiny piece of each membrane is investigated in the microscope. Therefore, what is observed in the images may not be representative for the whole membrane sample. Ideally, several samples taken from different parts of the membrane should have been analyzed.

The samples are susceptible to damage during preparation. This may affect the surface of the membrane and, further, its appearance in the SEM images. Finally, the interpretations of the SEM images are subjective. As a result, details may have been misinterpreted or overlooked.

9.3.2 Unexposed membranes

Figure 9-19 show SEM images of the upside and downside of a membrane of pure PTMSP. The membrane is prepared on glass. As the images show, the upside is quite even with a few bright spots visible at some areas on the surface. These are probably undissolved polymer particles. As Figure 9-19b shows, the white spots are much more prominent on the downside of the membrane. This indicates some degree of particle settling during the transformation from polymer solution to dry film.



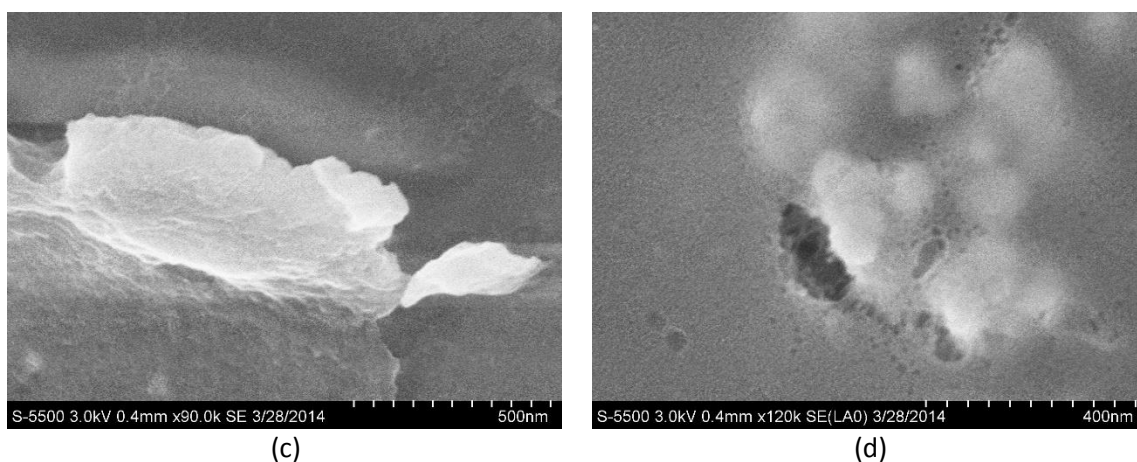


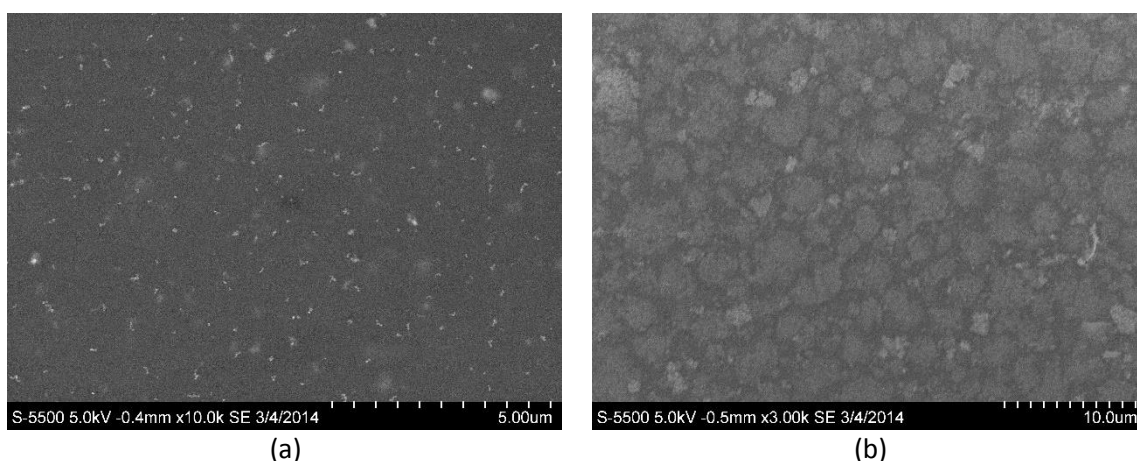
Figure 9-19: SEM images showing (a, c) upside and (b, d) downside of PTMSP membrane.

9.3.2.1 Membranes containing commercial T 805 TiO₂

Figure 9-20 and Figure 9-21 show the SEM images of the membranes containing 5 and 20 wt% commercial Aeroxide® T 805 TiO₂, respectively. Compared to the SEM images of the pure PTMSP, the presence of TiO₂ particles is obvious. Image c and d in Figure 9-21 show high-magnification images of TiO₂ particles on the surface of a membrane containing 20 wt% T 805.

The images show a clear difference between the upside and the downside of the flat sheet membranes. As stated in Section 7.1.5, the terms upside and downside of a membrane film refer to the air-side and casting plate-side, respectively. On the upside of the nanocomposite, some of the particles seem to be protruding from the surface. The downside appears more even, with larger white spots distributed across the surface. As mentioned for the membrane of pure PTMSP, this observation might indicate some settling of particles – both undissolved polymer and TiO₂ – during drying of the membrane films.

The two figures show how the density of particles on the surface increases as the fraction of TiO₂ increases from 5 to 20 wt%. When comparing the high-magnification images of the surfaces (Figure 9-20c and Figure 9-21c), it could seem as if the collection of particle aggregates are somewhat bigger at a content of 20 wt% than at 5 wt%. As mentioned in Section 6.1 an increase in aggregate size with particle loading is observed in other studies on nanocomposites of PTMSP and TiO₂. However, the observations made in this work could be mere coincidence. An analysis of the distribution of particles would be more accurate using TEM and/or AFM.



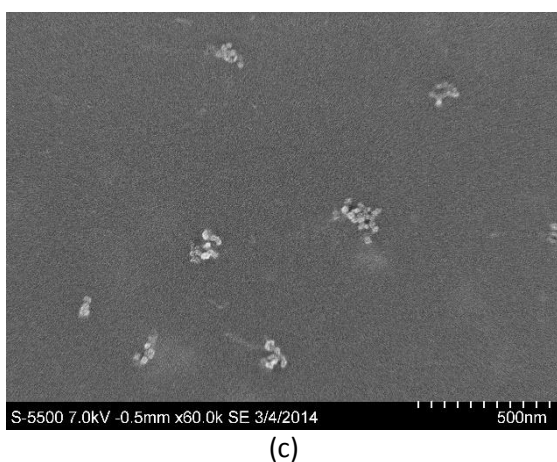


Figure 9-20: SEM images of (a and c) upside and (b) downside of membrane containing 5 wt% T 805 TiO_2 .

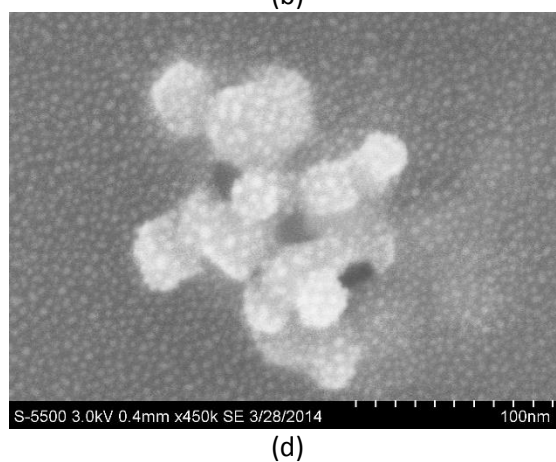
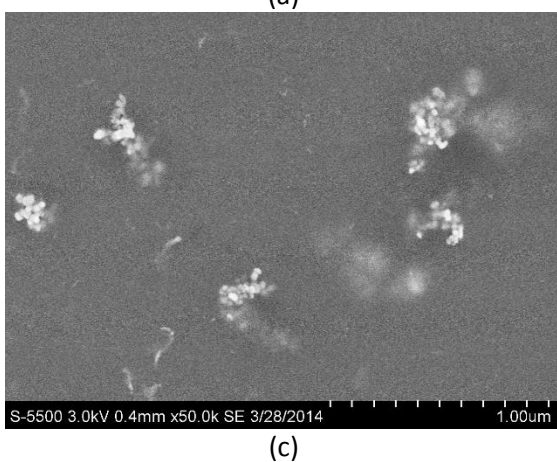
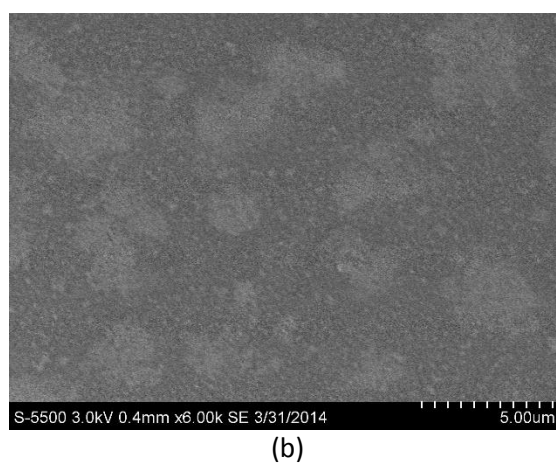
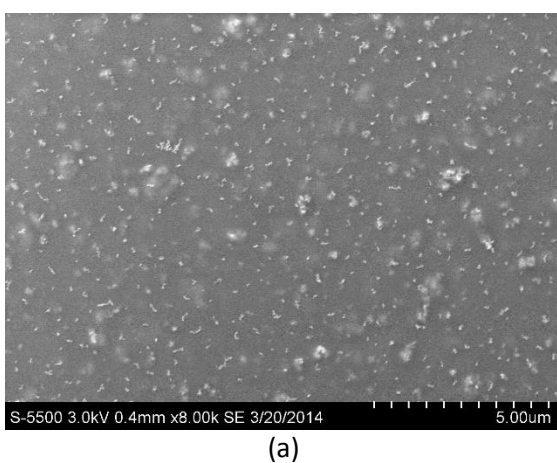


Figure 9-21: SEM images of (a, c, d) upside and (b) downside of membrane containing 20 wt% T 805 TiO_2 .

9.3.2.2 Membranes containing 5 wt% 15-400 nm TiO_2

Figure 9-22 shows the SEM images of membrane containing 5 wt% 15-400 nm TiO_2 from SINTEF Materials and Chemistry. Again, the presence of the TiO_2 nanoparticles is obvious. The high-magnification image (Figure 9-22d) suggests that this type of TiO_2 particles is smaller than the ones observed for the commercial particles. Additionally, both the upside and downside looks somewhat different than the ones observed in Figure 9-20 and Figure 9-21. The distribution of particles appears

more uneven and particles of different sizes are observed on both sides of the membrane. Additionally, scratches/stripes are observed on the upside of the nanocomposite which are not observed on any other surfaces. These may have arisen during preparation of the membrane or the SEM sample. The downside of the membrane also deviates from what is observed for the other types of membranes. The white spots are smaller and brighter than the ones observed on other downsides. The downside of this membrane seems somewhat rougher than the ones of the other types of membranes. The topography could explain why the water contact angles on the downside of this membrane are somewhat higher than for the others (see Table 9-4).

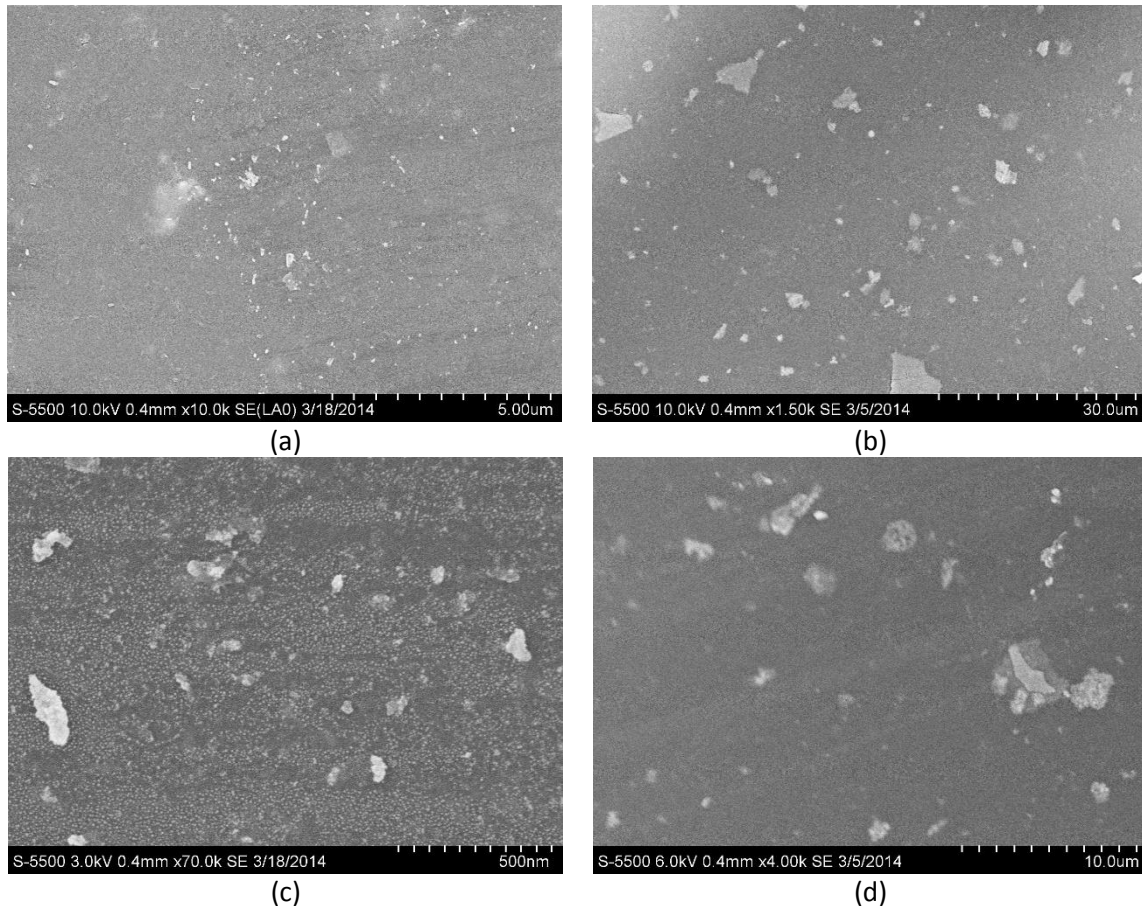


Figure 9-22: SEM images of (a and c) upside and (b and d) downside of membrane with 5 wt% 15-400 nm TiO_2 .

9.3.2.3 Membranes containing 5 wt% $>1 \mu\text{m}$ TiO_2

Figure 9-23 shows the SEM images of the membrane containing 5 wt% $>1 \mu\text{m}$ TiO_2 provided by SINTEF Materials and Chemistry. As for the other membranes, a difference between the upside and downside of the membrane is observed. On the upside, the particles seem to be protruding from the surface, while the downside seems somewhat more even. White spots are observed on the downside of this membrane, similar to what was observed for the three other types of membranes.

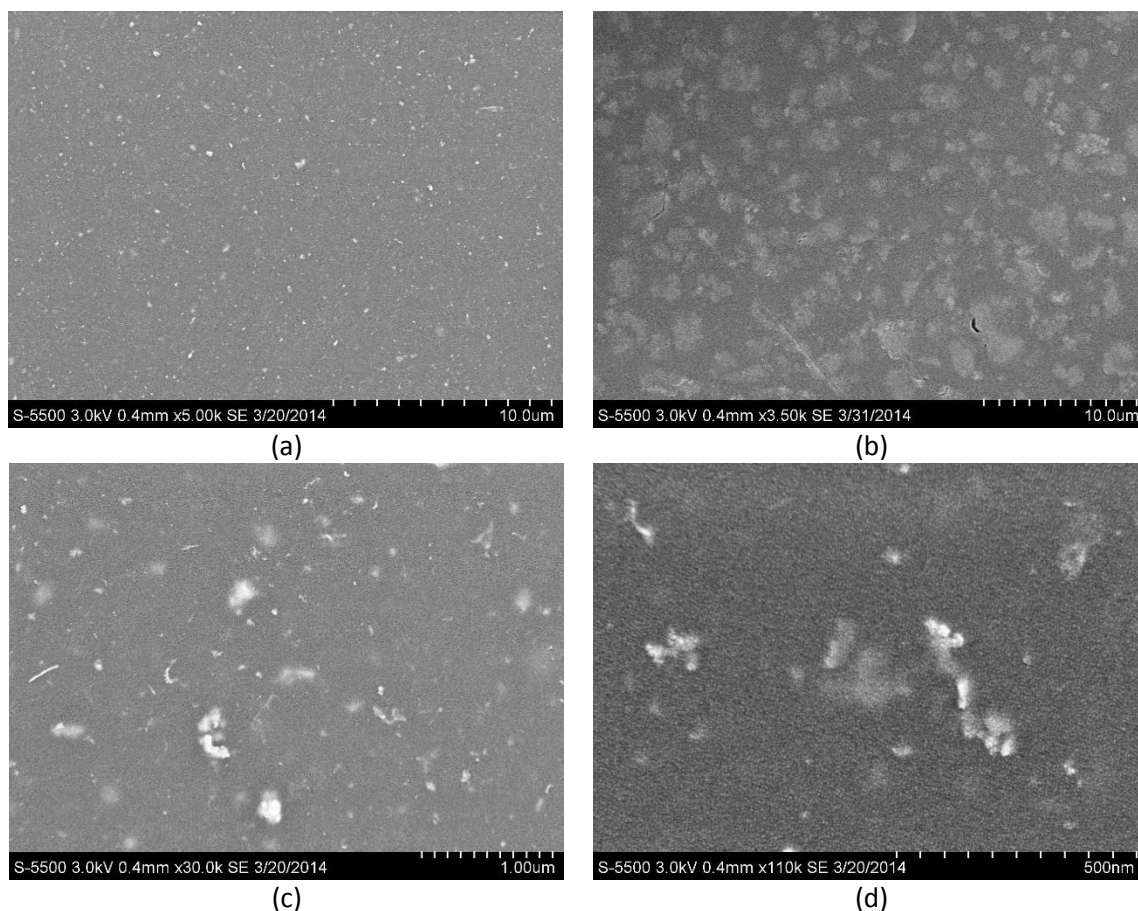


Figure 9-23: SEM images of (a, c, d) upside and (b) downside of membrane containing 5 wt% $>1 \mu\text{m}$ TiO_2 .

9.3.2.4 Cross-section images

Based on the images presented in the previous figures, the nanoparticles appear to be quite evenly distributed across the membrane surface. However, cross-section images of the nanocomposites would perhaps be better suited to study the distribution of particles in the membranes. Unfortunately, the membranes proved to be too soft to be able to break in liquid nitrogen. As a result, no clean cuts were obtained for the nanocomposites of PTMSP and TiO_2 .

The small membranes containing 20 wt% of the nanoparticles provided by SINTEF Materials and Chemistry did for some unknown reason become very brittle and could therefore be broken without the use of liquid nitrogen. However, as the membranes were very fragile, it was almost impossible to prepare the samples for SEM characterization. Only one sample was successfully mounted in the specimen holder without being destroyed. This was the membrane containing 20 wt% of the nanoparticles from SINTEF Materials and Chemistry in the size range 15-400 nm. The membrane was exposed to 2 M MDEA for 4 weeks. The cross-section image is shown in Figure 9-24. The blue and red line represents the upside and the downside of the membrane, respectively.

In the SEM image, particles is observed protruding from the membrane surface. Additionally, it could seem as if a settling of particles – either polymer, nanoparticles or both – is observed. However, it is not possible to draw any definite conclusion based on the images of only one membrane. Additionally,

the membrane has been exposed to MDEA solution for several weeks. As a result, the structure observed in the image above might have been affected by the liquid. Several cross-section SEM images of this membrane is included in the appendix.

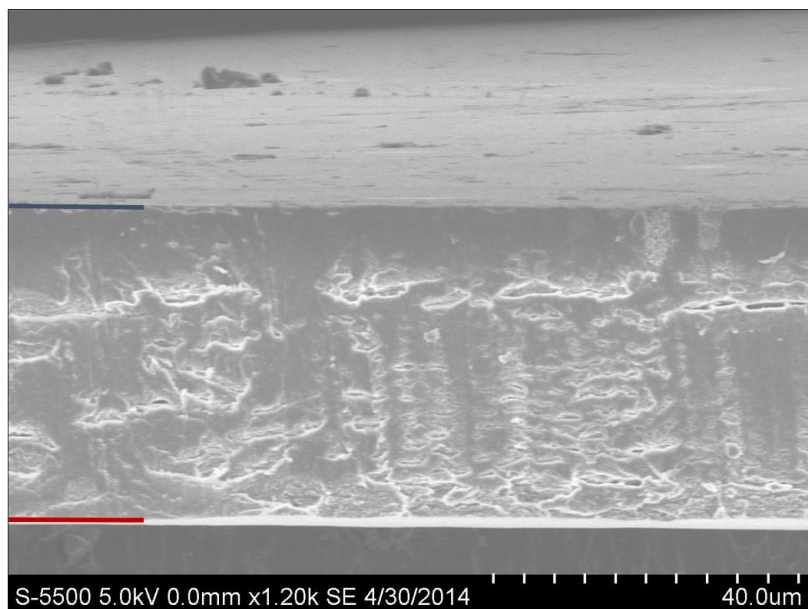


Figure 9-24: SEM image of the cross-section of a membrane containing 20 wt% 15-400 nm TiO₂. Blue and red line shows the upside and downside of the membrane, respectively.

9.3.3 Membranes prepared on casting plates of Teflon

Figure 9-25 shows SEM images of membranes prepared on casting plates of Teflon. The membranes contain 5 and 20 wt%, respectively, of the commercial Aeroxide[®] TiO₂ T 805. The dry nanocomposite films were carefully removed from the casting plates with the help of water to prevent any damage of the membrane. As the SEM images shows, the downside of the nanocomposite films are clearly uneven and different from the ones prepared on glass.

The uneven downside of the membranes prepared on Teflon may describe the higher water contact angle on this side of the membranes. Even though the apparent contact angle suggests that the downside of the membrane is more hydrophobic than the upside, and thus more resistance to wetting, this is not necessarily true. As previously mentioned, the experimental contact angle reflects the surface topography. As a result, the contact angle on a very rough surface is higher than on a perfectly smooth surface, and differs from the contact angle calculated from Young's equation for the given system.

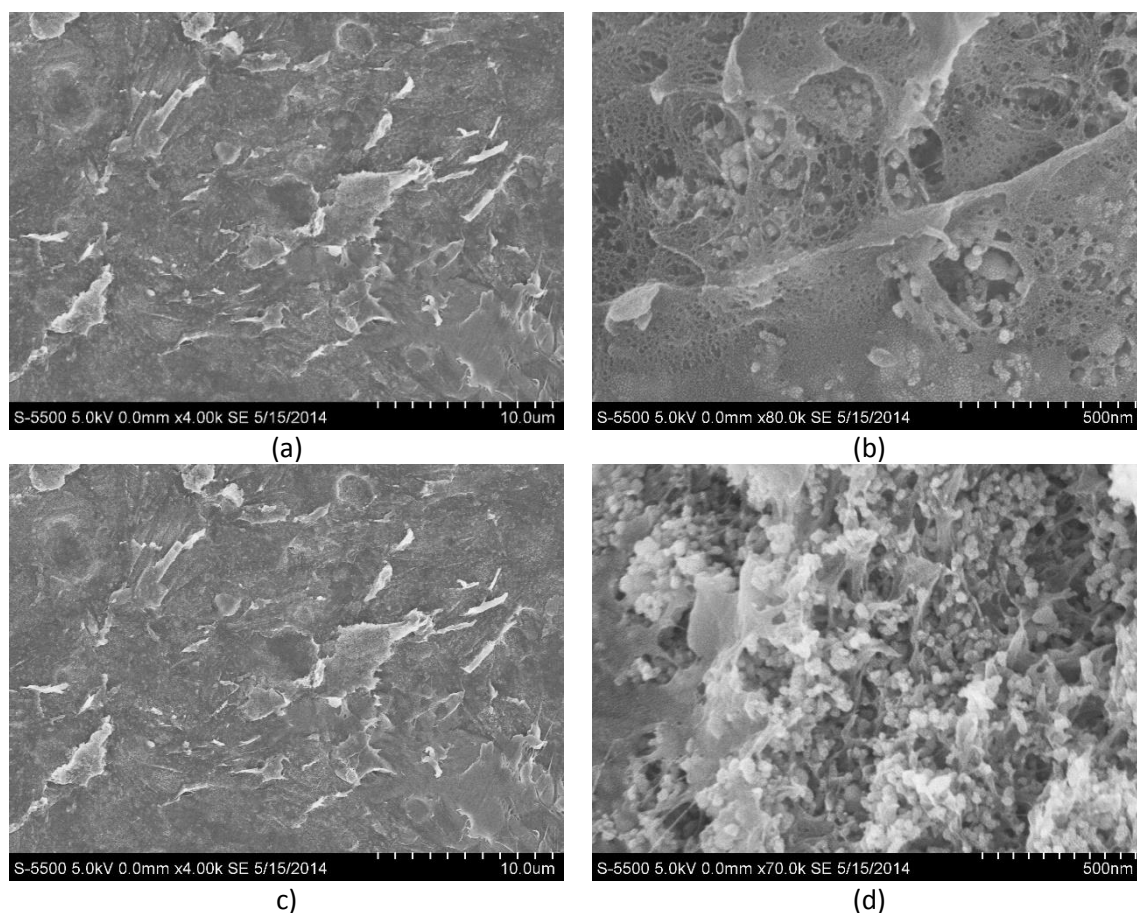


Figure 9-25: SEM images of the downside of membranes prepared on Teflon containing (a, b) 5 wt% and (c, d) 20 wt% T 805 TiO₂ nanoparticles.

9.3.4 Liquid-exposed nanocomposite membranes

This section presents the SEM images of nanocomposites exposed to water, 2 M MDEA and 4.2 M MDEA for an amount of time ranging from 1 day to nearly 10 weeks. As mentioned in previous parts of the report, only the upside of the membranes is exposed to liquid. The downside is kept dry. In some cases, however, liquid may have penetrated the exposure unit and come into contact with the underside of the membrane. This could have affected the results. Several images are included in the appendix.

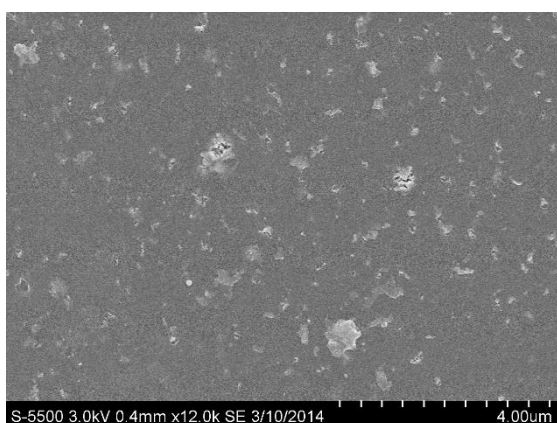
9.3.4.1 Membranes containing 5 wt% T 805 TiO₂

Figure 9-26 shows the SEM images of liquid-exposed nanocomposites containing 5 wt% commercial Aeroxide® T 805 nanocomposites. For the membrane exposed to water for 1 day, the upside appear unchanged compared to the unexposed membrane (see Figure 9-20). After 14 days of exposure to water, a change of the surface is observed. At this point, the upside of the membrane has become somewhat rippled, and is no longer as smooth as the unexposed surface. The membrane exposed to water for 67 days clearly differs from the unexposed membrane. This may indicate that the long-time exposure to water has had a strong effect on the surface.

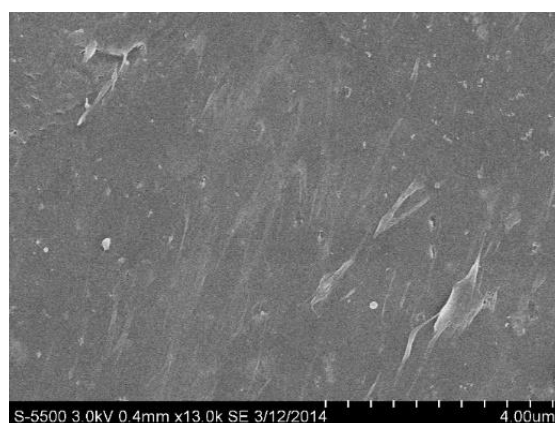
9. Results and discussion

For the membranes exposed to 2 M MDEA, a change on the surface is observed both after 14 and 64 days of exposure. The surface has become more uneven and appears rippled. These observations become more prominent as the time of exposure increases.

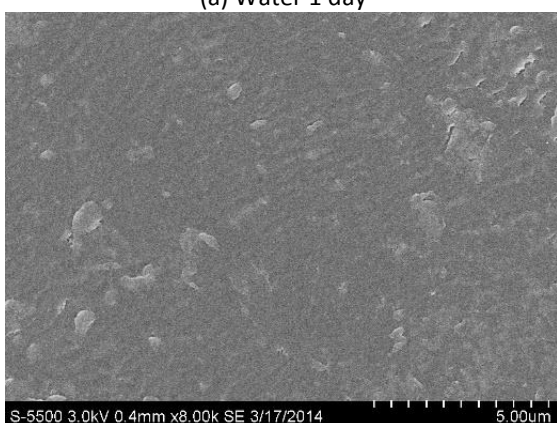
The membrane surfaces exposed to the MDEA solution of highest concentration (4.2 M) also appear to be affected by liquid exposure. This is especially true for the membrane exposed for 64 days. This surface is very rippled and uneven.



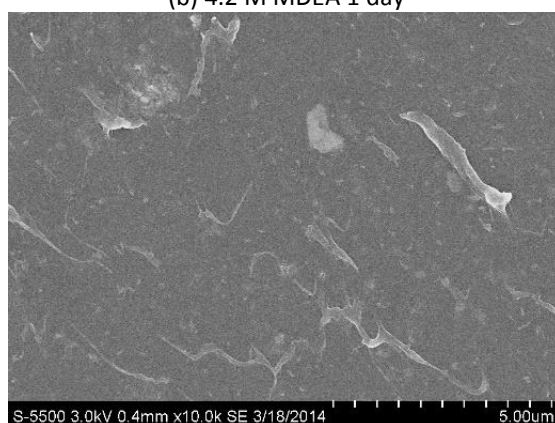
(a) Water 1 day



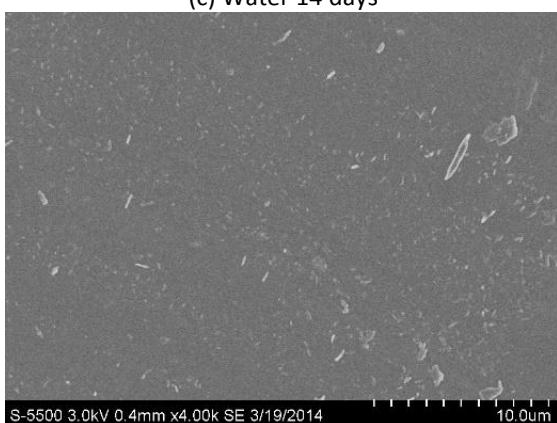
(b) 4.2 M MDEA 1 day



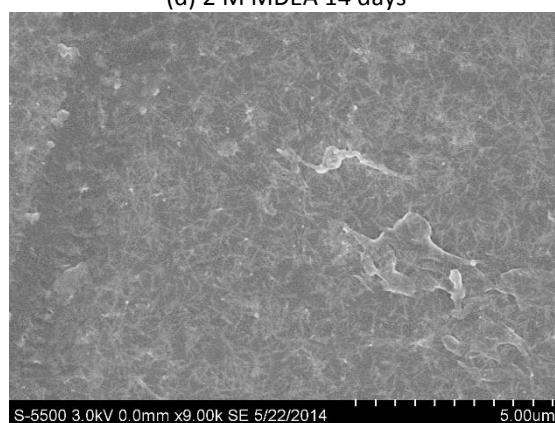
(c) Water 14 days



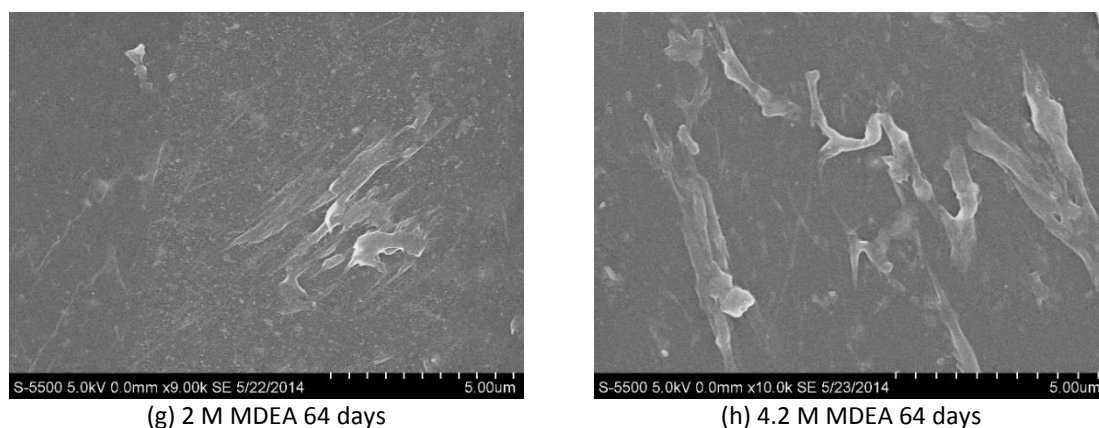
(d) 2 M MDEA 14 days



(e) 4.2 M MDEA 14 days



(f) Water 67 days

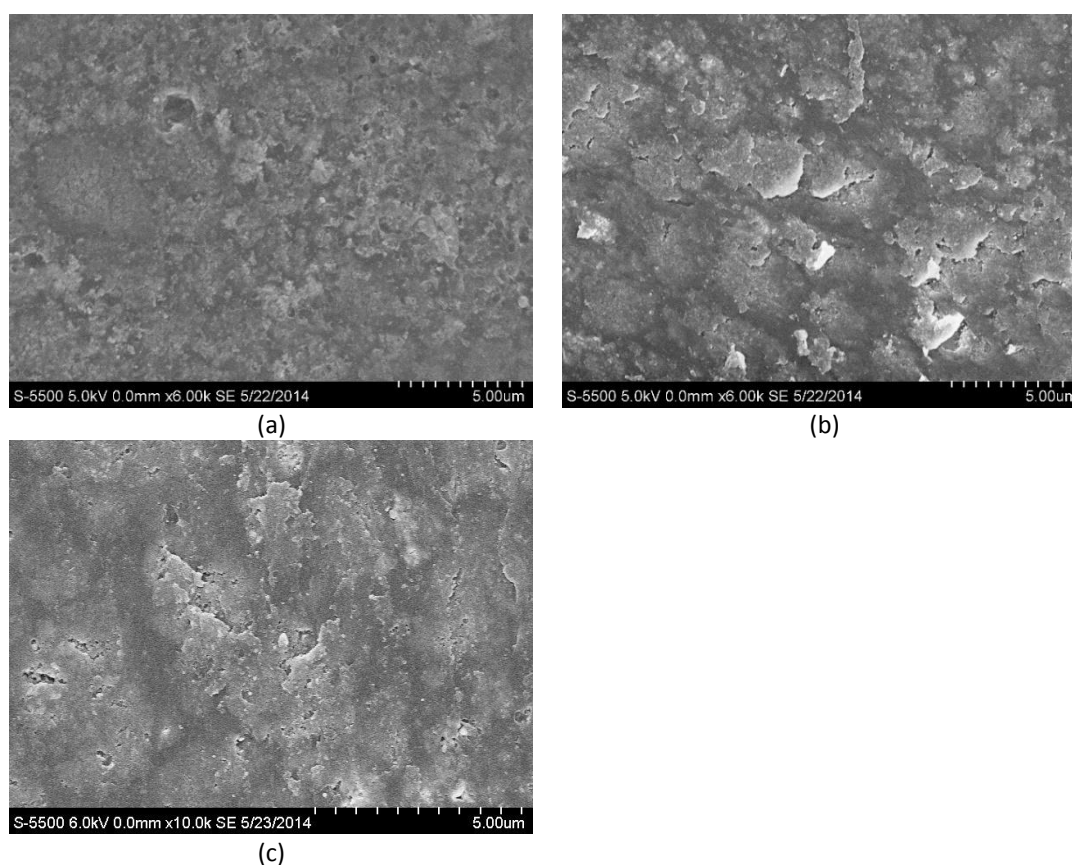


(g) 2 M MDEA 64 days

(h) 4.2 M MDEA 64 days

Figure 9-26: SEM images of the upside of liquid-exposed nanocomposites containing 5 wt% T 805 TiO₂.

Figure 9-27 shows SEM images of the downside of membranes containing 5 wt% T 805 exposed to water and aqueous amine solutions for 67 and 64 days, respectively. This side of the membrane is kept dry during immersion. Still, it appears as if the long-term exposure has had a strong impact on the downside of the membrane. This is true for all concentrations of liquid.



(a)

(b)

(c)

Figure 9-27: SEM images of downside nanocomposites containing 5 wt% T 805 TiO₂ exposed to (a) water for 67 days, (b) 2 M MDEA for 64 days and (c) 4.2 M MDEA for 64 days..

9.3.4.2 Membranes containing 20 wt% T 805 TiO₂

Figure 9-28 shows a selection of SEM images of liquid-exposed nanocomposites containing 20 wt% commercial Aeroxide® T 805 TiO₂. For the membrane exposed to 2 M MDEA for 4 weeks, the surface

has changed compared to the unexposed membrane shown in Figure 9-21. At the maximum time of exposure, all membrane surfaces have experienced changes compared to the unexposed membrane. The features are the same as the ones observed on the liquid-exposed membranes containing 5 wt% of the same type of nanoparticles.

The downside of the long-term exposed membranes is shown in Figure 9-27. As the figure shows, long-term exposure to liquid of all three concentrations appears to have had a strong effect also on the downside of the membranes, which has not been in direct contact with liquid.

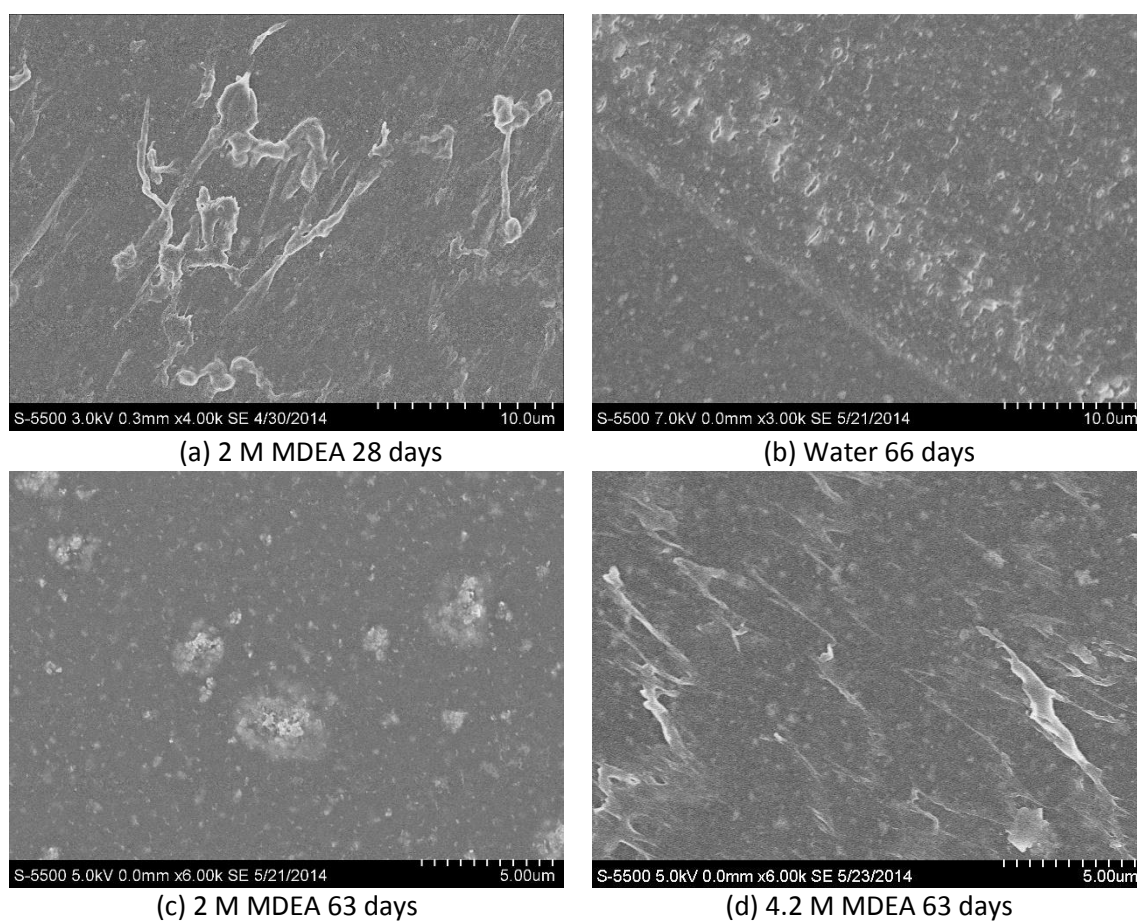


Figure 9-28: SEM images of liquid-exposed nanocomposites containing 20 wt% T 805 TiO_2 .

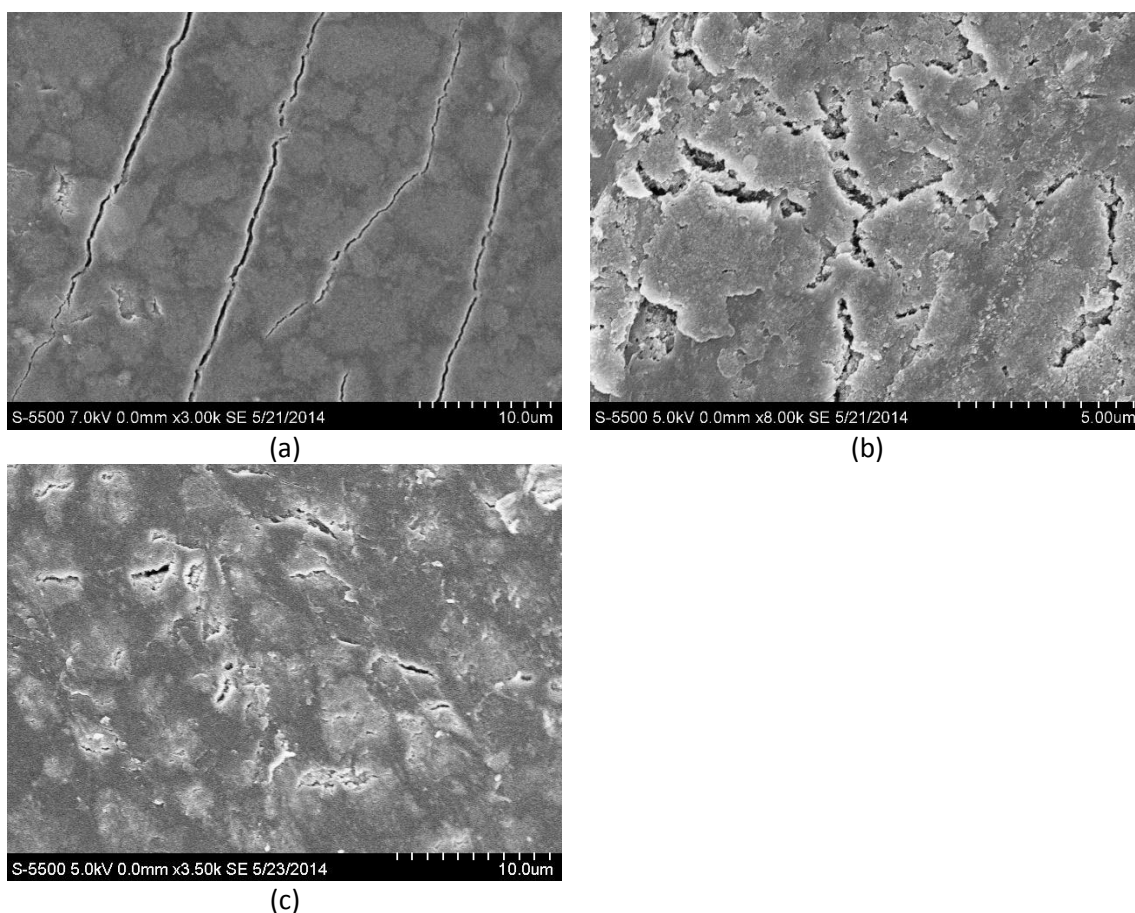
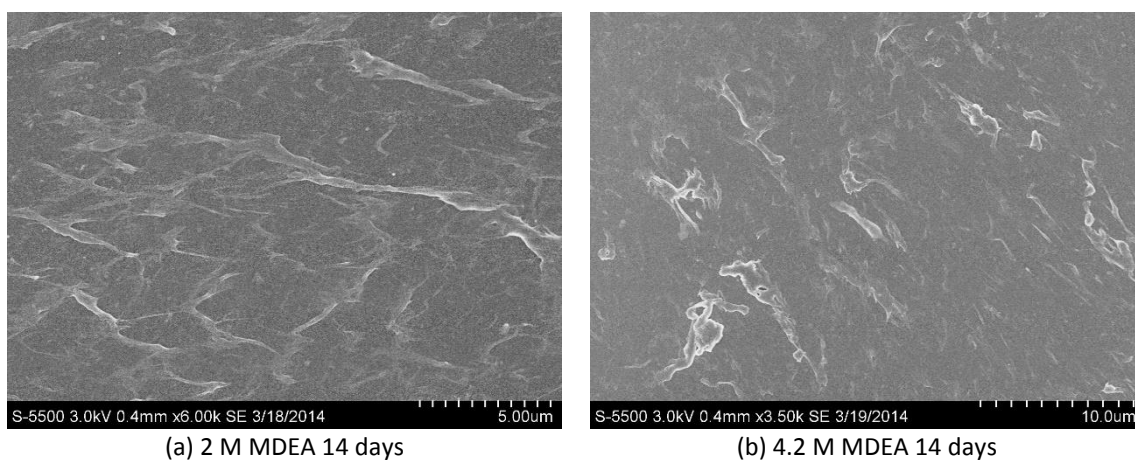
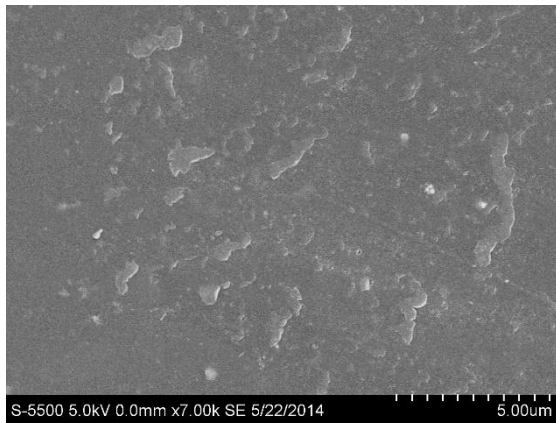


Figure 9-29: SEM images of downside nanocomposites containing 20 wt% T 805 TiO_2 . Upside exposed to (a) water for 66 days, (b) 2 M MDEA for 63 days and (c) 4.2 M MDEA for 63 days.

9.3.4.3 Membranes containing 5 wt% 15-400 nm TiO_2

Figure 9-30 shows the SEM images of the liquid-exposed membranes containing 5 wt% 15-400 nm TiO_2 provided by SINTEF Materials and Chemistry. The first images were taken after 14 days of exposure. All liquid-exposed surfaces showed in the figures differs from the ones observed for the unexposed membrane. This indicates that the surfaces have been affected by the liquid exposure.





(c) Water 67 days



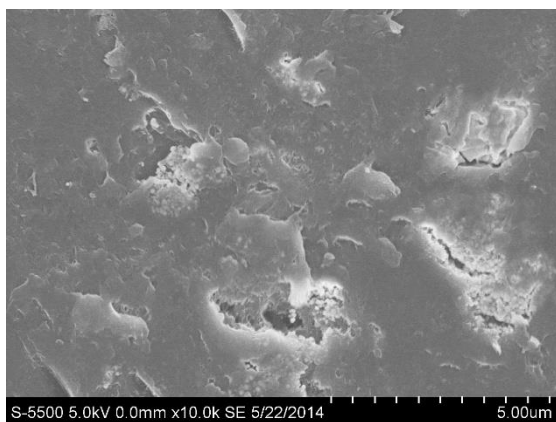
(d) 2 M MDEA 64 days



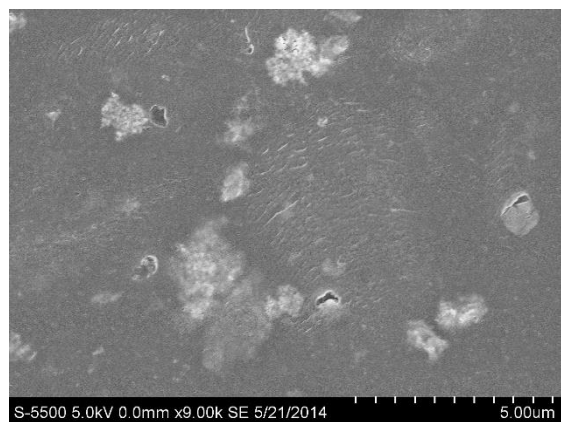
(e) 4.2 M MDEA 64 days

Figure 9-30: SEM images of liquid-exposed nanocomposites containing 5 wt% 15-400 nm TiO_2 .

SEM images of the downside of membranes containing 5 wt% 15-400 nm TiO_2 are shown in Figure 9-31. These membranes are exposed to water and aqueous MDEA solutions for 67 and 64 days, respectively. As for the other types of membranes, also the downside of the membranes appear to have been affected by the long-term exposure, even though they have not been in direct contact with liquid.



(a)



(b)

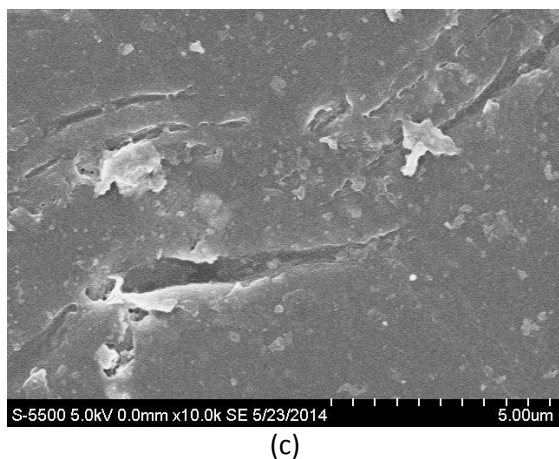


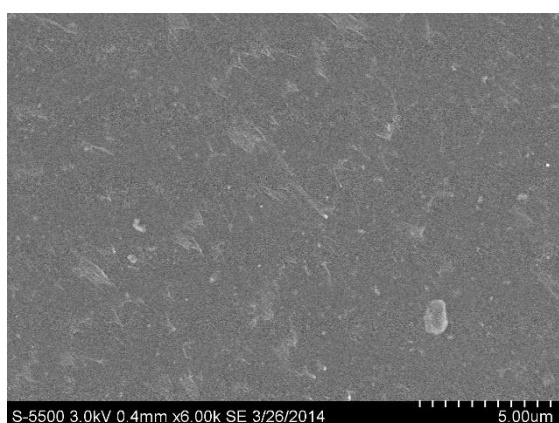
Figure 9-31: SEM images of downside nanocomposites containing 5 wt% 15-400 nm TiO_2 . Upside exposed to (a) water for 67 days, (b) 2 M MDEA 64 days and (c) 4.2 M MDEA 64 days.

9.3.4.4 Membranes containing 5 wt% $>1 \mu\text{m}$ TiO_2

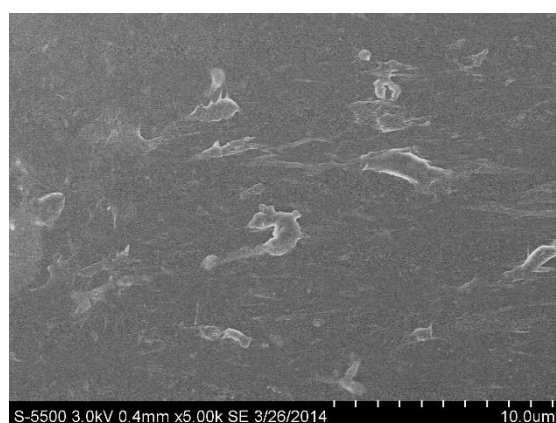
Figure 9-32 shows the SEM images of the liquid-exposed membranes containing 5 wt% $>1 \mu\text{m}$ TiO_2 provided by SINTEF Materials and Chemistry. Already after 1 day of exposure to 2 M MDEA, slight changes on the surface of the membrane are observed. The change is more apparent for the membrane exposed to 4.2 M MDEA for 1 day. The same trend is observed for the permeability (see Figure 9-7).

Long-term exposure to all concentrations of liquid appear to have had an effect on the surface morphology of the membranes. The changes are more apparent on these membranes than on the ones exposed to liquid for only a short period of time.

SEM images of the downside of membranes containing 20 wt% T 805 TiO_2 are shown in Figure 9-33. The membranes are exposed to water for 67 days and 2 M and 4.2 M MDEA for 64 days. The effect of liquid exposure on these membranes are not as evident as for the membranes presented in the previous figures. However, some damage is visible in the form of cracks etc., especially for the membrane exposed to 4.2 M MDEA.



(a) 2 M MDEA 1 day



(b) 4.2 M MDEA 1 day

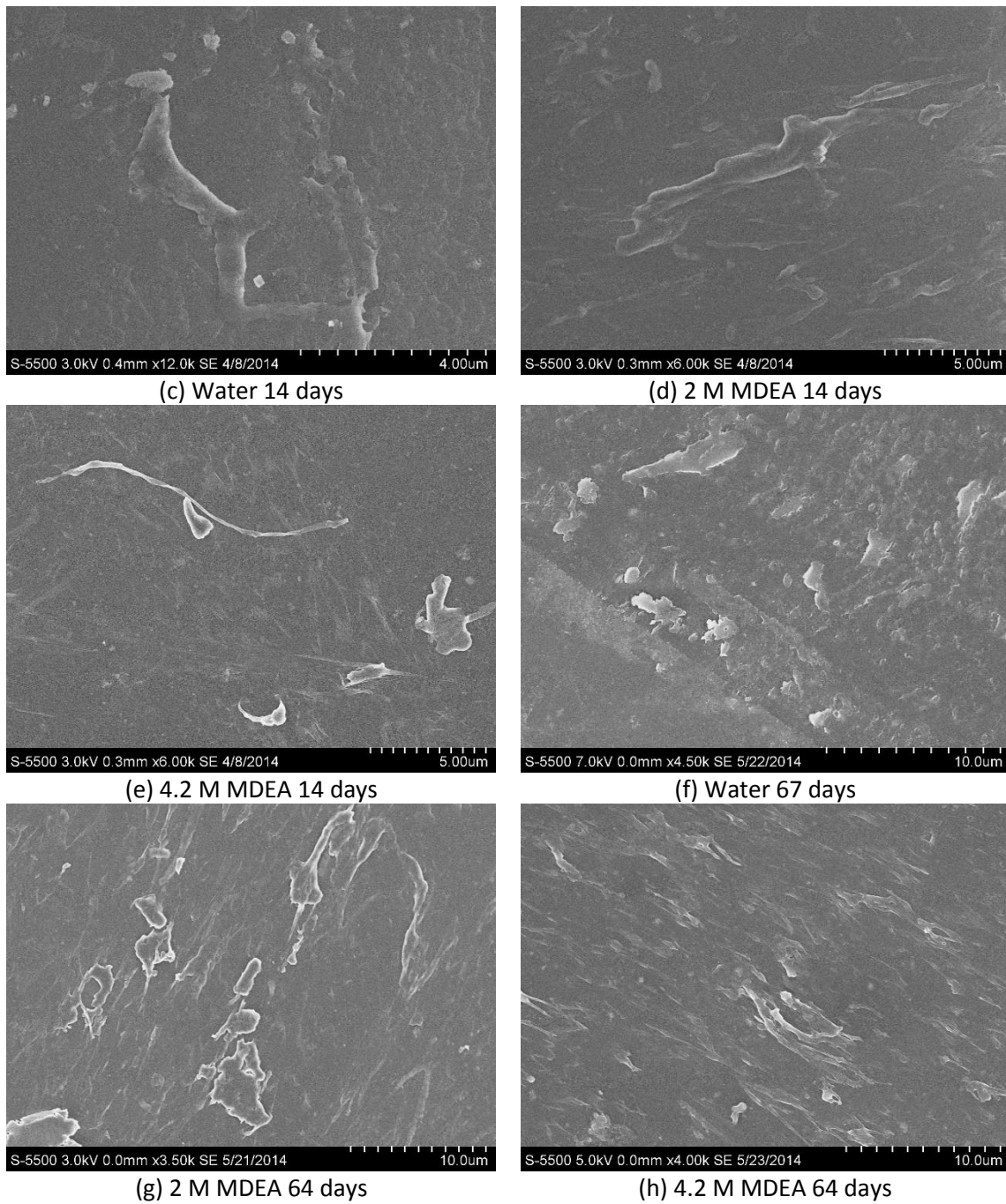


Figure 9-32: SEM images of liquid-exposed nanocomposites containing 5 wt% $>1 \mu\text{m}$ TiO_2 .

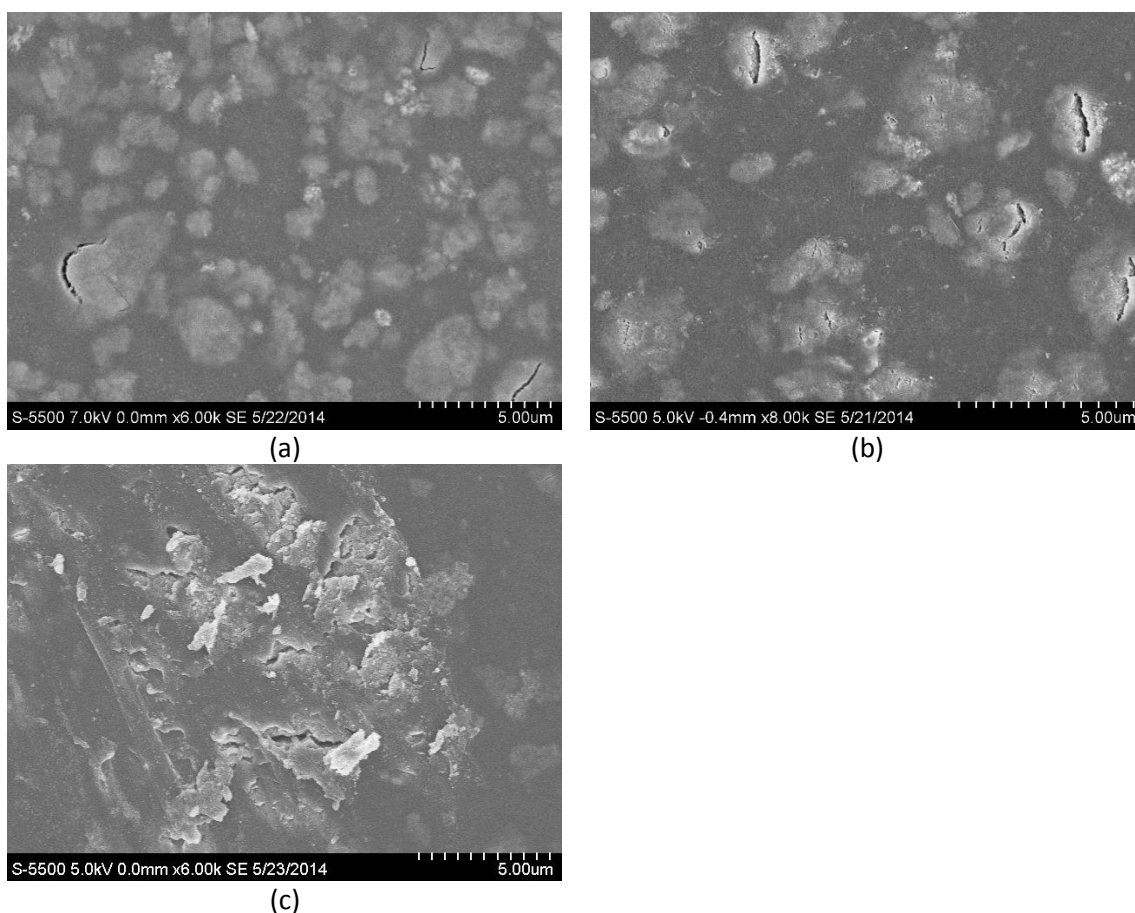


Figure 9-33: SEM images of downside nanocomposites containing 5 wt% $>1 \mu\text{m}$ TiO_2 . Upside exposed to (a) water for 67 days, (b) 2 M MDEA for 64 days and (c) 4.2 M MDEA for 64 days.

9.3.5 Summary of SEM images

The SEM images have showed that there is visible difference between the upside and downside of the flat sheet membranes. This is true both for pure PTMSP and nanocomposite membranes containing the different types of TiO_2 nanoparticles. No phase separation is observed for the PTMSP- TiO_2 nanocomposites. As previously mentioned, the morphology of the dispersed phase strongly influences the the gas transport properties of the mixed matrix membrane. For the membranes investigated in this work, the particles seems to be finely distributed in the polymer matrix. However, the membranes are only investigated using SEM and no cross-section images of good quality have been obtained. Therefore, it is difficult to draw any definite conclusions regarding the dispersion of the different types of particles.

The particles appears to be protruding from the surface on the upside of the membranes. The downside of the nanocomposites is covered with bright spots. The observations indicate that there might be some particle settling during the transformation from polymer solution to dry flat sheet membranes.

Nanocomposites prepared on casting plates of Teflon have a downside which is clearly different from the ones prepared on glass. The downside is very uneven with a lot of membrane flakes protruding from the surface. This could explain the surprisingly high water contact angles on the downside of the membranes prepared on Teflon.

The SEM images of the membrane surfaces exposed to water, 2 M MDEA and 4.2 M MDEA indicate that the surface morphology is affected by the liquid exposure. This is true for all liquid concentration, and is especially evident for the membranes exposed to liquid for the maximum amount of time. Changes are also observed on the downside of the membrane, despite the fact that they have not been in direct contact with liquid. Again, this is particularly evident for the membranes exposed for nearly 10 weeks.

9.4 Summary of results

For the membranes investigated in this work, the average CO₂ permeability is in the order: 5 wt% 15-400 nm (23 587 Barrer) > PTMSP (22 952 Barrer) > 5 wt% >1 μm (22 653 Barrer) > 20 wt% T 805 (22 631 Barrer) > 5 wt% T 805 (22 397 Barrer). Except for the membrane containing 5 wt% >1 μm, the standard deviation is several thousand Barrer. Therefore, it is difficult to draw any conclusions regarding the relative performance of the different types of nanocomposites. As regards the CO₂/CH₄ selectivities at 2 bar, all nanocomposites exhibit values below 3 and comparable to that of pure PTMSP. The average selectivity is in the order: 5 wt% T 805 (2.85) > 5 wt% >1 μm (2.82) > PTMSP (2.55) > 5 wt% 15-400 nm (2.54) > 20 wt% T 805 (1.09).

For the liquid-exposed nanocomposites, the pure-gas permeability decreases as the duration of exposure increases. The rate of change is highest during the first 14-35 days of exposure. For all nanocomposites exposed to 4.2 M MDEA, a drastic decrease in permeability is observed already after 1 day of exposure. At the maximum time of exposure, the permeability of the membranes exposed to 2 M MDEA lies at about the same low level as for the ones exposed to 4.2 M MDEA. For all membranes exposed to MDEA solutions, the permeability at this point is less than 10% of the initial value. For the majority of membranes exposed to these concentrations, the CO₂ permeability is well below 2 000 Barrer. In other words, these nanocomposites do not meet the requirement set by Nguyen et al. [44] (see Section 6.2). According these researchers, a dense layer in the micrometer range of a highly permeable polymer with CO₂ permeability above 3 000 Barrer is absolutely necessary to be able to compete with classical microporous membrane contactor materials.

For the membranes exposed to water, the decrease is not as dramatic as for the ones exposed to aqueous MDEA solutions. For the membranes containing 5 wt% T 805 and 5 wt% 15-400 nm, the CO₂ permeability at 2 bar seems to stabilize beyond 14 and 35 days of exposure, respectively. After 67 days of water-exposure, the CO₂ permeability of the two membranes is 15 200 and 17 300 Barrer, respectively. For the membrane containing 20 wt% T 805, the values are fluctuating, increasing from about 11 000 to 24 400 Barrer as the duration of water-exposure increases from 42 to 66 days. This could be a random error. Finally, for the membrane containing 5 wt% >1 μm TiO₂, the permeability continues to decrease as the time of exposure to water increases. After 67 days in water, the CO₂ permeability is slightly below 11 000 Barrer.

Based on the permeability results for the liquid-exposed membranes, it is difficult to draw any conclusion regarding the relative performance of the different types of nanocomposites. At the maximum time of exposure to water, the measured CO₂ permeability is in the order: 20 wt% T 805 > 5 wt% 15-400 nm > 5 wt% T 805 > 5 wt% >1 μm, ranging from 10 700 to 24 373 Barrer. However, as mentioned, the permeability of the membrane with 20 wt% T 805 could be too high. Additionally, as the tests involving the unexposed membranes demonstrated, the uncertainty in the measurements might be significant. For all membranes, a poor performance is observed for long-term exposure to 2 M and 4.2 M MDEA.

For a majority of the liquid-exposed membranes, the decrease in permeability is accompanied by an increase in the CO₂/CH₄ selectivity. This is due to the fact that the permeability of CH₄ has decreased more than that of CO₂. As the time of exposure increases, the selectivity continues to increase. The rate of change is highest during the first intervals of exposure. This is most notably for the membranes exposed to 4.2 M MDEA, for which the selectivity is almost 3 times higher after just 1 day of exposure. The increasing selectivity indicates that the transport of CH₄ is most affected by the liquid-induced changes of the membrane properties. This could be a result of a change in both diffusivity and solubility. After the maximum duration of exposure, the highest selectivity is observed for the membranes exposed to 2 M MDEA, followed by the ones exposed to 4.2 M MDEA. For the membranes exposed to water, the selectivity is lower than for the membranes exposed to MDEA solutions, but still significantly higher than for the unexposed membranes.

Contact angle measurements have confirmed the hydrophobicity of the membranes. The average water contact angle is in the order: 5 wt% 15-400 nm > 5 wt% >1 μm > 5 wt% T 805 > PTMSP > 20 wt% T 805, ranging from approximately 101° to 108°. However, the uncertainty in the measurements is expected to be significant. Therefore, it is difficult to draw any conclusions regarding the relative hydrophobicity of the different types of membranes. A distinction is made between the upside (air side) and downside (casting side) of the membranes. Without exception, all membranes prepared on casting plates of glass exhibit higher contact angles on the upside than on the downside. For membranes prepared on casting plates of Teflon, the opposite is observed, as the apparent contact angle is higher on the downside than on the upside of the membrane.

For the liquid-exposed nanocomposites, the water contact angles on the upside decreases after exposure. As for the permeability, the rate of change is highest during the first intervals of exposure. This matches the observations made for the permeability. The contact angles of the membranes exposed to aqueous MDEA solutions follows approximately the same trend. After 64 days, the measured contact angles of these nanocomposites are approximately between 80 and 90°. The contact angles of the water-exposed membranes are lower than those of the membranes exposed to aqueous MDEA solution. Based on the results, it appears as if the liquids have affected the surfaces of the nanocomposites in a different manner. The contact between the membrane material and the liquid may have changed both the chemistry (hydrophobicity) and the morphology of the membranes.

The SEM images of the membranes clearly indicate that there is a difference between the upside and downside of the flat sheet membranes. The fact that the upside of the membranes seems somewhat more uneven than the downside supports the observations made for the contact angles. As mentioned, the apparent contact angle is affected both by the surface chemistry and topography. Based on the SEM images, the topography of the two surfaces of the flat sheet membranes is obviously different. The rougher upside is expected to give a higher contact angles than the smoother downside. Additionally, the hydrophobic TiO₂ particles on the surface could contribute to the higher water contact angles. SEM images of the nanocomposites prepared on casting plates of Teflon help confirm that there is a difference between membranes casted on glass and Teflon, as was observed for the contact angles.

For the liquid-exposed membranes, changes are observed on membranes exposed to all three liquid concentrations even at short durations of contact. After the maximum time of exposure, it is obvious that the membranes have experiences a change compared to the unexposed membranes. At this point, surface alterations are obvious also on the downside of the membranes, which have not been in direct contact with the liquid. The images of the nanocomposites exposed to liquid for the maximum amount of time do not help explain why the apparent contact angles on the water-exposed membranes are lower than those exposed to aqueous MDEA solutions.

To summarize, long-term exposure to water, 2 M MDEA and 4.2 M MDEA has resulted in a decrease in pure gas permeability and water contact angle. Changes in surface morphology is also observed on both sides of the liquid-exposed membranes. The higher the concentration of liquid, the larger the change in morphology and permeation properties. The reduction in permeability may be caused by a reduction in both the diffusivity coefficient and the solubility coefficient. According to the contact angle measurements, the reduction in contact angle is more apparent for the membranes exposed to water. This may be a result of changes in both the surface chemistry and morphology.

Figure 9-34 summarizes the permeability results for the long-term exposed membrane materials investigated in different phases of the project. The results for the crosslinked nanocomposites exposed to liquid for 2 weeks are also included. For membranes of pure PTMSP, the CO₂ permeability at 2 bar is higher than 15 000 Barrer after exposure to liquid of all concentrations. The permeation properties seem to be equally affected by water, 2 M MDEA and 4.2 M MDEA. For crosslinked PTMSP, the CO₂ permeability of the long-term liquid-exposed membranes is significantly lower and no higher than 2 500 Barrer. Again, the membranes seem to be equally affected by the different concentrations of liquid. Crosslinked PTMSP with 20 wt% TiO₂ particles experienced a dramatic decrease in permeability already after 2 weeks of exposure. These membranes have shown the poorest performance of all the membrane materials investigated in this project. The uncrosslinked PTMSP/TiO₂ nanocomposites investigated in this work have not experienced the same dramatic reduction in permeability. However, long-term exposure to 2 M and 4.2 M MDEA has indeed resulted in permeabilities at the same low level as the crosslinked membranes without nanoparticles. The permeability of the water-exposed nanocomposites is significantly higher than for the crosslinked membranes. Thus, the nanocomposite membranes are more resistant towards long-term exposure to water than the crosslinked membranes without nanoparticles.

The results clearly indicate that the flat sheet membranes of pure PTMSP show the best performance after long-term exposure to 2 M and 4.2 M MDEA.

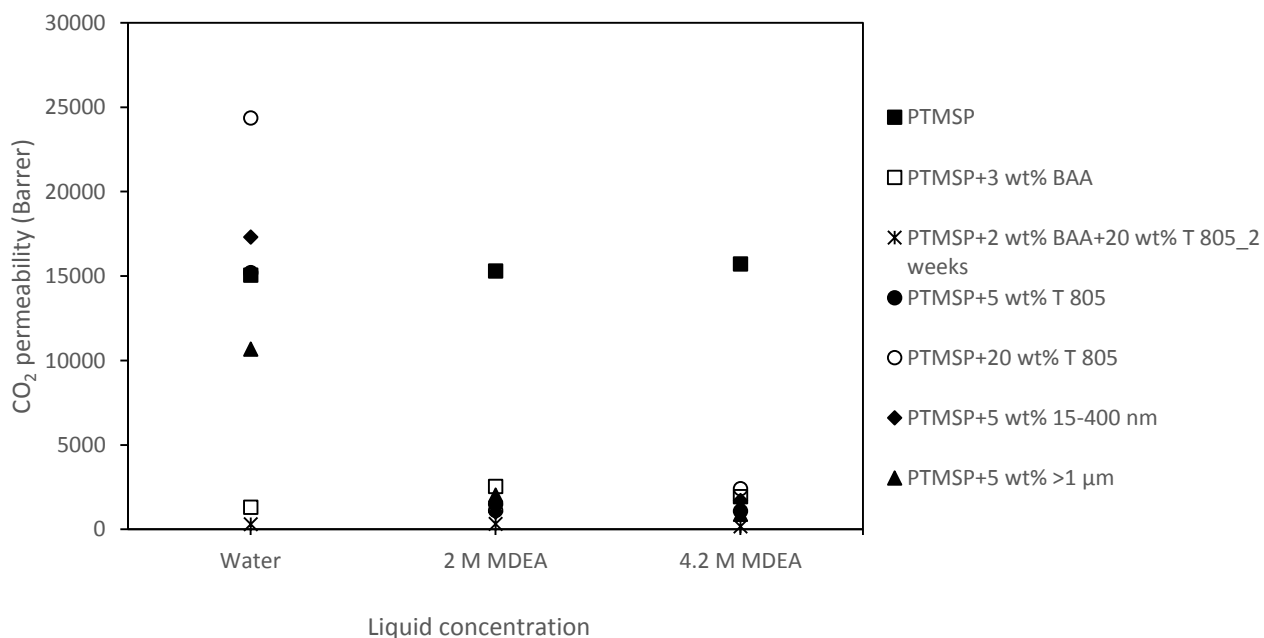


Figure 9-34: CO₂ permeability at 2 bar for PTMSP, crosslinked PTMSP, crosslinked nanocomposites and uncrosslinked nanocomposites of PTMSP and TiO₂. The membranes are exposed to water, 2 M MDEA and 4.2 M MDEA for 9-10 weeks. The crosslinked nanocomposites are exposed to liquid for 2 weeks.

10. Conclusion

10.1 Nanocomposite membranes of PTMSP and TiO₂

Flat sheet nanocomposite membranes of PTMSP and TiO₂ nanoparticles have been prepared by solvent evaporation. The membranes were prepared on casting plates of glass with a diameter of 17 cm. The resulting films were homogeneous with a thickness of 20–60 μm. Three different types of nanoparticles were applied, having different sizes and surface modifications. One was the commercial Aeroxide® T 805 TiO₂. These are in the form of hydrophobic, covalently bounded aggregates in the range of 100–250 nm. The commercial particles have previously been reported to give the expected increase in permeability. The other two types of particles were both provided by SINTEF Materials and Chemistry. These custom-made particles were delivered in the form of clustered particles in toluene. The size of the aggregates is 15–400 nm in the first solution and >1 μm in the second one. Membranes containing 5 and 20 wt% commercial TiO₂ were prepared. For the custom-made TiO₂, only membranes containing 5 wt% were characterized.

The measured CO₂ permeability of all membranes is located at approximately the same level, with an average value ranging from about 22 400 to 23 600 Barrer. No significant increase in permeability compared to the unfilled PTMSP was observed. For a majority of the nanocomposites, the standard deviation is several thousand Barrer. As a result, it is difficult to rank the performance of the nanocomposite membranes by the type of TiO₂ and by the weight fraction of particles. As regards the CO₂/CH₄ selectivities at 2 bar, all nanocomposites exhibit values below 3 and comparable to that of pure PTMSP. The lowest selectivity compared to PTMSP is observed for the membrane containing 20 wt% T 805. This could indicate that the fillers have enhanced the transport of CH₄.

Contact angle measurements have confirmed the hydrophobicity of the polymer and the nanocomposites. For all membranes, the water contact angle on the upside (air side) was higher than 100°. However, a majority of the measured water contact angles on the downside of the membrane (casting side) was lower than 90°. Thus, a difference between the two surfaces of the flat sheet membranes was confirmed. When aqueous MDEA solutions were used as liquid, the measured contact angles were lower than those of water. The values decreased as the MDEA concentration increased.

The morphology of the membranes was investigated using scanning electron microscopy. For the nanocomposites, no phase separation was observed and the particles appeared to be evenly distributed in the polymer. However, other characterization methods (AFM, TEM) are better suited to investigate particle dispersion. The SEM images confirmed the difference between the two sides of the flat sheet membranes. The upside seemed rougher than the downside, with particles protruding from the surface. This could explain why the contact angle is higher on the upside of the membrane. Additionally, observations made in the SEM images suggested that some settling of particles occurs during preparation. Cross-section images of high quality were not possible to obtain, as the membranes were not possible to break in liquid nitrogen.

10.2 Effects of liquid exposure

The nanocomposite membranes were exposed to deionized water, 2 M MDEA and 4.2 M MDEA. The time of exposure varied from 1 day to 67 days. The aim was to investigate both the short-term and long-term effects of liquid exposure on the membrane properties and performance. Only the upside of the membranes were in contact with liquid, as the contact angle measurements had suggested that this side would be less susceptible to wetting due to its higher contact angle.

As for the unexposed membranes, the liquid-exposed membranes were characterized by means of permeation tests, contact angle measurements and SEM analysis. For a majority of the nanocomposites, the most prominent decrease in permeability is observed during the first weeks of exposure. The membranes exposed to 4.2 M MDEA have suffered a drastic reduction in permeability already after 1 day. All nanocomposite membranes showed a poor performance after long-term exposure to 2 M and 4.2 M MDEA. After the maximum time of exposure, the CO₂ permeabilities of these membranes were less than 10% of the initial value. The long-term performance was better for the membranes exposed to water. After nearly 10 weeks of exposure, the permeability of all membranes was higher than 10 000 Barrer.

The decrease in permeability of the liquid-exposed membranes is accompanied by an increase in the CO₂/CH₄ selectivity. This is due to the fact that the permeability of CH₄ has decreased more than that of CO₂. This could be a result of a change in both diffusivity and solubility. After maximum duration of exposure, the highest selectivity is observed for the membranes exposed to 2 M MDEA, followed by the ones exposed to 4.2 M MDEA. For these membranes, the selectivity is about 3-6 times higher than the initial selectivity. Long-term exposure to water has resulted in a smaller increase in selectivity.

Contact angle measurements showed that the water contact angle decreased as the time of exposure increased. The contact angles of the water-exposed membranes are lower than those of the membranes exposed to 2 M and 4.2 M MDEA. The decrease in contact angle may be a combined effect of changes in surface morphology and chemistry (hydrophobicity).

To summarize, long-term exposure to liquid has resulted in a reduction in pure-gas permeability and water contact angles. Additionally, the surface morphology on both sides of the membranes has changed as a result of liquid exposure. With higher concentration of liquid and longer duration of exposure, the changes in morphology and permeability increase. The morphological changes therefore coincide with the decrease in permeability. The change in morphology may have affected both diffusivity coefficients and solubility coefficients of CO₂ and CH₄. Based on the selectivities, exposure to liquid has had a stronger effect on the transport of CH₄. According to contact angle measurements, the reduction in contact angle is more apparent for the membranes exposed to water. This may be a result of changes in both surface chemistry and morphology.

10.3 Effect of different types of TiO₂ particles

No obvious difference between the different types of TiO₂ particles have been observed in this work. The nanocomposite membranes exhibit permeabilities at approximately the same level. Liquid exposure has brought along a decrease in permeability for all types of membranes. A poor performance is observed for all membranes exposed to 2 M and 4.2 M MDEA regardless of the type of TiO₂ particles incorporated in the polymer matrix.

10.4 Comparison of results

Previous studies on the long-term exposure of crosslinked PTMSP without nanoparticles resulted in CO₂ permeabilities below 2 500 Barrer (Figure 8-1). When comparing these results to the ones obtained in this work, the performance of the membranes exposed to aqueous MDEA solutions lies at approximately the same level. For the long-term exposure to water, on the other hand, the permeabilities of the uncrosslinked nanocomposite membranes investigated in this work are higher.

In a previous phase of the project, a dramatic decrease in permeability was observed for crosslinked nanocomposite membranes of PTMSP, BAA and TiO₂ already after 14 days of liquid exposure. The uncrosslinked nanocomposite membranes investigated in this work have not suffered the same dramatic decrease in permeability. Even after long-term exposure to 2M and 4.2 M MDEA, the measured CO₂ permeabilities are not as low as the ones measured in the previous study.

These observations indicate that it is the combination of crosslinking and nanoparticles that has caused the poor performance of the membranes. The studies conducted in the different phases of the project have indicated that the flat sheet membranes of pure PTMSP show the best performance after long-term exposure to 2 M and 4.2 M MDEA.

11. Further work

The distribution of the TiO₂ particles in the polymer matrix should be further investigated using AFM or TEM. This could help explain the results presented in this report, as well as those obtained during previous phases of the project.

The changes in permeability should be further analyzed by investigating the diffusivity and solubility coefficients of the nanocomposites. A sorption apparatus is available at NTNU, but has been out of order. Sorption measurements would also provide an insight to how the incorporation of TiO₂ particles into the polymer matrix has effected to solubility coefficient and the diffusivity coefficient.

Cross-section images of high quality was not possible to obtain, as the membranes were not able to break in liquid nitrogen. The possibility of using other methods to prepare cross-section samples should be investigated. One option is to use an ultramicrotome apparatus, which uses diamond knives to cut samples. A sample preparation lab at NTNU (TEM Gemini Centre) has such an apparatus and several other specimen preparation devices.

Based on observations made in this work, the two permeation rigs are suspected to generate different results. Closer investigations are necessary to determine which of the two – if any – gives the correct permeability. To minimize the uncertainty in the measurements, the permeation rigs should perhaps be calibrated. Additionally, it would be advantageous to upgrade the second permeation rig (PR-2) so that the gas tubes are flexible as those in the first rig (PR-1). This would minimize the risk of leakage in the connection between the membrane cell and the gas tubes.

Finally, the developed membrane material should be coated on a microporous support. Development of this procedure as well as characterization of the resulting composite membrane should be included as further work. Another very important step is to test the membrane in a high pressure membrane contactor experimental rig.

12. References

1. Merkel, T.C., et al., *Effect of Nanoparticles on Gas Sorption and Transport in Poly(1-trimethylsilyl-1-propyne)*. *Macromolecules*, 2003. **36**(18): p. 6844-6855.
2. Shao, L., J. Samseth, and M.-B. Hägg, *Crosslinking and stabilization of nanoparticle filled poly(1-trimethylsilyl-1-propyne) nanocomposite membranes for gas separations*. *Journal of Applied Polymer Science*, 2009. **113**(5): p. 3078-3088.
3. Kelman, S.D., et al., *Crosslinking poly(1-trimethylsilyl-1-propyne) and its effect on solvent resistance and transport properties*. *Polymer*, 2007. **48**(23): p. 6881-6892.
4. Rufford, T.E., et al., *The removal of CO₂ and N₂ from natural gas: A review of conventional and emerging process technologies*. *Journal of Petroleum Science and Engineering*, 2012. **94–95**(0): p. 123-154.
5. Kohl, A.L. and R. Nielsen, *Gas Purification*. 1997: Elsevier Science.
6. Meisen, A. and X. Shuai, *Research and development issues in CO₂ capture*. *Energy Conversion and Management*, 1997. **38**(0): p. S37-S42.
7. Mulder, J., *Basic Principles of Membrane Technology*. 1996: Springer.
8. Koros, W.J. and G.K. Fleming, *Membrane-based gas separation*. *Journal of Membrane Science*, 1993. **83**(1): p. 1-80.
9. Gabelman, A. and S.-T. Hwang, *Hollow fiber membrane contactors*. *Journal of Membrane Science*, 1999. **159**(1–2): p. 61-106.
10. Feron, P.H.M. and A.E. Jansen, *Capture of carbon dioxide using membrane gas absorption and reuse in the horticultural industry*. *Energy Conversion and Management*, 1995. **36**(6–9): p. 411-414.
11. Baker, R., *Membrane Technology and Applications*. 2004: Wiley.
12. Merkel, T.C., et al., *Ultraparpermeable, reverse-selective nanocomposite membranes*. *Science*, 2002. **296**: p. 519-522.
13. Javaid, A., *Membranes for solubility-based gas separation applications*. *Chemical Engineering Journal*, 2005. **112**(1–3): p. 219-226.
14. Ismail, A.F. and W. Lorna, *Penetrant-induced plasticization phenomenon in glassy polymers for gas separation membrane*. *Separation and Purification Technology*, 2002. **27**(3): p. 173-194.
15. Bos, A., et al., *CO₂-induced plasticization phenomena in glassy polymers*. *Journal of Membrane Science*, 1999. **155**(1): p. 67-78.
16. Masuda, T., E. Isobe, and T. Higashimura, *Polymerization of 1-(trimethylsilyl)-1-propyne by halides of niobium(V) and tantalum(V) and polymer properties*. *Macromolecules*, 1985. **18**(5): p. 841-845.
17. Pinnau, I. and L.G. Toy, *Transport of organic vapors through poly(1-trimethylsilyl-1-propyne)*. *Journal of Membrane Science*, 1996. **116**(2): p. 199-209.
18. Witchey-Lakshmanan, L.C., H.B. Hopfenberg, and R.T. Chern, *Sorption and transport of organic vapors in poly[1-(trimethylsilyl)-1-propyne]*. *Journal of Membrane Science*, 1990. **48**(2–3): p. 321-331.
19. Merkel, T.C., et al., *Sorption and transport of hydrocarbon and perfluorocarbon gases in poly(1-trimethylsilyl-1-propyne)*. *Journal of Polymer Science Part B: Polymer Physics*, 2000. **38**(2): p. 273-296.
20. Toy, L.G., et al., *Gas-separation process*. 1994.
21. Nakagawa, T., et al., *Physical modification of poly [1(trimethylsilyl)-1-propyne] membranes for gas separation*. *Journal of Membrane Science*, 1994. **94**(1): p. 183-193.

22. Nagai, K., et al., *Poly[1-(trimethylsilyl)-1-propyne] and related polymers: synthesis, properties and functions*. Progress in Polymer Science, 2001. **26**(5): p. 721-798.
23. Takada, K., et al., *Gas permeability of polyacetylenes carrying substituents*. Journal of Applied Polymer Science, 1985. **30**(4): p. 1605-1616.
24. Robeson, L.M., *Polymer membranes for gas separation*. Current Opinion in Solid State and Materials Science, 1999. **4**(6): p. 549-552.
25. Gomes, D., S.P. Nunes, and K.-V. Peinemann, *Membranes for gas separation based on poly(1-trimethylsilyl-1-propyne)-silica nanocomposites*. Journal of Membrane Science, 2005. **246**(1): p. 13-25.
26. Merkel, T.C., *Organic-inorganic nanocomposite membranes for vapor separations*. 2001, North Carolina State University, USA.
27. Bi, J., et al., *Effects of solvent in the casting of poly(1-trimethylsilyl-1-propyne) membranes*. Radiation Physics and Chemistry, 2000. **58**(5): p. 563-566.
28. Robeson, L.M., et al., *High performance polymers for membrane separation*. Polymer, 1994. **35**(23): p. 4970-4978.
29. Jia, J. and G.L. Baker, *Cross-linking of poly[1-(trimethylsilyl)-1-propyne] membranes using bis(aryl azides)*. Journal of Polymer Science Part B: Polymer Physics, 1998. **36**(6): p. 959-968.
30. Morlière, N., et al., *Impact of thermal ageing on sorption and diffusion properties of PTMSP*. Journal of Membrane Science, 2006. **270**(1-2): p. 123-131.
31. Kelman, S.D., et al., *Crosslinking poly[1-(trimethylsilyl)-1-propyne] and its effect on physical stability*. Journal of Membrane Science, 2008. **320**(1-2): p. 123-134.
32. Chung, T.-S., et al., *Mixed matrix membranes (MMMs) comprising organic polymers with dispersed inorganic fillers for gas separation*. Progress in Polymer Science, 2007(32): p. 483-507.
33. Aroon, M.A., et al., *Performance studies of mixed matrix membranes for gas separation: A review*. Separation and Purification Technology, 2010. **75**(3): p. 229-242.
34. Moore, T.T., et al., *Hybrid membrane materials comprising organic polymers with rigid dispersed phases*. AIChE Journal, 2004. **50**(2): p. 311-321.
35. Cong, H., et al., *Polymer-inorganic nanocomposite membranes for gas separation*. Separation and Purification Technology, 2007. **55**(3): p. 281-291.
36. Merkel, T.C., et al., *Sorption, Transport, and Structural Evidence for Enhanced Free Volume in Poly(4-methyl-2-pentyne)/Fumed Silica Nanocomposite Membranes*. Chemistry of Materials, 2002. **15**(1): p. 109-123.
37. Matteucci, S., et al., *Gas transport in TiO₂ nanoparticle-filled poly(1-trimethylsilyl-1-propyne)*. Journal of Membrane Science, 2008. **307**(2): p. 196-217.
38. Merkel, T.C., et al., *Sorption and Transport in Poly(2,2-bis(trifluoromethyl)-4,5-difluoro-1,3-dioxole-co-tetrafluoroethylene) Containing Nanoscale Fumed Silica*. Macromolecules, 2003. **36**(22): p. 8406-8414.
39. Barrer, R.M., J.A. Barrie, and N.K. Raman, *Solution and diffusion in silicone rubber II—The influence of fillers*. Polymer, 1962. **3**(0): p. 605-614.
40. Hoff, K.A., et al., *Modeling and Experimental Study of Carbon Dioxide Absorption in Aqueous Alkanolamine Solutions Using a Membrane Contactor*. Industrial & Engineering Chemistry Research, 2004. **43**(16): p. 4908-4921.
41. Dindore, V.Y., et al., *CO₂ absorption at elevated pressures using a hollow fiber membrane contactor*. Journal of Membrane Science, 2004. **235**(1-2): p. 99-109.
42. Drioli, E., A. Criscuoli, and E. Curcio, *Membrane Contactors: Fundamentals, Applications and Potentialities: Fundamentals, Applications and Potentialities*. 2011: Elsevier Science.
43. Dindore, V.Y., *Gas purification using membrane gas absorption processes*. 2003, V.Y. Dindore: Enschede. p. IV, 205 s. ill.
44. Nguyen, P.T., et al., *A dense membrane contactor for intensified CO₂ gas/liquid absorption in post-combustion capture*. Journal of Membrane Science, 2011. **377**(1-2): p. 261-272.

45. Li, J.-L. and B.-H. Chen, *Review of CO₂ absorption using chemical solvents in hollow fiber membrane contactors*. Separation and Purification Technology, 2005. **41**(2): p. 109-122.
46. Wang, K.L. and E.L. Cussler, *Baffled membrane modules made with hollow fiber fabric*. Journal of Membrane Science, 1993. **85**(3): p. 265-278.
47. Rongwong, W., R. Jiratananon, and S. Atchariyawut, *Experimental study on membrane wetting in gas-liquid membrane contacting process for CO₂ absorption by single and mixed absorbents*. Separation and Purification Technology, 2009. **69**(1): p. 118-125.
48. Austgen, D.M., G.T. Rochelle, and C.C. Chen, *Model of vapor-liquid equilibria for aqueous acid gas-alkanolamine systems. 2. Representation of hydrogen sulfide and carbon dioxide solubility in aqueous MDEA and carbon dioxide solubility in aqueous mixtures of MDEA with MEA or DEA*. Industrial & Engineering Chemistry Research, 1991. **30**(3): p. 543-555.
49. Wang, R., et al., *Influence of membrane wetting on CO₂ capture in microporous hollow fiber membrane contactors*. Separation and Purification Technology, 2005. **46**(1-2): p. 33-40.
50. Decker, E.L., et al., *Physics of contact angle measurement*. Colloids and Surfaces A: Physicochemical and Engineering Aspects, 1999. **156**(1-3): p. 177-189.
51. De Sitter, K., et al., *Silica filled poly(1-trimethylsilyl-1-propyne) and poly(4-methyl-2-pentyne) membranes: similarities and differences in structural characteristics and membrane performances*. Desalination, 2006. **199**(1-3): p. 293-295.
52. De Sitter, K., et al., *Silica filled poly(1-trimethylsilyl-1-propyne) nanocomposite membranes: Relation between the transport of gases and structural characteristics*. Journal of Membrane Science, 2006. **278**(1-2): p. 83-91.
53. Ulutan, S. and T. Nakagawa, *Separability of ethanol and water mixtures through PTMSP-silica membranes in pervaporation*. Journal of Membrane Science, 1998. **143**(1-2): p. 275-284.
54. Pinnau, I., He, Z., *Filled superglassy membrane*. US Patent 6,316,684, 2001.
55. Kelman, S.D., et al., *The influence of crosslinking and fumed silica nanoparticles on mixed gas transport properties of poly[1-(trimethylsilyl)-1-propyne]*. Polymer, 2008. **49**(13-14): p. 3029-3041.
56. Qiu, J., J.M. Zheng, and K.V. Peinemann, *Gas Transport Properties in a Novel Poly(trimethylsilylpropyne) Composite Membrane with Nanosized Organic Filler Trimethylsilylglucose*. Macromolecules, 2006. **39**(12): p. 4093-4100.
57. Matteucci, S., et al., *Gas transport properties of MgO filled poly(1-trimethylsilyl-1-propyne) nanocomposites*. Polymer, 2008. **49**(6): p. 1659-1675.
58. Claes, S., et al., *Preparation and benchmarking of thin film supported PTMSP-silica pervaporation membranes*. Journal of Membrane Science, 2012. **389**(0): p. 265-271.
59. Shantarovich, V.P., et al., *Positron Annihilation Lifetime Study of High and Low Free Volume Glassy Polymers: Effects of Free Volume Sizes on the Permeability and Permselectivity*. Macromolecules, 2000. **33**(20): p. 7453-7466.
60. Matteucci, S., et al., *Transport of Gases and Vapors in Glassy and Rubbery Polymers*, in *Materials Science of Membranes for Gas and Vapor Separation*. 2006, John Wiley & Sons, Ltd. p. 1-47.
61. Esato, K. and B. Eiseman, *Experimental evaluation of Gore-Tex membrane oxygenator*. Vol. 69. 1975. 690-7.
62. Tsuji, T., et al., *Development and clinical evaluation of hollow fiber membrane oxygenator*. ASAIO Journal, 1981. **27**(1): p. 280-284.
63. Ho, W.S.W. and K.K. Sirkar, *Membrane Handbook*. 1992: Springer US.
64. Mansourizadeh, A. and A.F. Ismail, *Hollow fiber gas-liquid membrane contactors for acid gas capture: A review*. Journal of Hazardous Materials, 2009. **171**(1-3): p. 38-53.
65. Qi, Z. and E.L. Cussler, *Microporous hollow fibers for gas absorption : I. Mass transfer in the liquid*. Journal of Membrane Science, 1985. **23**(3): p. 321-332.
66. Qi, Z. and E.L. Cussler, *Microporous hollow fibers for gas absorption : II. Mass transfer across the membrane*. Journal of Membrane Science, 1985. **23**(3): p. 333-345.

67. Kreulen, H., et al., *Microporous hollow fibre membrane modules as gas-liquid contactors. Part 1. Physical mass transfer processes: A specific application: Mass transfer in highly viscous liquids*. Journal of Membrane Science, 1993. **78**(3): p. 197-216.
68. Kreulen, H., et al., *Microporous hollow fibre membrane modules as gas-liquid contactors Part 2. Mass transfer with chemical reaction*. Journal of Membrane Science, 1993. **78**(3): p. 217-238.
69. Cooney, D.O. and C.C. Jackson, *Gas absorption in a hollow fiber device*. Chemical Engineering Communications, 1989. **79**(1): p. 153-163.
70. Karoor, S. and K.K. Sirkar, *Gas absorption studies in microporous hollow fiber membrane modules*. Industrial & Engineering Chemistry Research, 1993. **32**(4): p. 674-684.
71. Rangwala, H.A., *Absorption of carbon dioxide into aqueous solutions using hollow fiber membrane contactors*. Journal of Membrane Science, 1996. **112**(2): p. 229-240.
72. Wang, R., et al., *Impact of DEA solutions with and without CO₂ loading on porous polypropylene membranes intended for use as contactors*. Journal of Membrane Science, 2004. **229**(1-2): p. 147-157.
73. Li, K. and W.K. Teo, *Use of permeation and absorption methods for CO₂ removal in hollow fibre membrane modules*. Separation and Purification Technology, 1998. **13**(1): p. 79-88.
74. Falk-Pedersen, O. and H. Dannström, *Separation of carbon dioxide from offshore gas turbine exhaust*. Energy Conversion and Management, 1997. **38**, Supplement(0): p. S81-S86.
75. Zhang, H.Y., et al., *Theoretical and experimental studies of membrane wetting in the membrane gas-liquid contacting process for CO₂ absorption*. Journal of Membrane Science, 2008. **308**(1-2): p. 162-170.
76. Khaisri, S., et al., *Comparing membrane resistance and absorption performance of three different membranes in a gas absorption membrane contactor*. Separation and Purification Technology, 2009. **65**(3): p. 290-297.
77. Nishikawa, N., et al., *CO₂ removal by hollow-fiber gas-liquid contactor*. Energy Conversion and Management, 1995. **36**(6-9): p. 415-418.
78. Nii, S. and H. Takeuchi, *Removal of CO₂ and/or SO₂ from gas streams by a membrane absorption method*. Gas Separation & Purification, 1994. **8**(2): p. 107-114.
79. Kim, Y.-S. and S.-M. Yang, *Absorption of carbon dioxide through hollow fiber membranes using various aqueous absorbents*. Separation and Purification Technology, 2000. **21**(1-2): p. 101-109.
80. Hoff, K.A., *Modeling and Experimental Study of Carbon Dioxide Absorption in a Membrane Contactor*. 2003, Norwegian University of Science and Technology, Department of Chemical Engineering. p. 210.
81. deMontigny, D., P. Tontiwachwuthikul, and A. Chakma, *Using polypropylene and polytetrafluoroethylene membranes in a membrane contactor for CO₂ absorption*. Journal of Membrane Science, 2006. **277**(1-2): p. 99-107.
82. Barbe, A.M., P.A. Hogan, and R.A. Johnson, *Surface morphology changes during initial usage of hydrophobic, microporous polypropylene membranes*. Journal of Membrane Science, 2000. **172**(1-2): p. 149-156.
83. Kamo, J., T. Hirai, and K. Kamada, *Solvent-induced morphological change of microporous hollow fiber membranes*. Journal of Membrane Science, 1992. **70**(2-3): p. 217-224.
84. Marzouk, S.A.M., et al., *Removal of carbon dioxide from pressurized CO₂-CH₄ gas mixture using hollow fiber membrane contactors*. Journal of Membrane Science, 2010. **351**(1-2): p. 21-27.
85. Al-saffar, H.B., B. Ozturk, and R. Hughes, *A Comparison of Porous and Non-Porous Gas-Liquid Membrane Contactors for Gas Separation*. Chemical Engineering Research and Design, 1997. **75**(7): p. 685-692.
86. Al-Marzouqi, M.H., et al., *CO₂ removal from CO₂-CH₄ gas mixture using different solvents and hollow Fiber Membranes*. Industrial and Engineering Chemistry Research, 2009. **48**(7): p. 3600-3605.

87. Stern, S.A., V.M. Shah, and B.J. Hardy, *Structure-permeability relationships in silicone polymers*. Journal of Polymer Science Part B: Polymer Physics, 1987. **25**(6): p. 1263-1298.
88. Teplyakov, V. and P. Meares, *Correlation aspects of the selective gas permeabilities of polymeric materials and membranes*. Gas Separation & Purification, 1990. **4**(2): p. 66-74.
89. Shelekhim, A.B. and I.N. Beckman, *Gas separation processes in membrane absorber*. Journal of Membrane Science, 1992. **73**(1): p. 73-85.
90. Yasuda, H. and K. Rosengren, *Isobaric measurement of gas permeability of polymers*. Journal of Applied Polymer Science, 1970. **14**(11): p. 2839-2877.
91. Kosaraju, P., et al., *Hollow Fiber Membrane Contactor Based CO₂ Absorption–Stripping Using Novel Solvents and Membranes*. Industrial & Engineering Chemistry Research, 2004. **44**(5): p. 1250-1258.
92. Chern, R.T., et al., *A note on the effects of mono-and di-bromination on the transport properties of poly(2,6-dimethylphenylene oxide)*. Journal of Membrane Science, 1990. **48**(2–3): p. 333-341.
93. Simons, K., K. Nijmeijer, and M. Wessling, *Gas–liquid membrane contactors for CO₂ removal*. Journal of Membrane Science, 2009. **340**(1–2): p. 214-220.
94. Ichiraku, Y., S.A. Stern, and T. Nakagawa, *An investigation of the high gas permeability of poly(1-Trimethylsilyl-1-Propyne)*. Journal of Membrane Science, 1987. **34**(1): p. 5-18.
95. Pinnau, I. and L.G. Toy, *Gas and vapor transport properties of amorphous perfluorinated copolymer membranes based on 2,2-bis(trifluoromethyl)-4,5-difluoro-1,3-dioxole/tetrafluoroethylene*. Journal of Membrane Science, 1996. **109**(1): p. 125-133.
96. Seglem, K.N., *Experimental results on first type of polymeric and hybrid membranes, in A Green Sea*. 2012.
97. Lin, H. and B. Freeman, in *Springer Handbook of Materials Measurement Methods*, H. Czichos, T. Saito, and L. Smith, Editors. 2006, Springer Berlin Heidelberg. p. 283-397.
98. Tomaša, T., *Development of membrane materials for gas-liquid membrane contactors for CO₂ capture from natural gas*. 2012, Norwegian University of Science and Technology, Department of Chemical Engineering.
99. Tomaša, T., *Development of Membrane Materials for Gas-liquid Membrane Contactors for CO₂ Capture from Natural Gas*. 2013, Norwegian University of Science and Technology, Department of Chemical Engineering. p. 119.
100. Yan, S.-p., et al., *Experimental study on the separation of CO₂ from flue gas using hollow fiber membrane contactors without wetting*. Fuel Processing Technology, 2007. **88**(5): p. 501-511.
101. Kumar, P.S., et al., *New absorption liquids for the removal of CO₂ from dilute gas streams using membrane contactors*. Chemical Engineering Science, 2002. **57**(9): p. 1639-1651.

APPENDIX

A. Permeation rig flowsheets

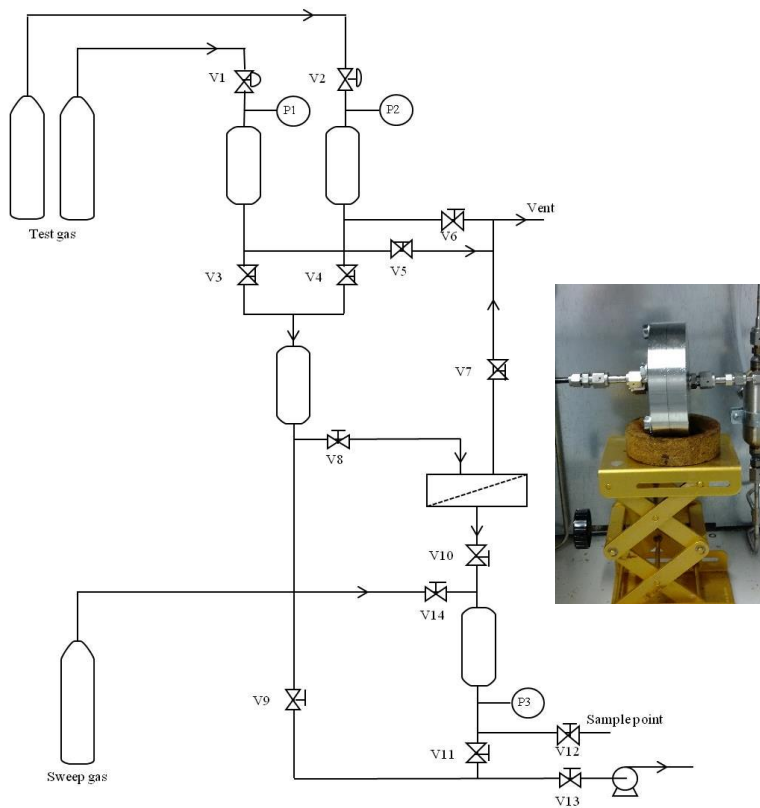


Figure A-2: Flowsheet of permeation rig 1 (PR-1)

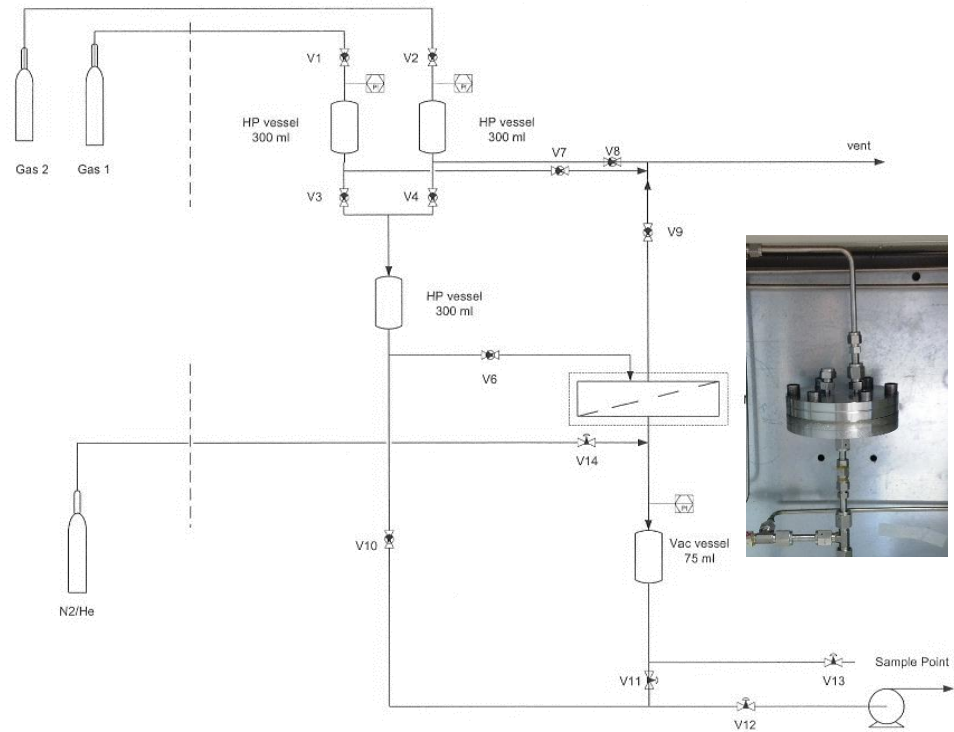


Figure A-1: Flowsheet of permeation rig 2 (PR-2).

B. Gas permeability results

The gas permeability was calculated using the equation:

$$P = \frac{lVT_0}{ATp_0(p_1 - p_2)} \frac{dp}{dt} \quad (\text{B.1})$$

This examples illustrates how the permeability, P, is generated using numbers for a membrane sample containing 5 wt% commercial T 805. The membrane is tested in the first permeation rig (PR-1), having a permeation volume of 134 cm³. CO₂ at 2 bar is used as the feed gas. Description and values of the individual parameters are given in Table B-1.

Table B-1: Description and values of variables in the permeability equation.

Variable	Description	Unit	Value
l	Membrane thickness	μm	52.4
V	Permeation volume	cm ³	134
T ₀	Standard temperature	K	273.15
A	Tested area of membrane sample	cm ²	1.5394
T	Temperature	K	295.15
p ₀	Standard pressure	bar	1.0133
p ₁	Feed pressure	bar	2.0717
p ₂	Permeate pressure	mbar	0.9633
dp/dt	Steady-state pressure change	mbar/s	0.9099

By using these variables, the permeability is calculated in the following manner:

$$\frac{(40 \cdot 10^{-4} \text{ cm}) \cdot 123 \text{ cm}^3 \cdot 273.15 \text{ K} \cdot (0.8729 \cdot 10^{-3} \cdot 75 \text{ cmHg} / \text{ s})}{(1.5394 \text{ cm}^2) \cdot 295.15 \text{ K} \cdot 1.0133 \cdot 75 \text{ cmHg} (2 - 0.8729 \cdot 10^{-3}) \cdot 75 \text{ cmHg}} = 2.44 \cdot 10^{-6} \frac{\text{cm}^3(\text{STP}) \cdot \text{cm}}{\text{cm}^2 \cdot \text{cmHg} \cdot \text{s}} \quad (\text{B.2})$$

Since 1 Barrer = 10⁻¹⁰ cm³(STP) · cm · cm⁻² · cmHg⁻¹ · s⁻¹, the CO₂ permeability at 2 bar is equal to 24 397 Barrer.

As the example shows, the permeate pressure, p₂, is so much lower than the feed pressure, p₁, that it may be neglected.

Table B-2: Measured permeabilities of pure PTMSP. One test conducted in each of the permeation rigs.

Test	Age (days)	Permeability (Barrer)						CO ₂ /CH ₄ selectivity		
		CH ₄			CO ₂			2 bar	4 bar	6 bar
		2 bar	4 bar	6 bar	2 bar	4 bar	6 bar			
1	8	8 289	8 463	8 459	23 669	23 702	23 409	2.86	2.80	2.77
2	8	9 898	10 231	10 239	22 235	23 375	23 475	2.25	2.28	2.29
Average		9 093	9 347	9 349	22 952	23 538	23 442	2.55	2.54	2.53
Standard deviation		1 138	1 250	1 259	1 014	231	47	0.43	0.36	0.34

Table B-3: Measured permeabilities of nanocomposites containing 5 wt% T 805 TiO₂. Three samples from same membrane tested in PR-1.

Test	Age (days)	Permeability (Barrer)						CO ₂ /CH ₄ selectivity		
		CH ₄			CO ₂			2 bar	4 bar	6 bar
		2 bar	4 bar	6 bar	2 bar	4 bar	6 bar			
1	18	6 739	7 033	7 106	18 279	18 407	18 452	2.71	2.62	2.60
2	45	9 145	9 435	9 396	24 517	24 509	24 193	2.68	2.60	2.57
3	55	7 704	8 003	8 094	24 397	25 049	24 819	3.17	3.13	3.07
Average		7 862	8 157	8 199	22 397	22 655	22 488	2.85	2.78	2.75
Standard deviation		1 211	1 208	1 149	3 567	3 689	3 509	0.27	0.30	0.28

Table B-4: Measured permeabilities of nanocomposites containing 20 wt% T 805 TiO₂. Three samples from same membrane tested in PR-2.

Test	Age (days)	Permeability (Barrer)						CO ₂ /CH ₄ selectivity		
		CH ₄			CO ₂			2 bar	4 bar	6 bar
		2 bar	4 bar	6 bar	2 bar	4 bar	6 bar			
1	35	8 772	9 637	10 059	17 584	21 149	24 080	2.00	2.19	2.39
2	39	13 963	14 461	14 350	25 586	26 956	27 351	1.83	1.86	1.91
3	45	12 680	13 154	13 426	24 721	27 669	28 838	1.95	2.10	2.15
Average		11 805	12 418	12 612	22 631	25 258	26 756	1.93	2.05	2.15
Standard deviation		2 704	2 495	2 258	4 391	3 576	2 434	0.09	0.17	0.24

Table B-5: Measured permeabilities of nanocomposites containing 5 wt% 15-400 nm TiO₂. Three samples from same membrane tested in PR-2.

Test	Age (days)	Permeability (Barrer)						CO ₂ /CH ₄ selectivity		
		CH ₄			CO ₂			2 bar	4 bar	6 bar
		2 bar	4 bar	6 bar	2 bar	4 bar	6 bar			
1	42	7 372	8 905	9 010	21 143	23 192	23 177	2.87	2.60	2.57
2	43	10 174	11 404	11 312	25 205	27 526	28 049	2.48	2.41	2.48
3	44	10 744	10 691	10 806	24 412	28 233	27 755	2.27	2.64	2.57
Average		9 440	10 333	10 376	23 587	26 317	26 327	2.54	2.55	2.54
Standard deviation		1 816	1 287	1 210	2 153	2 730	2 732	0.31	0.12	0.05

Table B-6: Measured permeabilities of nanocomposites containing 5 wt% >1 μm TiO_2 . Three samples from same membrane tested in PR-1.

Test	Age (days)	Permeability (Barrer)						CO ₂ /CH ₄ selectivity		
		CH ₄			CO ₂			2 bar	4 bar	6 bar
		2 bar	4 bar	6 bar	2 bar	4 bar	6 bar			
1	25	7 664	7 818	7 823	22 418	22 391	21 961	2.92	2.86	2.81
2	40	8 193	8 187	8 226	22 898	23 122	22 673	2.79	2.82	2.76
3	41	8 285	8 677	8 614	22 645	23 583	22 970	2.73	2.72	2.67
Average		8 047	8 228	8 221	22 653	23 032	22 534	2.82	2.80	2.74
Standard deviation		335	431	396	240	601	518	0.10	0.08	0.07

Table B-7: Pure gas permeability of CH₄ and CO₂ for membranes containing 5 wt% Aeroxide[®] T 805 TiO₂ nanoparticles exposed to solution (deionized water, 2 M MDEA and 4.2 M MDEA), the time of exposure varying from 1 day to 10 weeks. The numbers in grey gives the percentage change in permeability from the initial permeability of the unexposed nanocomposite membrane containing the same type and amount of nanoparticles.

Solution	Time of exposure (days)	Age (days)	Permeability (Barrer)						CO ₂ /CH ₄ selectivity		
			CH ₄			CO ₂			2 bar	4 bar	6 bar
			2 bar	4 bar	6 bar	2 bar	4 bar	6 bar			
Water	1	21	5 346	5 762	6 058	20 475	20 998	21 247	3.83	3.64	3.51
			-32%	-29%	-26%	-9%	-7%	-6%	34%	31%	28%
	7	27	8 681	9 017	9 107	25 274	26 268	25 915	2.91	2.91	2.85
			10%	11%	11%	13%	16%	15%	2%	5%	4%
	14	33	3 831	4 366	4 648	16 746	18 183	18 264	4.37	4.16	3.93
			-51%	-47%	-43%	-25%	-20%	-19%	53%	50%	43%
	35	86	4 173	4 465	4 640	16 151	16 573	16 893	3.87	3.71	3.64
			-47%	-45%	-43%	-28%	-27%	-25%	36%	33%	33%
	67	96	3 541	3 716	3 834	15 219	15 540	15 677	4.30	4.18	4.09
			-55%	-54%	-53%	-32%	-31%	-30%	51%	50%	49%

2 M MDEA	1	47	5 962	6 140	6 144	20 221	20 689	20 400	3.39	3.37	3.32
			-24%	-25%	-25%	-10%	-9%	-9%	19%	21%	21%
	7	28	2 922	3 167	3 375	14 289	15 123	15 426	4.89	4.77	4.57
			-63%	-61%	-59%	-36%	-33%	-31%	71%	72%	66%
	14	34	7 478	7 793	7 770	20 546	22 258	21 909	2.75	2.86	2.82
			-4.9%	-4.5%	-5.2%	-8.3%	-1.8%	-2.6%	-4%	3%	3%
	14 (2)	71	1 104	1 218	1 293	6 608	7 183	7 384	5.98	5.90	5.71
		-86%	-85%	-84%	-71%	-68%	-67%	110%	112%	108%	
	35	90	143	146	148	1 261	1 279	1 300	8.8	8.8	8.8
			-98%	-98	-98	-94%	-94%	-94%	208%	215%	220%
	64	94	179	183	182	1 515	1 553	1 545	8.47	8.50	8.48
			-98%	-98%	-98%	-93%	-93%	-93%	197%	206%	209%
4.2 M MDEA	1	26	462	486	487	3 556	3 627	3 617	7.69	7.47	7.43
			-94%	-94%	-94%	-84%	-84%	-84%	170%	169%	170%
	7	32	747	760	742	3 870	4 367	4 249	5.18	5.75	5.73
			-63%	-61%	-59%	-36%	-33%	-31%	82%	107%	109%
	14	35	161	169.9	172.5	1 558.3	1 592.4	1 598.2	9.68	9.37	9.27
			-98%	-98%	-98%	-93%	-93%	-93%	239%	237%	108%
	64	102	131	131	134	1 096	1 105	-	8.36	8.45	-
			-98%	-98%	-98%	-95%	-95%	-	193%	204%	-

Table B-8: Pure gas permeability of CH₄ and CO₂ for liquid-exposed membranes containing 20 wt% Aeroxide® T 805 TiO₂ nanoparticles. The numbers in grey gives the percentage change in permeability from the initial permeability of the unexposed nanocomposite.

Solution	Time of exposure (days)	Age (days)	Permeability (Barrer)						CO ₂ /CH ₄ selectivity		
			CH ₄			CO ₂			2 bar	4 bar	6 bar
			2 bar	4 bar	6 bar	2 bar	4 bar	6 bar			
Water	28	70	5 769	5 998	6 038	18 627	19 239	19 244	3.23	3.21	3.19
			-51%	-52%	-52%	-18%	-24%	-28%	67%	56%	48%
			2 741	2 766	2 870	11 019	11 403	11 539	4.02	4.12	4.02
Water	42	87	-77%	-78%	-77%	-51%	-55%	-57%	108%	101%	87%
			7 764	7 890	7 648	24 373	25 166	24 541	3.14	3.19	3.21
			-34%	-36%	-39%	8%	0%	-8%	63%	55%	49%
2 M MDEA	14	73	422	540	840	3 621	4 067	4 360	8.58	7.53	5.19
			-96%	-96%	-93%	-84%	-84%	-84%	345%	266%	141%
			168	174	184	1 555	1 666	1 734	9.28	9.59	9.43
			-99%	-99%	-99%	-93%	-93%	-94%	381%	367%	339%
			300	314	310	2 720	2 861	2 865	9.06	9.11	9.23
2 M MDEA	42	88	-97%	-97%	-98%	-88%	-89%	-89%	370%	343%	329%
			106	113	112	1 131	1 165	1 195	10.67	10.33	10.67
			-99%	-99%	-99%	-95%	-95%	-95%	453%	403%	396%
4.2 M MDEA	42	87	182	186	190	2 291	2 403	2 446	12.57	12.90	12.87
			-98%	-98%	-98%	-90%	-90%	-91%	552%	528%	499%
			276	-	271	2 425	-	2 513	8.79	-	9.28
4.2 M MDEA	63	102	-98%	-	-98%	-89%	-	-91%	356%	-	332%

Table B-9: Pure gas permeability of CH₄ and CO₂ for liquid-exposed membranes containing 5 wt% 15-400 nm TiO₂ nanoparticles. The numbers in grey gives the percentage change in permeability from the initial permeability of the unexposed nanocomposite.

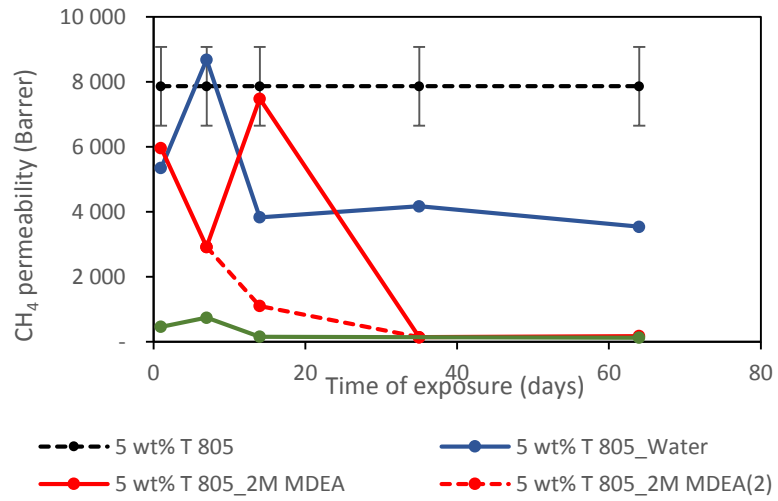
Solution	Time of exposure (days)	Age (days)	Permeability (Barrer)						CO ₂ /CH ₄ selectivity		
			CH ₄			CO ₂			2 bar	4 bar	6 bar
			2 bar	4 bar	6 bar	2 bar	4 bar	6 bar			
Water	1	21	8 690	8 959	9 210	28 451	30 184	30 384	3.27	3.37	3.30
			-8%	-13%	-11%	21%	15%	15%	29%	32%	30%
	7	27	4 009	4 304	4 534	18 303	21 218	23 403	4.57	4.93	5.16
			-58%	-58%	-56%	-22%	-19%	-11%	80%	93%	103%
	14	33	3 167	3 373	3 484	12 856	14 552	15 959	4.06	4.31	4.58
			-66%	-67%	-66%	-45%	-45%	-39%	60%	69%	80%
	35	88	3 000	3 112	3 208	17 578	18 260	18 682	5.86	5.87	5.82
			-68%	-70%	-69%	-25%	-31%	-29%	131%	130%	129%
	67	96	2 410	2 509	2 592	17 323	18 093	18 523	7.19	7.21	7.15
			-74%	-76%	-75%	-27%	-31%	-30%	183%	182%	181%
2 M MDEA	1	22	5 377	5 676	5 861	20 359	21 210	21 915	3.79	3.74	3.74
			-43%	-45%	-44%	-14%	-19%	-17%	49%	46%	47%
	7	28	294	297	292	2 131	2 338	2 274	7.25	7.88	7.78
			-97%	-97%	-97%	-91%	-91%	-91%	186%	209%	206%
	7 (2)	57	2 924	3 058	3 122	11 800	12 233	12 432	4.04	4.00	3.98
			-69%	-70%	-70%	-50%	-54%	-53%	59%	57%	57%
	14	34	1 361	1 428	1 454	8 121	8 502	8 592	5.97	5.96	5.91
			-86%	-86%	-86%	-66%	-68%	-67%	135%	133%	133%
	35	90	216	218	221	1 961	1 995	2 002	9.09	9.14	9.04
			-98%	-98%	-98%	-92%	-92%	-92%	258%	258%	256%
	64	94	97	101	102	1 031	1 057	1 080	10.66	10.46	10.54
			-99%	-99%	-99%	-96%	-96%	-96%	320%	310%	315%
4.2 M MDEA	1	26	808	836	831	5 809	5 986	5 932	7.19	7.16	7.14
			-91%	-92%	-92%	-75%	-77%	-77%	183%	180%	181%
	7	32	343	346	340	2 465	2 562	2 547	7.19	7.41	7.49
			-96%	-97%	-97%	-90%	-90%	-90%	183%	190%	195%
	14	35	117	121	122	1 115	1 167	1 181	9.54	9.63	9.65
			-99%	-99%	-99%	-95%	-96%	-96%	276%	277%	280%
	64	102	183	182	184	1 708	1 762	1 763	9.32	9.70	9.58

-98% 98% -98% -93% -93% -93% 267% 280% 277%

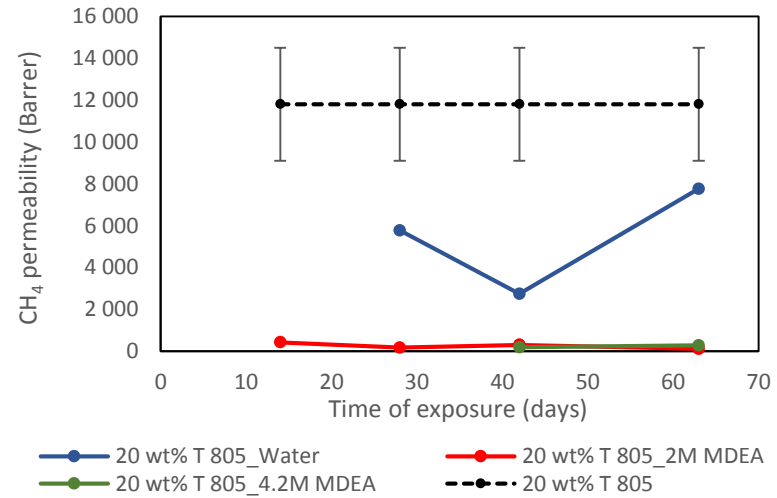
*Table B-10: Pure gas permeability of CH₄ and CO₂ for liquid-exposed membranes containing 5 wt% >1 μm TiO₂ nanoparticles. The numbers in grey gives the percentage change in permeability from the initial permeability of the unexposed nanocomposite. The membrane exposed to 4.2 M MDEA for 14 days (marked with *) was tested in PR-2 rather than PR-1.*

Solution	Time of exposure (days)	Age (days)	Permeability (Barrer)						CO ₂ /CH ₄ selectivity		
			CH ₄			CO ₂			2 bar	4 bar	6 bar
			2 bar	4 bar	6 bar	2 bar	4 bar	6 bar			
Water	1	36	5 648	5 982	6 195	15 803	16 918	16 911	2.80	2.83	2.73
			-30%	-27%	-25%	-30%	-27%	-25%	-1%	1%	0%
	7	49	6 415	6 671	6 690	20 728	21 153	21 011	3.23	3.17	3.14
			-20%	-19%	-19%	-9%	-8%	-7%	15%	13%	14%
	14	57	4 942	5 226	5 383	19 005	19 525	19 223	3.85	3.74	3.57
			-39%	-36%	-35%	-16%	-15%	-15%	36%	33%	30%
	35	87	3 614	3 870	4 153	17 479	17 936	18 130	4.84	4.63	4.37
			-55%	-53%	-49%	-23%	-22%	-20%	72%	65%	59%
	67	97	1 895	1 986	2 097	10 678	11 018	11 165	5.64	5.55	5.32
			-76%	-76%	-74%	-53%	-52%	-50%	100%	98%	94%
2 M MDEA	1	43	4 949	5 232	5 347	17 434	18 118	18 036	3.52	3.46	3.37
			-39%	-36%	-35%	-23%	-21%	-20%	25%	24%	23%
	7	50	234	239	249	1 873	1 962	1 945	8.01	8.20	7.82
			-97%	-97%	-97%	-92%	-91%	-91%	184%	193%	185%
	14	56	960	1 027	1 033	5 461	5 714	5 755	5.69	5.56	5.57
			-88%	-88%	-87%	-76%	-75%	-74%	102%	98%	103%
	35	93	348	358	352	2 580	2 579	2 572	7.41	7.21	7.31
			-96%	-96%	-96%	-89%	-89%	-89%	163%	157%	166%
	64	95	220	301	228	2 034	1 894	1 884	9.24	6.30	8.27
			-97%	-96%	-97%	-91%	-92%	-92%	228%	125%	201%
4.2 M MDEA	1	44	569	582	577	3 909	4 059	3 982	6.87	6.97	6.90
			-93%	-93%	-93%	-83%	-82%	-82%	144%	149%	152%
	7	51	141	143	147	1 598	1 713	1 715	11.31	11.95	11.65

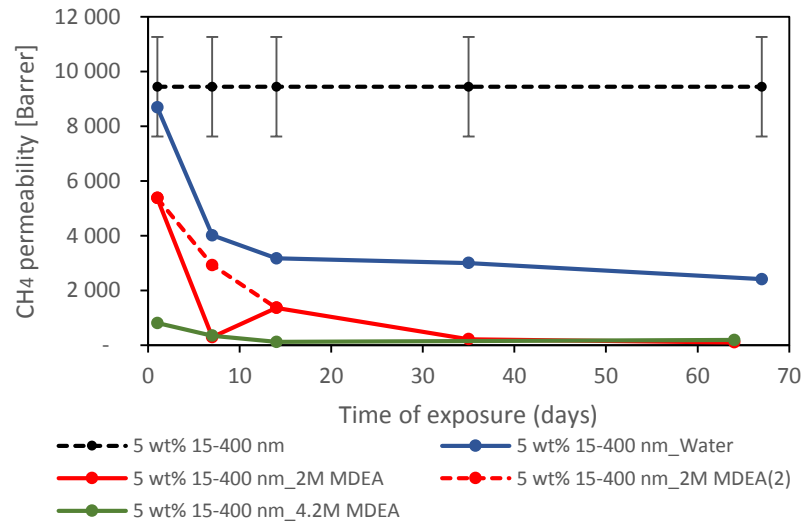
		-98%	-98%	-98%	-93%	-93%	-92%	301%	327%	3245%
14*	56	472	483	484	3 517	3 805	3 746	7.45	7.88	7.74
		-94%	-94%	-94%	-84%	-83%	-83%	165%	181%	182%
64	103	123	-	128	894	-	-	7.25	-	-
		-98%	-	-98%	-96%	-	-	157%	-	-



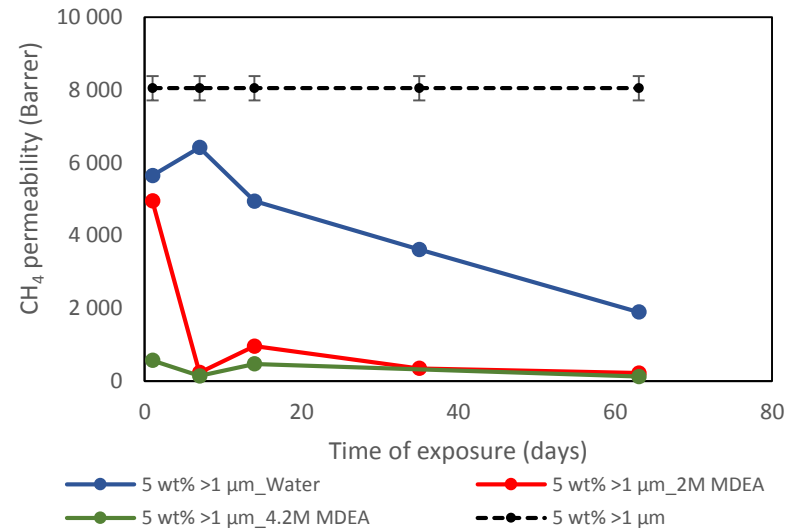
(a)



(b)



(c)



(d)

Figure B-3: CH₄ permeability of nanocomposites containing (a) 5wt% T 805, (b) 20 wt% T 805, (c) 5 wt% 15-400 nm and (d) 5 wt% >1 μm.

C. Contact angle measurements

Table C-11: Water contact angles on upside and downside of membranes containing 5 and 20 wt% T 805 TiO₂ prepared on casting plates of Teflon.

Membrane type	Contact angle (°)	
	Upside	Downside
5 wt% T 805	99.59 ± 1.21	125.71 ± 6.67
20 wt% T 805	94.46 ± 2.53	125.03 ± 4.69

Table C-12: Water contact angles on upside of membranes containing 5 and 20 wt% commercial T 805 TiO₂ exposed to water, 2 M MDEA and 4.2 M MDEA. Values in bold are measured before gas permeation test.

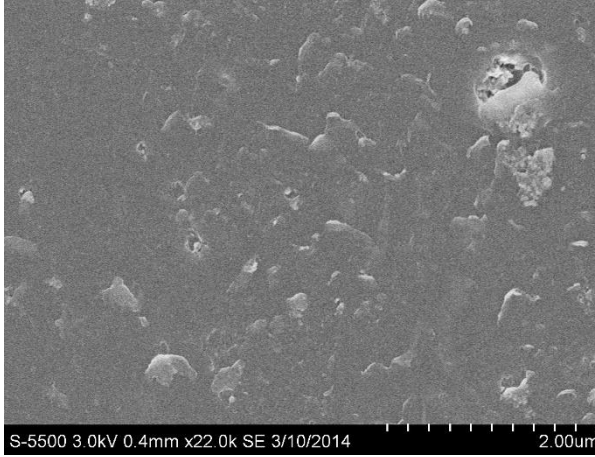
Time of exposure (days)	Contact angle (°)					
	5 wt% T 805			20 wt% T 805		
	Water	2 M MDEA	4.2 M MDEA	Water	2 M MDEA	4.2 M MDEA
1	-	88.30 ± 1.18	95.14 ± 0.84			
7	71.04 ± 5.42	-	-			
14	58.01 ± 3.37 57.89 ± 2.21	81.97 ± 2.04	86.31 ± 1.59	70.68 ± 1.41	95.70 ± 3.47	-
28				60.83 ± 3.70	89.69 ± 0.88	-
35/42	-	-	-	58.67 ± 0.93	82.37 ± 2.88 82.56 ± 2.79	89.48 ± 2.28
63	56.45 ± 3.19 65.50 ± 3.68	83.43 ± 2.62	80.44 ± 3.83	60.52 ± 0.37	88.36 ± 4.22	46.29 ± 0.60 86.14 ± 0.43

Table C-13: Water contact angles on upside of membranes containing 5 wt% 15-400 nm and >1 μm TiO₂ exposed to water, 2 M MDEA and 4.2 M MDEA. Values in bold are measured before gas permeation test.

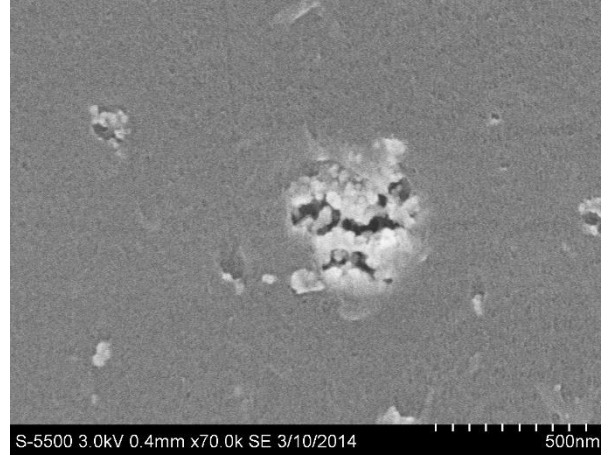
Time of exposure (days)	Contact angle (°)					
	5 wt% 15-400 nm			5 wt% >1 μm		
	Water	2 M MDEA	4.2 M MDEA	Water	2 M MDEA	4.2 M MDEA
1	89.30 ± 4.37	92.49 ± 1.93	95.27 ± 2.81	87.07 ± 2.91	96.82 ± 0.26	76.40 ± 3.21 100.69 ± 0.74
7	-	-	73.24 ± 3.54	-	-	61.99 ± 5.60
14	54.85 ± 2.63 69.74 ± 2.55	88.93 ± 1.56 82.46 ± 1.42	80.64 ± 1.11	67.07 ± 1.70 83.90 ± 0.68	91.43 ± 2.88	78.92 ± 1.95
35	-	78.53 ± 5.68	-	-	93.16 ± 7.68	-
63	51.56 ± 2.26 59.87 ± 5.46	78.69 ± 4.42	86.31 ± 2.68	46.84 ± 4.85 61.91 ± 4.88	86.88 ± 1.66	40.83 ± 2.70 80.08 ± 0.51

D. SEM images

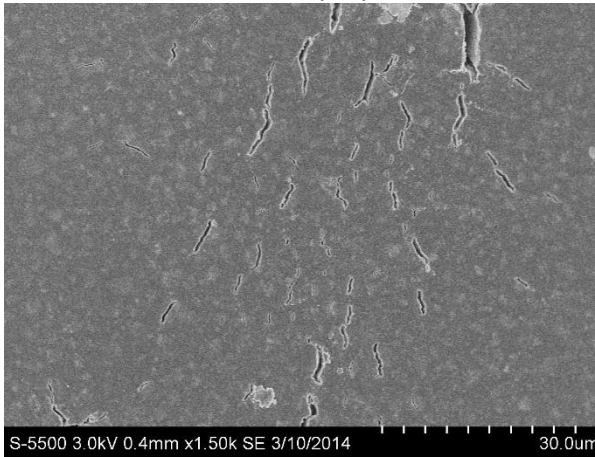
Nanocomposites containing 5 wt% commercial Aeroxide® T 805 TiO₂:



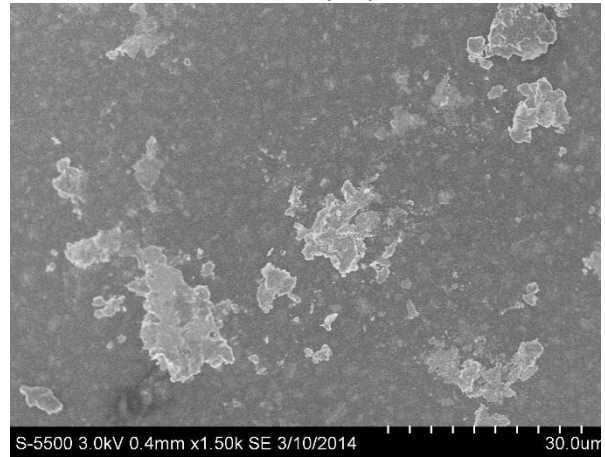
(a) Water 1 day, upside



(b) Water 1 day, upside



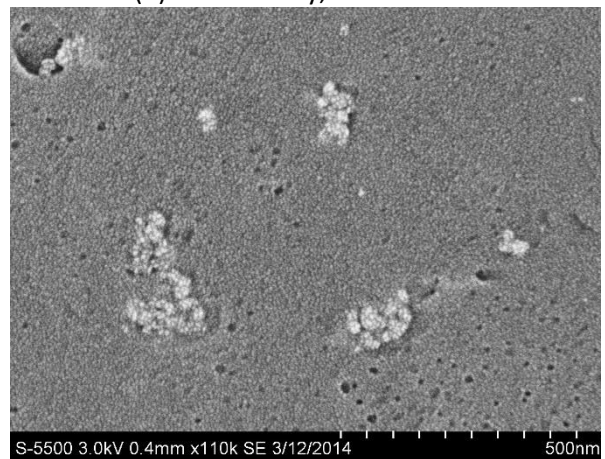
(c) Water 1 day, downside



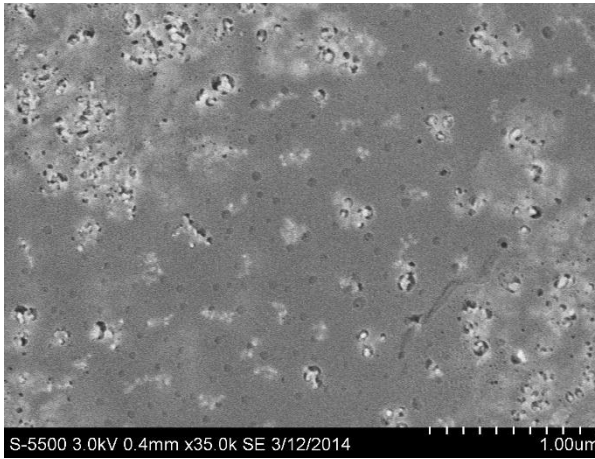
(d) Water 1 day, downside



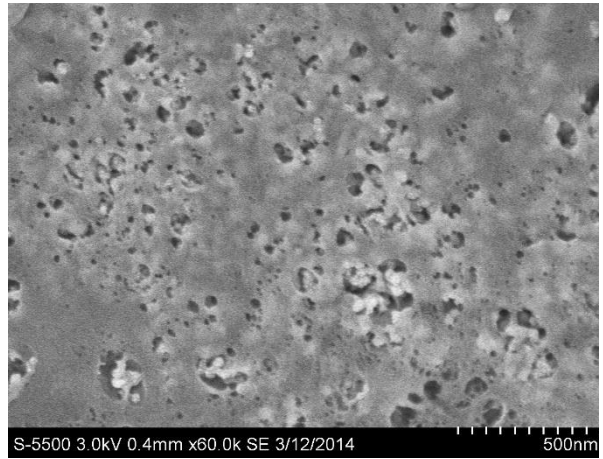
(e) 4.2 M MDEA 1 day, upside



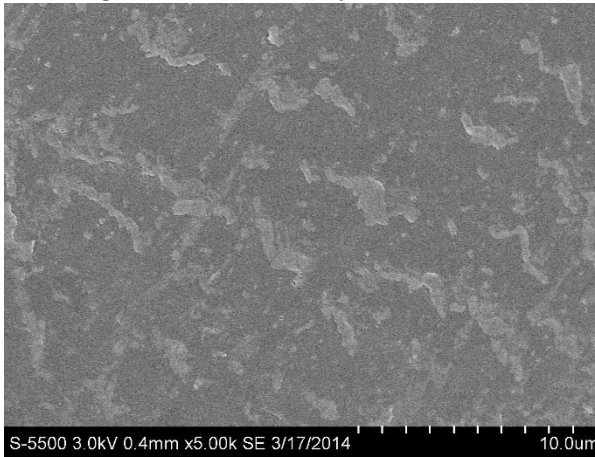
(f) 4.2 M MDEA 1 day, upside



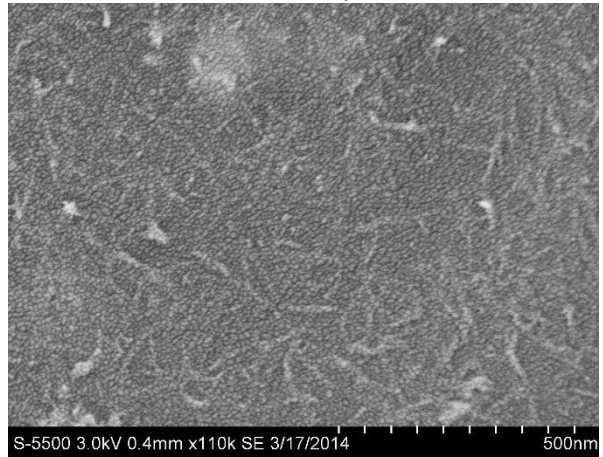
(g) 4.2 M MDEA 1 day, downside



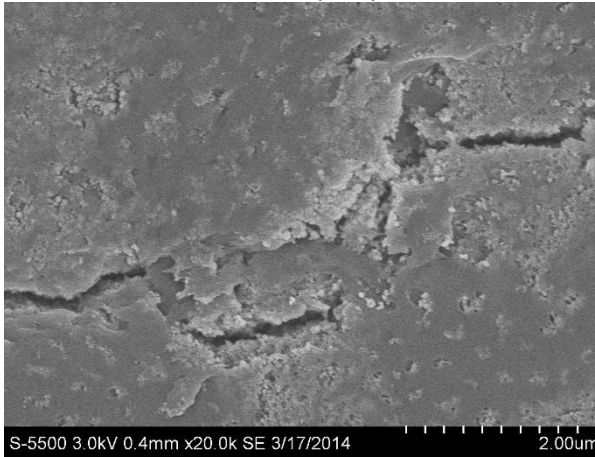
(h) 4.2 M MDEA 1 day, downside



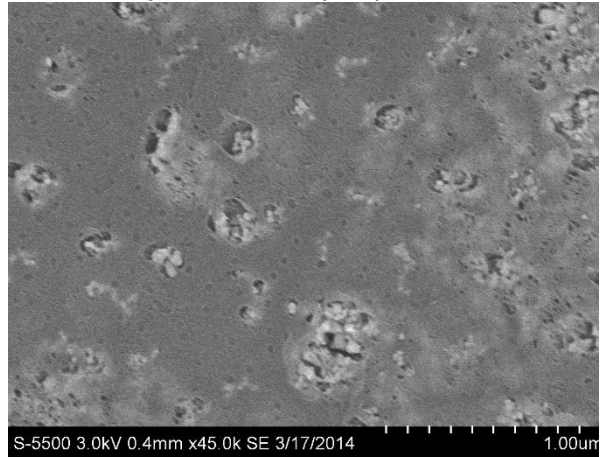
(i) Water 14 days, upside



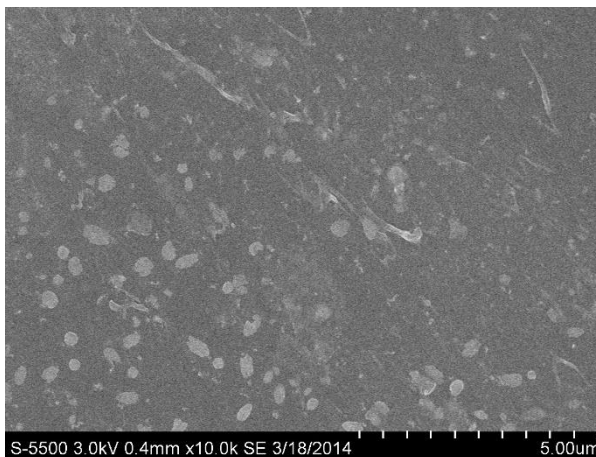
(j) Water 14 days, upside



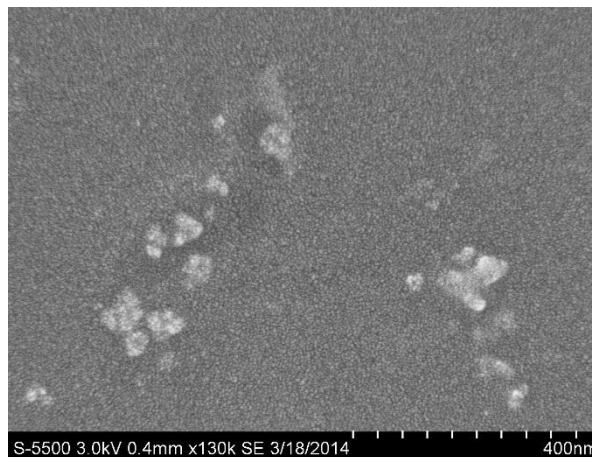
(k) Water 14 days, downside



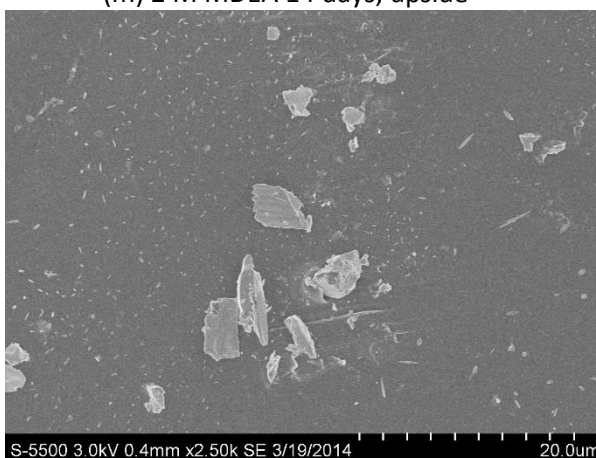
(l) Water 14 days, downside



(m) 2 M MDEA 14 days, upside



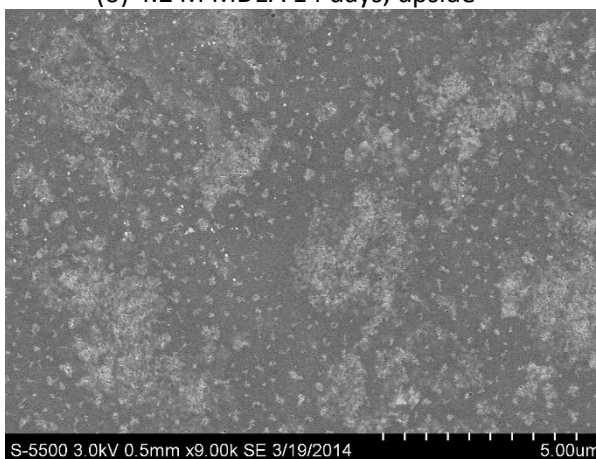
(n) 2 M MDEA 14 days, upside



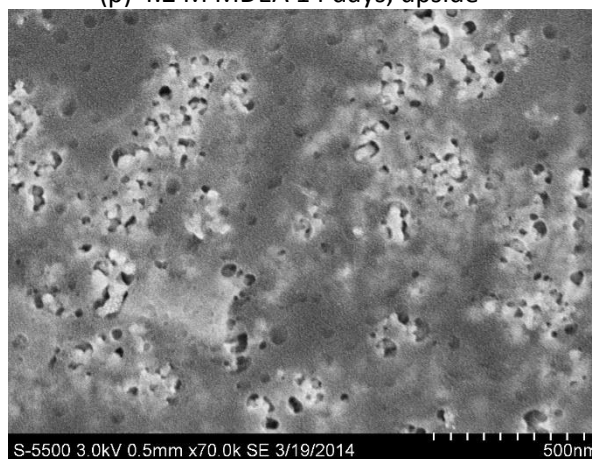
(o) 4.2 M MDEA 14 days, upside



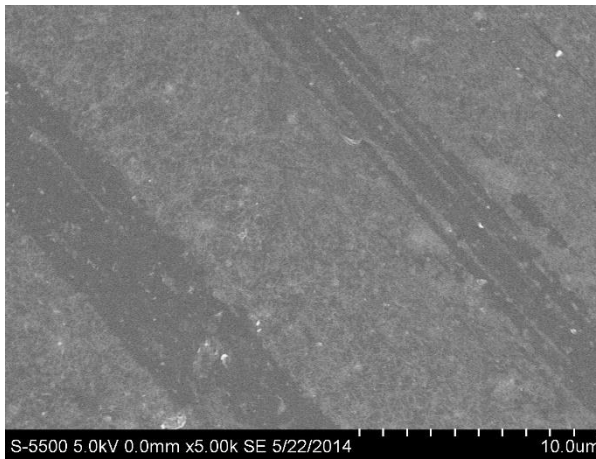
(p) 4.2 M MDEA 14 days, upside



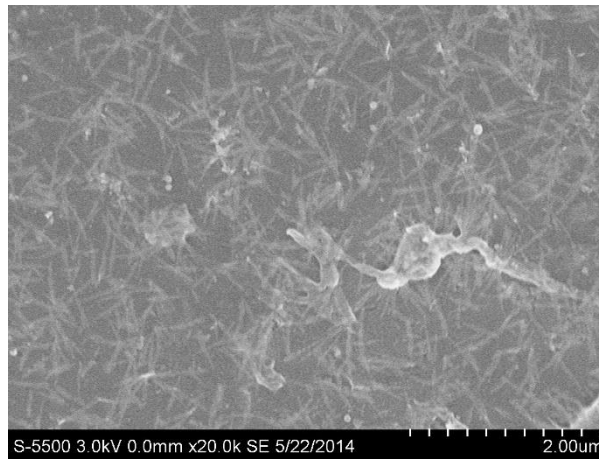
(q) 4.2 M MDEA 14 days, downside



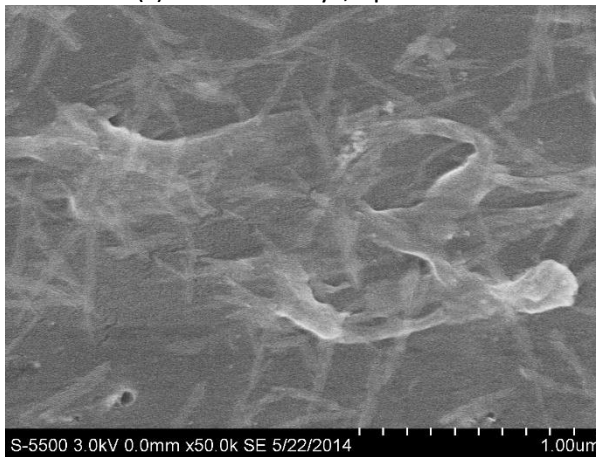
(r) 4.2 M MDEA 14 days, downside



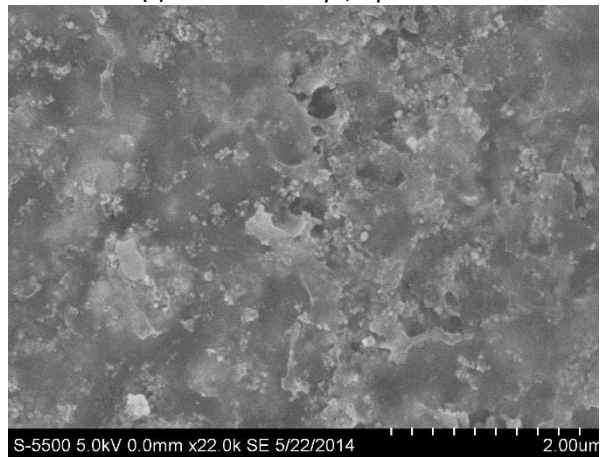
(s) Water 67 days, upside



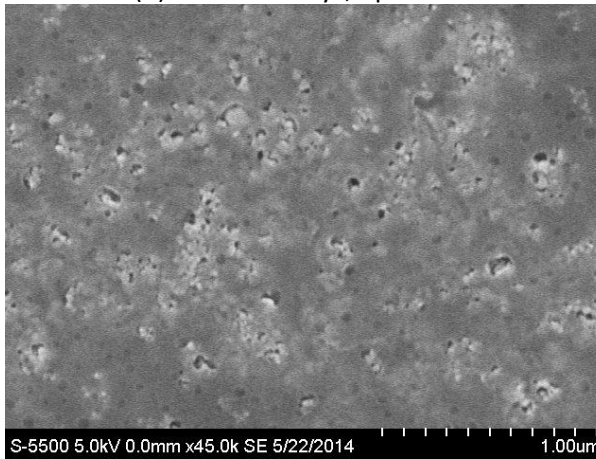
(t) Water 67 days, upside



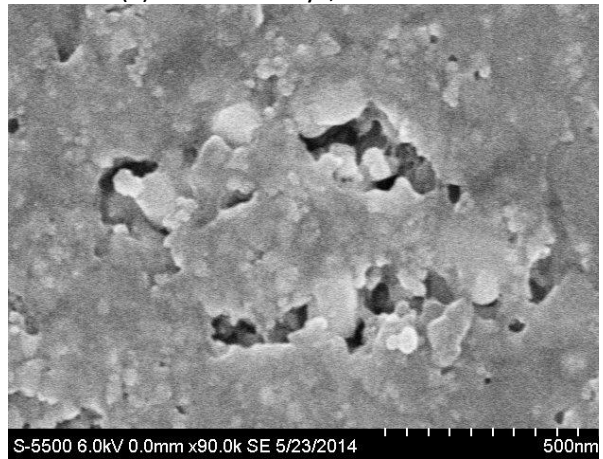
(u) Water 67 days, upside



(v) Water 67 days, downside



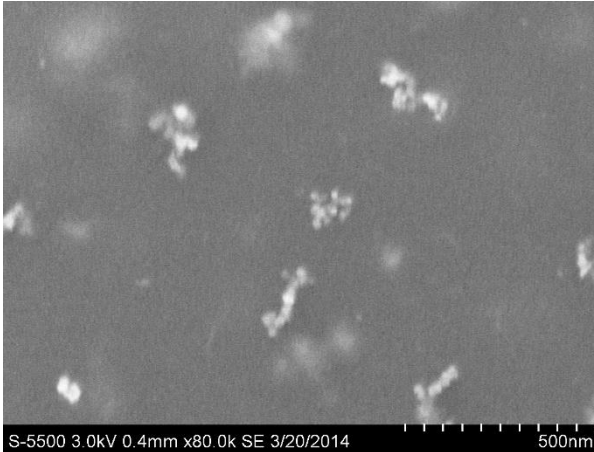
(w) 2 M MDEA 64 days, upside



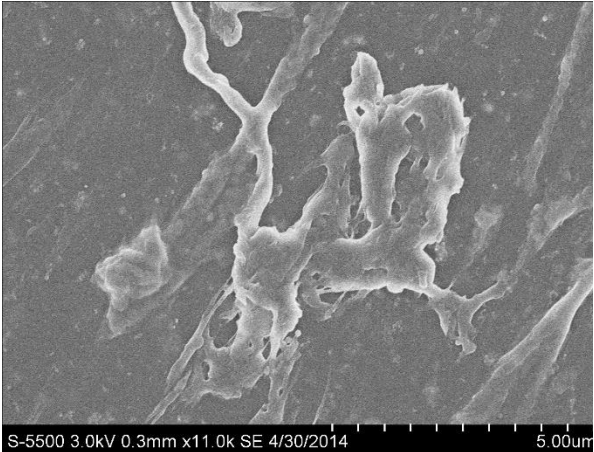
(x) 4.2 M MDEA 64 days, downside

Figure D-4: SEM images of membranes containing 5 wt% T 805 TiO₂.

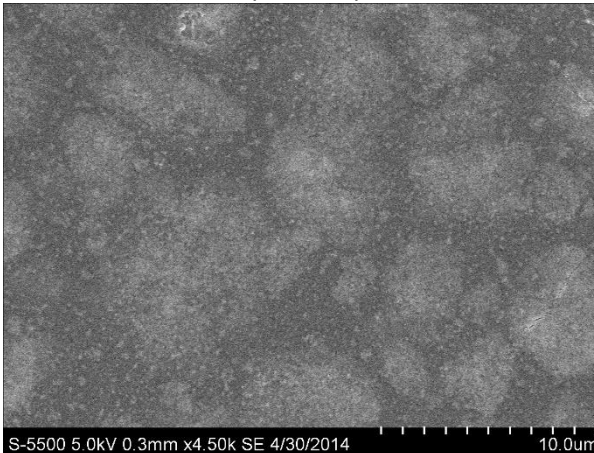
Nanocomposites containing 20 wt% commercial Aeroxide® T 805 TiO₂:



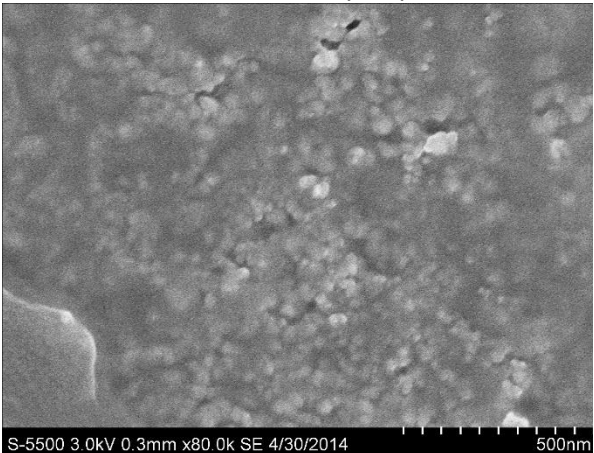
(a) Unexposed, upside



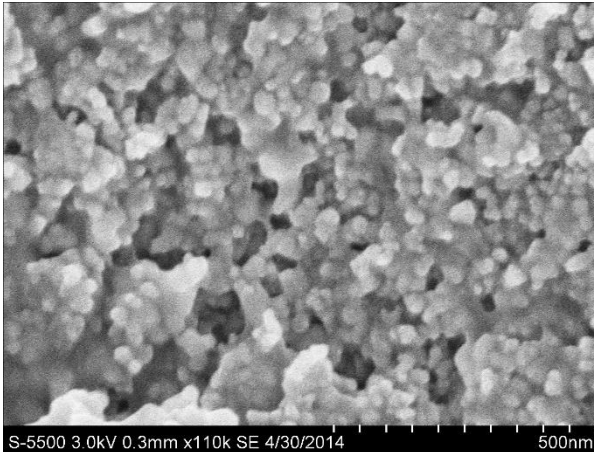
(b) 2 M MDEA 14 days, upside



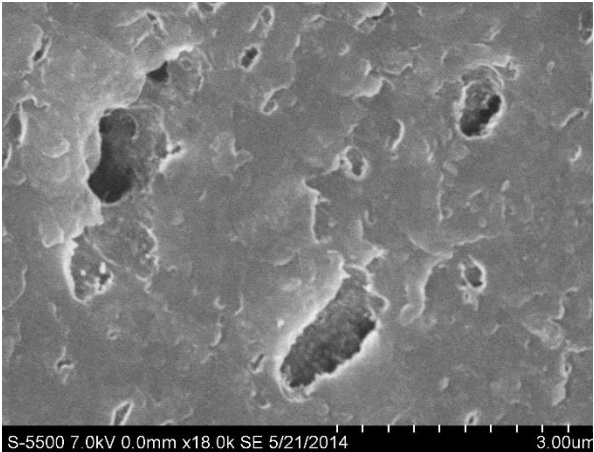
(c) 2 M MDEA 14 days, downside



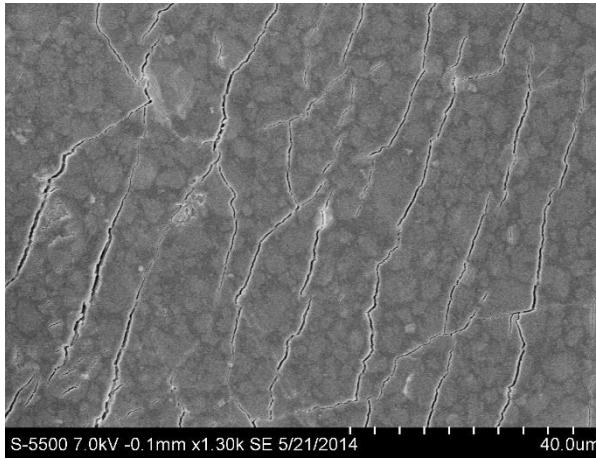
(d) 2 M MDEA 14 days, downside



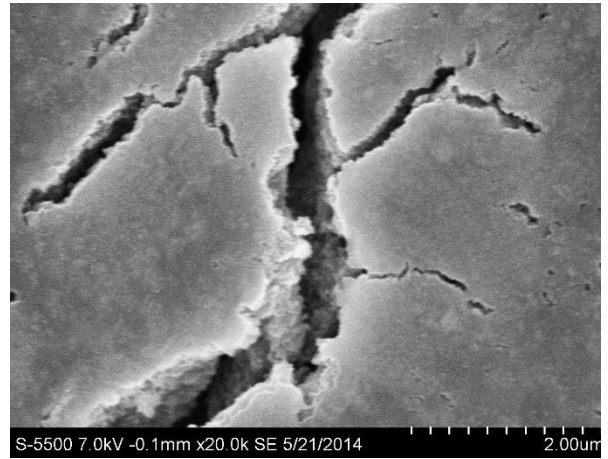
(e) 2 M MDEA 14 days, downside



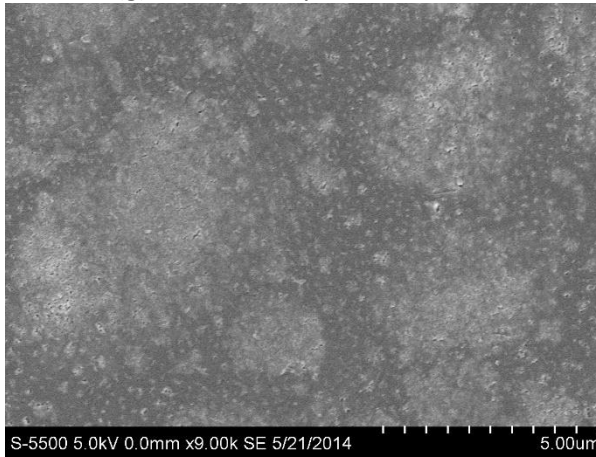
(f) Water 66 days, upside



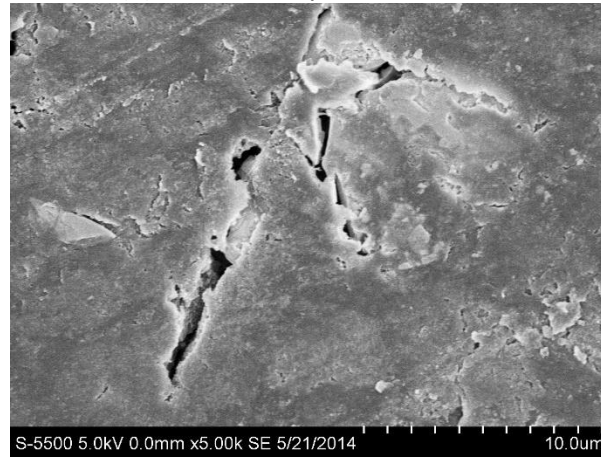
(g) Water 67 days, downside



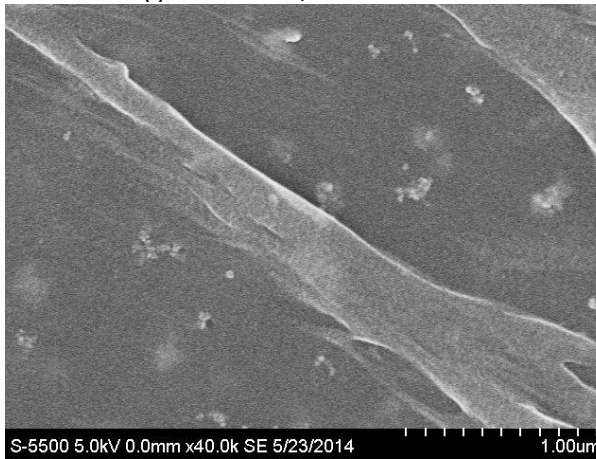
(h) Water 67 days, downside



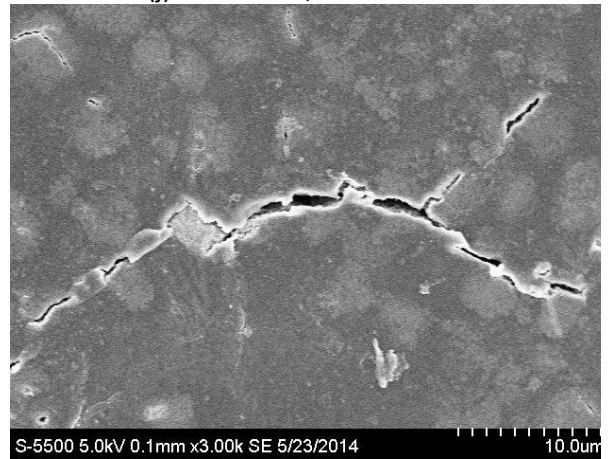
(i) 2 M MDEA, downside



(j) 2 M MDEA, downside



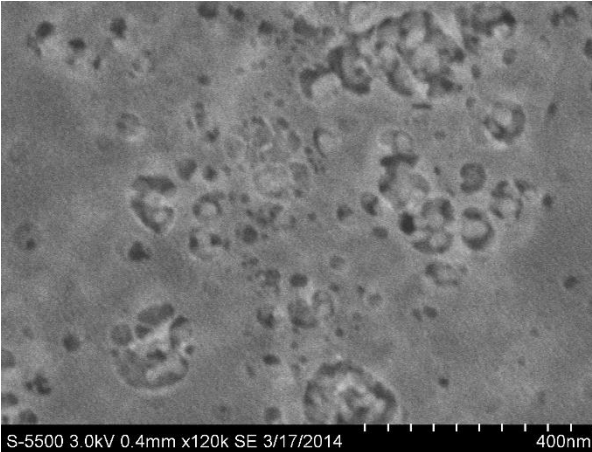
(k) 4.2 M MDEA 63 days, upside



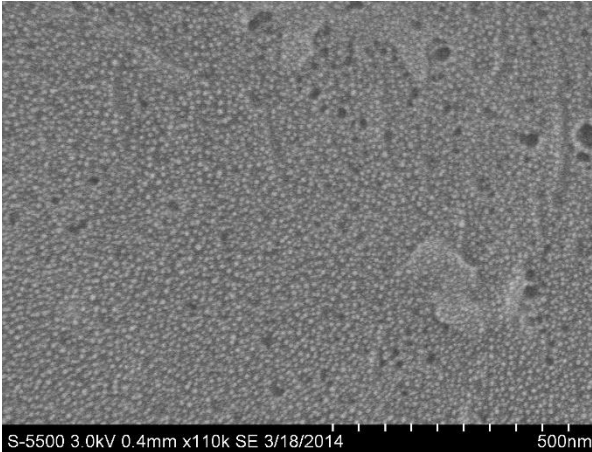
(l) 4.2 M MDEA 63 days, downside

Figure D-5: SEM images of membranes containing 20 wt% T 805 TiO₂.

Nanocomposites containing 5 wt% 15-400 nm TiO₂ from SINTEF Materials and Chemistry:



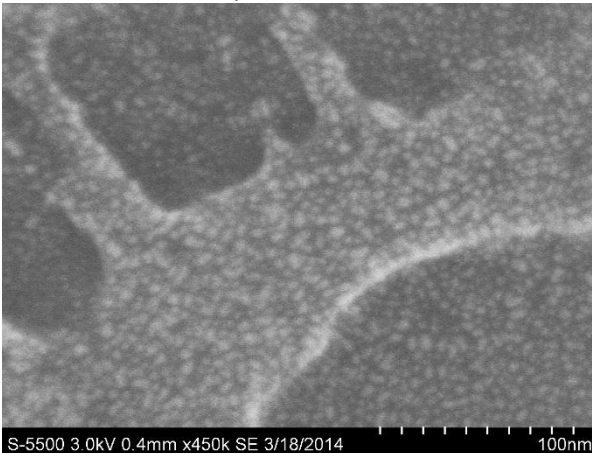
(a) Unexposed, downside



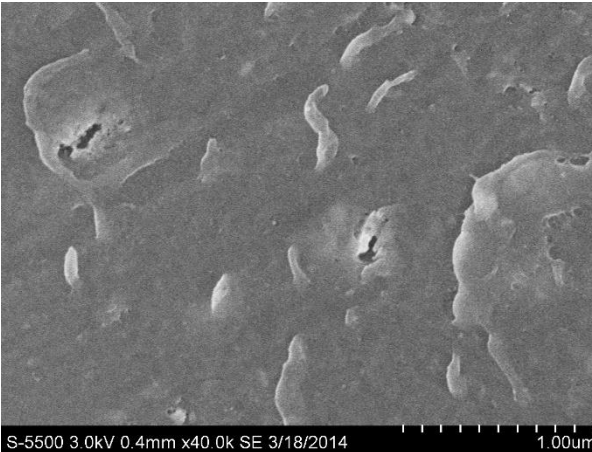
(b) Unexposed, downside



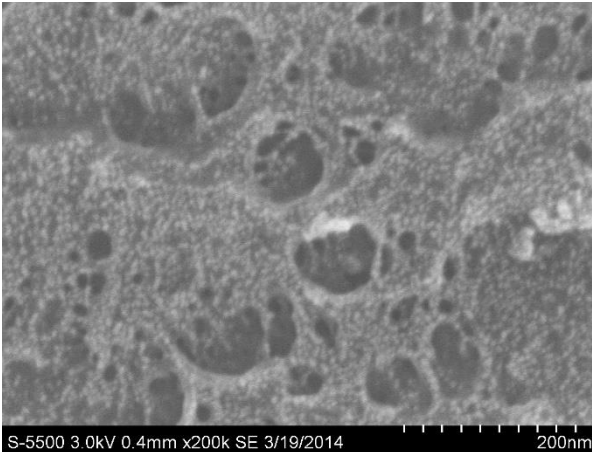
(c) 2 M MDEA 14 days, upside



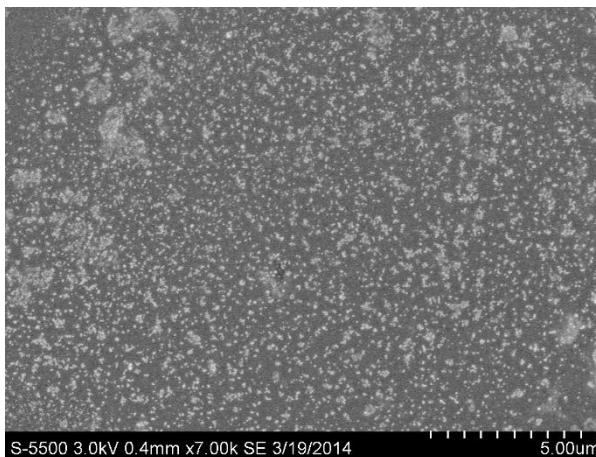
(d) 2 M MDEA 14 days, upside



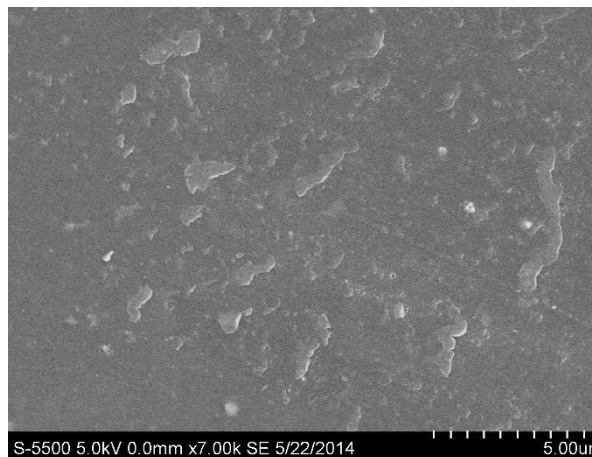
(e) 2 M MDEA 14 days, downside



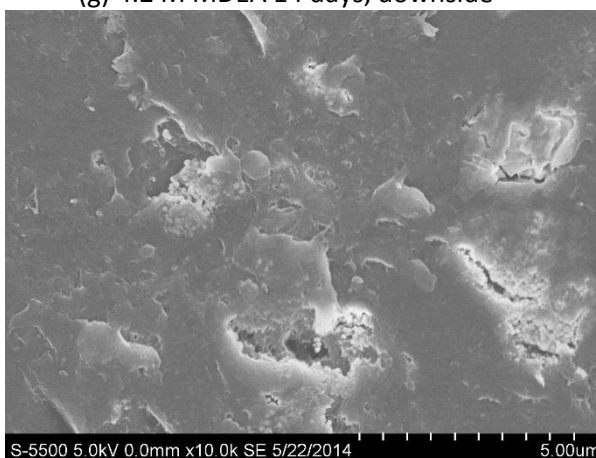
(f) 4.2 M MDEA 14 days, upside



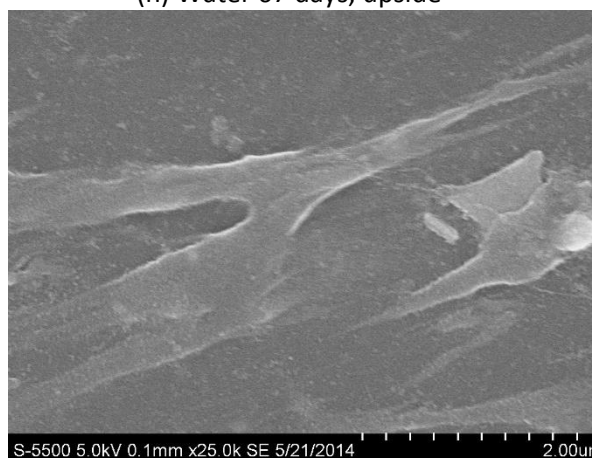
(g) 4.2 M MDEA 14 days, downside



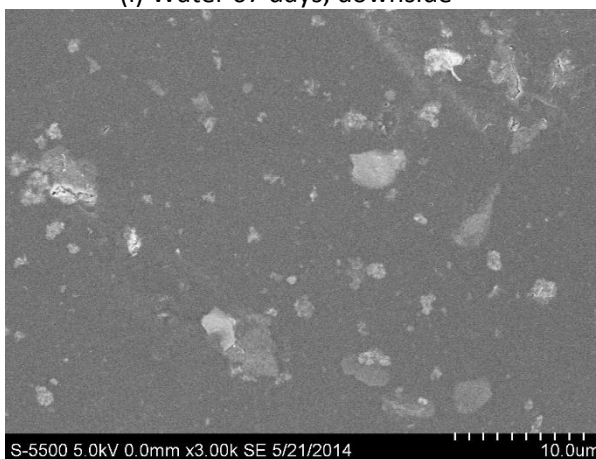
(h) Water 67 days, upside



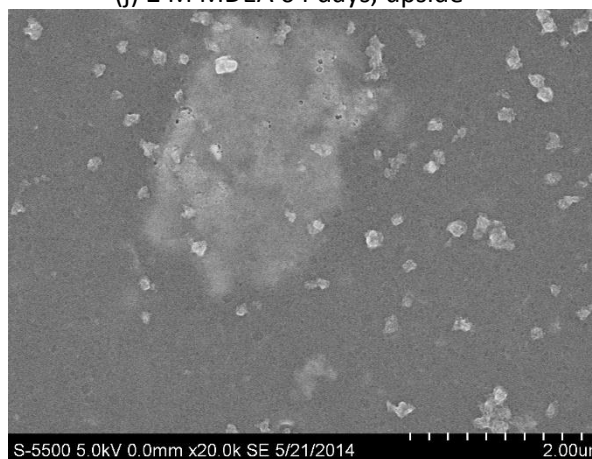
(i) Water 67 days, downside



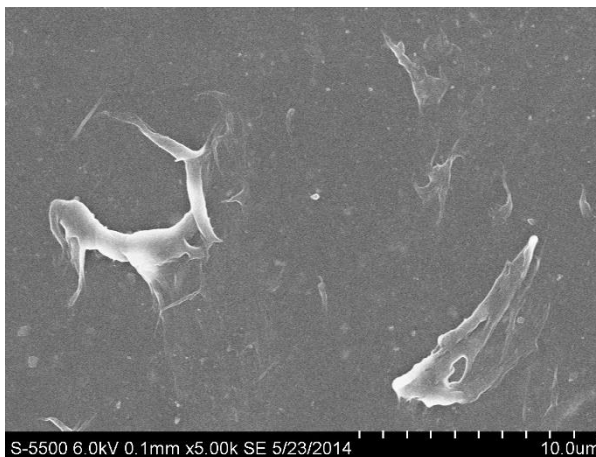
(j) 2 M MDEA 64 days, upside



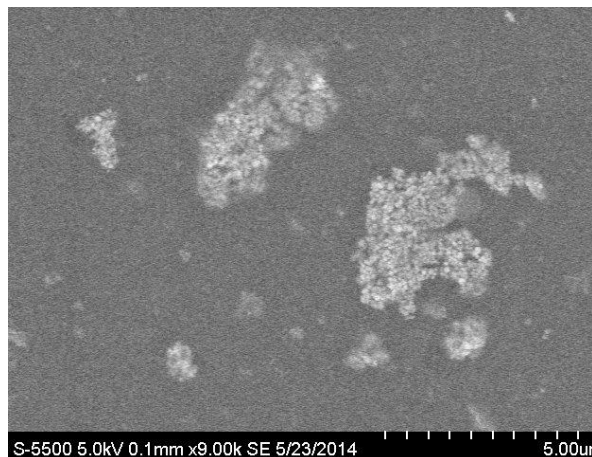
(k) 2 M MDEA 64 days, downside



(l) 2 M MDEA 64 days, downside



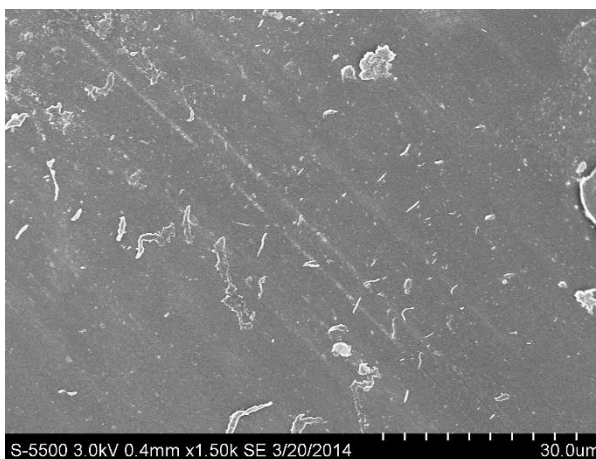
(m) 4.2 M MDEA 64 days, upside



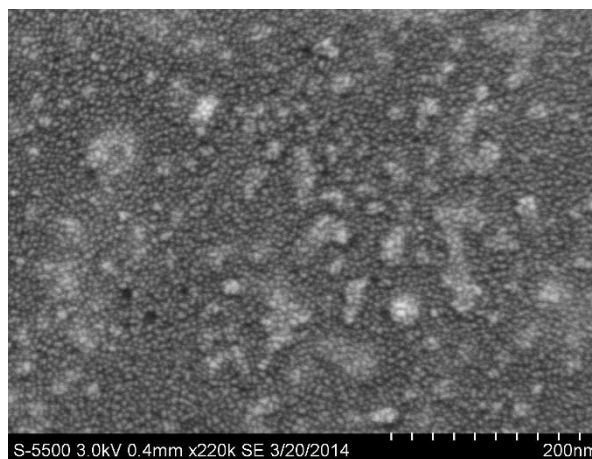
(n) 4.2 M MDEA 64 days, downside

Figure D-6: SEM images of membranes containing 5 wt% 15-400 nm TiO₂.

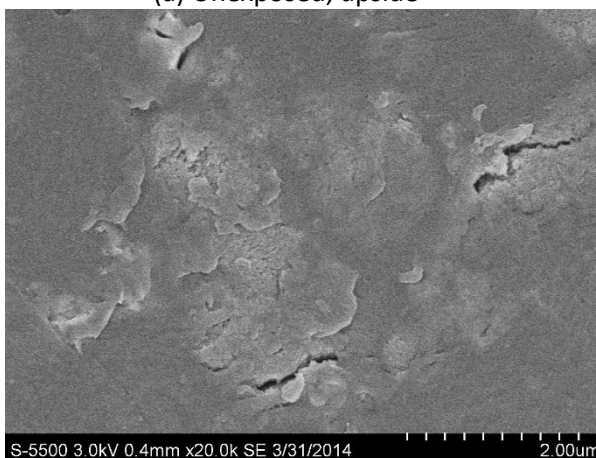
Nanocomposites containing 5 wt% >1 μm TiO₂ from SINTEF Materials and Chemistry:



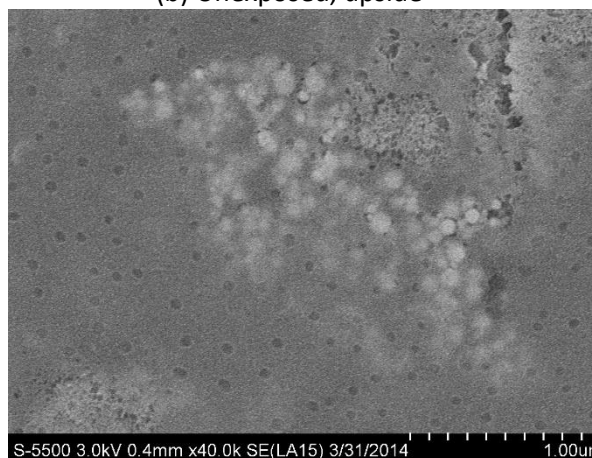
(a) Unexposed, upside



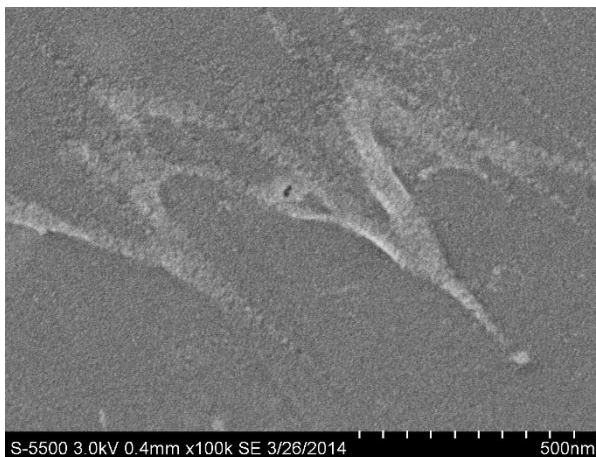
(b) Unexposed, upside



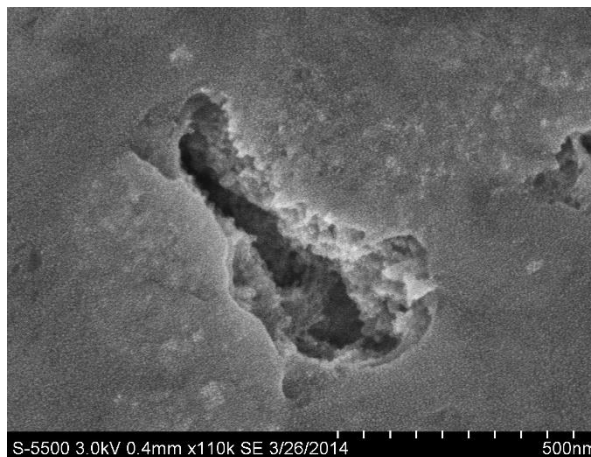
(c) Unexposed, downside



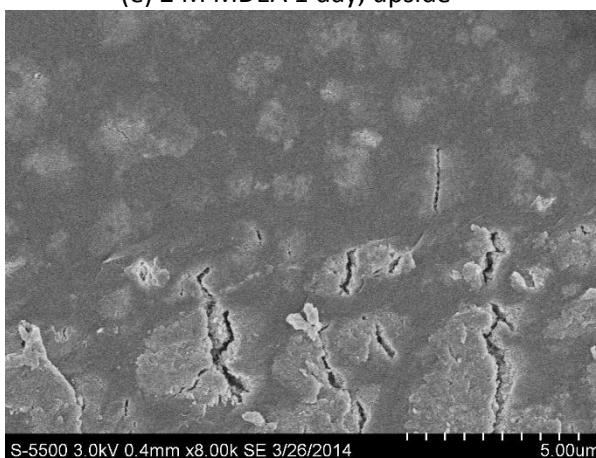
(d) Unexposed, downside



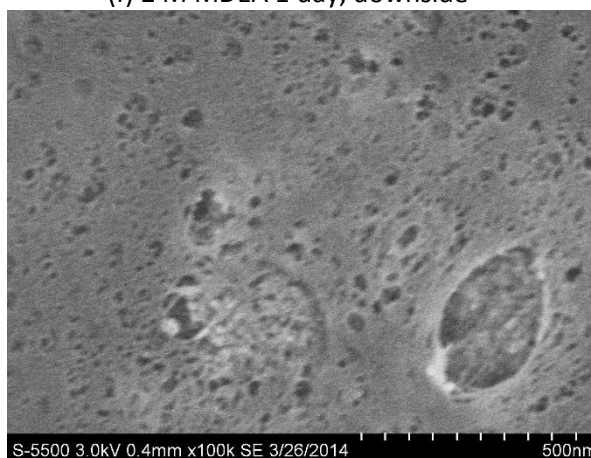
(e) 2 M MDEA 1 day, upside



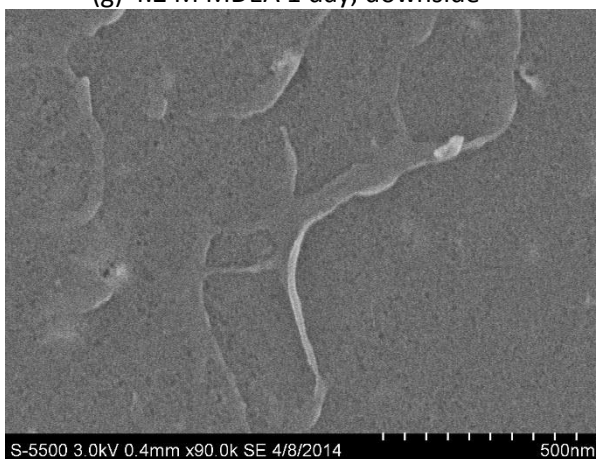
(f) 2 M MDEA 1 day, downside



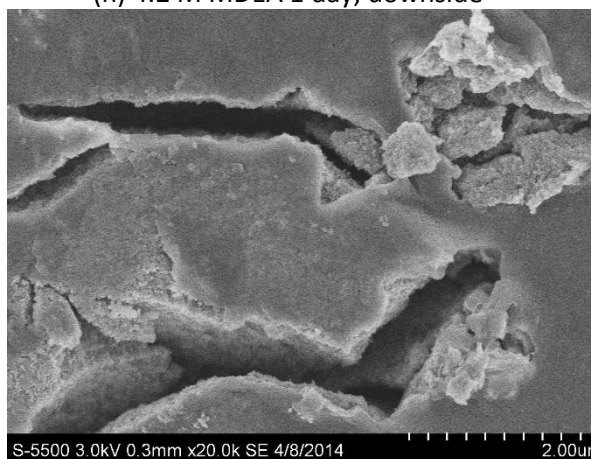
(g) 4.2 M MDEA 1 day, downside



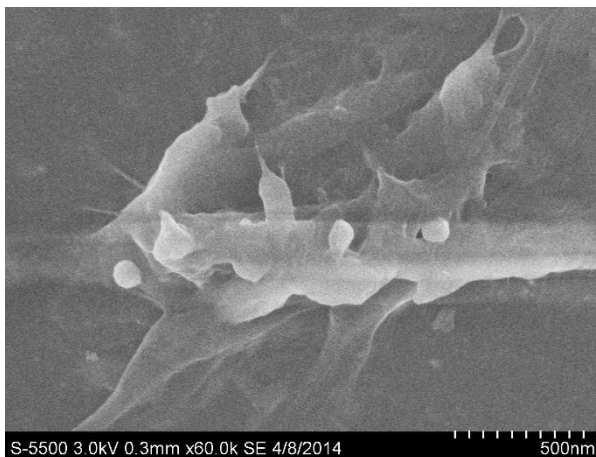
(h) 4.2 M MDEA 1 day, downside



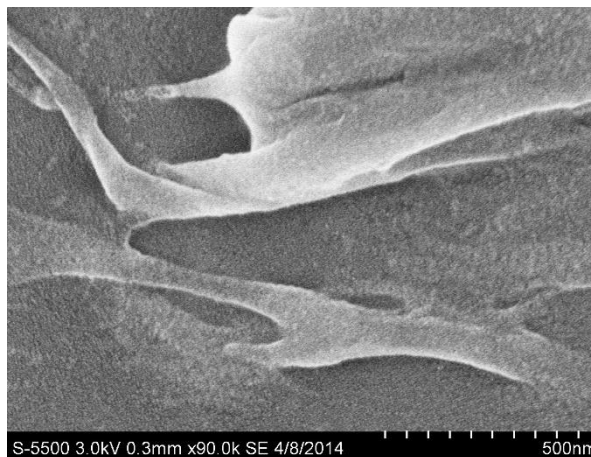
(i) Water 14 days, upside



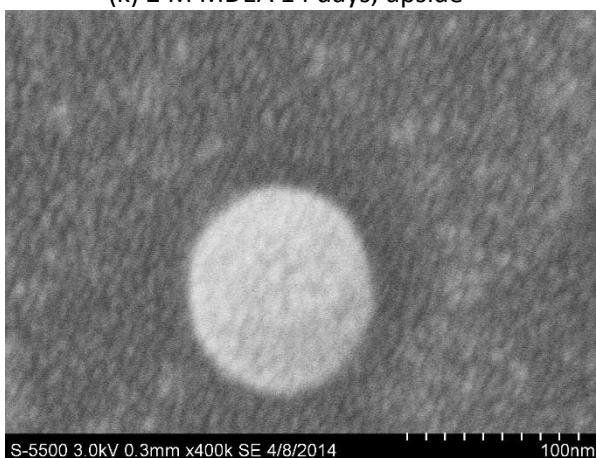
(j) Water 14 days, downside



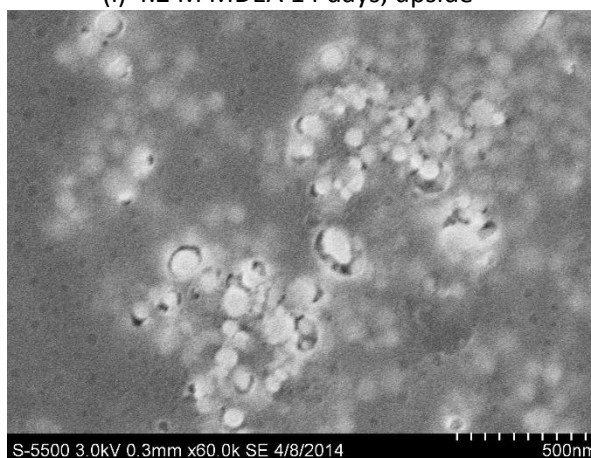
(k) 2 M MDEA 14 days, upside



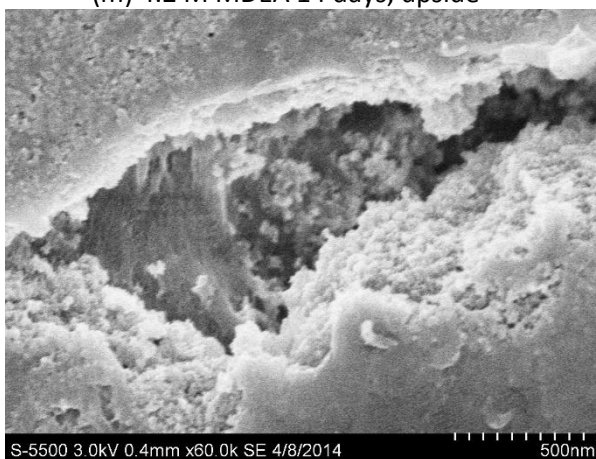
(l) 4.2 M MDEA 14 days, upside



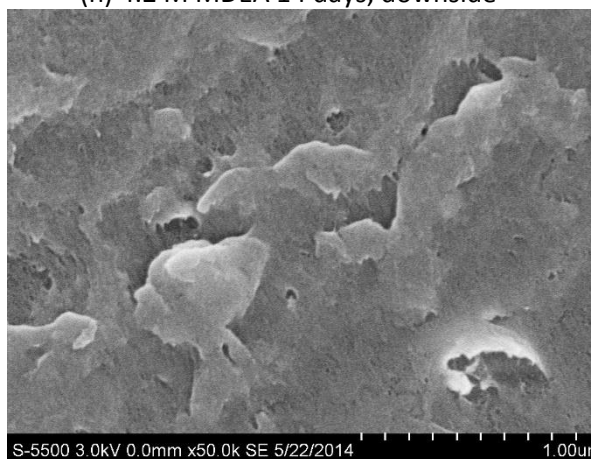
(m) 4.2 M MDEA 14 days, upside



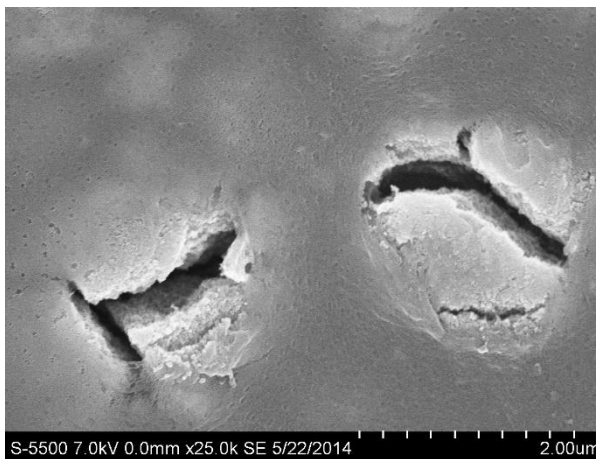
(n) 4.2 M MDEA 14 days, downside



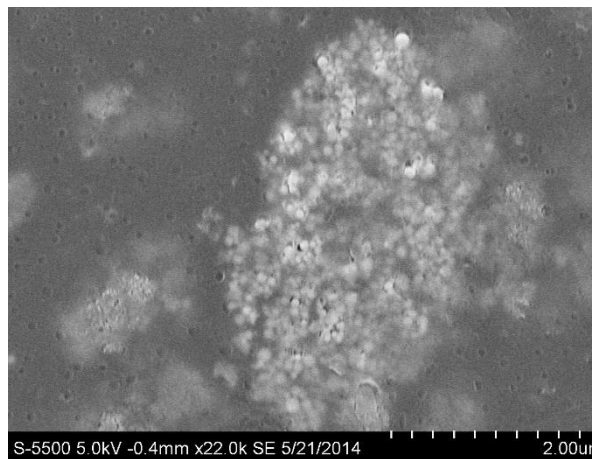
(o) 4.2 M MDEA 14 days, downside



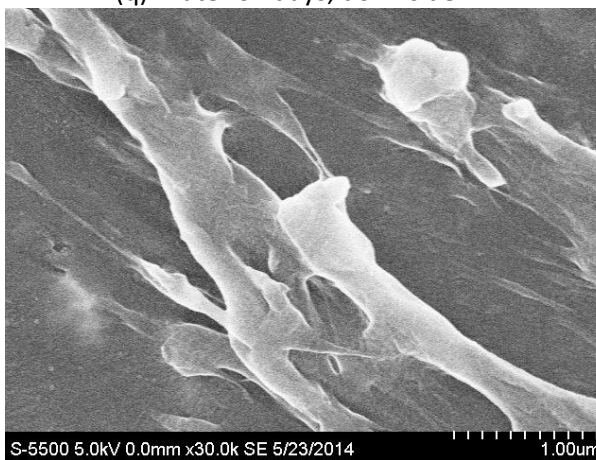
(p) Water 67 days, upside



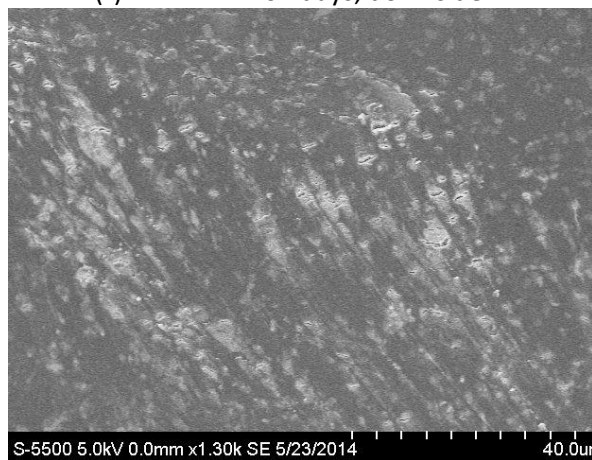
(q) Water 67 days, downside



(r) 2 M MDEA 64 days, downside



(s) 4.2 M MDEA 64 days, upside



(t) 4.2 M MDEA 64 days, downside

Figure D-7: SEM images of membranes containing 5 wt% $>1 \mu\text{m}$ TiO_2 .

Membranes containing 5 wt% commercial Aeroxide® T 805 TiO₂ prepared on casting plates of Teflon:

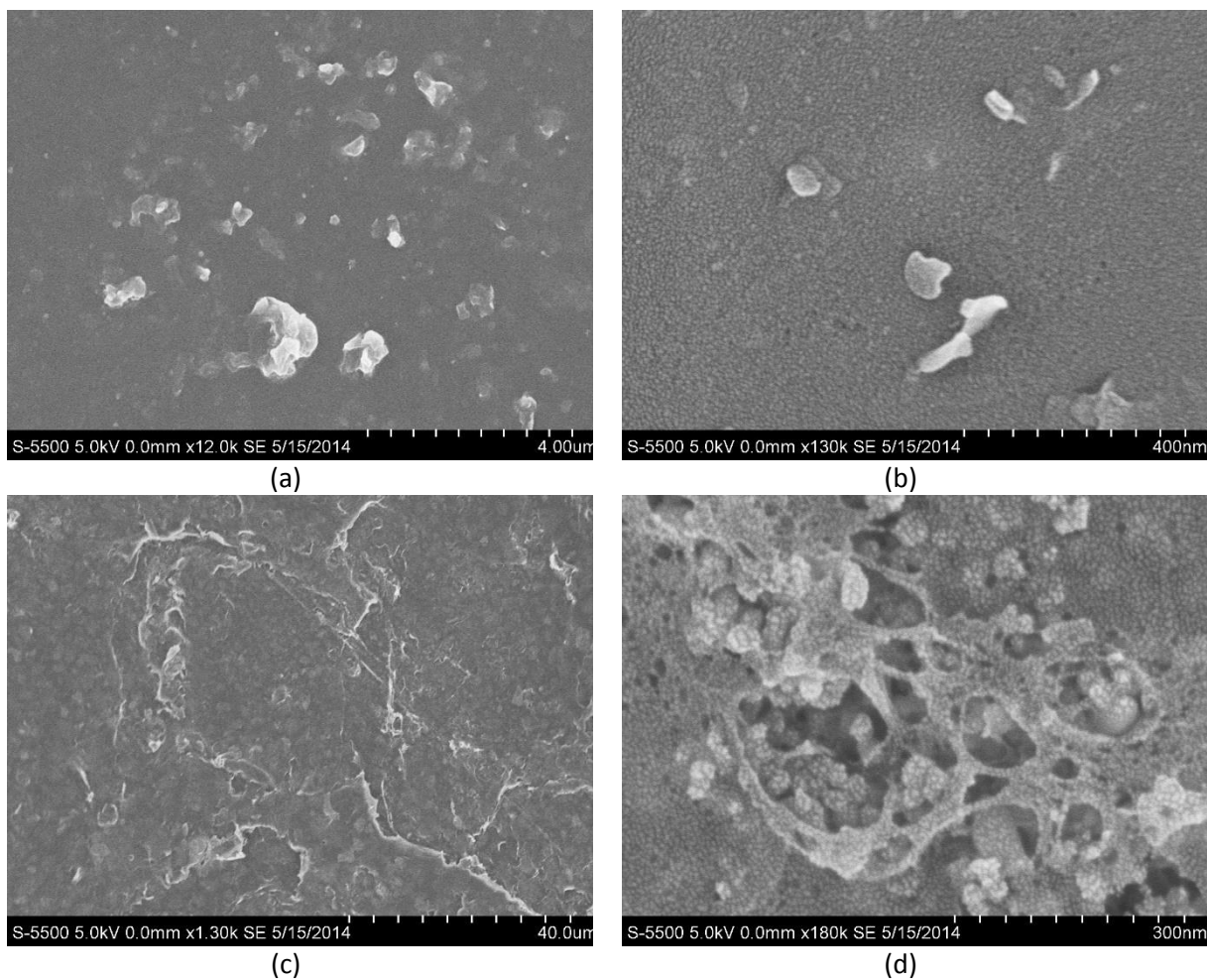


Figure D-8: SEM images (a and b) and (c and d) downside of membranes containing 5 wt% T 805 TiO₂ prepared on casting plates of Teflon.

Cross-section images of membranes containing 20 wt% 15-400 nm TiO₂:

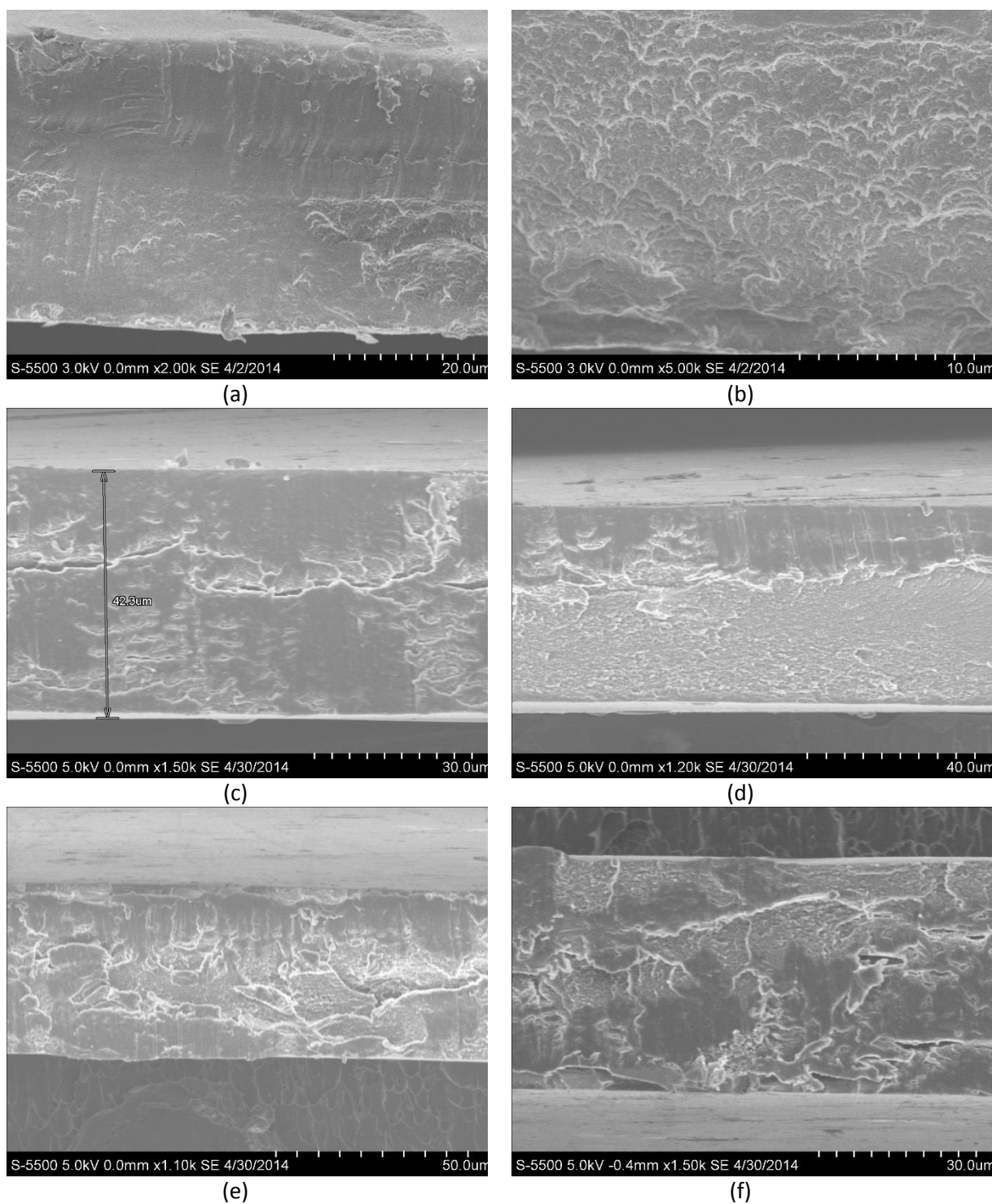




Figure D-9: Cross-section images of (a, b) unexposed and (c-f) membrane exposed to 2 M MDEA for 2 weeks containing 20 wt% 15-400 nm TiO₂. Upside is pointing upwards in image a-f, downside is pointing upwards in image f.

E. Risk assessments

NTNU	Hazardous activity identification process	Prepared by	Number	Date	
		HSE section	HMSRV2601	22.03.2011	
HSE		Approved by	Page	Replaces	
		The Rector		01.12.2006	

Unit: *(Institute)* Dep. of chemical eng. (IKP) Date: 15.01.2014

Line manager: Edd Blekkan

Participants in the identification process (incl. function): Henriette Mortensen (student), May-Britt Hägg (supervisor), Karen Nessler Seglem (co-supervisor)
(supervisor, student, co-supervisor, others)



Short description of the main activity/main process: _____

Is the project work purely theoretical? (YES/NO) No

Answer "YES" implies that supervisor is assured that no activities requiring risk assessment are involved in the work. If YES, skip rest of the form.

Signatures: Responsible supervisor: _____ Student: _____

ID nr.	Activity/process	Responsible person	Existing documentation	Existing safety measures	Laws, regulations etc.	Comment
1	Use of N-Methyldiethanolamine (MDEA)	Karen Nessler Seglem	Lab safety equipment	HSE-datasheet	HSE-datasheet	

NTNU	Risk assessment	Prepared by	Number	Date	
		HSE section	HMSRV2603	04.02.2011	
HMS/KS		Approved by	Page	Replaces	
		The Rector		09.02.2010	

Unit: *(Institute)* Dep. of chemical eng. (IKP) Date: 15.01.2014



Line manager: Edd Blekkan

Participants in the identification process (incl. function): Henriette Mortensen (student), May-Britt Hägg (supervisor), Karen Nessler Seglem (co-supervisor)
(supervisor, student, co-supervisor, others)

Risk assessment of: _____ 0

Signatures: Responsible supervisor: _____ Student: _____

ID nr.	Activity from the identification process form	Potential undesirable incident/strain	Likelihood: (1-5)	Consequence:			Risk value (human)	Comments/status Suggested measures
				Human (A-E)	Environment (A-E)	Economy/material (A-E)		
1	Use of N-Methyldiethanolamine (MDEA)	Inhalation	4	A	A	A	A4	Use fume hood, gloves and safety glasses.
		Spill	4	A	A	A	A4	
		Skin and eye irritation	3	A	A	A	A3	

 HSE	<h2 style="margin: 0;">Hazardous activity identification process</h2>	Prepared by	Number	Date	
		HSE section	HMSRV2801	22.03.2011	
		Approved by	Page	Replaces	
		The Rector		01.12.2008	

Unit: (Institute)

Dep. of chemical eng. (IKP) Date:

15.01.2014

Line manager:

Edd Blekkan

Participants in the identification process (incl. function)

(supervisor, student, co-supervisor, others)

Henriette Mortensen (student), May-Britt Hägg (supervisor), Karen Nessler Seglem (co-supervisor)

Short description of the main activity/main process: Membrane preparation

Is the project work purely theoretical? (YES/NO)

NO


Answer "YES" implies that supervisor is assured that no activities requiring risk assessment are involved in the work. If YES, skip rest of the form.

Signatures:

Responsible supervisor:



Student:

ID nr.	Activity/process	Responsible person	Existing documentation	Existing safety measures	Laws, regulations etc.	Comment
1	Preparation of polymer solutions - transfer of toluene from main container to beaker	Karen Nessler Seglem	MSDS	Fumehood, safety goggles, lab coat, Ansell Barrier® gloves		
2	Preparation of polymer solutions - weighing of toluene/toluene solutions with nanoparticles	Karen Nessler Seglem	MSDS	Movable fumehood, safety goggles, lab coat, Ansell Barrier® gloves	See MSDS	
3	Preparation of polymer solutions - weighing of dry nanoparticles	Karen Nessler Seglem	MSDS	Movable fumehood, safety goggles, lab coat, double, longer nitril gloves, filter mask, P2 filter		Very little known about the consequences of exposure to nanoparticles
4	Preparation of polymer solutions - weighing of polymer, poly-1-trimethylsilyl-1-propyne (PTMSP)	Karen Nessler Seglem	MSDS	Movable fumehood, Safety goggles, lab coat, nitril gloves,		
5	Ultrasound treatment of polymer solution with nanoparticles	Karen Nessler Seglem	MSDS toluene	Movable fumehood, safety goggles, lab coat, Ansell Barrier® gloves. Solution put on ice and covered with parafilm to avoid evaporation	Local operation manual	
6	Preparation of small membranes - weighing of polymer solution	Karen Nessler Seglem	MSDS toluene	Movable fumehood, safety goggles, lab coat, Ansell Barrier® gloves	See MSDS	Main component is toluene
7	Transportation of membrane casting plate from scale to fumehood	Karen Nessler Seglem	MSDS toluene	Safety goggles, lab coat, Ansell Barrier® gloves. Casting plate covered with upsidedown funnel with partially closed		

NTNU	Risk assessment	Prepared by	Number	Date
		HSE section	HMSRV2803	04.02.2011
HMS /KS		Approved by	Page	Replaces
		The Rector		09.02.2010



Unit: (Institute) Dep. of chemical eng. (IKP) Date: 15.01.2014
 Line manager: Edd Blekkan
 Participants in the identification process (incl. function): Henriette Mortensen (student), Karen Nessler Seglem (co-supervisor)
 Risk assessment of: Membrane preparation
 Signatures: Responsible supervisor: _____ Student: _____

ID nr.	Activity from the identification process form	Potential undesirable incident/strain	Likelihood:	Consequence:			Risk value (human)	Comments/status Suggested measures
			(1-5)	Human (A-E)	Environment (A-E)	Economy/material (A-E)		
1	Preparation of polymer solutions - transfer of toluene from main container to beaker	Inhalation	3	A	A	A	3A	
		Spill - inhalation	3	A	A	A	3A	
		Spill - skin contact	3	A	A	A	3A	
2	Preparation of polymer solutions - weighing of toluene/toluene solutions with nanoparticles	Inhalation	4	A	A	A	4A	Be careful to keep the solution under the movable hood. Reduce continuous exposure.
		Spill - inhalation	4	A	A	A	4A	
		Spill - skin contact	3	A	A	A	3A	
3	Preparation of polymer solutions - weighing of dry nanoparticles	Inhalation	3	B - see comment	A	A	3B - see comment	Very little known about the consequences of exposure to nanoparticles. Nanoparticles may stick to clothing etc.
		Skin contact	4	B - see comment	A	A	4B - see comment	
4	Preparation of polymer solutions - weighing of polymer, poly-1-trimethylsilyl-1-propyne (PTMSP)	Spill	4	A	A	A	4A	
5	Ultrasound treatment of polymer solution with nanoparticles	Inhalation	4	A	A	A	4A	
6	Preparation of small membranes - weighing of polymer solution	Inhalation	4	A	A	A	4A	Be careful to keep the solution under the movable hood. Reduce continuous exposure, take breaks from the work
		Spill - inhalation	4	A	A	A	4A	
		Spill - skin contact	3	A	A	A	3A	
7	Transportation of membrane casting plate from scale to fumehood	Inhalation	3	A	A	A	3A	
		Spill - inhalation	4	B	A	A	4B	
		Spill - skin contact	3	B	A	A	3B	

NTNU	Hazardous activity identification process	Prepared by	Number	Date	
		HSE section	HMSRV2601	22.03.2011	
HSE		Approved by	Page	Replaces	
		The Rector		31.12.2008	

Unit: (Institute) Dep. of chemical eng. (IKP) Date: 15.01.2014
 Line manager: Edd Blekkan
 Participants in the identification process (incl. function): Henriette Mortensen (student), May-Britt Hägg (supervisor), Karen Nessler Seglem (co-supervisor)
 Short description of the main activity/main process: Gas permeation tests
 Is the project work purely theoretical? (YES/NO) NO
 Answer "YES" implies that supervisor is assured that no activities requiring risk assessment are involved in the work. If YES, skip rest of the form.
 Signatures: Responsible supervisor: _____ Student: _____

ID nr.	Activity/process	Responsible person	Existing documentation	Existing safety measures	Laws, regulations etc.	Comment
1	Gas permeation of N2	Karen Nessler Seglem	Local operation manual	Use safety glasses	-	
2	Gas permeation of CH4	Karen Nessler Seglem	Local operation manual	Use safety glasses	-	
3	Gas permeation of CO2	Karen Nessler Seglem	Local operation manual	Use safety glasses	-	

 NTNU HMS/KS	<h2 style="margin: 0;">Risk assessment</h2>	Prepared by	Nummer	Date	
		HSE section	HMSRV2803	04.02.2011	
		Approved by	Page	Replaces	
		The Rector		08.02.2010	

Unit: *(Institute)*

Dep. of chemical eng. (IKP)

Date:

15.01.2014

Line manager:

Edd Blekkan

Participants in the identification process (incl. function):

Henriette Mortensen (student), May-Britt Hägg (supervisor), Karen Nessler Seglem (co-supervisor)

(supervisor, student, co-supervisor, others)

Risk assessment of:

Gas permeation tests

Signatures:

Responsible supervisor:

Student:

ID nr.	Activity from the identification process form	Potential undesirable incident/strain	Likelihood:	Consequence:			Risk value (human)	Comments/status Suggested measures
			(1-5)	Human (A-E)	Environment (A-E)	Economy/material (A-E)		
1	Gas permeation of N2	Pressure build-up can cause rupture of membranes due to malfunction of valves.	2	A	A	A	2A	Check the pressure, vent the system, change membranes or valves if they have lost some of their function.
		Leakage	2	A	A	A	2A	
		Explosion	1	C	C	C	1C	
2	Gas permeation of CH4	Pressure build-up can cause rupture of membranes due to malfunction of valves.	2	A	A	A	2A	Check the pressure, vent the system, change membranes or valves if they have lost some of their function.
		Leakage	2	A	A	A	2A	
		Fire, flammable gas	1	B	B	B	1B	
		Explosion	1	C	C	C	1C	
3	Gas permeation of CO2	Pressure build-up can cause rupture of membranes due to malfunction of valves.	2	A	A	A	2A	Check the pressure, vent the system, change membranes or valves if they have lost some of their function.
		Leakage	2	A	A	A	2A	
		Explosion	1	C	C	C	1C	